

DISSERTATION

SIMPLE MADE CONTINUOUS BRIDGES WITH STEEL DIAPHRAGMS: TENSION AND
COMPRESSION TRANSFER MECHANISMS

Submitted by

Robert I. Johnson

Department of Civil and Environmental Engineering

In partial fulfillment of the requirements

For the Degree of Doctor of Philosophy

Colorado State University

Fort Collins, Colorado

Spring 2015

Doctoral Committee:

Advisor: Rebecca Atadero

Suren Chen
Caroline Clevenger
Paul Heyliger
Hussam Mahmoud

Copyright by Robert I. Johnson 2015

All Rights Reserved

ABSTRACT

SIMPLE MADE CONTINUOUS BRIDGES WITH STEEL DIAPHRAGMS: TENSION AND COMPRESSION TRANSFER MECHANISMS

Simple-made-continuous (SMC) steel bridges are a relatively new innovation in steel bridge design. The SMC concept has been used for quite some time in the construction of precast concrete bridges and based on current statistics, precast concrete bridge construction is outpacing steel bridge construction by a factor of two to one. The SMC concept is a viable solution for steel bridges to recover market share of the bridges constructed in the United States. The majority of SMC bridges currently in use are constructed with concrete diaphragms. This dissertation presents the results of numerical analysis and laboratory testing of an alternative simple-made-continuous connection scheme that uses steel diaphragms in lieu of concrete diaphragms. A bridge using steel diaphragms was constructed by the Colorado Department of Transportation in 2005 and the connections on this bridge serve as a basis for the research presented herein.

Preliminary numerical analysis was performed by hand; this analysis discovered potential design flaws in the current bridge connection. Subsequent numerical analysis using Abaqus finite element analysis software provided results which were indecisive in regard to the flaws found in the hand analysis. The finite element analysis however, did provide valuable insight into some of the connection behavior, which was also verified with the physical test.

Physical testing was subsequently performed on a full size model of the connection. The physical model consisted of double cantilever composite girders loaded at their ends with 300

kip actuators to simulate negative moments at the center connection. The physical test verified that there were design flaws in the original design.

The results of analysis and physical testing provided information necessary to correct the design flaws and data required for the development of a design methodology based on the actual physical behavior of the SMC connection. Also, particular behaviors noted in the finite element analysis were corroborated with the physical test and the design methodology recognizes these behaviors.

The research also compares the steel diaphragm SMC connection to concrete diaphragm connection and demonstrates that the steel diaphragm design has several desirable features. The steel diaphragm design provides for a more economical and quicker to construct steel bridge design and requires less total construction time than other SMC schemes. Additionally, since the girder ends are exposed, the girders are able to fully weather and they may be easily inspected.

TABLE OF CONTENTS

ABSTRACT	ii
LIST OF TABLES	ix
LIST OF FIGURES	xii
Chapter 1 - Introduction.....	1
1.1 Background /Motivation	1
1.2 Basics of Steel Girder Bridge SMC Connections	3
1.3 Summary of Currently Constructed Bridges using the SMC Concept	7
1.4 Study Objectives	8
1.5 Study Methodology.....	9
Chapter 2 - Literature Review.....	11
2.1 Simple Made Continuous Concept for Steel Bridges	11
2.2 Research to Develop Steel SMC Connections.....	13
2.3 Findings of Nebraska Experimental Program.....	22
2.3.1 Details of Finite Element Modeling.....	23
2.3.2 Lab Testing of SMC Bridge Connections.....	26
2.4 Code Mandated Requirements	29
2.5 Field Testing of Bridges Constructed with SMC Connections.....	30
2.6 Summary and General Publications.....	35

2.7 A Summary of Bridges Constructed with the SMC Concept	37
2.8 Selection of a Study Bridge	42
Chapter 3 – Preliminary Analysis	45
3.1 Research Overview	45
3.2 AASHTO Requirements	48
3.2.1 General.....	48
3.2.2 Bridge Load Requirements and Load Factors	48
3.2.3 Bridge Material Limit States and Resistance Requirements.....	53
3.3 Design Load Calculations and Determination of Controlling Loads.....	56
3.3.1 Preliminary Analysis.....	56
Chapter 4 Finite Element Analysis	64
4.1 Material Modeling	64
4.2 Element Selection and Modeling	73
4.3 Constraints and Contacts.....	78
4.4 Sensitivity Analysis	79
4.5 Finite Element Analysis of the Study Girder Connection	87
4.5.1 Basic Finite Element Modeling	87
4.5.2 Loads and boundary conditions	89
4.5.3 Contacts and Constraints.....	90
4.5.4 Convergence Criteria	91

4.5.5 Discussion of Results	92
Chapter 5 Physical Test	99
5.1 Lab Description and Constraints.....	99
5.2 Self-Reacting Load Frame	99
5.3 Test Specimen Description	100
5.4 Test Specimen Instrumentation.....	107
5.5 Physical Test	114
5.6 Test Results	119
5.6.1 Day 1 Test Results	119
5.6.2 Day 2 Test Results	127
5.7 Analysis of Test Results.....	139
5.7.1 Internal Forces and Model Equilibrium.....	139
5.7.2 Deflection and deformation compatibility	141
5.7.3 Discussion/Conclusions from experimental test.....	142
5.7.4 Comparison with Abaqus Results	143
5.7.5 Post-Test Attempts to Correlate Results to Hand and Abaqus Analysis	147
Chapter 6 Parametric Study	152
6.1 Bridged Roadway Geometry Limitations	152
6.2 Deck Slab Geometry and Reinforcing	154
6.2.1 General.....	154

6.2.2 AASHTO Limitations	154
6.3 Girder Selection Criteria	156
6.3.1.....	156
6.3.2 Girder Serviceability Criteria.....	157
6.5 Final Ranges of Parameters	157
6.6 Analysis Considerations.....	158
6.7 Final Truck Load Analysis.....	160
Chapter 7 Proposed Design Formulation	164
7.1 Preliminary Considerations.....	164
7.2 Formulation Development	169
7.3 Verification/Validation of Design Formulation.....	175
7.4 Cost Analysis	180
Chapter 8 Summary and Recommendations.....	183
8.1 Summary	183
8.2 Recommendations for Future Research	185
Bibliography	187
Appendix 1 – Current SMC Bridges.....	191
Appendix 2 – Hand Calculations	211
Appendix 3 – Model Construction Drawings	214
Appendix 5 – Plate Girder Dimensions	236

Appendix 6 – Acceptable Bridge Girders	237
Appendix 7 – Maximum SMC Negative Moments	239
Appendix 8 – Deflection Equation Development	241

LIST OF TABLES

Table 1 - Summary of Instrumentation Type and Placement	26
Table 2 - Study Objectives.....	47
Table 3 - Applicable Load Combinations.....	50
Table 4 - AASHTO Load Factors, γ 's	50
Table 5 – AASHTO Ultimate Capacity Calculations.....	53
Table 6 – AASHTO resistance factors.....	55
Table 7 - Comparison of SMC Moment Capacities of Study Connection	60
Table 8 – Steel stress-strain curve values for $F_y = 50$ ksi (Salmon, 2009).....	65
Table 9 – Steel stress-strain curve values for $F_y = 50$ ksi (Salmon, 2009).....	65
Table 10 - Steel Reinforcing Stress-Strain Curve Values for $F_y = 60$ ksi (Groom, 2010).....	66
Table 11 – Weld Stress-Strain Properties for E70 Electrodes	66
Table 12 – Steel Stud Material Properties for Stress-Strain Diagram	68
Table 13 – Damaged stress/strain values for 4712 psi concrete in uniaxial tension.....	70
Table 14 - Damaged stress/strain values for 4712 psi concrete in uniaxial compression.....	72
Table 15 - Additional variables to effectively model "CONCRETE DAMAGED PLASTICITY"	73
Table 16 - Possible element types and their descriptions	73
Table 17 - Moments along Beam Span.....	82
Table 18 – Sensitivity Analysis Matrix (Shaded areas indicate the choices being analyzed)	83
Table 19 – Sensitivity analysis matrix (continued).....	84
Table 20 - Sensitivity Analysis - Comparison of Increments and Run Times.....	87

Table 21 - Final Part Element Types	87
Table 22 - Final Constraint Types	88
Table 23 - Final Interaction Types.....	88
Table 24 - Location of Resultants for Various Loadings.....	141
Table 25 - North Girder End Deflections	141
Table 26 - Span and Spacing Ranges for the Parametric Study	157
Table 27- Girder Span to Girder Size Table	158
Table 28 - Girder Acceptance Table - 80 ft. Span	161
Table 29 - Maximum SMC Negative Moments (kip-feet) - 80 ft. Span.....	162
Table 30 - Sample SMC Reinforcing and Moment Calculations	177
Table 31 - Minimum SMC Bar Size based on Girder Area/Flange Area.....	180
Table 32 - Cost Comparison - Concrete vs. Steel Diaphragm.....	181
Table 33 - Construction Man-hour Comparison.....	182
Table 34 – Girder Cost Comparison Fully Continuous Bridge to SMC Bridge.....	182
Table 35	191
Table 36	193
Table 37	195
Table 38	198
Table 39	200
Table 40	201
Table 41	204
Table 42	206
Table 43	208

Table 44	209
Table 45 - Plate Girder Dimensions.....	236
Table 46 - Girder Acceptance Table - 92 ft. Span	237
Table 47 - Girder Acceptance Table - 104 ft. Span	237
Table 48- Girder Acceptance Table - 116 ft. Span	237
Table 49 - Girder Acceptance Table - 128 ft. Span	238
Table 50 - Girder Acceptance Table - 140 ft. Span	238
Table 51 - Maximum SMC Negative Moments (kip-feet) - 92 ft. Span.....	239
Table 52 - Maximum SMC Negative Moments (kip-feet) - 104 ft. Span.....	239
Table 53 – Maximum SMC Negative Moments (kip-feet) – 116 ft. Span	239
Table 54 - Maximum SMC Negative Moments (kip-feet) - 128 ft. Span.....	240
Table 55 - Maximum SMC Negative Moments (kip-feet) - 140 ft. Span.....	240

LIST OF FIGURES

Figure 1 - Comparison New Bridges by Type of Construction Material from 2003-2012 (FHWA, 2005 through 2012).....	1
Figure 2 - Typical Continuous Girder Bridge Bolted Splice over Roadway	3
Figure 3 - Girders Placed on Supports	4
Figure 4 - Bridge Deck Slab Cast on Girders	4
Figure 5 - Slab Strength Attained	5
Figure 6 – Basic SMC Connection Elements and Behavior	6
Figure 7 - SMC Connection Elements – Variation without Concrete Diaphragm	6
Figure 8 - Girder connection specimen modeled at University of Nebraska - Lincoln (Lampe N. J., 2001).....	14
Figure 9 - Girder Connection Specimens Tested at University of Nebraska-Lincoln (Farimani M. , 2006)	16
Figure 10 - Connection with diaphragm and slab in place	17
Figure 11 - Accelerated connection detail modeled at U of N - Lincoln (Niroumand, 2009).....	19
Figure 12 - Detail at SMC Connection showing reinforcing layout in diaphragm and slab	20
Figure 13 - Bridge over the Scioto River SMC detail	31
Figure 14 - Bridge over the Scioto River pier detail.....	31
Figure 15 - U.S. 70 over Sonoma Ranch Road SMC detail	33
Figure 16 - DuPont Access bridge SMC detail.....	34
Figure 17 - DuPont Access bridge slab and diaphragm.....	34
Figure 18 - Wedge plate detail.....	35

Figure 19 - Revised Concrete Diaphragm SMC Detail	36
Figure 20 - SMC Detail with a Steel Diaphragm.....	42
Figure 21 - SH 36 Over Box Elder Creek (reprinted courtesy of AISC).....	44
Figure 22 - SH 36 Over Box Elder Creek – Girder Details (reprinted courtesy of AISC).....	44
Figure 23 - Simplified girder model	46
Figure 24 - AASHTO Design Truck.....	49
Figure 25 - AASHTO Design Tandem	49
Figure 26 - AASHTO Dual Truck	50
Figure 27 – Weld Load Directions (AASHTO 6.13.3.2.4b).....	56
Figure 28 - Shear Diagram.....	58
Figure 29 - Moment Diagram	59
Figure 30 - Service Load Level Shear Diagram	63
Figure 31 – Service Load Level Moment Diagram	63
Figure 32 - Stress-Strain Diagram for Weld Metal (Ricles).....	67
Figure 33 - Stress-strain diagram for stud shear connectors.....	68
Figure 34 - Softening Response to Uniaxial Loading Based on Plain Concrete Tensile Damage (Gopalaratnam, 1985)	69
Figure 35 – Damage Model for Concrete in Uniaxial Compression for $f'_c = 4712$ psi.....	72
Figure 36 - Meshed Girders - Solid Brick Elements (left) and Shell Elements (right)	75
Figure 37 - Meshed Sole Plate.....	75
Figure 38 - Shear Stud Connector Dimensions and as Modeled (brick elements).....	76
Figure 39 - Weld (left), Weld and Girder (right)	76
Figure 40 - Meshed Slab and Haunch.....	77

Figure 41 - Meshed Pier.....	77
Figure 42 - Sensitivity Analysis Composite Girder - Elevation	80
Figure 43 - Sensitivity Analysis Composite Girder - Section.....	80
Figure 44 - Sensitivity Girder - ABAQUS Model	81
Figure 45 - Comparison of Bending Moments from Sensitivity Analysis	86
Figure 46 – Modeling of Study Connection	89
Figure 47 - Contacts and Constraints at Support Pier.....	91
Figure 48 - Slab, Studs and Reinforcing Constraints.....	91
Figure 49 - Centerline Negative Moment at SMC Connection	93
Figure 50 - Axial Force at Pier	94
Figure 51 - Axial Force at Sole Plate.....	94
Figure 52 - Concrete Surface Axial Stress after Dead Load Application.....	95
Figure 53 - Concrete Surface Axial Stress after 75% of Concentrated Load Application	95
Figure 54 - Concrete Surface Axial Stress after 100% of Concentrated Load Application	96
Figure 55 - von Mises Stress in Weld after Dead Load Application.....	97
Figure 56 - von Mises Stress in Weld after 75% of Concentrated Load Application	97
Figure 57 - von Mises Stress in Weld after 100% of Concentrated Load Application	98
Figure 58 - Self-Reacting Load Frame – Upper Frames for Actuators (March 2014)	100
Figure 59 - Safety Device Details.....	102
Figure 60 - Bridge Girders with Studs (March 2014).....	102
Figure 61 - Steel Diaphragm Beam (March 2014)	103
Figure 62 - Slab Reinforcing Placement (March 2014).....	103
Figure 63 - Concrete Deck Slab (April 2014).....	104

Figure 64 - 220 kip Actuator and Load Application Beam (May 2014)	104
Figure 65 - (2) 110 kip Actuators and Load Application Beam (May 2014)	105
Figure 66 - Plan of Constructed Physical Model	106
Figure 67 - Legend for Instrumentation Layouts	107
Figure 68 - Instrumentation Layout at the Girder Ends – 1	108
Figure 69 - Pots 3, 4, 5 and 6 in Position during Testing (July 2014)	109
Figure 70 - Instrumentation at the Girder Ends -2.....	109
Figure 71 - Instrumentation Layout at the Sole Plate	110
Figure 72 - Gage Placement at 5/8" Sole Plate Fillet Weld (July 2014)	111
Figure 73 - Strain Gage Attached to Top of Slab (July 2014)	111
Figure 74 - Instrumentation Layout on the Top and Bottom of Slab.....	112
Figure 75 - Instrumentation Layout on the Slab Reinforcing	113
Figure 76 – Strain Gages Attached to Reinforcing Steel (April 2014).....	114
Figure 77 - Free Body Diagram of Sole Plate.....	117
Figure 78 - Failed Weld on East Side of North Girder (July 2014).....	118
Figure 79 - Failed Weld on West Side of North Girder (July 2014)	118
Figure 80 - Actuator Force vs. Displacement – Day 1 Test.....	120
Figure 81 - Shear Lag in Top SMC Bars - Day 1 Test	121
Figure 82 - Concrete Top Surface Strains vs. Actuator Force – Day 1 Test	122
Figure 83 - Concrete Bottom Surface Strains vs. Actuator Force – Day 1 Test.....	123
Figure 84 - Sole Plate Strains and Stresses at the end of Day 1 Test	124
Figure 85 - Displacement at North End of North Girder vs. Actuator Force – Day 1	126
Figure 86 - Displacement at South End of South Girder vs. Actuator Force – Day 1.....	126

Figure 87 - Displacement of North Elastomeric Bearing vs. Actuator Force – Day 1	127
Figure 88 - Displacement of South Elastomeric Bearing vs. Actuator Force – Day 1	127
Figure 89 - Actuator Force vs. Displacement - Day 2 Test	128
Figure 90 - Comparison of Days 1 and 2 Actuator Load and Reinforcing Strain	130
Figure 91 - Comparison of Days 1 and 2 Actuator Load and Reinforcing Strain - Scheme 1 ...	130
Figure 92 - Comparison of Days 1 and 2 Actuator Load and Reinforcing Strain - Scheme 2 ...	131
Figure 93 - Shear Lag in Top SMC Bars - Day 2 Test - Safety Device Activation	131
Figure 94 - Shear Lag in Top SMC Bars - Day 2 Test - End of Test	132
Figure 95 - Bottom Concrete Strains vs. Actuator Force - Day 2.....	133
Figure 96 - Strains at Center of Sole Plate – Day 2 Test	134
Figure 97 - Sole Plate Strains and Stress at Safety Device Activation - Day 2 Test	134
Figure 98 - Strains at Center of Safety Device vs. Actuator Force - Day 2 Test.....	135
Figure 99 - Detail of Safety Device Showing Bevel at Weld	135
Figure 100 - Displacement of North Girder - Day 2 Test.....	136
Figure 101 - Displacement of South Girder - Day 2 Test.....	137
Figure 102 - Distorted Potentiometer Anchorages - Day 2 (July 2014).....	137
Figure 103 - Final Crack Pattern in Top of Deck Slab Looking South (July 2014).....	138
Figure 104 - Crack Pattern in Top of Deck Slab	139
Figure 105 - Girder Support Behavior	140
Figure 106 - Normal Forces on Sole Plate – Abaqus.....	145
Figure 107 - Axial Stress in SMC Top Reinforcing Steel	145
Figure 108 - Comparison of SMC Reinforcing Strains	146
Figure 109 - Early Shear Lag in Top of Concrete Slab	146

Figure 110 - Profile of Modulus of Elasticity across Slab.....	150
Figure 111 – Third Approach - Moduli of Elasticity	150
Figure 112 - Comparison of Reduced Stiffness Abaqus Shear Lag to Physical Test.....	151
Figure 113 Roadway Limitations.....	153
Figure 114 Slab Reinforcing Placement	156
Figure 115 Maximum and Minimum Moments vs. Spans (note: moment scales are different)	160
Figure 116 - SMC Girder Support Detail 1 – Side View.....	166
Figure 117 - SMC Girder Support Detail 1 - Plan View	166
Figure 118 – SMC Girder Support Detail 2 – Side View	167
Figure 119 - SMC Girder Support Detail 2 - Plan View	167
Figure 120 - SMC Girder Support Detail 3 - Side View	168
Figure 121 - SMC Girder Support Detail 3 - Plan View	168
Figure 122 - SMC Behavior.....	175
Figure 123 - Day 2 SMC Reinforcing Strains vs. Actuator Force.....	178
Figure 124 - Girders.....	191
Figure 125 – Diaphragm and Slab	191
Figure 126 - Girders.....	193
Figure 127 – Girders and Slab	193
Figure 128 - Girders.....	195
Figure 129 – Diaphragm and Slab	195
Figure 130 - Girders.....	198
Figure 131 – Diaphragm and Slab	198
Figure 132 - Girders.....	201

Figure 133 – Diaphragm and Slab	201
Figure 134 - Girders.....	204
Figure 135 – Diaphragm and Slab	204
Figure 136 - Girders.....	206
Figure 137 – Diaphragm and Slab	206
Figure 138 - Girders.....	209
Figure 139 – Diaphragm and Slab	209

CHAPTER 1 - INTRODUCTION

1.1 BACKGROUND /MOTIVATION

An annual inventory of new bridges by material type has been performed by the Federal Highway Administration (FHWA) since 2003 (FHWA, 2005 through 2013). At the time of this writing, complete data is available through 2012 and is presented in Figure 1. As may be seen, the market share of steel bridges is consistently less than that of both reinforced concrete and prestressed concrete and is actually dropping based on the most current data.

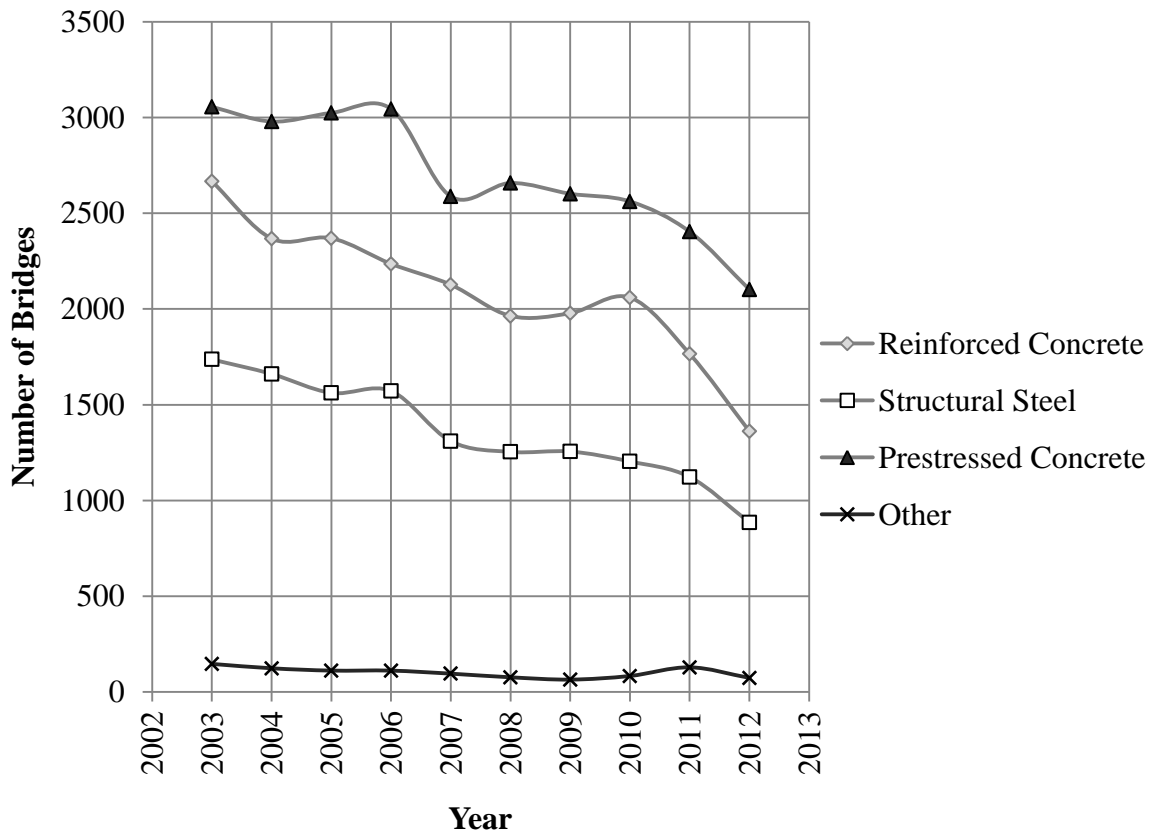


Figure 1 - Comparison New Bridges by Type of Construction Material from 2003-2012 (FHWA, 2005 through 2012)

The popularity of pre-stressed concrete for bridge construction in comparison to steel may be largely attributed to the lower initial cost of pre-stressed concrete bridges. The impetus

for the development of the Simple Made Continuous (SMC) concept came from the desire for steel bridges to be able to compete economically against precast/prestressed concrete bridges for medium to long girder spans. The SMC concept is also known as “simple for dead - continuous for live” or SD-CL (Azizinamini, 2005).

Typically, continuous bridges are more economical than simple span bridges because they develop smaller positive interior span moments due to the negative moments at the continuous ends. Conventional continuous steel bridges cannot compete against continuous prestressed concrete bridges due primarily to differences in construction techniques. The steel continuity connections must be made in the field and these connections typically occur in portions of the spans over the bridged roadway, thus requiring shoring of the girders over the roadway until the continuity connection (welded or bolted) can be made. This scheme has many drawbacks (Azizimanini & Vander Veen, 2004), including:

- Blocking existing roadways
- Danger to ironworkers
- Considerable cost
- Effects on construction schedule

In addition to the preceding drawbacks, spliced bridges require tight placement and fit-up tolerances for proper fastening of the splice plates, Figure 2.

SMC bridge construction is able to overcome these limitations, and thus, the prime mover of the majority of the SMC research is the steel industry and its desire to increase its share of the bridge market. Additional motivation has been provided by the various state departments of transportation/roads which want to encourage competition and thereby increase the economy of both steel and concrete bridges in the medium to long span range.



Figure 2 - Typical Continuous Girder Bridge Bolted Splice over Roadway

1.2 BASICS OF STEEL GIRDER BRIDGE SMC CONNECTIONS

In the past ten plus years, considerable research has gone into the development of details for Simple Made Continuous (SMC) bridge connections for steel girder bridges. In brief, SMC connections behave as simple or hinged connections for permanent dead load and continuous for live loads and superimposed dead loads. The typical method of obtaining continuity involves placing steel girders and formwork for cast-in-place concrete slabs. Reinforcing steel for slabs, which spans perpendicular to the girders, is installed and additional top reinforcing oriented parallel to the girders is placed over the girder ends that are to act continuously. Once the concrete has set, negative moment continuity exists and is taken through the composite slab and various means of steel girder attachments. The overall concept results in lighter weight steel girders.

SMC connections are made over the bridge support piers, the only place to develop negative moments in continuous spans. The basic steps in developing the behavior and elements

of a SMC connection are shown in Figure 3 through Figure 5. In Figure 3 the girders have been placed and are loaded only by their self-weight. Their deflection is very small and loads are taken by simple beam behavior.

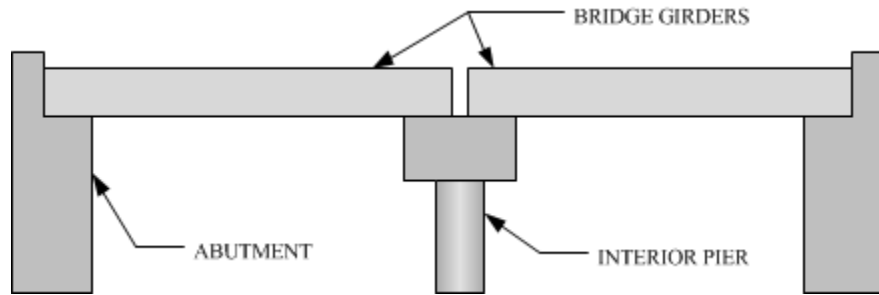


Figure 3 - Girders Placed on Supports

In Figure 4, the slab is cast on the bridge girders and they will deflect considerably more under the dead load of the wet concrete; again, loads are taken by simple beam behavior. Typically, bridge girders are cambered during fabrication in order to offset the effects of permanent dead load deflection from the self-weight of the girders and slabs. The camber does not usually include the deflection from replaceable dead loads such as a protective wearing course.

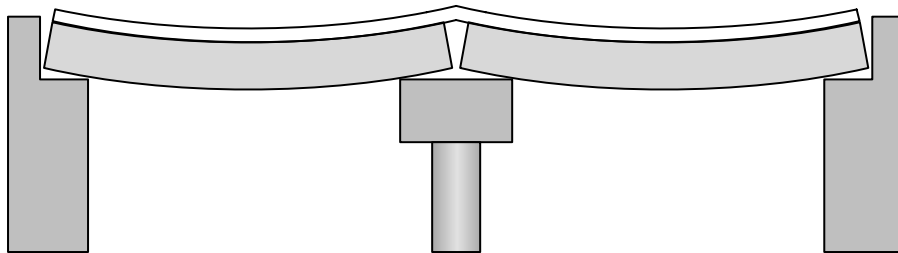


Figure 4 - Bridge Deck Slab Cast on Girders

In Figure 5, the slabs have attained their design strength and negative moment resistance has been developed over the center support; superimposed loads, such as the wearing course and traffic, are now taken by continuous behavior.

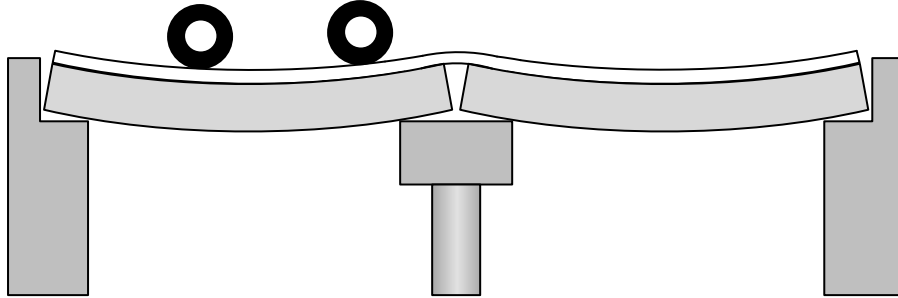


Figure 5 - Slab Strength Attained

The minimum components of a SMC connection are a tension zone (top reinforcing in the concrete deck), a compression zone (concrete, fastening by welds or a steel block) and a shear transfer mechanism (shear studs). The basic construction of a common SMC connection is detailed in Figure 6, which shows one half of the symmetric connection. This connection has variations where the beam end is also encased in the diaphragm concrete. There are many variations of this arrangement, the most extreme variation is the case where there is no concrete diaphragm and compression forces are transferred by the bridge girder bearing plate through welds of the bottom flanges as shown in Figure 7.

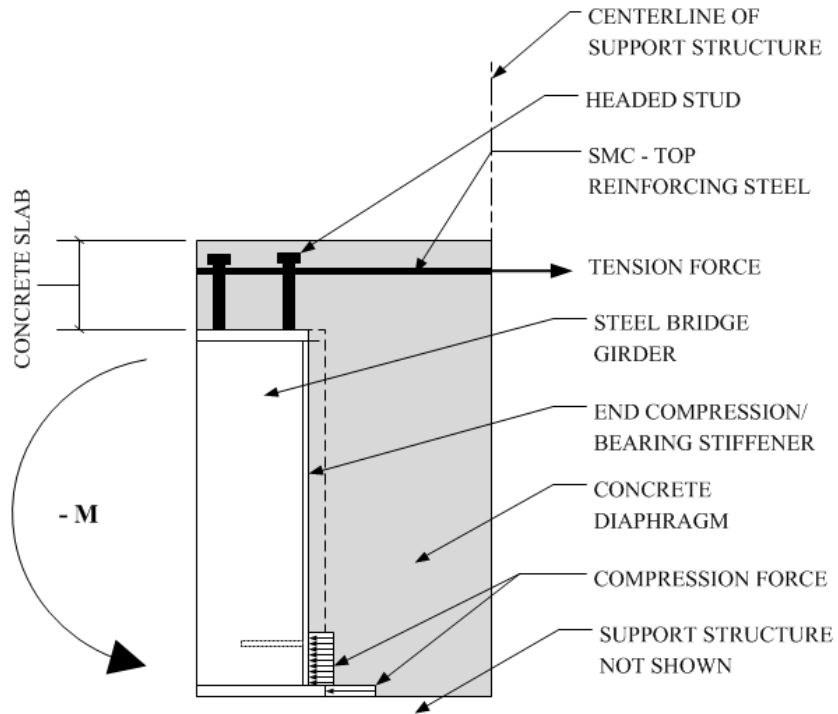


Figure 6 – Basic SMC Connection Elements and Behavior

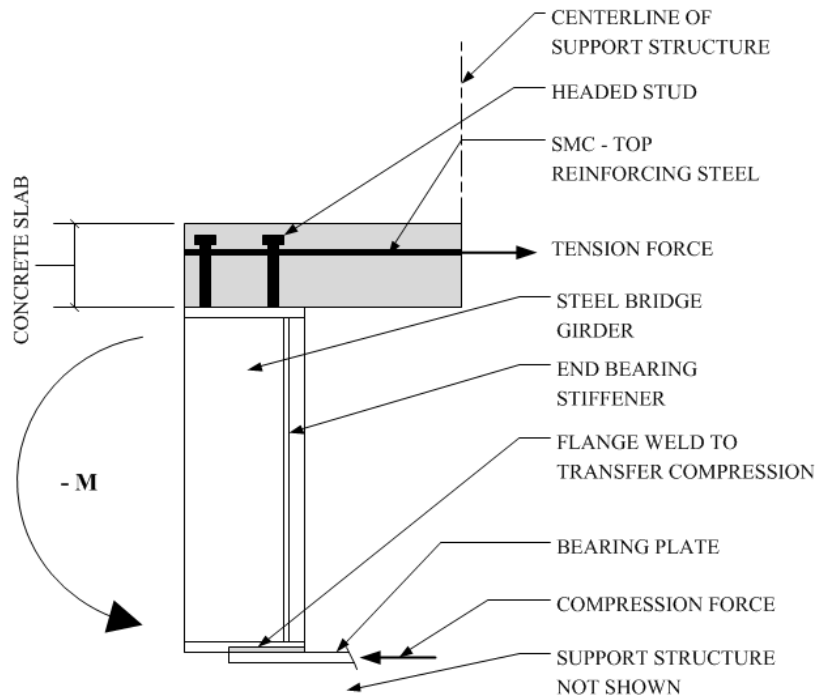


Figure 7 - SMC Connection Elements – Variation without Concrete Diaphragm

1.3 SUMMARY OF CURRENTLY CONSTRUCTED BRIDGES USING THE SMC CONCEPT

One SMC bridge has been built in Nebraska using a scheme developed in research conducted at the University of Nebraska - Lincoln (Azizinamini, 2005) and uses the basic configuration as shown in Figure 6. Two additional Nebraska bridges have been constructed using a slight modification of the research scheme. Another Nebraska bridge was constructed using “tub” girders; this SMC scheme was also based on an extrapolation of the University of Nebraska - Lincoln work. SMC bridges of various SMC continuity schemes have also been constructed on S.H. 36 and S.H. 16 in Colorado (NSBA, 2006), New Mexico (Barber, 2006) and Ohio (Lin, 2004) and partial SMC bridges have been constructed in Tennessee (Talbot, 2005). While some of the aforementioned bridge’s SMC connection schemes appear to be based on those researched for the Nebraska Bridges (S.H. No. 16 in Colorado and S.H. No. 56 in Ohio), the others use unique, and apparently previously uninvestigated configurations. The bridge in New Mexico uses a bolted top flange splice plate which is not tightened until after the concrete has attained design strength and appears to use this plate rather than the composite slab reinforcing for negative moment resistance; this design methodology is basically a typical beam moment splice, but the continuity is not invoked until the bolts are tightened. The later tightening of the bolts makes the girder continuous for superimposed loads and simple for the permanent dead loads. While achieving SMC behavior, this connection is basically no different than a conventional bolted splice and thus its design requires no special considerations over those provided by existing American Association of State Highway and Transportation Officials [AASHTO Bridge Design Specifications, hereinafter referred to as AASHTO] design requirements. All four Tennessee bridges are even simpler than the bridge in New Mexico in that the splice connections are bolted prior to placement of the slab, thus making them simple for

only the dead load of the framing in place prior to bolting. This connection also requires no special considerations over those currently provided by AASHTO.

The one aspect that all of the previous schemes have in common is that their behavior involves a concrete diaphragm, and in most instances, the diaphragm is necessary for the SMC behavior to develop by resisting the compression developed due to the negative moment over the pier as shown in Figure 6. By far, the most unique of the SMC concepts currently in use is that on the S.H. 36 bridge in Colorado. This bridge develops its SMC continuity through tension in the composite slab top reinforcing steel and compression in welds to a sole (base) plate on top of the pier that is common with the adjacent girder as shown in Figure 7. This connection works without the need for a concrete diaphragm for compression and thus has steel diaphragm beams connected to the bearing stiffener at the pier. The behavior and design of this type of SMC connection is the subject of this dissertation for reasons given in section 2.8 Selection of a Study Bridge.

1.4 STUDY OBJECTIVES

The goal of this work was to develop a methodology for the analysis and design of the steel continuity connection for simple made continuous bridge construction for bridges that have exposed steel diaphragms in lieu of being encased in concrete diaphragms. In order to develop this methodology, the following objectives were considered by this research:

- Use analytical models and experimental testing to understand the behavior/performance of this SMC connection using rolled girders with loading representative of bridges with spans in the range of 80 -160 feet.
- Develop complete design provisions for this type of connection including:

- Consideration of the effect of shear lag in the top deck reinforcement and development of design procedures to specify the optimal rebar placement.
 - Investigation of the transfer of load through the girder such that all compression forces are capable of being transferred through only a bottom flange connection.
 - Understanding of the interaction between the bottom girder flange and the sole plate and identification of all design parameters required.
 - Determination of calculations necessary for the welds between the sole plate and girder flange.
 - If weld sizes and/or lengths became excessive, development of formulations and design criteria for steel wedge bearing plates to transfer bottom flange compression across the joint.
 - If wedge plates were required, consideration of details to prevent lateral movement of the SMC girders.
- Throughout the investigation and the development of a design methodology, the economy and constructability of the connection details were key considerations.

1.5 STUDY METHODOLOGY

The study began with a literature review which included investigation of available past research on the SMC concept for steel girder bridges, code mandated requirements for these bridges, application of the finite element method to SMC bridges and concepts of modeling structures of this type and concludes with a brief inventory of bridges constructed with the SMC concept. Subsequently, an analytical evaluation of the connection detail using ABAQUS finite element analysis software. Modeling was an iterative process in order to perfect the material properties, load application method, load stepping and convergence criteria for the model.

Subsequently, a full size test of the ABAQUS modeled connection was performed on a full simple made continuous joint. In order to accommodate the space available in the laboratory, the joint was constructed with reduced beam lengths and load application locations calculated to simulate the moments and shears at the joint from a full span beam.

Following the full scale modeling, a comparison of results is performed and the ABAQUS model modified to correlate it with the physical test. Once correlation was achieved with reasonable accuracy, a parametric study considering additional configurations were modeled in ABAQUS and analyzed as necessary and design methodology and equations developed to match or closely approximate the results of the analysis and testing.

Certain limitations are required in any study of this nature; the limitations of this study were as follows:

1. Only gravity loads due to typical roadway loading have been considered. No lateral loads such as vehicular centrifugal force, vehicular braking force, wind, earthquake, soil pressure, etc. were included in any analysis or design check.
2. Since the subject connection is primarily a moment transfer mechanism, the analysis considers only the effects of the applied maximum moment and corresponding shear.
3. Thermal effects such as temperature gradient or thermal expansion forces due to environmental temperature changes were not considered in any analysis or design check.
4. Other incidental forces such as effects due to shrinkage or down drag were not considered.

CHAPTER 2 - LITERATURE REVIEW

Literature directly relevant and tangentially or somewhat relevant to the subject was reviewed and was categorized as it related to the concepts of:

1. Simple made continuous
2. General research to develop the SMC concept
3. Findings at University of Nebraska - Lincoln including details of finite element analysis (FEA) modeling and physical testing performed in the lab
4. Existing code requirements for design of affected elements
5. Previous physical testing performed in the field on completed structures
6. A review of bridge deck structures known to have been constructed with the SMC concept.

This section concludes with the selection of a bridge using the SMC concept which was then investigated.

2.1 SIMPLE MADE CONTINUOUS CONCEPT FOR STEEL BRIDGES

The earliest mention of the idea of SMC found was in a paper that discussed the integral construction of steel girders into concrete piers to achieve continuity after the concrete had attained its design strength (set). The reasons for the continuity however, were not for using smaller steel sections but for increased seismic strength of the completed structure. The details of this methodology were extremely complex and correspondingly expensive to construct and is therefore only mentioned in a historic context (Nakamura, 2002).

While not in wide distribution, a master's thesis (Lampe, 2001) presented a study of steel bridge economics and presented a preliminary analysis and physical testing of a simple made continuous bridge girder connection. Based on this research, it became clear that steel bridges

made with the SMC concept could be competitive with precast concrete bridges. Details of the testing will be discussed in Section 2.3.2.

The earliest publicly published relevant mention of the SMC concept as used in the United States was in, appropriately enough, “Roads and Bridges” (Azizimanini & Vander Veen, 2004) , in which the following benefits of the SMC concept were presented:

- Negative moments at piers are less for SMC than for beams continuous for all loads, dead and live.
- Mid- span moments will be larger due to locked-in dead load moment from simple beam action; however this balances positive and negative moments better than standard continuous beams in which negative moments may be significantly larger than positive moments.
- Eliminates welded and/or bolted field splices altogether.
- Moment of inertia of the beam is increased after composite action is invoked for both positive and negative bending.

The same article also points out the following improvements in the fabrication and erection processes of the SMC concept:

- Shop detailing of the bridge girders is simplified as no flange holes are necessary for splice plates, and, no detailing of the splice plates themselves is required.
- Smaller and hence cheaper cranes will be required for bridge erection since they won't be required to reach over the roadway to support partial span girders.
- Time savings in overall erection compared to conventional continuous girders, which are typically constructed with bolted field splices. These splices are generally made at low stress locations near the points of inflection of the continuous girders.

- Significantly less disruption of traffic on existing roadways since splices are constructed over the bridge piers.

2.2 RESEARCH TO DEVELOP STEEL SMC CONNECTIONS

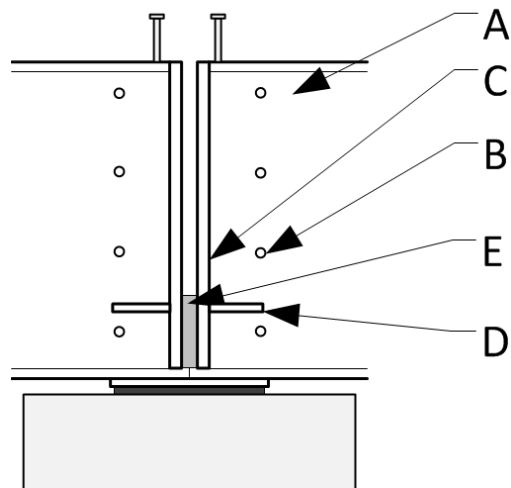
This work was done at the University of Nebraska - Lincoln and is described in a series of theses and reports Lampe (2001), Farimani (2006) and Niroumand (2009). The goals of this research were to:

- Work toward the development of an economically competitive concept for steel bridges to compete against prestressed concrete bridges.
- Comprehend the force transfer mechanism at the SMC girder connection
- Develop a mechanistic model to predict the behavior of the connection under design loads and a design methodology

All specimens considered had concrete diaphragms at the supports based on the thought that since these were specified in NDOR standards (NDOR, 1996) for SMC bridges constructed with precast/prestressed girders, they should also be used on steel girder bridges.

Research started with Lampe (2001) who modeled and tested the connection shown in Figure 8. Lampe started with SAP2000 modeling of the connection shown along with two other variations (Lampe N. J., 2001). The results of the SAP2000 analysis were very approximate and will not be discussed further except to say:

- This was a quick way to obtain preliminary results and fine tune an analytical model before going into a full finite element analysis with more complex software such as ANSYS or ABAQUS
- A full span analysis was performed in order to determine initial rotations induced by the dead load on the simple spans, which were then used in the physical model.



Legend:

- A = Girder
- B = Web openings for reinforcing
- C = End vertical stiffener plate
- D = Horizontal stiffener plate
- E = Concrete compression block

Figure 8 - Girder connection specimen modeled at University of Nebraska - Lincoln (Lampe N. J., 2001)

Of the three variations investigated, that shown in Figure 8 was chosen for physical testing primarily because the computer analysis showed that the contact of the bottom flanges resulted in ductile behavior of the connection. The physical testing of the connection configuration shown in Figure 8 consisted of first initiating end rotation in the beam ends to simulate the initial dead load end rotation by adjusting the slab support shoring in stages. This involved the lowering of the temporary supports and taking potentiometer readings of the girder end displacements. Based on an increase in horizontal separation of the girders, the end rotation could be calculated. Once the theoretical rotation was achieved, shores would remain in place until the concrete had attained its design strength. Of all of the literature reviewed on the subject of SMC connections testing, this is the only work that mentioned applying the simple span end rotation prior to testing.

The completed model was then subjected to fatigue testing prior to ultimate strength testing. The fatigue testing resulted in the largest cracks occurring in the slab at the edges of the concrete diaphragm, which was attributed to an abrupt change in rigidity from the slab over the diaphragm to the slab alone. In over two million cycles, the stress in the reinforcing steel varied

less than 0.5 ksi and remained in the elastic range. Although there were several pump failures before failure load was achieved, failure of the specimen occurred at a load of 350 kips, which induced a moment at the SMC connection of 4200 ft-kips. The failure was due to yielding of the top tension reinforcing bars; a ductile failure.

Farimani (2006) considered three specimens as described below and shown in Figure 8:

Specimen 1 – Two girders with abutting bottom flanges to directly transfer compression and thick end compression stiffeners which develop a portion of the interstitial concrete in compression.

Specimen 2 – Two girders separated by a gap and no stiffeners, so that compression in the girder and webs must be transferred by only a small region of the concrete.

Specimen 3 – Two girders with a gap and thick end compression stiffeners which develop the interstitial concrete in compression.

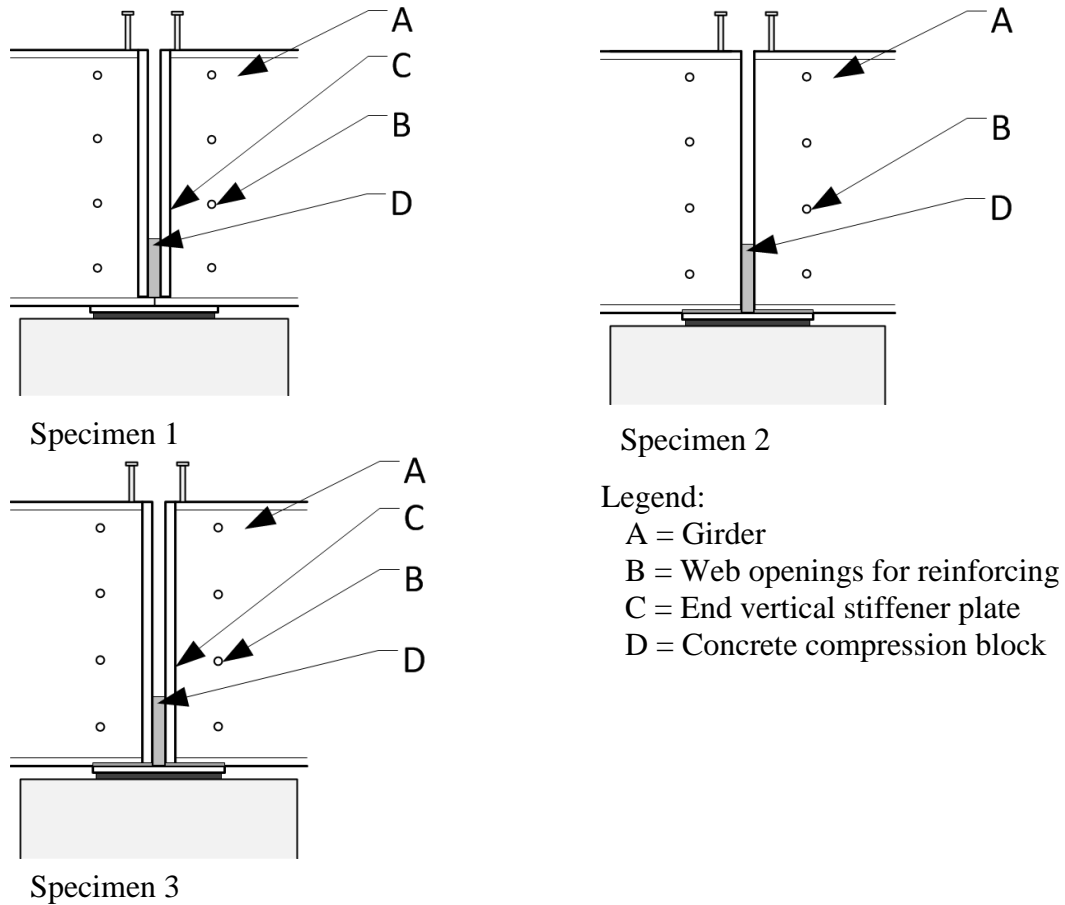


Figure 9 - Girder Connection Specimens Tested at University of Nebraska-Lincoln (Farimani M., 2006)

All of the specimens evaluated had holes either punched or drilled through the girder webs to allow the longitudinal reinforcing of the diaphragm to pass through in order to behave continuously. It's noteworthy that this is not the case in the NDOR standards for precast concrete girders in which the longitudinal diaphragm reinforcing is terminated on either side of the girder. The girders with the diaphragm and composite slab installed are shown in Figure 10.

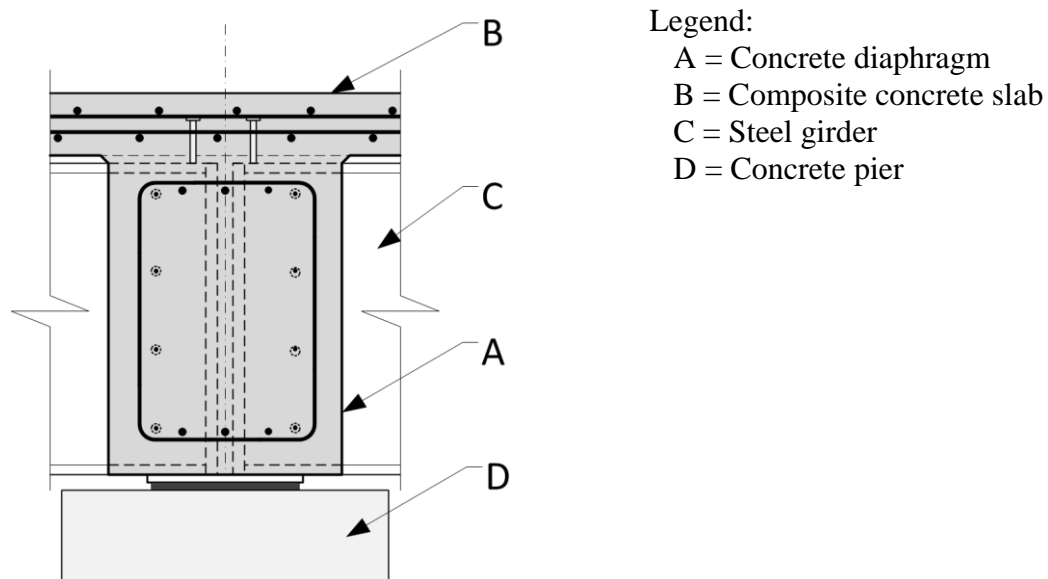


Figure 10 - Connection with diaphragm and slab in place

In this case, physical testing was conducted prior to the FE analysis. Fatigue testing was performed on all three specimens. The appropriate number of cycles for the testing was determined to be 135,000,000, which was based on AASHTO and the S-N curves for the girder material; this number of cycles was deemed to be excessive for testing. It was decided to alternatively increase the applied load and reduce the number of cycles using AASHTO equation (6.6.1.2.5-2) (AASHTO, 2012) in an attempt to achieve the same effect. Following 2,780,000 cycles in fatigue, ultimate load tests were performed on the same specimens. Faults in the loading due to failing load pumps required unloading and reloading of the specimens during pump replacement. Due to instrumentation failures, values for the many strains in the second and third specimens were unavailable.

Based on the test results, composite action was verified to be effective in all of the tests as there was virtually no slip measured between the top girder flange and the bottom of the concrete slab. This was discussed as being the result of bond between the concrete and the

headed shear studs; bond seems unlikely to be stronger than the actual contact bearing between the slab concrete and the stud heads and shafts. In the test of the second specimen, excessive deformation/movement of the bottom flanges occurred due to failure of the interstitial concrete; enough such that the diaphragm bars through the girder web failed or were sheared through. In the test of the third specimen, an increase in concrete compressive stresses was noted between the girder end stiffeners; this is obviously due to the bottom flanges not being connected as they were in the first specimen and thus the specimen failed due to concrete crushing.

Based on the physical testing, the following is a summary of what were determined to be the modes of failure of the specimens:

Specimen 1 – Yielding of top reinforcing steel (ductile failure)

Specimen 2 – Crushing of diaphragm concrete at the girder bottom flange (crushing or brittle failure)

Specimen 3 – Crushing of concrete between the end stiffener plates (crushing or brittle failure)

The finite element analysis was performed using ANSYS software to obtain more information about the connection behavior beyond that of the physical test. By exploiting symmetry, only half of the model was required and necessary constraints were placed at the center of the SMC connection. The analysis used a static non-linear analysis due to the low rate of load application.

Investigation of the load displacement curves of the physical tests and FEA analysis indicated that they compared well. Numerical instabilities occurred in some of the results for the second specimen, which also performed poorly in the physical tests. Otherwise, these results corresponded well with the results of the physical test specimen's results.

Another study by Niroumand (2009) was performed at University of Nebraska / Lincoln to evaluate a SMC connection intended for accelerated construction and to look at SMC connections for skew bridges; the portion specific to skew bridges will not be discussed herein. A distinguishing feature of the connection intended for accelerated construction is that the top flanges are coped so that the longitudinal slab reinforcing may be hooked into the diaphragm at the location of the girders, Figure 11 and Figure 12. Neither the compression plate sizes nor their attachment method was given. The compression plate is used in lieu of the full height end girder stiffeners and actually abuts the compression plate of the adjacent girder, thus taking the concrete compression block out of the connection behavior. From examination of Figure 11, it may be seen that the compression blocks (C) at the end of the beam are stiffened towards their outside edges by vertical stiffeners (F) and at the center by the web of the girder (A). Erection of this type of connection in the field will require very tight fabrication tolerances in the shop. If a girder is too short, there will be a gap between the compression plates, whereas if a girder is too long, the girders will not be able to be set since portions of the compression plates will be trying to occupy the same space.

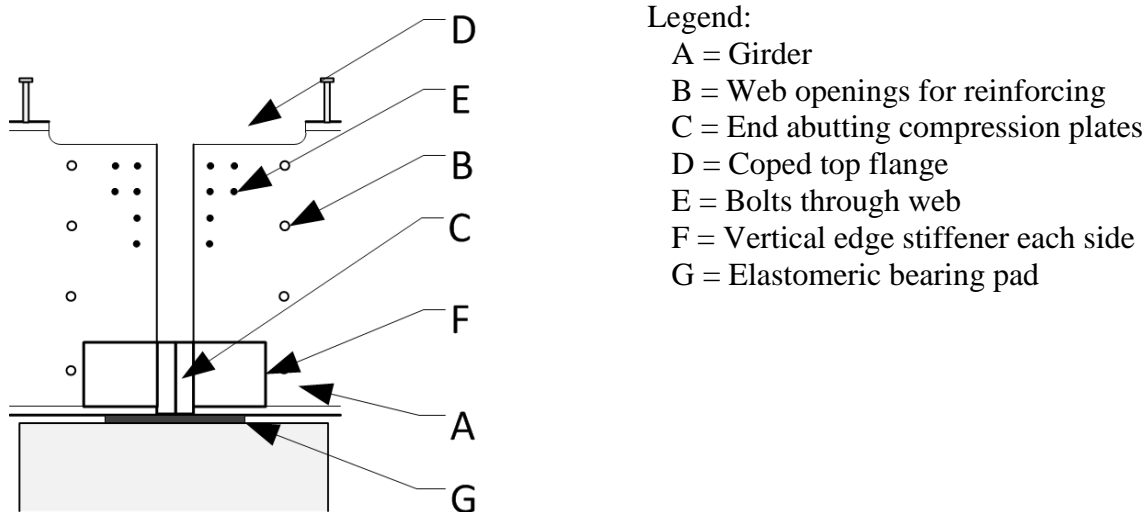


Figure 11 - Accelerated connection detail modeled at U of N - Lincoln (Niroumand, 2009)

The accelerated idea in this detail is that the SMC (lower) layer of top slab reinforcing is to be placed in two pieces; each has a hooked lap bar placed into the far end of the diaphragm, Figure 12, thus also lapping nearly the full width of the diaphragm. This area is already very congested and how this method would be accelerated versus placing a single bar is not clear; additionally, it will be much more costly in material and labor, which seems to defeat the purpose of the SMC concept altogether. The center of the haunch also happens to be the location of the highest stress in the top reinforcing, which is the worst possible place to splice bars. Additional detailing of the connection included bolts that were connected to either side of the beam web for “additional resistance”, however, no documentation was provided as to the bolt diameter, length, type, etc. The redeeming aspect of this detail is the compression plates, which don’t involve the compression concrete in the SMC behavior.

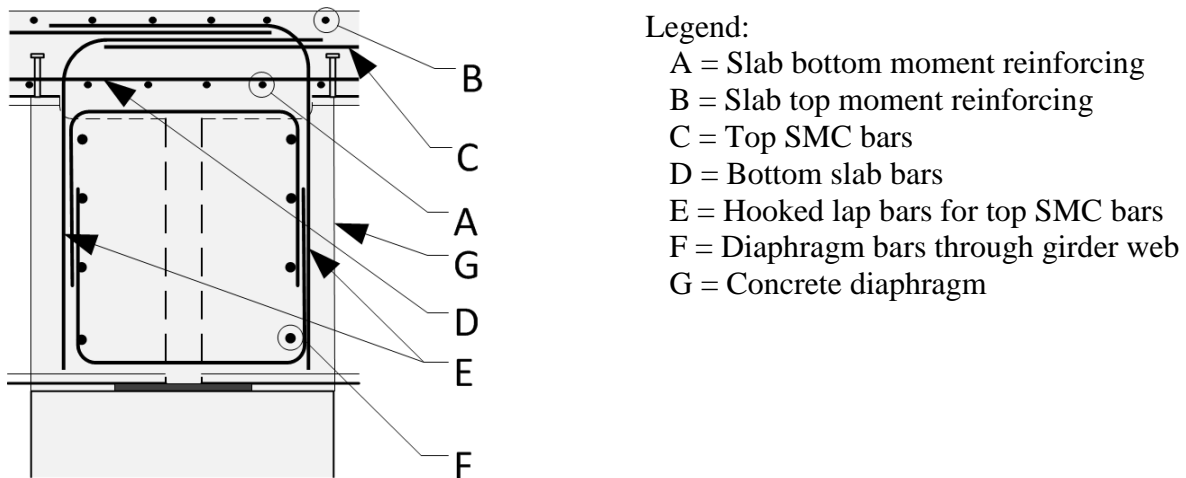


Figure 12 - Detail at SMC Connection showing reinforcing layout in diaphragm and slab

Physical testing was again conducted prior to the FE analysis. Fatigue testing was on the model preceded ultimate load testing and as in the previous University of Nebraska - Lincoln study, the number of cycles was reduced from 135,000,000 to 4,000,000 through the use of AASHTO equation (6.6.1.2.5-2). By use of this method, the applied fatigue moment had to be

increased from 532 foot-kips to 1137 foot-kips or approximately double the load to reduce the number of cycles to 1/34 of the original number.

Subsequent to the fatigue testing, the ultimate load test was performed. Due to load application issues, the test was stopped, corrections made and then started all over. When loaded the second time there was evidence of some nonlinear behavior at a load that had previously behaved linearly during the stopped first test; no explanation was provided for this phenomenon, but it was likely due to crack initiation in the tension zone of the slab.

In addition to the physical model testing, material tests were performed on the various materials, i.e., structural steel, reinforcing steel, concrete and elastomeric material to obtain their engineering properties for later validation of results with a finite element analysis of the connection.

Significant conclusions drawn at the end of the ultimate load testing and evaluation of instrumentation results are summarized below:

- The strain profile at the end of the girder was linear
- The cantilever end of the girder had considerable displacements, up to 13 in. vertically without concrete failure and thus exhibited significant ductility.
- The strain profile of the longitudinal reinforcing bars at the diaphragm dropped significantly at the face of the diaphragm; this was likely due to the increase in the amount of reinforcing in this area.
- While the concrete in the vicinity of the steel blocks had the highest compressive strains, these strains were lower than those that would cause cracking or crushing.

The finite element analysis of this scheme was performed using ABAQUS finite element software and was conducted subsequent to the physical testing of the model. Material properties

based on the previously discussed material tests were used in the model. The verification process was considered complete when the load-displacement curves for the FEA and physical test were in agreement. Once the finite element analysis was verified with the physical test, it would give the ability to evaluate different scenarios. As ABAQUS was the finite element analysis software selected for use in the research project described in this dissertation, additional details of this analysis is provided in section 2.3.1.

2.3 FINDINGS OF NEBRASKA EXPERIMENTAL PROGRAM

In total, the University of Nebraska - Lincoln studies investigated five different connection types. All had the similarity of being encased in concrete pier diaphragms, with holes drilled through the girder webs so that the diaphragm reinforcing could pass through the web and act continuously. Three of the six specimens, Figure 8 (Lampe), Figure 9, (Farimani) and Figure 11 (Niroumand), had the benefit of some sort of interconnection between the bottom (compression) flanges of the girders at the center of the SMC connection; these connections failed by steel yielding, a ductile failure. The remaining specimens had no connection between the girders in the compression area and failed in concrete compression, a brittle failure. It is evident that connection details involving the interconnection of the bottom flanges had a more desirable failure mode and the authors did not hesitate to point this out.

Of the three ductile connections, the most economical and likely quickest to construct was that investigated by Lampe, which was subsequently the basis of the work by Farimani. This connection had the simplest reinforcing steel details and a straightforward steel compression transfer mechanism between the steel girders. However, this connection still has complexities and unknowns, specifically:

- The diaphragm steel passing through the girder webs, which require that holes be punched, drilled or flame cut through the webs.
- The concrete diaphragm is cast prior to the bridge slab and thus, will engage the girder ends prior to the slab concrete; this could cause changes between the behavior in the lab and the field
- By the girders being embedded in the concrete diaphragms, they are susceptible to moisture seepage due to gaps caused by concrete shrinkage that will occur at their perimeters

Important considerations from review of the preceding research:

- Use high quality, properly installed instrumentation to avoid erroneous or missing results, however, as equipment does fail, it may be wise to install some redundant instrumentation.
- Inspect and make sure all load application equipment is in good working order prior to commencing testing and have sources for replacement parts on hand in case of failure or malfunction during testing
- Exploit symmetry wherever possible to save both modeling and analysis time

The previous work at University of Nebraska – Lincoln also provided valuable insight in terms of finite element modeling and physical testing.

2.3.1 Details of Finite Element Modeling

Of the SMC connections studied for which FEA was performed, three types of FEA software were used, specifically, SAP2000 (Lampe, 2001), ANSYS version 5.7 (Farimani, 2006) and ABAQUS 6.9 (Niroumand, 2009). While SAP2000 is relatively simple to use, this simplicity comes at the cost of restrictions in the size of the analysis that may be performed and

the lack of ability to model complex behaviors between surfaces and embedded elements.

ANSYS and ABAQUS perform basically all of the same types of analysis, i.e., linear, nonlinear, static, dynamic, etc., but function differently in the creation of models, particularly in the definition of elements and their associated materials. For the tasks to be performed for the analysis of SMC connections, they are functionally equivalent.

Finite element models of SMC connections involve at a minimum, the material properties for structural steel, steel studs, reinforcing steel and concrete. Depending upon the software used, the material may in fact be part of the element definition such as in ANSYS or it may have its own definition and the ability to only be applied to particular element types such as in ABAQUS.

In the third study (Niroumand, 2009), two methods to model concrete in both tension and compression available in ABAQUS were considered for the modeling, specifically, Concrete Smearred Cracking and Concrete Damaged Plasticity. For the subject model, Concrete Damaged Plasticity was chosen as it models the nonlinear behavior of concrete in both tension and compression more accurately than Concrete Smearred Cracking, although at the cost of more significantly more processing time. Five different tension failure models were discussed for concrete in uniaxial tension and in the end, the Barros et al. (2002) method was selected; this method is somewhat complex as it involves the evaluation of more than six equations. Three different compression failure models were considered for concrete in uniaxial compression. The Carreira and Chu (1985) method was selected as its peak value matches the ultimate compressive strength of the concrete under consideration while in the other methods, the peak values were less than the ultimate compressive strength. It is odd that there was no discussion of

the material model used for the steel girder, compression plates and stiffeners; these are key elements of the SMC behavior, if not the most critical.

The study's (Niroumand, 2009) discussion on element type selection was fairly brief in comparison to the material selection discussion. The steel girder was modeled using shell elements as this provided not only nodal displacements, but also nodal rotations. Nodal rotations cannot be obtained by the use of first order solid elements, but can be provided by second order solid elements at the cost of additional processing time. Timoshenko beam elements were chosen to model the shear studs as these would also provide shear deformation results. Three dimensional two node truss elements were selected to model the slab reinforcing. The slabs were modeled as first order eight node brick elements; no explanation was given as to why a second order element was not required.

Constraints consisted of embedding the reinforcing bars and studs in the slab; while this method simplifies analysis, modeling the stud as an embedded beam may not capture the effect of the head of the stud locking the slab down since the beam is only a line type element. However, this should not have a significant effect on the overall results. The lower nodes of the studs were tied to the girder top flange. Although not very clear, it appears that lateral constraints were applied to the bottom flanges of the girders and the vertical load was carried through part contact with the elastomeric bearing. Additional contacts were modeled between the end steel compression plates. No mention of contact between the interstitial concrete and the ends of the girders was mentioned.

Sensitivity analyses were carried out on variations of mesh size, omitting studs and tying the slab to the girder, load application methodology, etc. A summary of the findings of this analysis follows:

- While a finer overall mesh was no better than a coarse mesh for the entire model, more accurate results were obtained using a finer mesh in the vicinity of the concrete diaphragm.
- The load application applied to the top of the slab vs. the bottom flange of the girder gave better correlation to the actual physical test results.
- The girder connected directly to the deck in lieu of being tied with studs caused considerable elongation in the slab reinforcing bars over the girder, thus, shear studs should be used to correctly model this interaction.

2.3.2 Lab Testing of SMC Bridge Connections

Lab testing of physical models involved construction of the model simultaneous with the placement of embedded and surface mounted instrumentation; the instrumentation is subsequently wired to a data acquisition device. Additionally, the method of actuator control must be determined either force or displacement.

Lampe (2001) went into great detail about instrumentation types, their use and their placement. The types of monitoring instrumentation used, their mounting locations and other details of their installation are summarized in Table 1.

Table 1 - Summary of Instrumentation Type and Placement

Gage Type	Use/Placement
Steel surface electrical strain gages	mounted to the surface on the top and sides of the girder flanges, mounted to embedded reinforcing bars
Concrete embedment vibrating wire strain gages	placed in the composite slab and the concrete pier and diaphragm
Steel embedded electrical strain gages	placed on girder flanges and web outside of the concrete diaphragm and slab
Concrete surface electrical strain gages	mounted on the concrete surface

Gage Type	Use/Placement
Potentiometers (linear transducers)	positioned at the girder ends to determine and set initial simple beam end rotation and at the location of load application to measure beam deflection

Farimani (2006) provided instrumentation to obtain results for the two load stages tested, cyclic fatigue loading and ultimate loading. Instrumentation used included electrical strain gages, vibrating wire embedment gages and potentiometers. Electrical strain gages were mounted to the steel girder webs and flanges and the steel reinforcing bars, vibrating wire embedment gages were positioned and mounted within the concrete slab and diaphragm. These gages were also attached to the reinforcing steel in the diaphragm between the girder ends.

Potentiometers were used to measure the vertical deflection of the beam ends and in the test of the third specimen, Figure 9a, they were used to measure the movement of the girder bottom flanges into the concrete diaphragm. Malfunctioning of gages in this study occurred due to the following reasons:

- Limitations of the measurement range strain gages in areas of particularly high strain.
- Damage of embedment gages at the construction stage due to concrete placement.
- Damage of embedment gages from the concrete vibrator during concrete consolidation in the pier.
- Failure of the glue used to attach the gages due to its strength decreasing over time.

For the cyclic fatigue loading, two 220 kip MTS actuators were used, one at the cantilever end of each girder. The load was applied to a spreader beam so as not to subject the bridge deck to a concentrated load. The load range of 2 kips to 106 kips was then applied by means of displacement control. After cyclic fatigue test, it was found that the stiffness of the specimen had decreased such that the load for the specified displacement had decreased to 74

kips from 106 kips. At the conclusion of the fatigue test, it was noted that there was a reduction in stiffness of approximately 12 percent.

It should be noted that the physical testing of this model was performed prior to the finite element analysis. If the FEA had been performed prior to the physical test, the limitations of the gages may have been overcome if the range of strains was known in advance, since then gages with adequate ranges could have been selected.

Niroumand (2009) provided instrumentation to monitor both the fatigue and ultimate load tests. This work provides considerable detail on the types and uses of strain gages. The types of gages and their utilization were similar to those listed in Table 1, with the addition of a crack meter between the girder webs at the top flange at the center of the connection.

For the cyclic fatigue loading, the load applied as in the Farimani (2006) test. The load was then applied by means of displacement control by considering the stiffness of the system and the displacement corresponding to a given load. This issue could have possibly been circumvented by performing the Abaqus modeling prior to the physical testing.

For the ultimate strength test, the MTS actuators were replaced by four 300 ton hydraulic rams placed at locations where they would provide the correct moment based on the applied load, which would correspond to the beam end shear. The rams applied the load to the slab by means of a spreader beam with a rod from each ram at the ends. The test load was increased gradually in load steps which varied from 10 kips to 25 kips during the test. There was no mention of any instrumentation or load application malfunction.

2.4 CODE MANDATED REQUIREMENTS

The code used for determination of design requirements is “AASHTO LRFD BRIDGE DESIGN SPECIFICATIONS 2012” (AASHTO, 2012). The current version of AASHTO does not directly address SMC construction, however it does allude to the concept of SMC in Section 6.10.10.4.2 –Nominal Shear Force (in studs), where it says: “For continuous spans that are composite for negative flexure in the final condition....” This paragraph is in regards to the determination of the number of studs required at the point of contra flexure when continuity exists.

In general and applicable to this study, AASHTO specifies requirements for determination of:

- Nominal material strengths to be used in “Load and Resistance Factor Design” (LRFD).
- Resistance factors to be used in conjunction with ultimate material strengths.
- Ultimate load factors and corresponding load combinations for required load conditions.
- Required service live loads to be applied to a bridge structure to determine the largest load effects (moments, shears, etc.) in combination with applicable load factors.
- Factors for impact of moving loads under normal and fatigue conditions
- Formulas for calculation of factors for distribution of wheel loads based on bridge girder spacing, number of design lanes, drive lane widths and drive lanes tributary to the girder under consideration.
- General dimension and detail requirements for steel shapes, including
 - Dead load camber
 - Minimum steel thickness
 - Diaphragm and cross-frame locations and spacing

- I-shaped beam proportions for compactness
- Fatigue considerations, which were not analyzed in this study.

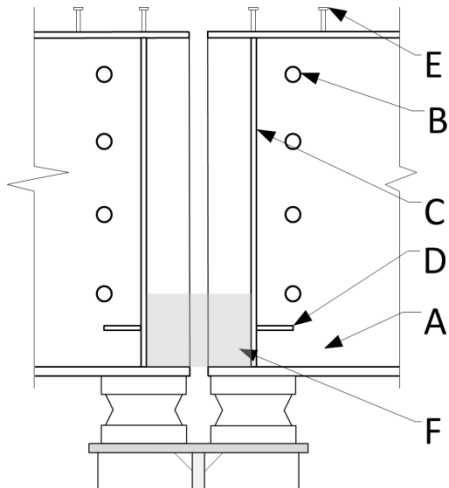
These requirements were applied to the analysis of the SMC connection as applicable and expanded as necessary and if possible in order to determine design requirements for SMC connections with steel diaphragms.

2.5 FIELD TESTING OF BRIDGES CONSTRUCTED WITH SMC CONNECTIONS

Several bridges designed and constructed with the SMC concept were tested in the field to verify their efficacy in continuous behavior for live load. Of the bridges tested, there was no evidence found of any previous specific lab testing or finite element analysis as in the Nebraska bridges.

The earliest published field test information was by Lin (2004); this work investigated/verified the AASHTO specification live load distribution factors for two different bridges. However, also in this study, the author investigated the live load continuity of one of the bridges, Ohio State Highway 56 over the Scioto River (2003), constructed with the SMC concept to verify its SMC behavior.

The SMC detail of this bridge is shown in Figure 13 and Figure 14 and bears a strong resemblance to the Nebraska detail shown in Figure 8. The bridge was instrumented with four pairs of strain gages on two adjacent girders, two feet from the support pier. Based on information from the strain gages, the bending moments from a known truck as a function of position along the bridge were able to be calculated. Upon review of the bending moments, the bridge was indeed found to be acting continuously for the live load of the truck.



Legend:

- A = Girder
- B = Web openings for reinforcing
- C = End vertical stiffener plate
- D = Horizontal stiffener plate
- E = Headed studs
- F = Concrete compression block

Figure 13 - Bridge over the Scioto River SMC detail

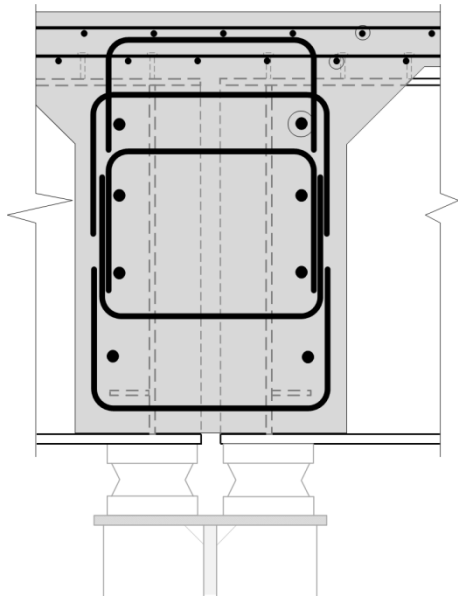


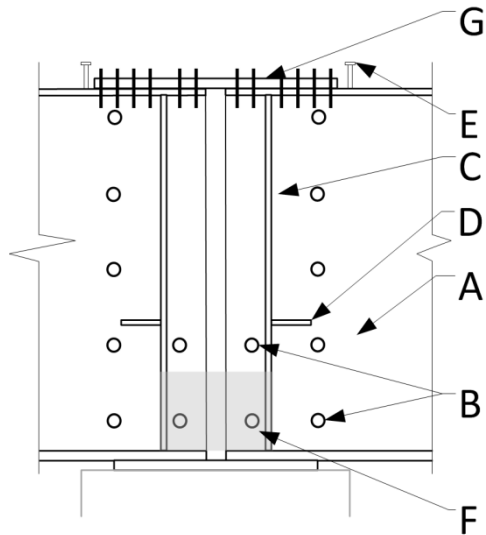
Figure 14 - Bridge over the Scioto River pier detail

Subsequent field evaluation by (Solis, 2007) on a bridge on U.S. 70 over Sonoma Ranch Road (2004) in Las Cruces, New Mexico was performed to verify SMC behavior at the interior bridge piers. As shown in Figure 15, this appears to be a variation of the Nebraska detail shown in Figure 8 with the main difference being the addition of a bolted splice plate connecting the top flanges and more web openings. From review of the construction documents the procedure for fastening the top plates involves tightening the bolts after the concrete has fully cured; this along with the concrete compression block being ineffective until it has attained design strength insures

that the connection will not resist any dead load moment. In addition to the top flange splice plate, the composite slab has additional reinforcing in the negative moment zone over the pier. The top flange splice plate also has shear studs, which have been omitted from the figure for clarity.

The field study involved the installation of 56 strain transducers at select locations along the bridge where they were attached to the center of the web and either the top of the bottom flange or the underside of the top girder flange, depending upon location in the span. For the test, a truck with a total weight of approximately 56,000 lbs. was positioned along the bridge at eight different locations. Based on strain readings, the neutral axes of the girder were determined and compared to the assumed theoretical values. The evaluation of the experimental vs. the theoretical showed that the results compared well and also showed that the actual composite action included the effects of the longitudinal reinforcing steel and the concrete haunch being effective.

Additional study was done by comparing the experimental results with those obtained with a SAP 2000 model. The model in SAP 2000 was calibrated as much as possible to agree with the behavior of the actual bridge. Based on the experimental and the SAP 2000 results, the bridge behavior was found to be simple for dead load and continuous for live load. Also, the studies showed that although there was a top flange splice plate, in order for the bridge to behave as it had, the top reinforcing steel was also necessary to resist the negative moments over the supports.



Legend:

- A = Girder
- B = Web openings for reinforcing
- C = End vertical stiffener plate
- D = Horizontal stiffener plate
- E = Headed studs
- F = Concrete compression block
- G = Bolted splice plate

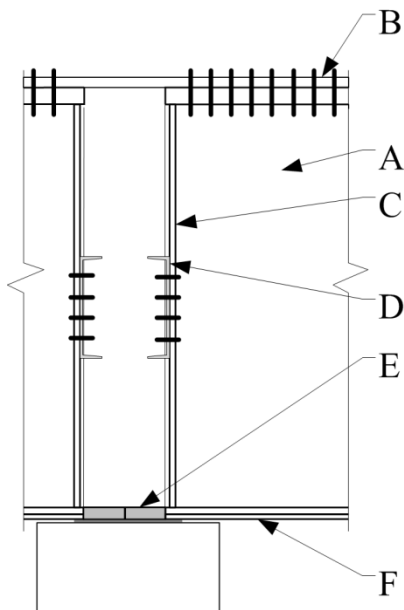
Figure 15 - U.S. 70 over Sonoma Ranch Road SMC detail

Field studies were also performed on the DuPont Access Road Bridge in Humphreys County, Tennessee, Figure 16 and Figure 17 (Chapman, 2008). This bridge is somewhat of a hybrid due to the following variations in its construction:

- The top flange has no studs in the negative moment tension zone
- The bottom flange has a lower reinforcing plate in the negative moment compression zone
- Wedge compression plates are field welded between the bottom flanges prior to placement of the concrete diaphragm

This bridge does not actually meet the definition of having SMC connections; however, it is noted in this literature review because it does have an interesting feature in that the continuous connection of this bridge is developed by the use of field installed and welded wedge plates between the bottom girder flanges, Figure 18. This is a novel approach to connecting the bottom flanges for continuity as it allows for adjustment in the field and does not require the tight tolerances as would be required in the Nebraska details. Also, while not studied in the work (Chapman, 2008), the behavior of the wedge plates would be the same as the abutting end plates

of the Nebraska detail and, thus, would most likely result in more ductile behavior in the connection.



Legend:

- A = Girder
- B = Splice plate and bolts
- C = End vertical stiffener/compression plate
- D = Horizontal channel stabilizers
- E = Wedge compression plates
- F = Bottom flange reinforcing plate

Figure 16 - DuPont Access bridge SMC detail

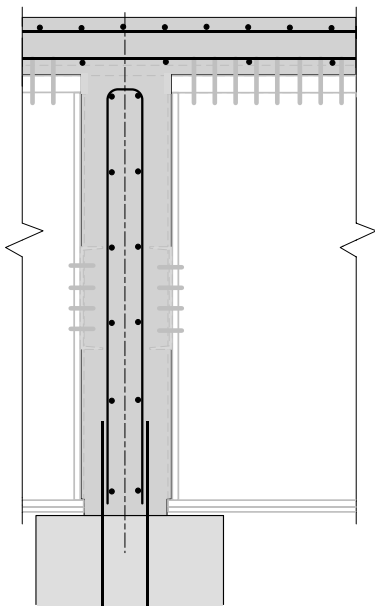
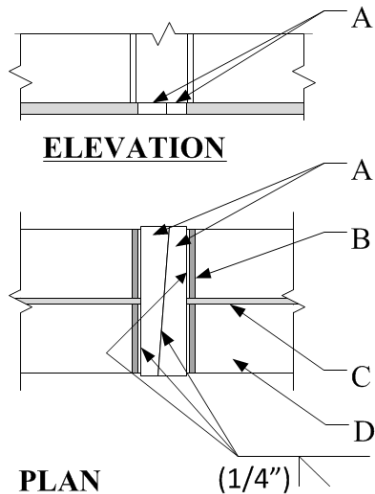


Figure 17 - DuPont Access bridge slab and diaphragm



Legend:
 A = Wedge plates
 B = End stiffener
 C = Girder web
 D = Girder bottom flange

Figure 18 - Wedge plate detail

2.6 SUMMARY AND GENERAL PUBLICATIONS

Several pieces of very recently published literature reviewed were summaries of previous research with additional comments or slightly expanded content, which really doesn't add to the current knowledge base; these documents are briefly discussed herein.

Two consecutive quarterly AISC Engineering Journals were published with a total of seven articles relating to the SMC concept. Of these articles, five were rehashing or slight expansion of work performed at the University of Nebraska/Lincoln (Azizinamini A. , 2014), (Lampe N. M., 2014), (Farimani R. S., 2014), (Yakel, 2014) and (Javidi, 2014) with the only really new information being a revised detail to alleviate cracking in the concrete diaphragm and is shown in Figure 19. As may be seen, this detail is significantly more involved than the original detail shown in Figure 10.

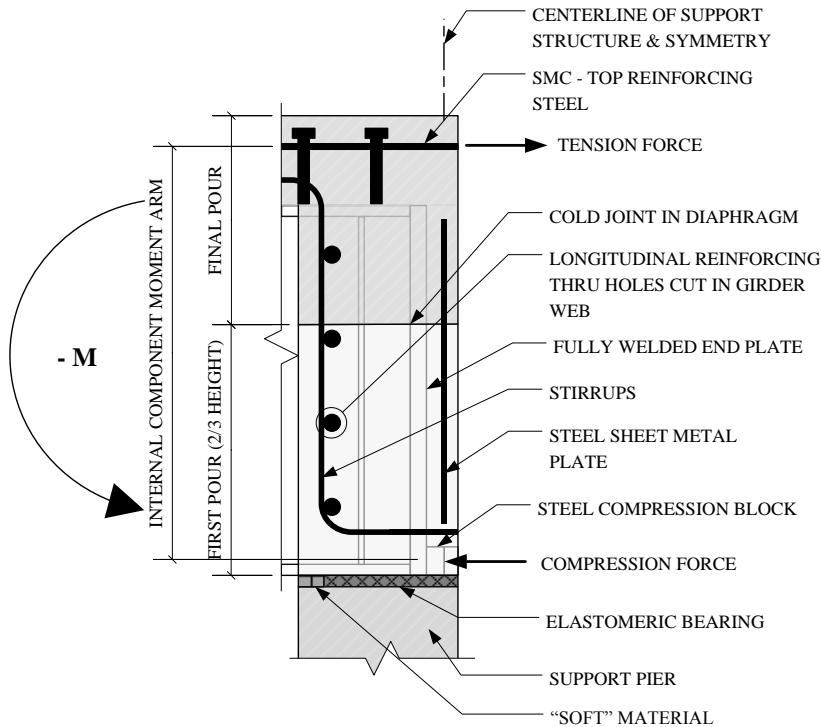


Figure 19 - Revised Concrete Diaphragm SMC Detail

Also presented in the AISC Journal article, was a cost benefit analysis, which compared the costs of fully continuous girder construction vs. simple made continuous girders (Yakel, 2014). The results of this comparison came out in favor of the favor of the SMC girder construction scheme by about 15%. However, the cost comparison failed to include the cost of the additional top reinforcing to resist the SMC behavior as well as the additional cost of the reinforcing in the pier in order to use the accelerated method. The study also compared time for completion of the erection of the connection, but did not include the additional time required for the placement of the SMC top reinforcing or the time required for placement of the reinforcing for accelerated method of construction. It was also stated that the diaphragm was poured to two thirds of its height and allowed to cure for seven days prior to the placement of the remainder of the pier, which was placed monolithically with the deck slab; this seven day wait is longer than it would take to install field splices in fully continuous girders.

2.7 A SUMMARY OF BRIDGES CONSTRUCTED WITH THE SMC CONCEPT

At the time of this writing, there were at least sixteen known constructed and operational bridges found in the United States that have used the SMC concept or variations thereof; there are quite possibly more in design and planning or construction stages, which are not considered. These operating bridges and relevant points about their SMC details/behavior are summarized in chronological order below; dates provided are the dates that the drawings were issued for construction. Detailed information about each bridge is provided in Appendix 1 – Current SMC Bridges.

Massman Drive over Interstate 40, Davidson County, Tennessee – November, 2001

This is a two span, two lane composite rolled girder bridge with concrete diaphragms at interior supports; maximum span is 145'-6". Continuity is achieved by steel compression blocks between bottom flanges and a steel top flange splice plate, which is fastened prior to concrete placement, thus this bridge is actually simple for only the girder self-weight and continuous for all other loads..

State Highway N-2 over Interstate 80, Hamilton County, Nebraska – November, 2002

This is a tub (box) girder bridge and is not directly within the scope of this study but it is noted that it uses the SMC concept at its interior piers.

U.S. 70 over Sonoma Ranch Blvd. – Las Cruces, New Mexico – August, 2002

This structure consists of two nearly identical bridges one in each direction. Each is a three span, two lane, composite plate girder bridge with concrete diaphragms and a tension flange splice plate, which is bolted subsequent to the concrete setting; maximum span is 119'-9". Continuity is achieved by girder bearing stiffeners compressing the diaphragm concrete and tension in the top flange splice plate, which also has headed studs and top slab reinforcing steel.

The top splice plate is unique to this bridge and it takes the place of providing additional reinforcing steel in the top of the slab to develop the SMC behavior.

Dupont Access Road over State Route 1, Humphrey's County, Tennessee – December, 2002

This is a two span, two lane composite rolled girder bridge with concrete diaphragms at interior supports, maximum span is 87'-0". Continuity is achieved in the same manner as the Massman Drive bridge.

Sprague St. over Interstate 680, Omaha, Nebraska – May, 2003

This is a two span, two lane bridge with composite rolled steel girders with concrete diaphragms at interior supports; maximum span is 97'-0". Continuity is achieved by end bearing plates on the girder compressing the diaphragm concrete and top tension steel in the deck slab.

Ohio S.H. 56 over the Scioto River – Circleville, Ohio – June 2003

This is a six span, two lane bridge with composite plate girders with concrete diaphragms at interior supports, maximum span is 112'-8". Continuity is achieved by girder bearing stiffeners compressing the diaphragm concrete and tension in the top flange splice plate.

State Highway No. 16 over US 85, Fountain, Colorado – February, 2004

This is a four span, two lane bridge with composite steel plate girders embedded in concrete diaphragms at the interior supports, maximum span is 128'-2". Continuity is achieved by end bearing plates on the girder compressing the diaphragm concrete and top tension steel in the deck slab.

New Mexico 187 over Rio Grande River – Arrey/Derry, New Mexico – June, 2004

This is a five span, two lane composite plate girder bridge with concrete diaphragms and a top flange tension splice plate, which is bolted subsequent to the concrete setting; maximum span is 105'-0". Continuity is achieved by girder bearing stiffeners compressing the diaphragm

concrete and tension in the top flange splice plate, which also has headed studs and top slab reinforcing steel.

State Route 210 over Pond Creek, Dyer County, Tennessee – June, 2004

This is a five span, two lane composite rolled girder bridge with concrete diaphragms at interior supports; maximum span is 132'-2". Continuity is achieved in the same manner as the Massman Drive bridge. Three of the five spans of this bridge also have full midspan bolted plate splices.

Church Ave. over Central Ave., Knox County, Tennessee – January, 2005

This is a six span, three lane, composite rolled girder bridge with concrete diaphragms at interior supports, maximum span is 100'-0". Continuity is achieved in the same manner as the Massman Drive bridge.

State Highway No. 36 over Box Elder Creek, Watkins, Colorado – June, 2005

This is a six span, two lane bridge with composite rolled steel girders with steel diaphragms at the interior supports; maximum span is 77'-10". Continuity is achieved by compression being transferred between girders by connection to a common sole plate and top tension steel in the deck slab. This is the only completely SMC bridge to not use a concrete diaphragm.

Three Springs Drive Bridge over U.S. Route 22, Weirton, W. Virginia, 2007

This is a two span, two lane bridge with composite rolled steel girders with concrete diaphragms at all supports; spans are 125'-6" and 95'-0". Continuity is achieved by compression being transferred by compression plates at the end of each girder with a field installed shim pack between them and a top flange splice plate, which is bolted to the flanges prior to concrete placement.

I-476 Bridge over the Schuylkill River, Philadelphia, Pennsylvania, 2008

This project consisted of the modification of two existing bridges, one each way with 17 spans. The reason for the modification was to eliminate troublesome control joints. The center ten spans of each bridge were combined into three continuous sections each, one of three spans, one of four spans and another of three spans. No modifications appear to have been made to the approach spans of either side of the bridge.

The detail used for bottom flange continuity in this bridge were wedge plates, which are the same as those used in the Massman County Bridge; the report on this bridge (Griffith, 2014) erroneously attributes this detail to the Colorado Department of Transportation detail, which is the subject of this work and has no wedge plates. This document also provides another initialization for this type of bridge, SSMC or Simple Spans Made Continuous, which may be a fitting name for existing bridges modified in this manner.

Washington Avenue Bridge over Interstate 70, Wheeling, W. Virginia, 2008

This is a two span, two lane bridge with composite rolled steel girders with concrete diaphragms at all supports; spans are 96'-0" and 112'-0". Continuity is achieved by compression being transferred by compression plates at the end of each girder with a field installed shim pack between them and a top flange splice plate, which is bolted to the flanges prior to concrete placement.

US 75 over North Blackbird Creek – Macy, Nebraska – May 2010 and US 75 over South Blackbird Creek – Macy, Nebraska – May 2010

These are almost identical three span, two lane bridges with composite rolled steel girders with concrete diaphragms at interior supports, maximum spans are 65'-8" and 73'-6",

respectively. Continuity is achieved by end bearing plates on the girder compressing the diaphragm concrete and top tension steel in the deck slab.

The behavior of these bridges may be summarized as being in one of the following categories:

1. Simple made continuous with an integral concrete diaphragm and abutting bottom flanges, as shown in Figure 9a or similar.

State Highway No. 16 over US 85, Fountain, Colorado

Sprague St. over Interstate 680, Omaha, Nebraska

State Highway N-2 over Interstate 80, Hamilton County, Nebraska

US 75 over North Blackbird Creek – Macy, Nebraska

US 75 over South Blackbird Creek – Macy, Nebraska

Ohio S.H. 56 over the Scioto River – Circleville, Ohio

2. Simple made continuous for all superimposed loads with flange interconnections, i.e., simple for girder dead load only, Figure 16.

Church Ave. over Central Ave., Knox County, Tennessee

Dupont Access Road over State Route 1, Humphrey's County, Tennessee

Massman Drive over Interstate 40, Davidson County, Tennessee

State Route 210 over Pond Creek, Dyer County, Tennessee

Three Springs Drive Bridge over U.S. Route 22, Weirton, W. Virginia

Washington Avenue Bridge over Interstate 70, Wheeling, West Virginia

3. Simple made continuous for live loads with post connected flange interconnection(s), Figure 15.

New Mexico 187 over Rio Grande River – Arrey/Derry, New Mexico

U.S. 70 over Sonoma Ranch Blvd. – Las Cruces, New Mexico

4. Simple made continuous with steel diaphragms and exposed ends, Figure 20.

State Highway No. 36 over Box Elder Creek, Watkins, Colorado

I-476 Bridge over the Schuylkill River, Philadelphia, Pennsylvania (Retrofit)

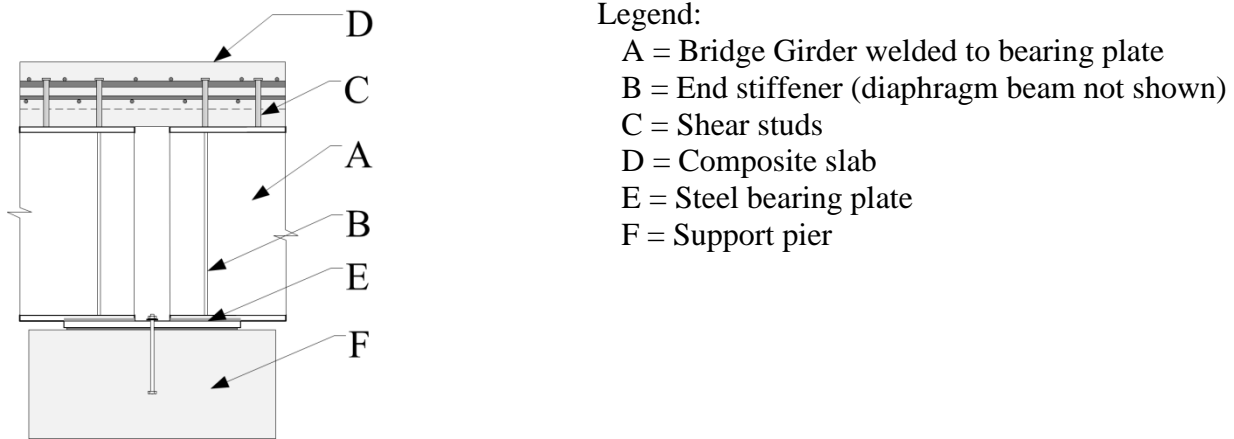


Figure 20 - SMC Detail with a Steel Diaphragm

2.8 SELECTION OF A STUDY BRIDGE

A SMC connection with ductile behavior is the most desirable. Ductility in a structure is desirable as it provides warning of overload before ultimate failure, usually in the form of excessive deflections or deformations. Based on the preceding research and review of existing SMC bridge details, it is apparent that ductility is ensured by having tension reinforcing in the top of the composite slab for negative bending and a steel to steel connection at the bottom of the connection to transfer the compressive component of the negative moment. In other words, the concrete should not be directly involved in carrying tension or compression load at the extremities of the connection.

Many studies have been performed and many bridges have been constructed with a detail using steel to steel contact, however, this steel detail is encased in a concrete diaphragm. The

one exception, which is similar to details with steel to steel contact is the State Highway No. 36 over Box Elder Creek bridge (Figure 21 and Figure 22), in which the end of the steel girder and its connection are completely exposed. However, this detail does not have direct steel to steel contact; but instead, each girder end is welded to a common bearing plate. This detail has many desirable traits as noted below:

- Appears to be more economical than encased diaphragm designs.
- Involves less construction time as there is no need to wait for the diaphragm concrete to be placed and set prior to placing deck slabs, which will accelerate construction.
- Simple and straightforward.
- Allows for slight deviations in longitudinal girder dimensions without the accuracy required for exact fit-up as in the other steel to steel details.
- Absence of the concrete diaphragm makes the connection accessible for future inspection and to allow the steel girder to properly weather for corrosion protection, when weathering steel is used.
- No need to rely on the additional concrete strength afforded by confinement, which is a necessity with some of the Nebraska schemes.
- It is a unique concept that hasn't been subject to any previous analytical study or physical testing.
- Most importantly, both the compression and tension components of the SMC behavior are taken through ductile steel elements.

This connection involves field welding of the bottom girder flange to a common sole plate to transfer the compression component of the SMC connection forces as opposed to direct bearing connections in most of the other SMC schemes.

On the basis of the preceding points, this bridge girder and its SMC detail were selected as the subject of this study.

A possible drawback to the otherwise positive aspects of this connection may be the method of transferring the compression component of the SMC behavior; this will be considered in the analysis, testing and final recommendations for design of future connections.



Figure 21 - SH 36 Over Box Elder Creek (reprinted courtesy of AISC)



Figure 22 - SH 36 Over Box Elder Creek – Girder Details (reprinted courtesy of AISC)

CHAPTER 3 – PRELIMINARY ANALYSIS

3.1 RESEARCH OVERVIEW

The study objectives identified in section 1.4, were accomplished through a combination of preliminary load analysis, finite element analysis and testing of a full scale physical model. The study began with a review of the AASHTO specification requirements for determination of bridge loading.

After completion of the maximum load investigation, material properties of all of the bridge component materials were determined. These values were then used for preliminary and final finite element analyses.

Non-linear static finite element analysis was performed on a partial model to simulate the maximum negative moment along with the corresponding applied shears on either side of the connection. The model used the respective end shears placed at distances from the center of the support that resulted in equal and opposite applied moments on either side of the SMC connection as shown in Figure 23. The results of the finite element analysis provided an analytical model of the behavior of the components of the SMC connection as load was applied. The FEA results provided reference point data and benchmarks for correlation with instrumentation data obtained during the physical model test.

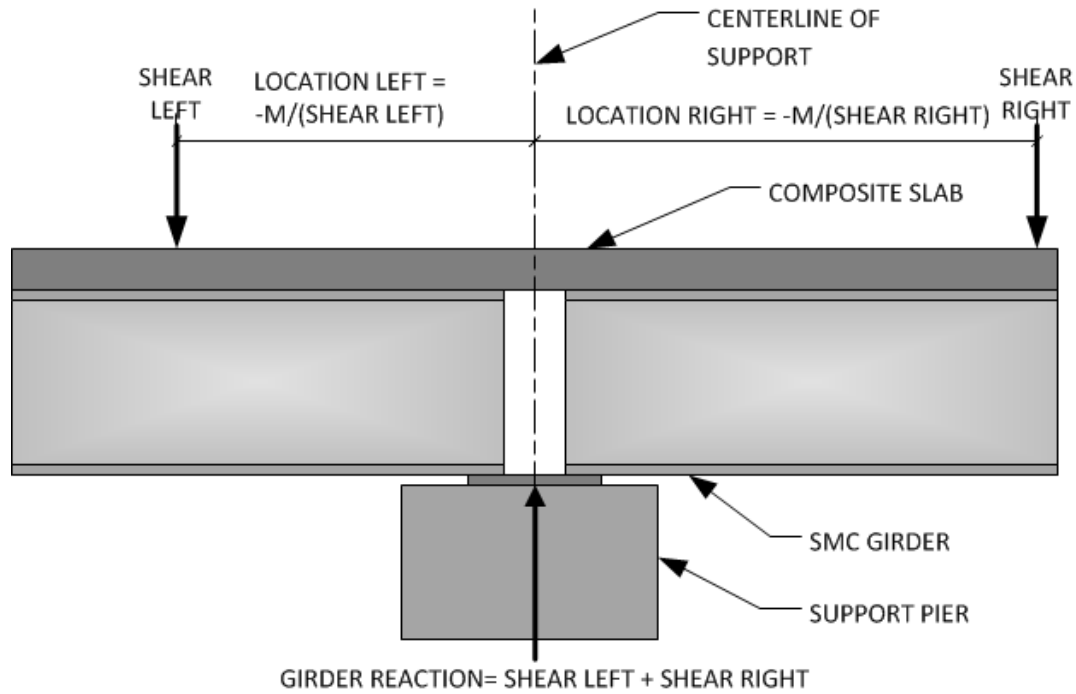


Figure 23 - Simplified girder model

After completion of the FEA, a physical test was performed on a specimen similar to that shown in Figure 23. The test specimen was instrumented to determine strains, displacements, etc., at various key locations. Based on the results of the data collected from the physical model test, the ABAQUS model was verified/calibrated for use in further analysis. The calibrated FE model was then used to perform a parametric study and to assist in achieving the study objectives outlined in Table 2.

Table 2 - Study Objectives

Objective	Approach
<p>Determine the effect of shear lag in the top deck reinforcement and develop design procedures to specify the rebar placement</p>	<p>Examine the results of the ABAQUS analysis to determine the stresses in the top reinforcing bars and the variation in stress away from the center of the composite girder. In the physical model, instrument the top reinforcing bars near the center of the connection for comparison to the ABAQUS results. Use the validated ABAQUS model to run additional analysis and propose design equations for reinforcing steel placement.</p>
<p>Investigate the transfer of load through the girder such that all load is capable of being transferred through only a bottom flange connection</p>	<p>Use ABAQUS results to plot stress distributions through the girder in the vicinity of the end connection. Install strain gages at various heights and distances from the bottom and end of the bottom of the girder to be instrumented. Use the ABAQUS results to estimate strain gage placement locations.</p>
<p>Understand/define the possible interaction between the bottom girder flange and the sole plate and identify all design parameters required</p>	<p>Use ABAQUS results to examine stresses from stiffeners transferring to the sole plate through the bottom flange of the girder. Also, use results to check stresses in welds due to moment couple effects for comparison to design values. Install strain gages on the sole plate in the vicinity of the bearing stiffeners and on longitudinal and lateral welds between the girder bottom flange and the sole plate to determine stresses for comparison to ABAQUS results.</p>
<p>Specify calculations necessary for the welds between the sole plate and girder flange</p>	<p>Based on ABAQUS and physical model results, develop design equations for weld of bottom flanges of girders to common steel sole plate by making modifications to AASHTO design provisions if necessary or developing a weld analysis methodology that will use the current design provisions.</p>
<p>If weld sizes and/or lengths in the preceding objective become excessive, develop formulations and design criteria for wedge bearing plates to transfer bottom flange compression across the joint</p>	<p>Perform additional ABAQUS analysis to analyze a compression plate between the bottom girder flanges to take some load away from welds. Subsequently, develop design equation based on the FEA results.</p>

3.2 AASHTO REQUIREMENTS

3.2.1 General

The AASHTO design specification was used for load determination, analysis methods and design checks. AASHTO (AASHTO, 2012) equation numbers are given when available, otherwise equations are numbered sequentially. The AASHTO specifications require all bridges to be designed with the load and resistance factor method (LRFD). In essence, this requires satisfaction of the general equation:

$$\phi R_n \geq \sum \eta_i \gamma_i Q_i \quad (\text{AASHTO 3.4.1-1})$$

Where:

- ϕ = Resistance factor for the particular limit state
- R_n = Nominal resistance
- η = Load modifier specific to AASHTO
- γ = Load factor for the specific load and load case
- Q = Force effects from specified load

Thus, the left hand side of this equation, ϕR_n , is the resistance portion and the right hand side is the load portion.

3.2.2 Bridge Load Requirements and Load Factors

The actual bridge is subjected to both dead and live loads. Of the dead loads, there are permanent loads that will cause only simple moments in the girders. Permanent dead loads include the self-weight of the steel framing, the concrete slab and anything cast into the slab such as drain grates, hangers, etc. Then there are superimposed dead loads, which are installed after the SMC connection has become effective. Superimposed dead loads would include wearing course pavement, downspouts, signage, railings, etc.

The code required live loads on bridges designated as HL-93 consist of a lane load along with any of three specified truck loadings. The lane loading is 0.64 klf over a ten foot wide lane or 0.064 ksf. The truck loadings consist of:

The design truck with 6'-0" wide axles and front axle spacing, L1 of 14'-0" and rear axle spacing, L2 of 14'-0" through 30'-0", at one foot increments, this would create a total of 19 possible trucks, Figure 24.

The design tandem truck with 6'-0" wide axles as shown in Figure 25.

The dual trucks with 6'-0" wide axles as shown in Figure 26.

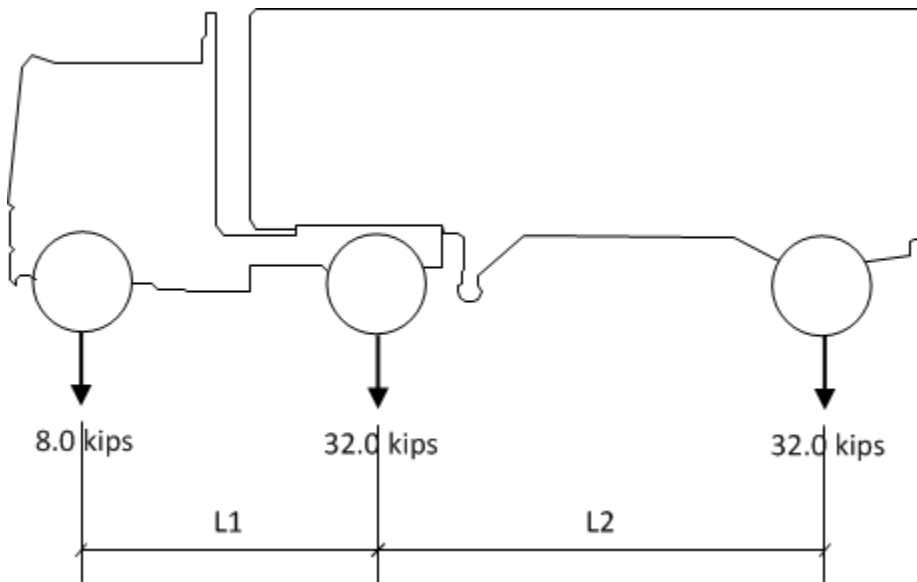


Figure 24 - AASHTO Design Truck

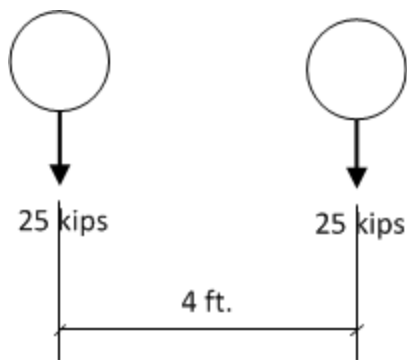


Figure 25 - AASHTO Design Tandem

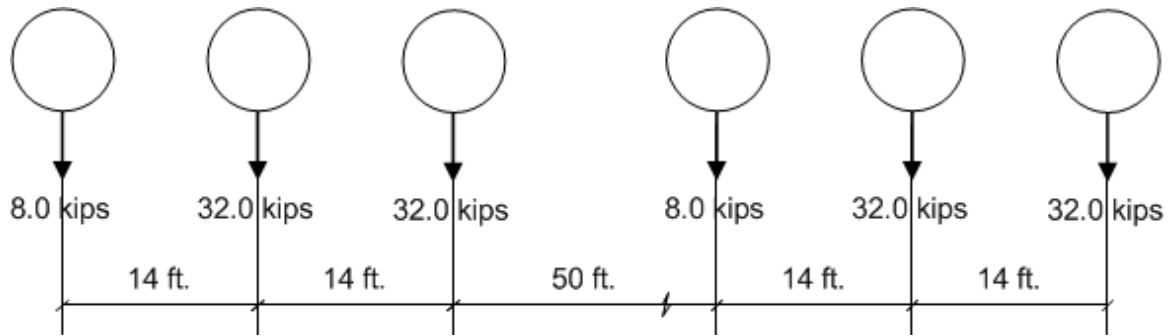


Figure 26 - AASHTO Dual Truck

For the type of bridge selected, AASHTO specifies five applicable load combinations, which are shown in Table 3. Once the appropriate combination has been selected, applicable load factors, γ 's, based on the combination will be used (Table 4). For the purpose of this study, the 'Strength I' combination will be used since it will create the largest wheel loads and consequently, the largest absolute internal moments and shears.

Table 3 - Applicable Load Combinations

Combination Name	Description
Strength I	Basic load combination relating to the normal vehicular use of the bridge without wind.
Service I	Load combination relating to normal operational use of the bridge. Also related to deflection control.
Service II	Load combination intended to control yielding of steel structures due to vehicular live load.
Fatigue I	Fatigue and fracture load combination related to infinite load-induced fatigue life.
Fatigue II	Fatigue and fracture load combination related to finite load-induced fatigue life.

Table 4 - AASHTO Load Factors, γ 's

Combination Name	Dead(DC)	Vehicular Live(LL)	Pedestrian Live(PL)	Vehicular Dynamic Load Allowance (IM)
Strength I	1.25	1.75	1.75	33%
Service II	1.00	1.00	--	--
Service II	1.00	1.30	1.30	33%
Fatigue I	--	1.50	--	15%

Combination Name	Dead(DC)	Vehicular Live(LL)	Pedestrian Live(PL)	Vehicular Dynamic Load Allowance (IM)
Fatigue II	--	0.75	--	15%

The vehicular dynamic load allowance (AASHTO Table 3.6.2.1.1) is determined in accordance with Equation 1. The IM shall only be applied to the truck wheel loads and not to the uniform lane loading. The IM shall be applied as an additional load factor to the static loads in combination with the values for IM in

Table 4.

$$1.0 + IM/100 \quad \text{Equation 1}$$

The final form of the load equation is $Q = \sum \eta_i \gamma_i Q_i$, where for the bridge considered,

η_i = Load modifiers as follows:

$$\eta_D = \text{factor relating to ductility} = 1.00$$

$$\eta_R = \text{factor relating to redundancy} = 1.00$$

$$\eta_I = \text{factor relating to operational classification} = 1.00$$

Q_i = the various loadings

γ_i = the applicable load factor for the load under consideration

While the η values are all 1.00 for this particular bridge, this is not always the case.

Distribution of live loads for moments to interior and exterior beams is determined based on bridge supporting component (girder) type and deck type. In this study, the girders are steel beams and the deck type is a cast-in-place concrete slab, which according to AASHTO Table 4.6.2.2.1-1, is a cross-section type (a). Thus, in accordance with AASHTO Table 4.6.2.2.2b-1, the design loads shall be determined based on Equation 2 for one design lane loaded and on Equation 3 for two or more design lanes loaded. It should be noted that the distribution factors are to be applied to the axle loads, not the wheel loads which are one half of the axle loads.

$$0.06 + \left(\frac{S}{14}\right)^{0.4} \left(\frac{S}{L}\right)^{0.3} \left(\frac{K_g}{12.0L_s^3}\right)^{0.1} \quad \text{Equation 2}$$

$$0.075 + \left(\frac{S}{9.5}\right)^{0.6} \left(\frac{S}{L}\right)^{0.2} \left(\frac{K_g}{12.0Lt_s^3}\right)^{0.1} \quad \text{Equation 3}$$

In these equations, the variables used are defined as follows:

I_g = moment of inertia of girder (in.⁴)

A = girder area (in.²)

E_B = modulus of elasticity of girder (ksi)

E_C = modulus of elasticity of concrete (ksi)

S = spacing of beams or webs (ft.)

t_s = depth of concrete slab (in.)

L = span of beam (ft.)

N_b = number of beams, stringers or girders

e_g = distance between the centers of gravity of the
basic beam and deck (in.)

And the limits of applicability are:

$$3.5 \leq S \leq 16.0$$

$$4.5 \leq t_s \leq 12.0$$

$$20 \leq L \leq 240$$

$$N_b \geq 4$$

$$10,000 \leq K_g \leq 7,000,000$$

In addition, the variable L may vary depending on the desired force effect and is defined in AASHTO Table C4.6.2.1.1-1. Should all of the girder spans be the same, then L would be the same for all force effects such as minimum/maximum moments, shears and reactions.

Alternatively, AASHTO allows another methodology, the lever method, which provides more conservative (Barker, 2007) loads than the distribution factor method and thus was not considered.

3.2.3 Bridge Material Limit States and Resistance Requirements

AASHTO provides the formulations and the methodology to determine the nominal structural element capacities to use for different components of force and the applicable resistance factors to be applied to them for the specific limit state involved.

Specific materials considered in the study were:

- Structural steel for girders and plates
- Reinforcing steel
- Steel for headed studs
- Filler metal for welds
- Concrete for the slab, haunch and support pier

Detailed ultimate capacity or ultimate stress requirements based on AASHTO are presented in Table 5. These values were used in hand calculations for determination of the ultimate moment and shear capacity of the connection as detailed. The hand calculations followed the standard practice of ignoring the tensile capacity of the concrete.

Table 5 – AASHTO Ultimate Capacity Calculations

Material	Stress/Load Description	Formula for Determination	Source (AASHTO eqn. number unless noted)
Structural Steel	Nominal Flexural Resistance $D_p \leq 0.1D_t$	$M_n = M_p$	(6.10.7.1.2-1)
Structural Steel	Nominal Flexural Resistance $D_p > 0.1D_t$	$M_n = M_p \left(1.07 - 0.7 \frac{D_p}{D_t} \right)$	(6.10.7.1.2-2)

Material	Stress/Load Description	Formula for Determination	Source (AASHTO eqn. number unless noted)
Structural Steel	Nominal Flexural Resistance (continuous span limitation)	$M_n \leq 1.3R_h M_y$	(6.10.7.1.2-3)
Structural Steel	Nominal Shear Resistance of Stiffened Webs	$V_n = V_p \left[C + \frac{0.87(1-C)}{\sqrt{1 + \left(\frac{d_0}{D}\right)^2}} \right]$	(6.10.9.2-1)
Structural Steel	Nominal Shear Resistance of Unstiffened Webs	$V_n = V_{cr} = CV_p$ and $V_p = 0.58F_{yw}Dt_w$	(6.10.9.2-1)
Structural Steel - Bearing Stiffeners	Nominal Axial Load Capacity	$P_e = \frac{\pi^2 E}{\left(\frac{Kl}{r_s}\right)^2} A_g$	(6.9.4.1.2-1)
Fillet Welds	Nominal Shear Resistance	$R_r = 0.6F_{exx}$	(6.13.3.2.4b-1)
Shear Connectors	Nominal Shear Resistance	$Q_r = Q_n$	(6.10.10.4.1-1)
Concrete	Modulus of Elasticity	$E_c = 1,820\sqrt{f'_c}$	(C5.4.2.4-1)
Concrete	Modulus of Rupture	$0.24\sqrt{f'_c}$	(Sect. 5.4.2.6)
Concrete	Tensile Strength	$0.23\sqrt{f'_c}$	(Sect. C5.4.2.7)

Variable definitions:

- C = ratio of the shear-buckling resistance to the shear yield strength from Eqs. 6.10.9.3.2-4,-5 or -6 as applicable, with $k_v = 5.0$
- D = clear distance between the flanges less the inside corner radius on each side
- D_p = distance from the top of the concrete deck to the neutral axis of the composite section at the plastic moment (in.)
- D_t = total depth of the composite section (in.)
- M_p = plastic moment capacity of the composite section (kip-in.) per AASHTO D6.1
- M_u = ultimate moment at the strength limit state (kip-in.)
- R_h = hybrid factor per AASHTO article 6.10.1.10.1 (1.0 for rolled girders and girders with constant F_y)

Once the nominal strength values for the various limit states are determined, resistance factors in accordance with Table 6 will be applied to complete the left side of AASHTO equation 3.4.1-1.

Table 6 – AASHTO resistance factors

Limit State	Resistance Factor and Value
Flexure (structural steel)	$\phi_f = 1.00$
Compression (structural steel only)	$\phi_c = 0.90$
Tension in gross section (structural steel)	$\phi_y = 0.95$
Tension (reinforcing steel)	$\phi_y = 0.90$
Shear (structural steel)	$\phi_v = 1.00$
Shear (concrete)	$\phi_v = 0.90$
Shear Connectors in Shear	$\phi_{sc} = 0.85$
Shear Connectors in Tension	$\phi_{st} = 0.85$
Web Crippling	$\phi_w = 0.80$
Weld metal in fillet welds with tension or compression parallel to axis of weld	$\phi_{e1} = 1.00$ (same as base metal) (Figure 27 b)
Weld metal in fillet welds with shear in throat of weld metal	$\phi_{e2} = 0.80$ (Figure 27 a)

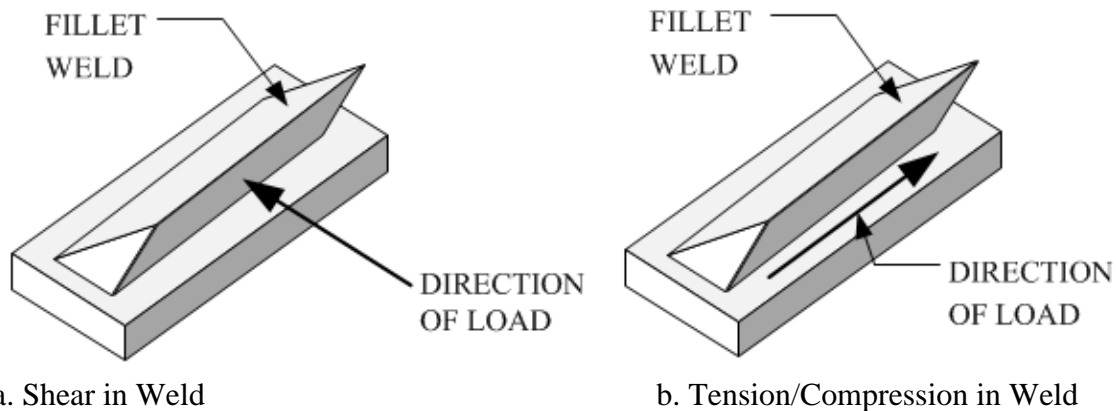


Figure 27 – Weld Load Directions (AASHTO 6.13.3.2.4b)

3.3 DESIGN LOAD CALCULATIONS AND DETERMINATION OF CONTROLLING LOADS

3.3.1 Preliminary Analysis

For the study bridge, preliminary load determination for the girder was made with a computer analysis of the effects of the design trucks, Figure 24, Figure 25 and Figure 26. This analysis provided the maximum negative moment developed at an interior support. A design check of the SMC components of the connection was then performed by hand calculation considering several variations of components and combinations thereof which were effective in the SMC behavior (Appendix 2 – Hand Calculations).

For multi-span bridges, each of the trucks were moved along the bridge until the desired maximum load effect for a particular span is obtained. At a minimum step of one foot along the bridge, this meant 19 different load cases times the total length of the bridge plus the length of the truck for the given case. For example, a 200 foot long bridge for the design truck with $L_2 = 16'-0''$ would require $200 + 14 + 16 = 230$ steps along the bridge girders and the corresponding shear and moment calculations; this is just for one particular truck. For all trucks, a similar calculation set was required 19 times. This would be daunting to complete by hand, so

spreadsheet software was developed by the author to perform this task. While some cases could obviously be omitted, it was simpler to create the programmed spreadsheet software to consider all possibilities as the additional time involved was negligible. This software provided the maximum positive/negative moments in the span and at each support as well as the maximum/minimum reactions at the each support for all 19 trucks. Simultaneously to providing the moment and reaction values, the software also provides the position of the first wheel of the truck that produces the maximum. The user then selects the case for the desired result, minimum or maximum moment, shear, etc., and requested a detailed analysis of that truck and its first wheel location.

Results of the detailed analysis were shear and moment diagrams for the maximum selected load. For the selected study bridge, S.H. 36 over Box Elder Creek, the shear diagram is shown in Figure 28 and the moment diagram is shown in Figure 29. The blue (dashed) line indicates the loading due to the superimposed wheel, lane and wearing course loads and the red (solid) line indicates sum of the superimposed loads and the simple dead load.

**Shear Diagram for Bridge: S.H. 36 over Box Elder Creek (Truck No. 19 at
136 ft. from start)**

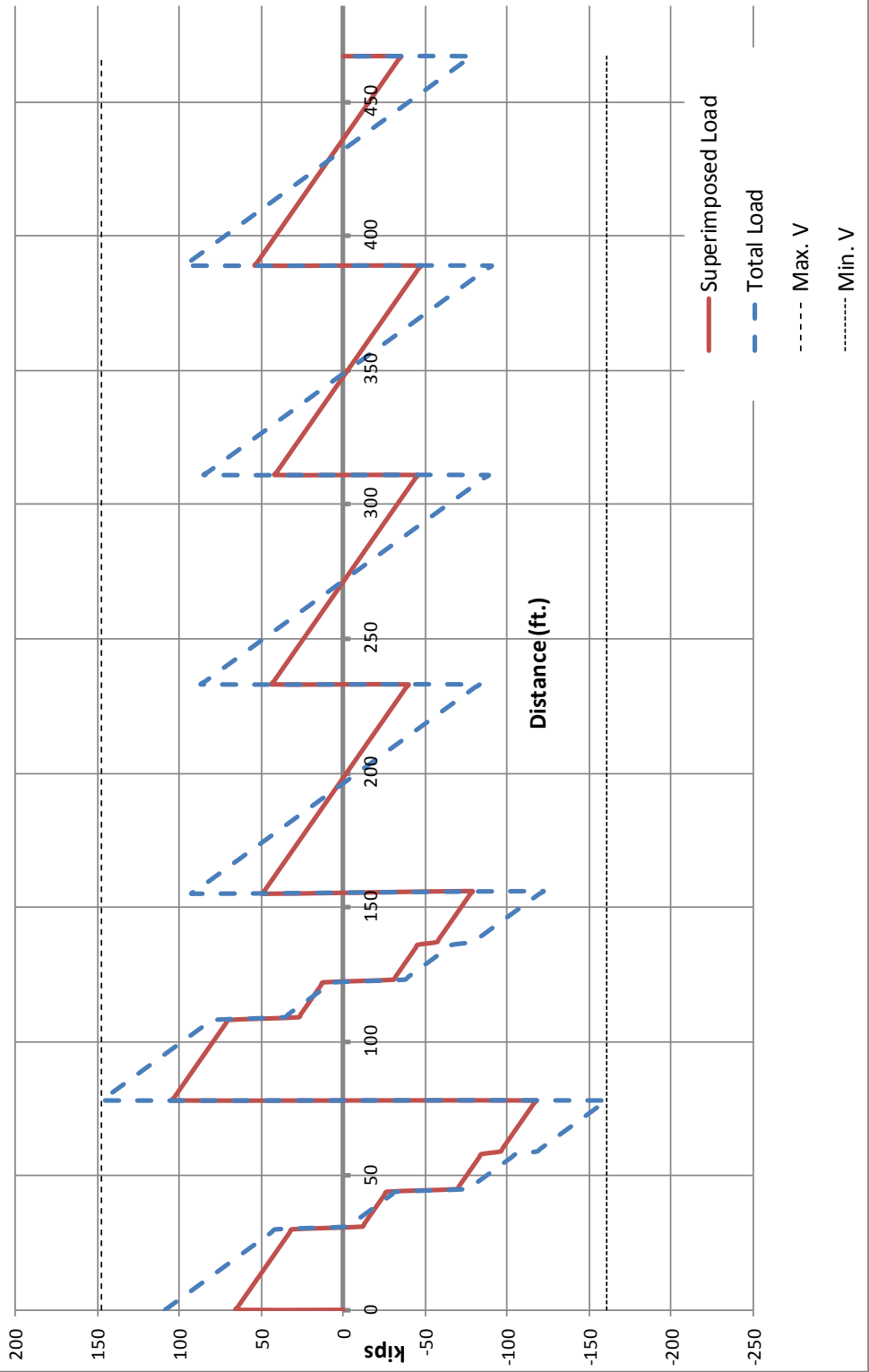


Figure 28 - Shear Diagram

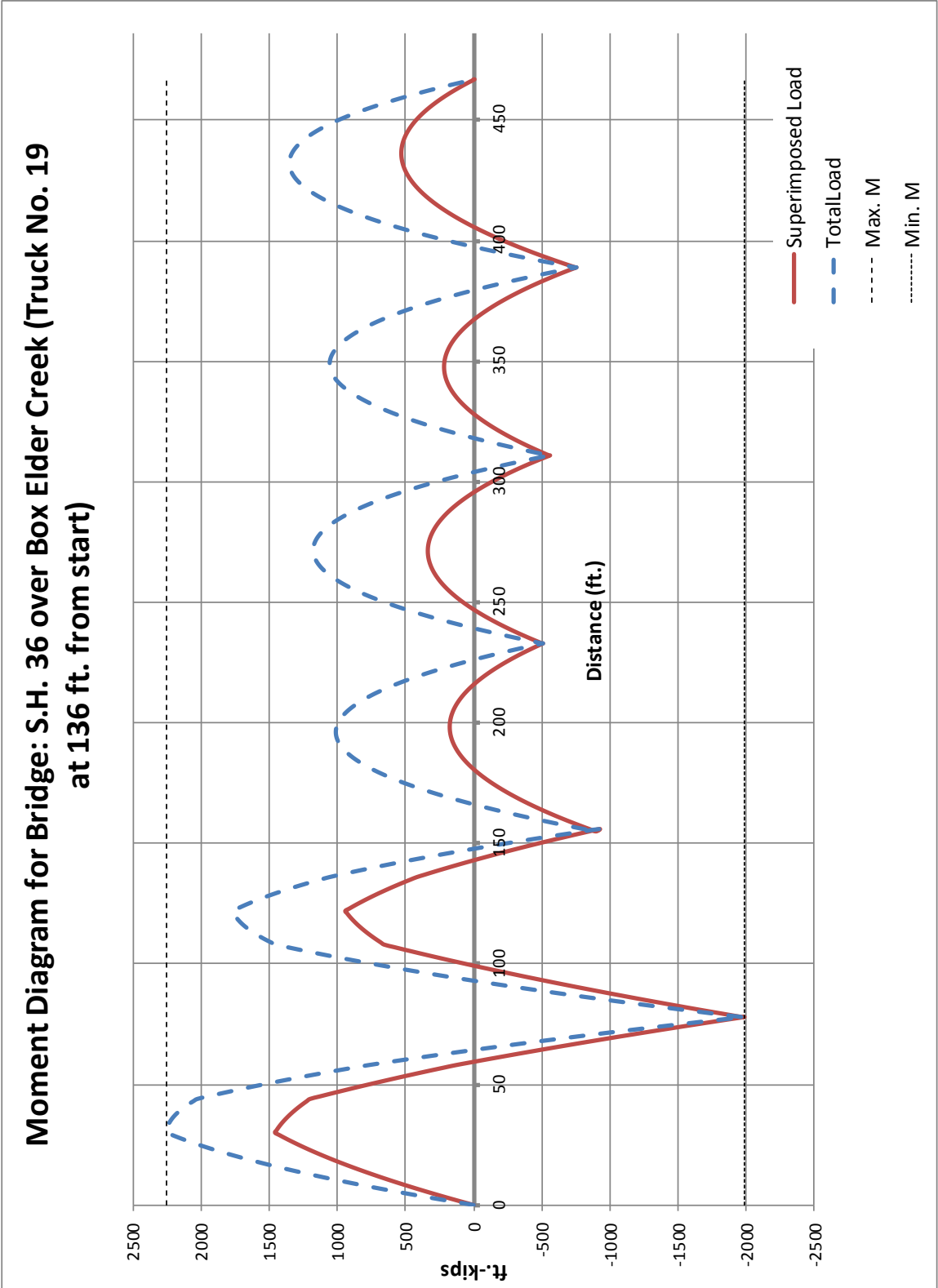


Figure 29 - Moment Diagram

The particular load condition shown in the preceding figures is the condition that resulted in the maximum negative moment at the first interior support and is caused by the dual truck

(Figure 26) with its first wheel 136 feet from the beginning of the bridge. The dead load moments used in the total were based on the weight of the bridge girder, steel diaphragms and concrete slab. These loads were used in the finite element analysis to evaluate the study girder. Based on the preceding analysis results, the ultimate loads to be applied to the study connection were $V_{\text{left}} = 160.6$ kips, $V_{\text{right}} = 147.7$ kips and $-M_{\text{max}} = 1,968$ ft-kips (see Figure 20). The resulting moment arms that were applied to a partial model (Figure 23) were 12.3 ft. to the left and 13.3 ft. to the right respectively. In order to shorten the length of the analytical and physical test models, a load application point of 12.0 feet from either side was chosen with an applied test load of 164 kips in order to achieve a moment of 1,968 ft-kips. The vertical resultant based on the actual truck was 308 kips, whereas the applied loads to the analytical and physical models resulted in a slightly higher reaction of 328 kips due to the shorter moment arm. The analysis effects of the increased shear/reaction were negligible. This is discussed in depth in Chapter 5 Physical Model Test.

The study connection was analyzed by hand (Appendix 7) to determine the controlling moment capacity of the various components. Moment capacities were determined by calculating the nominal capacities of the various components, applying their respective resistance factors and multiplying by their moment arms. The moment results of these calculations are presented in Table 7. The applied maximum ultimate moment from the analysis as shown in Figure 29, is 1,968 kip-feet.

Table 7 - Comparison of SMC Moment Capacities of Study Connection

Component	ϕP_n	Moment Arm	ϕM_n Moment Capacity
Slab Reinforcing #8+#5	1129 kips	41.375 inches	3890 kip-feet
W33 Bottom Flange	615 kips	40.345 inches	2070 kip-feet
Welds to Sole Plate	421 kips	40.875 inches	1434 kip-feet
Sole Plate	700 kips	41.375 inches	2414 kip-feet

As can be seen, the moment capacity of the welds to the sole plate (1434 kip-feet) is over 25% less than the required moment capacity of 1,968 kip-feet for the worst case truck load. The anticipated actual ultimate load to the welds is 578 kips. For this reason, modifications were made to the test model to anticipate failure prior to reaching moment capacity of the welds; this included installation of a safety device and increasing the weld sizes on one of the girders to meet the required capacity. See Section 5.1 for details.

For the actual finite element analysis and testing, the bridge was analyzed for the service level dead and live loads with the appropriate impact factors. The results of this analysis are shown in Figure 30 and Figure 31. The reaction force at the first interior support is 212 kips and the negative moment at the SMC connection is 1172 ft-kips.

Shear Diagram for Bridge: S.H. 36 over Box Elder Creek (Truck No. 19 at 136 ft. from start)

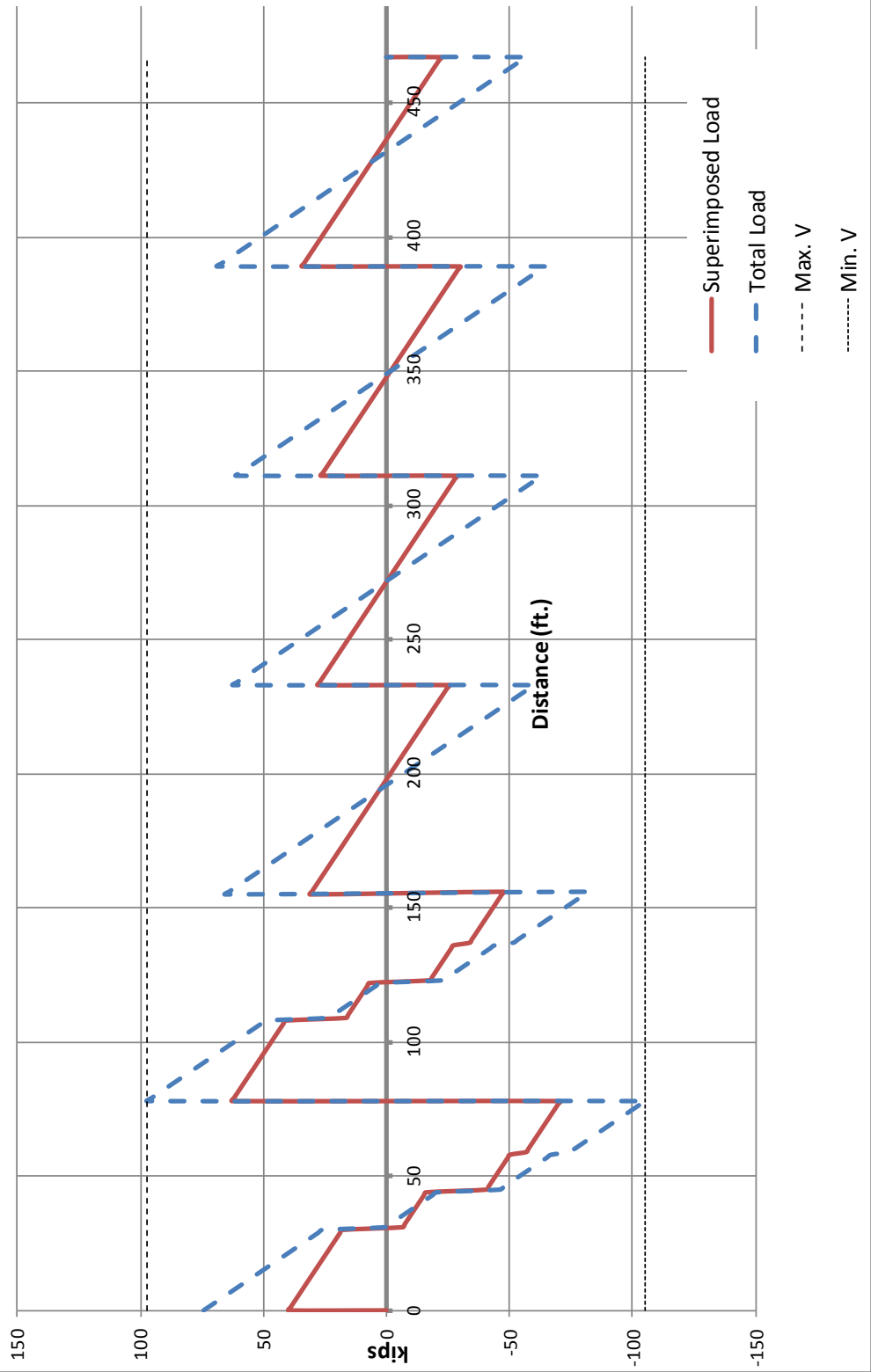


Figure 30 – Service Load Level Shear Diagram

**Moment Diagram for Bridge: S.H. 36 over Box Elder Creek (Truck No. 19
at 136 ft. from start)**

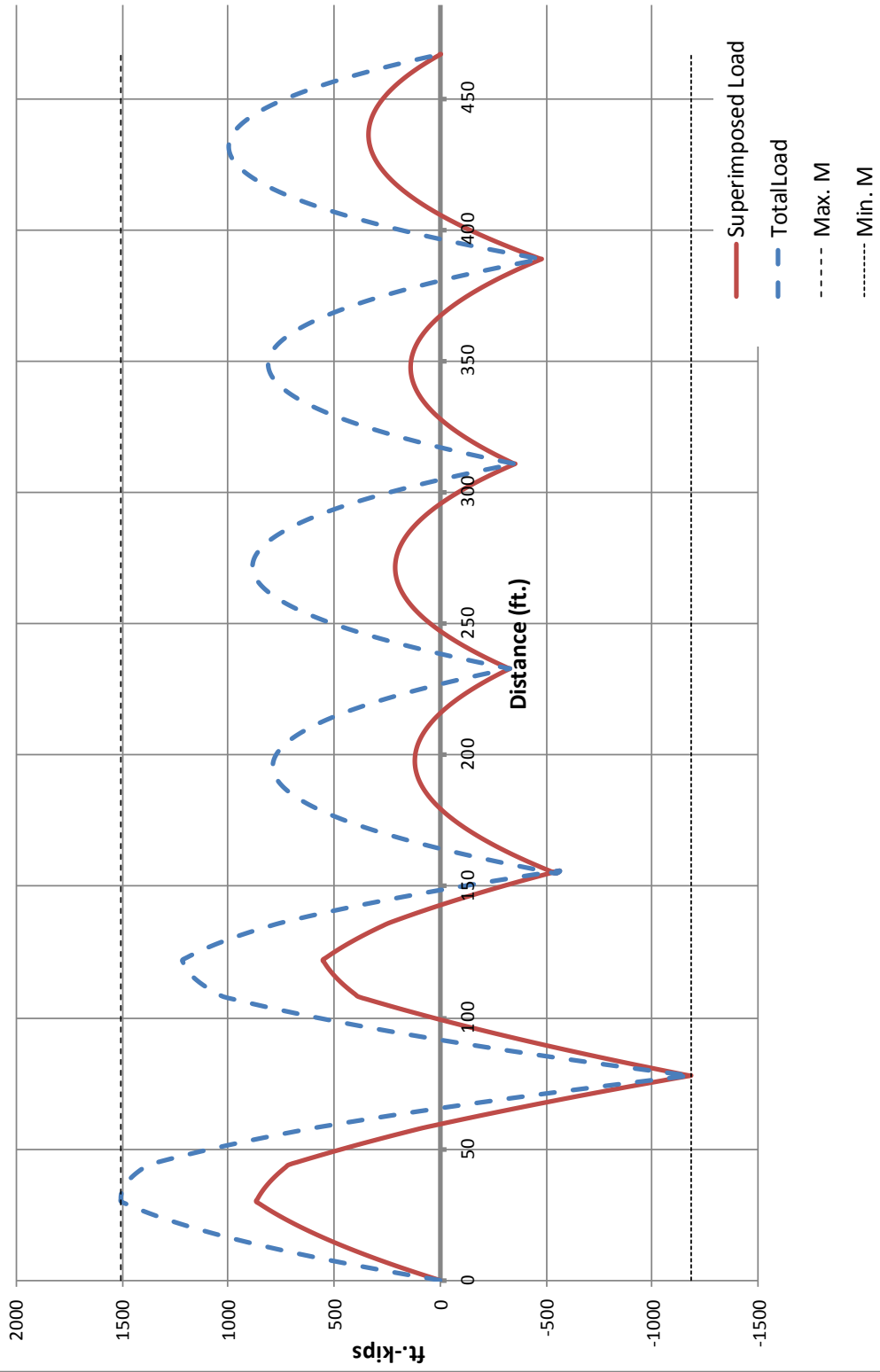


Figure 31 – Service Load Level Moment Diagram

CHAPTER 4 FINITE ELEMENT ANALYSIS

This section discusses modeling of the study connection in ABAQUS finite element software. Material modeling methods are discussed and the material properties to be used are developed. The first finite element analysis (FEA) performed was a sensitivity analysis of a double cantilever girder to optimize the meshing, element selection, element order, contact and constraint types to be used, boundary conditions and load application methodology. Finally, the study girder connection was modeled and analyzed using ABAQUS. The final ABAQUS results were anticipated to be used for monitoring of and comparison with the physical model test.

4.1 MATERIAL MODELING

Materials modeled were steel for beams, steel for stiffener plates, steel for sole (bearing) plates, weld metal for welds, steel for reinforcing bars, steel for headed stud anchors, concrete for slabs and concrete for support piers. Steel members were expected for the most part to remain in the elastic range however, some areas, particularly in the area of the welded connection might have possibly extended into the plastic range. The properties for the structural steel were the same for both tension and compression so the same material model was used throughout for its properties. Concrete on the other hand is brittle and has very low tensile capacity, thus its properties were defined on the basis of both tensile failure and compressive failure.

Steel beams: No damage of beams was anticipated except for the possibility of some plastic behavior thus, the beam material was modeled in ABAQUS as follows:

General=>Density = 2.935×10^{-4} kips/inch³ (use gravity value of -1)

Mechanical=>Elasticity=>Elastic Young's Modulus = 29,000 ksi, Poisson's Ratio = 0.30

Mechanical=>Plasticity=> per Table 8

Table 8 – Steel stress-strain curve values for $F_y = 50$ ksi (Salmon, 2009)

No.	Yield Stress (ksi)	Plastic Strain (in/in)
1	52	0
2	54	0.0193
3	69	0.0283

Steel stiffeners and sole (bearing) plates: No yielding of the stiffener plates nor the bearing plates was anticipated however, the stiffener and bearing plate material will be modeled as follows:

General=>Density = 2.935×10^{-4} kips/inch³ (use gravity value of -1)

Mechanical=>Elasticity=>Elastic Young's Modulus = 29,000 ksi; Poisson's Ratio = 0.3

Mechanical=>Plasticity=> per Table 9

The elasticity properties were used until yield and then the plasticity properties were used for all of the plates modeled.

Table 9 – Steel stress-strain curve values for $F_y = 50$ ksi (Salmon, 2009)

No.	Yield Stress (ksi)	Plastic Strain (in/in)
1	50	0
2	54	0.0193
3	69	0.0283

Elastomeric bearing: The elastomeric bearing was not anticipated to fail, although it would have severe displacements. A compression test of a sample was made in the lab and the only mechanical property used was Mechanical=>Elasticity=>Elastic Young's Modulus = 1.12 ksi. The density and Poisson's ration were not anticipated to have an effect on the model behavior.

Steel reinforcing bars: Damage might have occurred to the reinforcing bars over the support at the location of the SMC action and therefore the material was modeled as follows:

General=>Density = 2.935×10^{-4} kips/inch³ (use gravity value of -1)

Mechanical=>Elasticity=>Elastic Young's Modulus = 29,000 ksi; Poisson's Ratio = 0.3

Mechanical=>Plasticity=> per Table 10.

Table 10 - Steel Reinforcing Stress-Strain Curve Values for $F_y = 60$ ksi (Groom, 2010)

No.	Stress (ksi)	Plastic Strain (in/in)
1	60	0
2	63.9	0.0155 (0.0175-0.002)
3	74.9	0.0380
4	88.0	0.0780
5	91.6	0.1180
6	86.8	0.1580
7	81.9	0.1830

Weld Metal: E70XX electrodes were used on both the actual bridge and the physical model. Stress-strain information about welds was difficult to find and many times was found to be specious at best. The selected reference, Ricles (Ricles, 2000), appears to have been used in a considerable amount of studies up until the present. The weld material information presented therein was based upon coupon testing of samples welded with E70 electrodes. The weld metal was anticipated to yield and most likely fail prior to the final total moment.

General=>Density = 2.935×10^{-4} kips/inch³ (use gravity value of -1)

Mechanical=>Elasticity=>Elastic Young's Modulus = 29,000 ksi; Poisson's Ratio = 0.3

Mechanical=>Plasticity=> per Table 11 and Figure 32.

Table 11 – Weld Stress-Strain Properties for E70 Electrodes

No.	Stress (ksi)	Plastic Strain (in/in)
1	71.0 (yield)	0.0000
2	78.0	0.0205
3	80.0	0.0206
4	86.6	0.0455
5	89.0	0.0955
6	90.0	0.1205
7	89.0	0.1455
8	86.6	0.1955
9	75.0	0.2455

No.	Stress (ksi)	Plastic Strain (in/in)
10	53.0	0.2955
11	1.0	0.2956

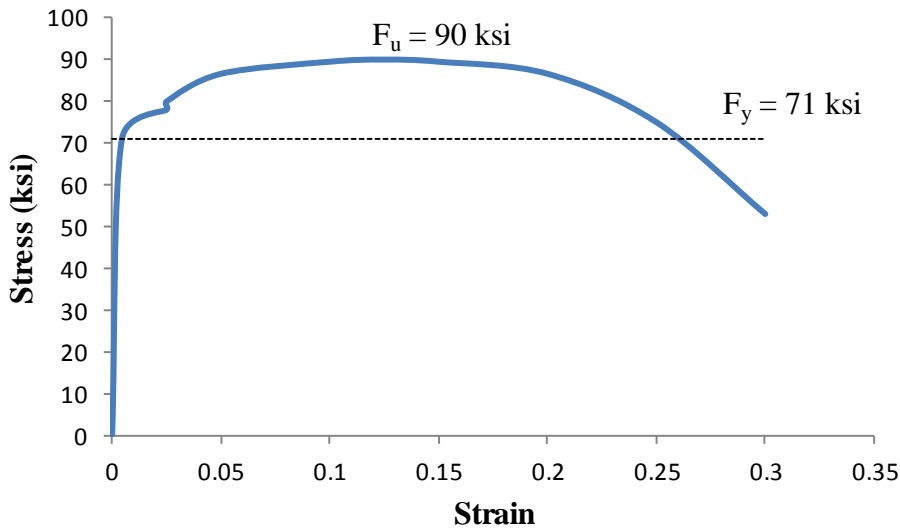


Figure 32 - Stress-Strain Diagram for Weld Metal (Ricles)

Shear Studs: No yielding of the shear studs was anticipated nonetheless, the material was modeled as follows:

General=>Density = 2.935×10^{-4} kips/inch³ (use gravity value of -1)

Mechanical=>Elasticity=>Elastic Young's Modulus = 29,000 ksi; Poisson's Ratio = 0.3

Mechanical=>Plasticity=> per Table 12.

Mechanical properties for headed studs were given in the Nelson Stud Welding Catalog (Nelson, 2011). These studs conform to ASTM A-108 specifications for 1010 through 1020 mild steels.

A graph of their stress-strain diagram is presented in Figure 33. It should be noted that the locations of strain hardening and ultimate strain were estimated as 25 times and 40 times yield strain respectively based on review of the behavior of other similar steels; these did not have an effect on the analysis since their interaction with the concrete did not cause significant strains nor plastic strains in the studs.

Table 12 – Steel Stud Material Properties for Stress-Strain Diagram

Minimum Values	Mild Steel Shear and Concrete Anchors
Yield, 0.2% offset (ksi), R_e	51
Ultimate Tensile (ksi), R_m	65
% Elongation, A_s , in 2" gage length	20
% Area Reduction	50 (ICC, 2012)

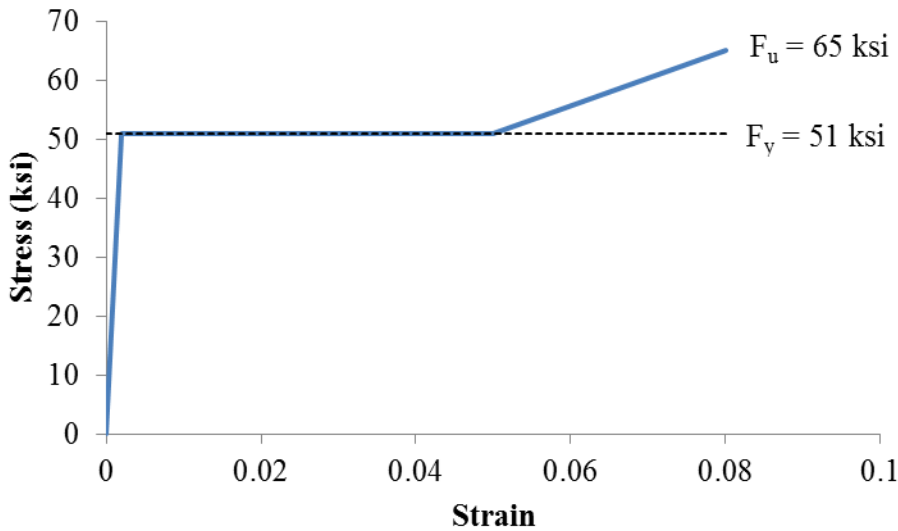


Figure 33 - Stress-strain diagram for stud shear connectors

Concrete: It was anticipated that for the SMC action to be invoked, there would be cracking in the upper concrete when it was subjected to tensile loads from the negative moment over the support. The concrete material model that modeled this effect most properly was “CONCRETE DAMAGED PLASTICITY”. Characteristics of this model are two failure mechanisms, tensile cracking of the concrete and compressive crushing of the concrete. A suitable concrete response curve and formulation for concrete subject to uniaxial tension was presented by Godalaratnam (1985). This formulation provides a peak at the determined tensile strength and then a curved softening response after tensile failure, which accurately models the effects of widening cracks, Figure 34. This response occurs due to tension from bending action

on the concrete causing micro cracking over the support. The tensile damage behavior became effective initially over the supports and then extended further into the slab as more load was applied at the girder ends.

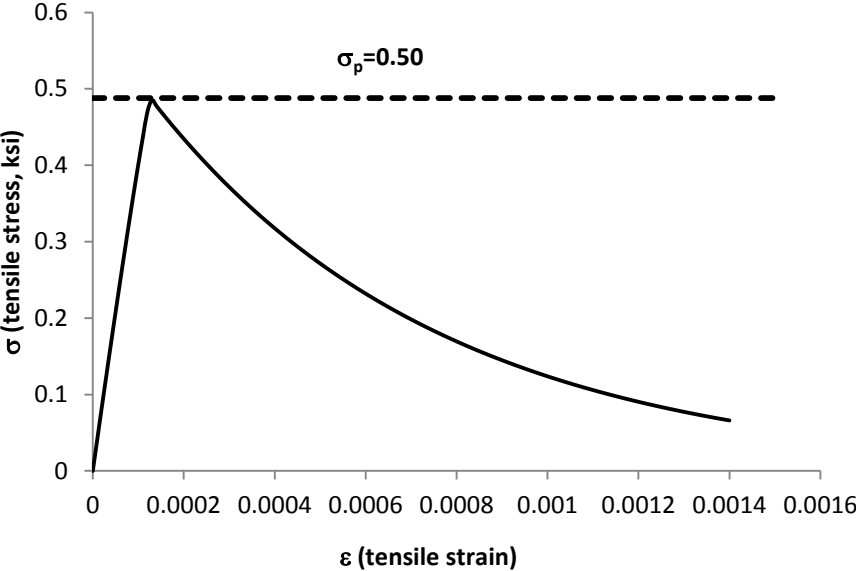


Figure 34 - Softening Response to Uniaxial Loading Based on Plain Concrete Tensile Damage (Gopalaratnam, 1985)

Where:

For the ascending portion:

$$\sigma = \sigma_p \left[1 - \left(1 - \frac{\varepsilon}{\varepsilon_p} \right)^A \right]$$

Where:

σ = tensile stress

σ_p = peak value of σ

ε = tensile strain

ε_p = value of ε at σ_p

$$A = \frac{E_t \varepsilon_p}{\sigma_p}$$

E_t = initial tangent modulus

For the descending portion:

$$\sigma = \sigma_p (e^{-k\omega\lambda})$$

Where:

ω = crack width (μin)

λ = 1.01 a factor

$k = 1.554 \times 10^{-3}$ a factor

The values used in the model are summarized in Table 13; these values were determined using $f'_c = 4712$ psi for the actual physical model concrete, which came from the concrete cylinder tests.

Table 13 – Damaged stress/strain values for 4712 psi concrete in uniaxial tension

Stress (ksi)	Strain	Plastic Strain
0	0	0
0.500	0.00013	0
0.481	0.00015	0.00002
0.459	0.00018	0.00005
0.431	0.00022	0.00009
0.325	0.00040	0.00027
0.305	0.00044	0.00031
0.255	0.00058	0.00045
0.173	0.0008	0.00067
0.067	0.0014	0.00127

Niroumand (2009) considered several models for damage of concrete under uniaxial compression loading. The study compared the work of three sources and settled on a reasonably simple approach (Carreira & Chu, 1985); this model uses only concrete ultimate compressive strength, strain at ultimate strength and strains to determine the values of useable compressive

strength (f_c'). In addition, it was the only model investigated, which allowed the concrete to reach its ultimate compressive strength before failure; all others peaked at values less than the ultimate strength. The basic formula for this model is given in Equation 4. This equation uses a factor β , which is determined by using Equation 5. However, Equation 5 is dependent upon f_c' in units of MPa; this was converted for ksi in Equation 6. For verification purposes, the Carreira & Chu study was compared against an older, frequently used (Simula, 2011) method (Karsan, 1969), which somewhat conservatively underestimates the compressive strength of the concrete. Comparisons of both methodologies for 4712 psi concrete are presented in the chart in Figure 35. Corresponding tabular values, based on Carreira and Chu were used in the analysis are presented in Table 14.

Another, more recent concrete uniaxial compressive damage model was found that showed promise (Lu, 2010). However, on evaluation of the formulations, the values for this model could not be reproduced by the author using the formulations presented. Additionally, the formulation depended primarily on the initial tangent modulus of the concrete being considered; this is not a value that is normally provided for concrete mixes, thus this model was considered unusable for multiple reasons.

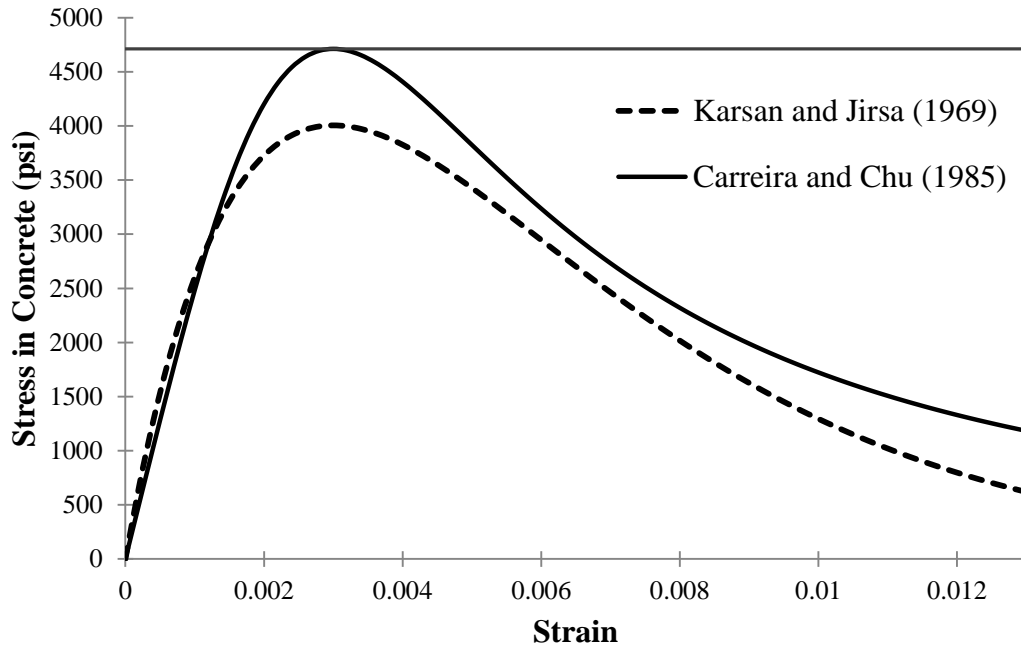


Figure 35 – Damage Model for Concrete in Uniaxial Compression for $f'_c = 4712$ psi

$$f_c = \frac{f'_c \beta \left(\frac{\varepsilon}{\varepsilon'_c} \right)}{\beta - 1 + \left(\frac{\varepsilon}{\varepsilon'_c} \right)^\beta}$$

Equation 4

$$\beta = \left[\frac{f'_c}{32.4} \right]^3 + 1.55$$

Equation 5

$$\beta = \left[\frac{f'_c}{4.7} \right]^3 + 1.55$$

Equation 6

Where:

ε = strain in concrete ($< \varepsilon_u$)

ε'_c = strain corresponding to the maximum stress, f'_c

f'_c = maximum compression stress (ksi)

Table 14 - Damaged stress/strain values for 4712 psi concrete in uniaxial compression

Stress (ksi)	Strain	Plastic Strain
0	0	0
3.66	0.0016	0
4.20	0.0020	0.0004
4.63	0.0026	0.0010
4.71	0.0030	0.0014
4.70	0.0032	0.0016
4.65	0.0034	0.0018

Stress (ksi)	Strain	Plastic Strain
4.41	0.0040	0.0024
3.95	0.0050	0.0034
3.24	0.0060	0.0044
2.73	0.0070	0.0054

In addition to tension and compression failure curves, the “CONCRETE DAMAGED PLASTICITY” model also requires several variables to fully model the behavior of the concrete; the values used are presented in Table 15.

Table 15 - Additional variables to effectively model "CONCRETE DAMAGED PLASTICITY"

Variable	Symbol	Value	Source
Dilatation angle	ψ (degrees)	31° (based on a concrete friction angle of 37°)	(Malm, 2009)
Eccentricity	ϵ	0.1	Default value (Simula, 2011)
$\frac{\text{Equibiaxial}}{\text{Uniaxial}}$ compressive yield stress	$\frac{\sigma_{b0}}{\sigma_{c0}}$	1.16	(Lubliner, 1989)
Ratio of tensile meridian stress to compressive meridian stress without Hydrostatic pressure	$K_c = \bar{q}_{(TM)} / \bar{q}_{(CM)}$	2/3	Default value (Simula, 2011)
Viscosity parameter	μ	0	Default Value (Simula, 2011)

4.2 ELEMENT SELECTION AND MODELING

Element types: ABAQUS offers a substantial number of element types, when all of the standard elements and their variations are considered. Selection of the appropriate element type for a given structural part and material can decrease processing time as well as provide more accurate results. The element types which were anticipated to be used in this study are presented in Table 16.

Table 16 - Possible element types and their descriptions

Element Name	Description	Possible Use	Notes
S4R	4-node doubly curved thin or thick	Girder Flanges	1

Element Name	Description	Possible Use	Notes
	shell, reduced integration, hourglass control, finite membrane strains.	Girder Web Girder Stiffeners	
S8R	8-node doubly curved thick shell, reduced integration with 5 or 6 degrees of freedom per node		
C3D8R	8-node linear brick with reduced integration and hourglass control (only provides nodal displacements)	Solid Girder Steel Plates Welds	
C3D20R	20-node linear brick with reduced integration (provides both nodal rotations and displacements)		2
T3D2	2-node linear 3D truss element	Reinforcing Steel	
T3D3	3-node quadratic 3D truss element	Reinforcing Steel	
B31	2-node linear 3D beam element (shear flexible)	Shear Connectors Reinforcing Steel	
B32	3-node quadratic 3D beam element (shear flexible)		

Notes:

1. Shell elements do not provide output of internal forces for comparison to the moments calculated by hand. Extracting and assembling the nodal forces and resultant moments from a beam created with shell elements is a major task.
2. Quadratic brick elements for the slab become severely distorted when modeled with elements embedded within them.

Structural steel: Structural steel shapes and stiffener plates were modeled as either shell or solid elements. The shell elements had the advantage of not only providing the three components of displacement, but also providing the three components of rotation at nodes, which were not provided by first order solid elements, Figure 36. The final determination of the element type was based on the results of the sensitivity analysis, Section 4.4 Sensitivity Analysis.

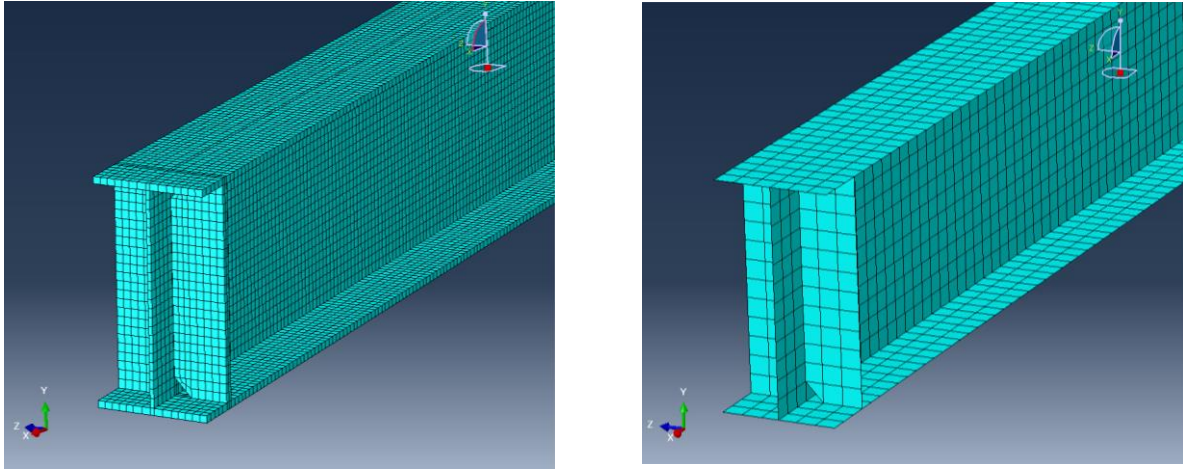


Figure 36 - Meshed Girders - Solid Brick Elements (left) and Shell Elements (right)

Steel Sole plate: Due to its simplicity, structural steel for the sole plate was modeled using linear brick elements, Figure 37.

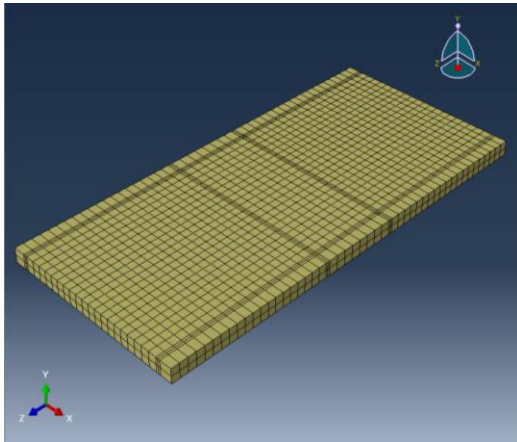


Figure 37 - Meshed Sole Plate

Headed studs (shear connectors): Headed stud anchors for composite action were modeled as either linear brick elements, linear beam elements or quadratic beam elements. Dimensional information for modeling of the shear stud and the connector as modeled and meshed are shown in Figure 38.

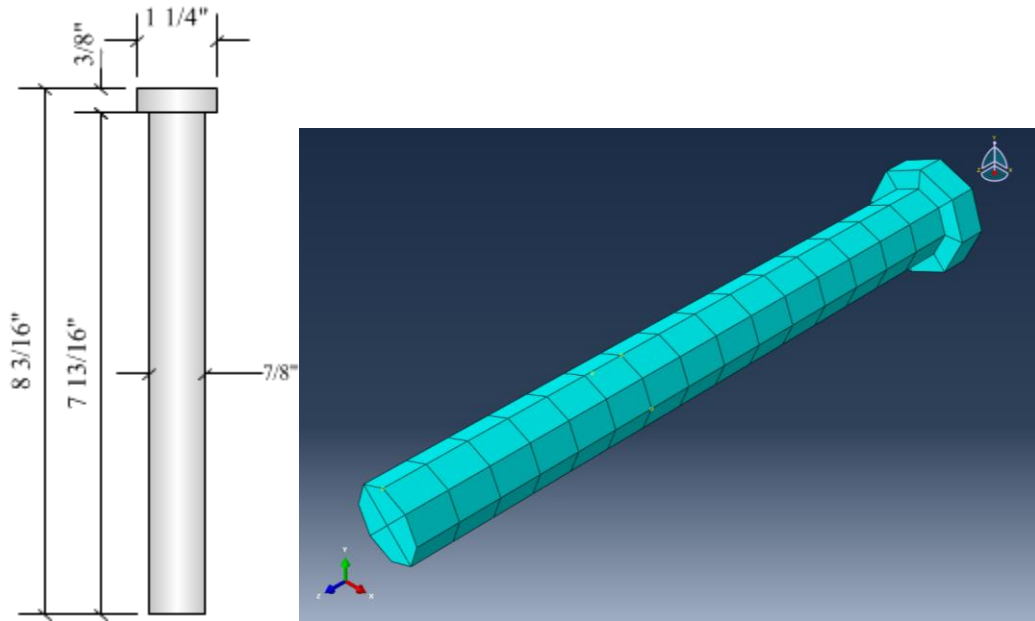


Figure 38 - Shear Stud Connector Dimensions and as Modeled (brick elements)

Welds: Welds were modelled as either linear or quadratic brick elements, Figure 39.

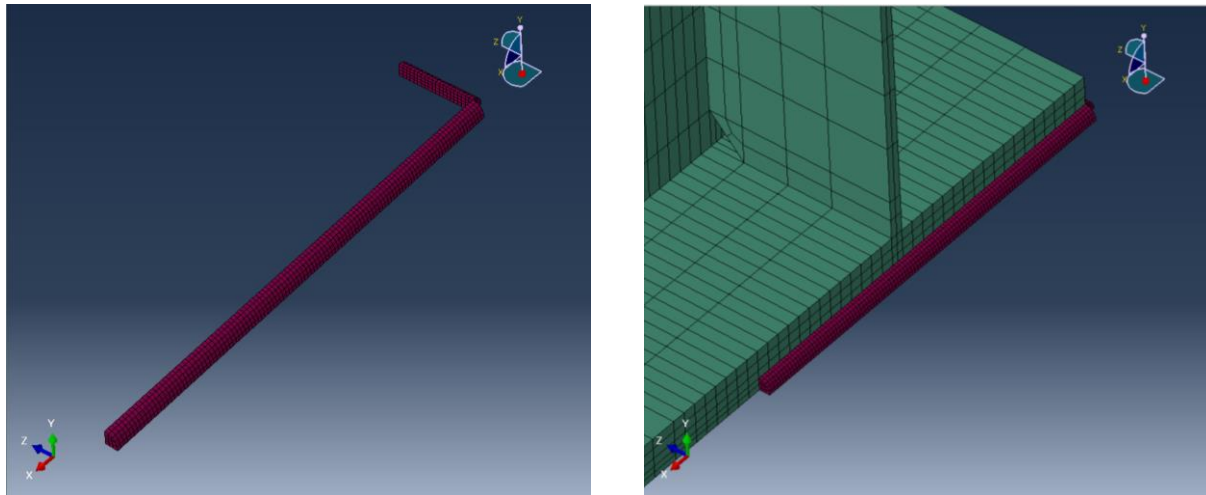


Figure 39 - Weld (left), Weld and Girder (right)

Reinforcing Steel: Reinforcing steel was modeled as either two or three node truss elements, linear beam elements or solid linear brick elements. Linear beam elements would include shear deformations.

Concrete Slab and Haunch: These members were created as a single member to allow common meshing and material definition. The combined section was modeled with either linear or quadratic brick elements, Figure 40.

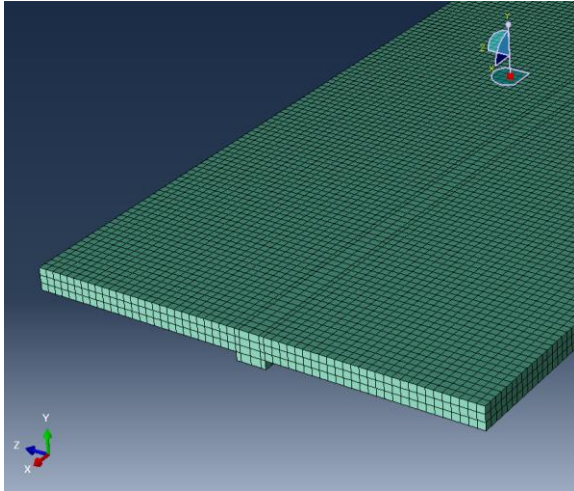


Figure 40 - Meshed Slab and Haunch

Concrete Support Pier: The pier, Figure 41, was modeled with linear brick elements as variations in element selection for this part would have little effect on the SMC behavior and the pier is only acting as a support.

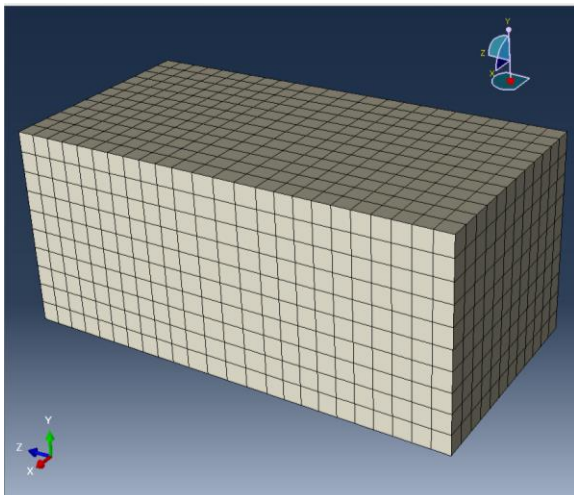


Figure 41 - Meshed Pier

4.3 CONSTRAINTS AND CONTACTS

In order to obtain the maximum benefits of using ABAQUS, the different types of constraints and part contacts available were considered for application to the FEA model. Constraints consist of boundary conditions such as rigid supports and springs to restrain the structure from displacing or rotating depending upon actual support conditions and the anticipated behaviors. However, constraints can provide much more than just boundary conditions; they may specify tied behavior between dissimilar parts or materials so that they behave as a unit. Ties may also indicate to the software that one part is partially in another and tie the two together at the intruding portion, such as shear studs tied to the top of the girder and extending into the concrete. They may also be used to specify parts embedded in other parts, such as reinforcing steel in concrete slabs.

Boundary condition constraints are available for all nodal displacements and rotations. When using linear brick elements, rotational constraints may cause errors since only displacement constraints are necessary to develop fixity. Boundary condition constraints were used on the base of the pier for only translational displacements since the pier was modeled with linear brick elements.

The embedded region or the tie constraint may be used for the interaction between the reinforcing steel and the slab concrete; the final selection is based on the results of the sensitivity analysis. The embedded region or the tie constraint may also be used for the interaction between the shear studs and the slab. The shear studs were in effect tied to the girder by making the two a combined shape and thus, no constraint was necessary; this is discussed in detail in Section 4.4 Sensitivity Analysis.

Contacts allow the definition of interactions between two parts. If contacts are not defined or improperly defined, Abaqus does not have the ability to determine interactions and the contacting parts will just move through each other as the model displaces. By defining contacts the user is able to control the behavior of the interaction between parts in order to achieve correct results.

The interaction type 'Surface to Surface contact' was chosen for all of the possible interactions between adjacent parts which were not interconnected. The contact types available include tangential behavior, normal behavior, damping, damage, fracture criterion and cohesive behavior; for this study, only tangential and normal behaviors were considered. Tangential behavior is defined by the friction between the two surfaces, which is selected by using the 'Penalty' option and entering a coefficient of friction between the two materials or zero for no friction. For steel on concrete and concrete on steel, the coefficient chosen was 0.40; this interaction occurred between the load application girders and the top of the slab, between the bottom of the concrete haunch and the top of the girder and between the bottom of the sole plate and the top of the concrete support pier. For steel on steel a coefficient of 0.5 was used; this condition occurred between the bottom of the girder and the top of the sole plate. It is unlikely that any movement between the girder and the sole plate occurred since the two are also tied together with welds.

4.4 SENSITIVITY ANALYSIS

A sensitivity analysis was conducted to determine the most accurate and best performing element types for use in the finite element analysis of the final model. The basic scheme of the girder used in the sensitivity analysis was similar, but significantly simplified from the final

model and is as shown in Figure 42 and Figure 43. The girder as modeled in ABAQUS is shown and annotated in Figure 44.

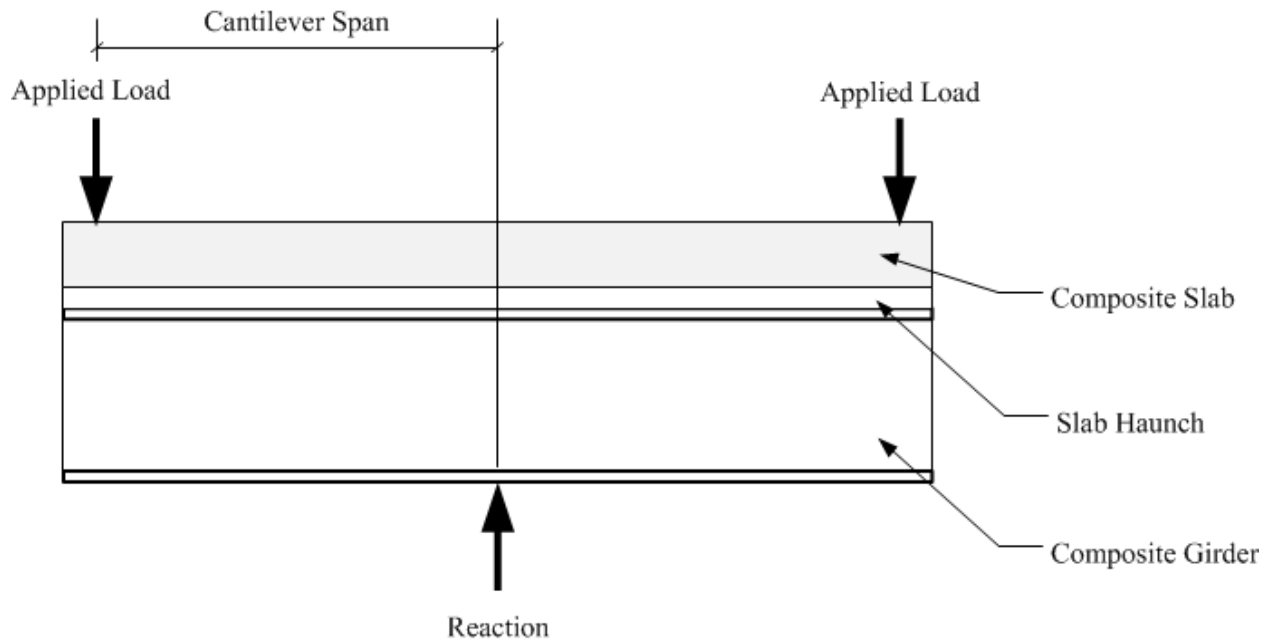


Figure 42 - Sensitivity Analysis Composite Girder - Elevation

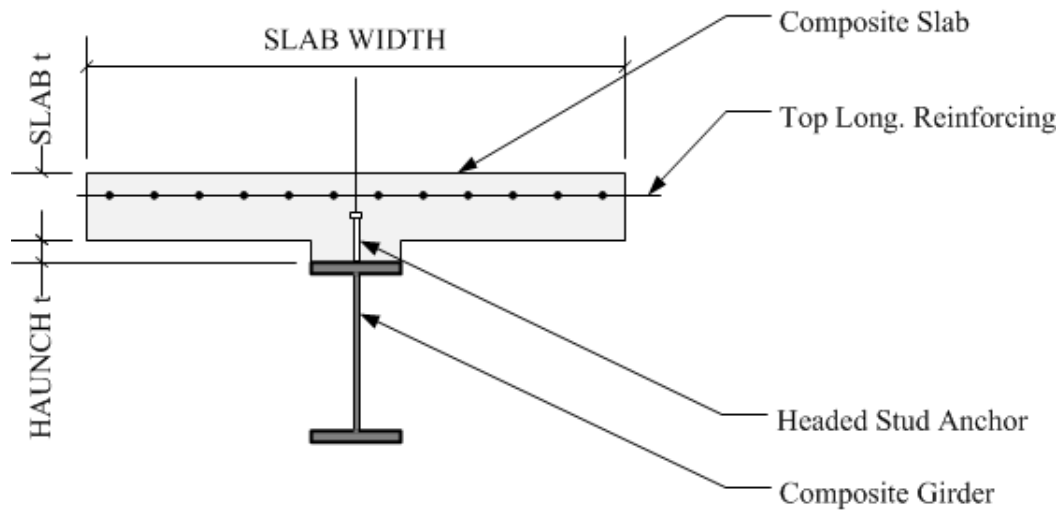


Figure 43 - Sensitivity Analysis Composite Girder - Section

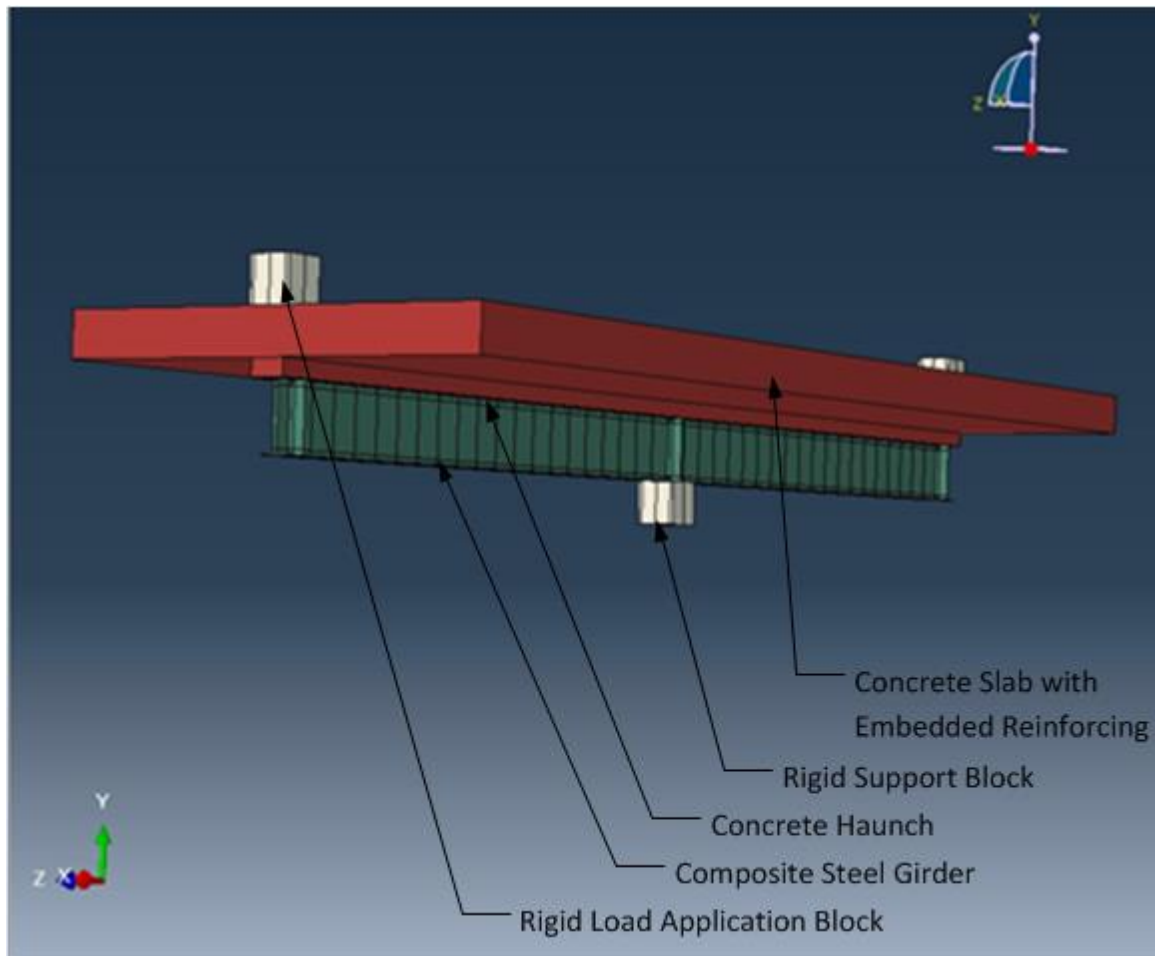


Figure 44 - Sensitivity Girder - ABAQUS Model

To simplify modeling and meshing and to reduce run time errors due to constraining two parts together by using the ‘Tie’ constraint to form a common part, large parts were created by combining smaller parts in ABAQUS’ assembly module and then these larger, more complex parts were used in the final assembly. Of equal importance to the selection of element types were the constraint and contact methodologies and properties. Constraints for boundary conditions were constant throughout the sensitivity analysis, consisting of the base of the support block constrained in all three component directions. Additional constraints involved how the reinforcing interacted with the slab and how the beam with studs was connected to the slab. Both the tie and embedded region methods were evaluated in the sensitivity analysis with mixed

results. These same two methodologies were also applied to the studs on the beam and the slab, also with mixed results.

Contacts used in the sensitivity analysis were between the bottom of the haunch and the top of the girder, between the bottom of the rigid load application blocks and the top of the slab and between the bottom of the girder and the top of the rigid support block.

Prior to the start of the sensitivity analysis, an attempt was made to prepare hand calculations to determine values of displacements end displacements at the end of the cantilever beams.

However, this task became overwhelming due to the model complexity and the number of variables that would affect the calculation of the deflection at the end of the girder and, thus, was abandoned. Hand calculations of bending moments along the beam span were calculated and are presented in Table 17.

Table 17 - Moments along Beam Span

	Distance from the Support (inches)									
	0	11	33	55	66	77	88	99	110	118
M(in-k)	2360	2140	1700	1260	1040	820	600	380	160	0

The sensitivity analysis stepped through variations in element types and constraints as shown in summarized in Table 18 in order to consider the 36 different models. Section cuts of the girder were taken at the specified points along the beam and internal moments were compared to those tabulated in Table 17. The internal moments were the only measure of accuracy available for validation of the FEA results.

Table 18 – Sensitivity Analysis Matrix (Shaded areas indicate the choices being analyzed)

Case	Girder				Slab & Haunch			Loads	Reinforcing			Studs	Constraints				Contacts		Run name using 10 processors	Total run Time (min.)
	Shell Elements	Solid Linear Elements	Solid Quadratic Elements	Second Order Accuracy	Solid Linear Elements	Second Order Accuracy	Solid Quadratic Elements		SMC Live Load	Truss Elements	Solid Linear Elements		Beam Elements	Linear Beam Elements	Embedded Reinforcing	Tied Reinforcing	Embedded Studs	Tied Studs		
1	1"			3"				3"			1"								CT1	26
2	1"			3"				3"			1"								CT2	26
3	1"			3"				3"			1"								CT3	26
4	1"					3"		3"			1"								CT4	208
5		1"		3"				3"			1"								CT5	43
6	1"			3"				3"			1"								CT6	21
7	1"					3"		3"			1"								CT7	222
8		1"		3"				3"			1"								CT8	48
9	1"			3"				3"			1"								CT9	21
10	1"					3"		3"			1"								CT10	123
11		1"		3"				3"			1"								CT11	38
12	1"			2"				3"			1"								CT12	27
13	1"					2"		3"			1"								CT13	1505
14		1"		2"				3"			1"								CT14	174
15	1"			3"				3"			1"								CT15	26
16	1"					3"		3"			1"								CT16	191
17		1"		3"				3"			1"								CT17	50
18	1"			3"				3"			1"								CT18	19
19	1"					3"		3"			1"								CT19	134
20		1"		3"				3"			1"								CT20	30

Table 20 – Sensitivity Analysis Matrix (continued)

Case	Girder				Slab & Haunch			Loads	Reinforcing			Studs	Constraints				Contacts	Run name using 10 processors	Total run Time (min.)
	Shell Elements	Solid Linear Elements	Solid Quadratic Elements	Second Order Accuracy	Solid Linear Elements	Second Order Accuracy	Solid Quadratic Elements		SMC Live Load	Truss Elements	Solid Linear Elements		Beam Elements	Linear Beam Elements	Embedded Reinforcing	Tied Reinforcing			
21	1"	3"								3"-Q	1"							CT21	32
22	1"				3"					3"-Q	1"							CT22	732
23	1"	3"								3"-Q	1"							CT23	66
24	1"	3"								3"-Q	1"							CT24	17
25	Q	3"								3"-Q	1"							CT25	28
26	1"				3"					3"-Q	1"							CT26	194
27	1"	3"								3"-Q	1"							CT27	11
28	Q	3"								3"-Q	1"							CT28	31
29	1"	3"								3"-Q	1"							CT29	14
30	Q	3"								3"-Q	1"							CT30	23
31	1"	3"								3"-Q	1"							CT31	N/A
32	Q	3"								3"-Q	1"							CT32	N/A
33	1"	3"							3"-3D		1"							CT33	348
34	1"				3"				3"-3D		1"							CT34	183
35	1"	3"							3"-3D		1"							CT35	57
36	1"	3"									1"							CT36	34

1" = 1" element size, etc.

Q = Quadratic elements

The results of the sensitivity analysis provided information on the correctness of the internal forces and deflections, run times and quantity of increments required to complete the analysis. Also discovered during the sensitivity analysis were schemes of element type combinations, which failed to produce useable results or much less, run at all.

Internal moments were the primary measure of acceptability of a particular run or runs. A large number of increments indicate convergence issues, which were to be expected when using higher order elements, however, convergence issues also occurred with contact interactions. If contacts had no effect on the overall behavior of a model, they were omitted and run time decreased, sometimes considerably.

Since the cantilever section of the model is statically determinate, the moments at various points along these sections must be correct if calculated by hand using statics. Based on comparison of moments along the span for the various sensitivity models to the moments based on hand calculations, the models that compared well were numbers 4, 7, 16, 19, 22, 33, 34 and 36 as shown in the plot in Figure 45. A summary of the runs, execution times and number of increments for these models is shown in Table 20.

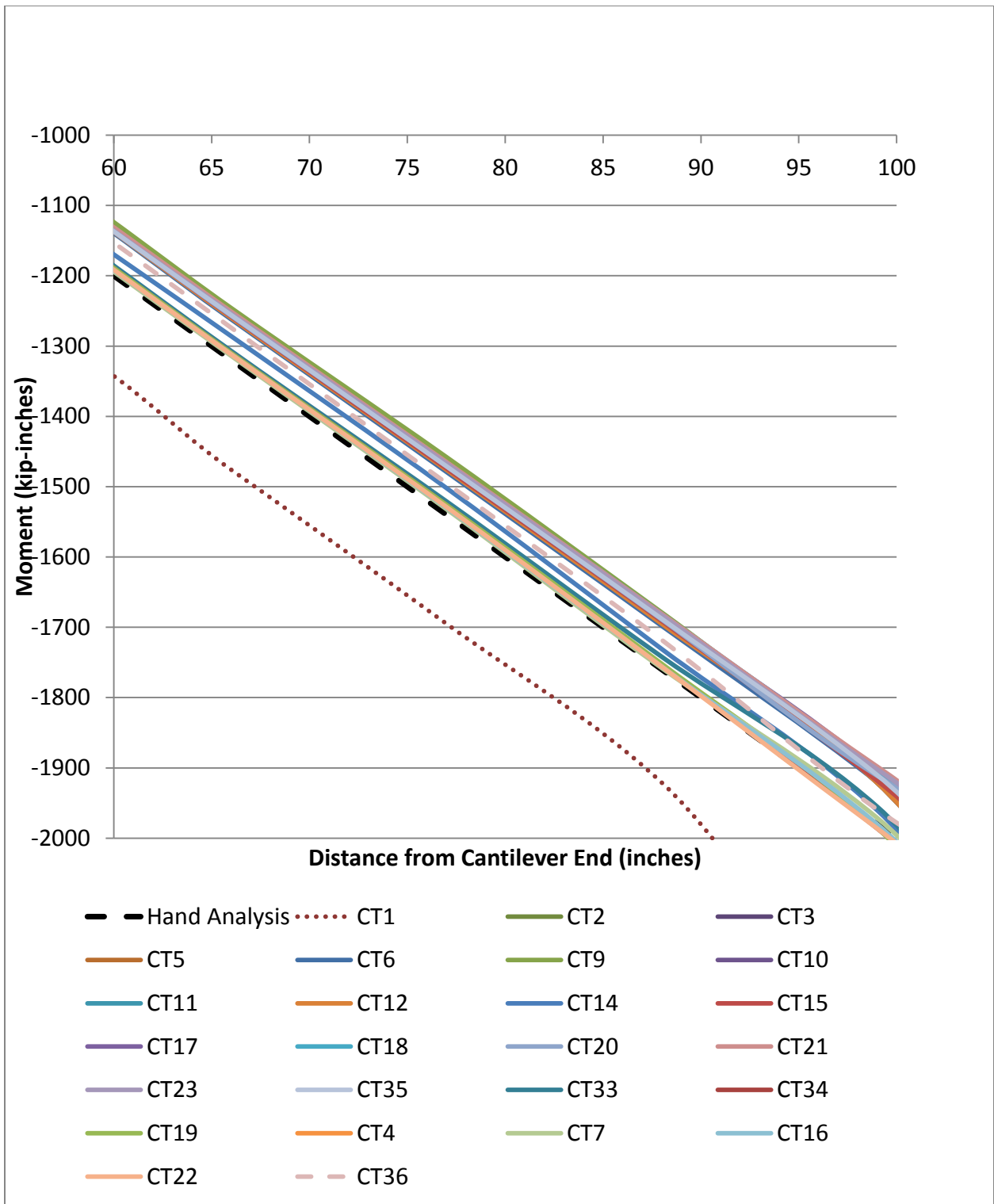


Figure 45 - Comparison of Bending Moments from Sensitivity Analysis

Table 20 - Sensitivity Analysis - Comparison of Increments and Run Times

Sensitivity Model Number	Execution Time (minutes)	Number of Increments
4	208	556
7	222	611
16	191	471
22	732	577
33	348	989
34	183	678
36	34	354

Reviewing Table 20, the run with the shortest execution time is number 36; this was the only run to use solid linear elements for the reinforcing bars in lieu of the supposedly simpler truss and beam elements. It's interesting to note that none of the runs that used smaller meshing for the slab (12, 13 and 14, where the element size is noted in the shaded box) provided any more accurate results than the runs with the coarser meshing of the slab. The finer meshed slabs also had the highest run times, between four and eight times longer than for the coarser meshed slabs.

4.5 FINITE ELEMENT ANALYSIS OF THE STUDY GIRDER CONNECTION

4.5.1 Basic Finite Element Modeling

Based on the results of the sensitivity analysis, the finite element model of the study connection was created. From the sensitivity analysis, the element types and sizes given in Table 21 were selected for the respective parts.

Table 21 - Final Part Element Types

Part	Element Type	Element Size
Girder and Stiffeners	Linear brick elements	1 inch
Shear Studs	Beam elements	1 inch
Slab and Haunch	Linear brick elements	3 inches
Reinforcing Steel	Linear brick element	3 inches
Sole Plate	Linear brick elements	1 inch
Concrete Support Pier	Linear brick elements	3 inches
Elastomeric Bearing	Linear brick elements	0.25 inches

The constraint types selected for use between the given parts are presented in Table 22.

Table 22 - Final Constraint Types

Master	Slave	Constraint Type
Slab and Haunch	Reinforcing Steel	Embed
Slab and Haunch	Shear Studs	Embed
Steel Girder	Welds to Sole Plate	Tie
Sole Plate	Welds to Steel Girder	Tie

The interaction types selected for use between the given parts are given in Table 23.

Table 23 - Final Interaction Types

Master	Slave	Interaction Type
Load Application Beams	Slab and Haunch	Hard Contact – $\mu = 0.4$
Sole Plate	Steel Girder	Hard Contact – $\mu = 0$
Elastomeric Bearing	Sole Plate	Hard Contact - $\mu = 0.2$
Concrete Support Pier	Elastomeric Bearing	Hard Contact – $\mu = 0.2$
Steel Girder	Slab and Haunch	None

Notes on interactions:

1. μ is the coefficient of static friction.
2. A value of $\mu = 0$ was used for contact between the bottom of the steel girder and sole plate to ensure that the total axial load component of the SMC behavior is transferred through the welds to the sole plate. Although somewhat unrealistic, it would also have been unconservative to consider friction as resisting part of a load that may possibly overload the connection.
3. No interaction was necessary between the girder and slab since the two are constrained by the studs being embedded in the slab.

The final model was used to help predict and anticipate the behavior of the physical test.

The initial finite element model of the study connection is shown in Figure 46.

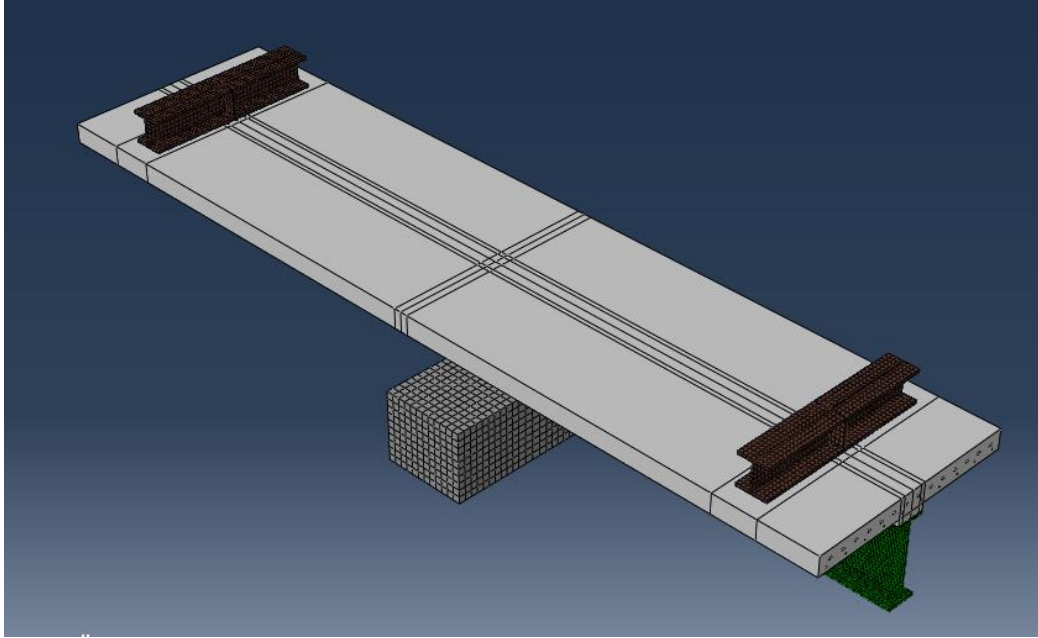


Figure 46 – Modeling of Study Connection

4.5.2 Loads and boundary conditions

The FEA loads were applied in two steps. In the first step the dead load of the structure was applied. The second step induced a moment in each girder to simulate the effects of the controlling design truck. In order to correctly represent the physical test model, the dead loads of model elements had to be considered in ABAQUS. The dead loads of the model consisted of the self-weight of the load application beams, slab and haunch, reinforcing bars, steel girders and steel studs. In lieu of using mass densities, unit weights were used with a gravity acceleration of -1 inch/second^2 . The truck loading to be applied was a 90.0 kip concentrated load acting on each of the load application beams.

Boundary conditions consisted only of x, y and z support reactions at the bottom of the pier. Since all elements of the FEA model were tied together and all loads were concentric and symmetric, no stabilizing boundary conditions were necessary. While the physical model had

bottom flange stabilizers at the ends of the cantilevers, no such supports were necessary in the FEA model as it did not buckle laterally.

4.5.3 Contacts and Constraints

Contacts on the model of the SMC connection were created between the anchor bolts and the holes in the sole plate, the anchor bolt nuts and the top of the sole plate, the bottom of the steel girders and the top of the sole plate and the bottom of the sole plate and the top of the pier (Figure 47). Contact was also created between the bottom of the load application beam and the top of the slab.

Tie constraints were used between the girder bottom flanges and the welds and between the welds and the sole plates (Figure 47). Tie constraints were also used between the headed studs on the top of the girder and the concrete slab, thus enforcing the composite behavior of the girder and slab (Figure 48). Embedded region constraints were used to define the top SMC reinforcing and the bending/shrinkage reinforcing in the slab (Figure 48).

It should be noted that preliminary Abaqus analyses, with the elastomeric bearing plate modeled, failed to converge due to its excessive displacement, thus, for the final model it was omitted.

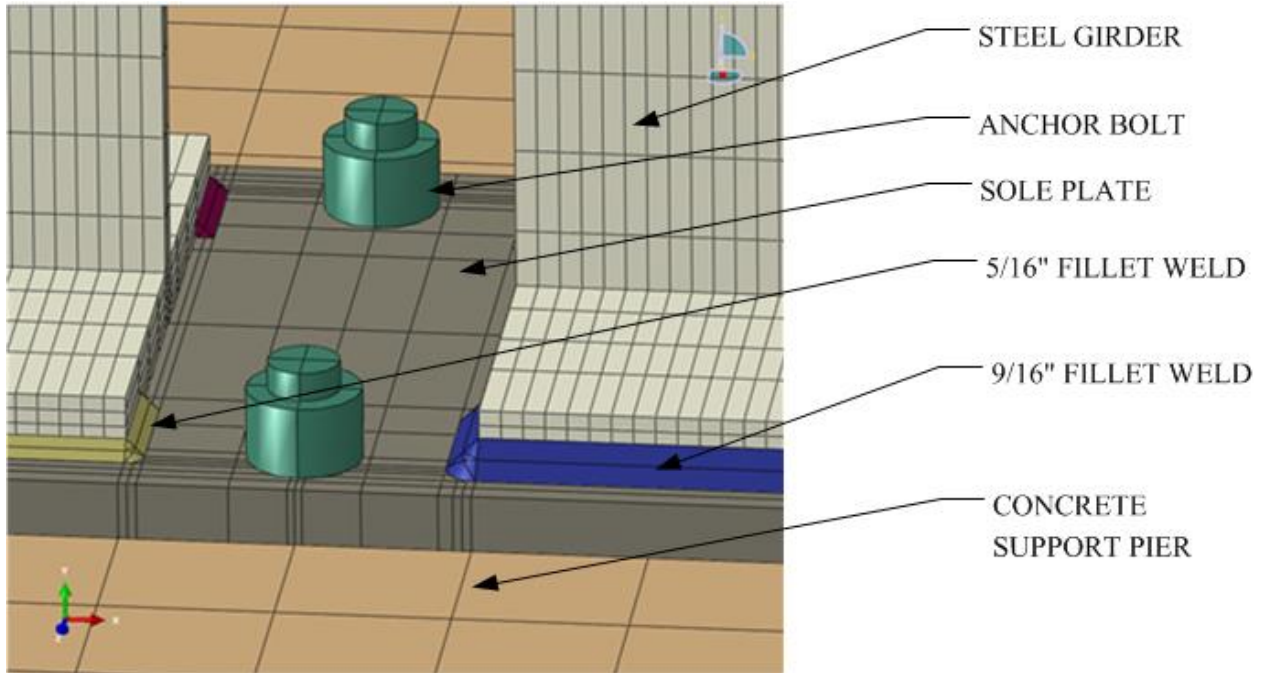


Figure 47 - Contacts and Constraints at Support Pier

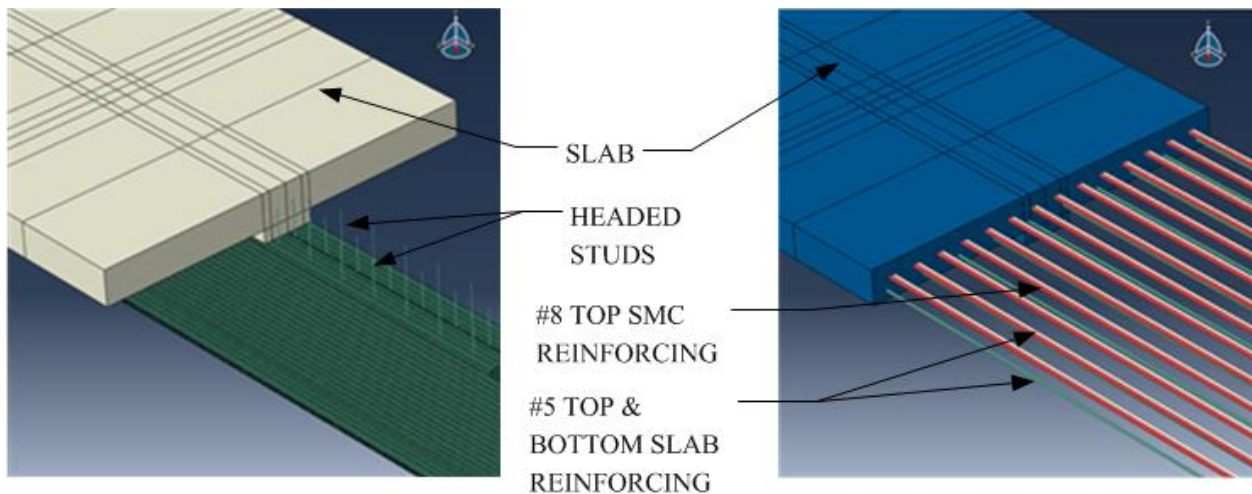


Figure 48 - Slab, Studs and Reinforcing Constraints

4.5.4 Convergence Criteria

Convergence in Abaqus is a function of solution method, convergence tolerances, number of equilibrium iterations allowed before time cutbacks are made and factors for time cutbacks. The solution method chosen for the analysis was the direct method instead of iterative since the structure will have a sparse stiffness matrix due to its geometry and creation technique,

which went through multiple revisions and modifications. The direct solver uses a “multi-front” technique which may have reduced computational time. The matrix storage method was chosen as the solver default, which is the unsymmetric method; the unsymmetric method enforces the use of Newton’s method as the numerical technique for solving nonlinear equations.

Convergence tolerances were ‘loosened’ to account for the nonlinear behavior of the slab and its interaction with the shear studs and reinforcing. Additionally, numbers of increments available for each particular step were modified depending on the magnitude of load to be applied in the step. The larger the load, the more likely that the time increment would require reduction to converge and if enough increments were not allowed the run would have terminated prematurely.

4.5.5 Discussion of Results

The model completed successfully with a combination of the model dead load and a simulation live/superimposed dead load of 90 kips at each end. The run required a total of 137 increments, one for the gravity effects of the dead load of the model and the remaining 136 for analysis of the effects of the two symmetrically placed 90 kip loads.

4.5.5.1 Internal Force Results

The FEA moment induced at the center of the support was 13,560 inch-kips or 1130 ft-kips (Figure 49), which agrees very well with 1172 ft-kips determined in section 3.3.1 Preliminary Analysis. It is reasonable that the moment from the FEA would be smaller than from conventional analysis since in reality the shear in the girders diminishes as the girder begins to be supported by the sole plate whereas the conventional analysis considers the girders to be point supported at the center of the support.

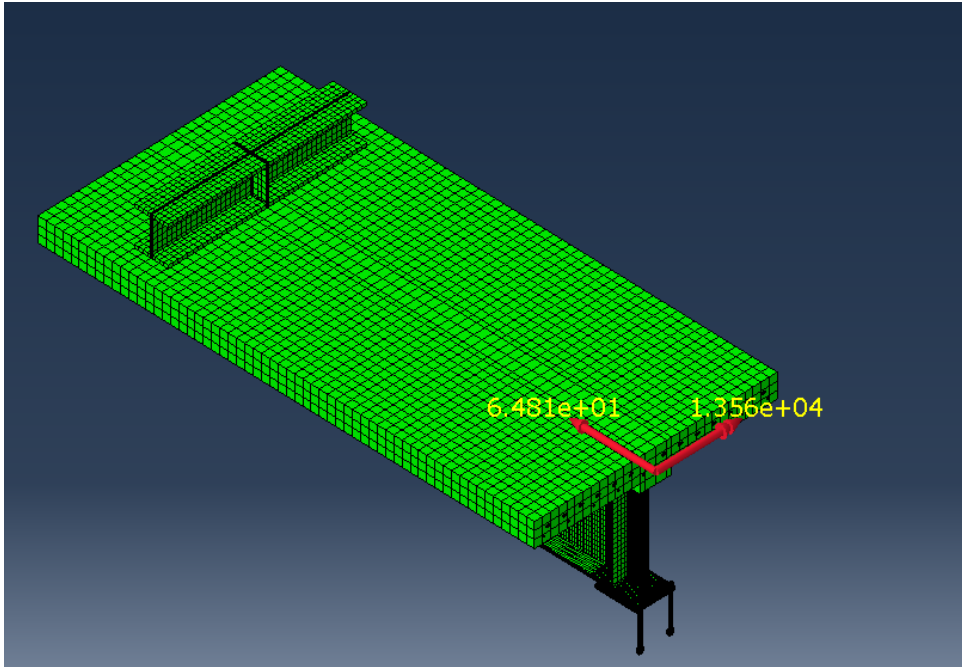


Figure 49 - Centerline Negative Moment at SMC Connection

The axial load, which is transferred by a combination of compression in the sole plate (Figure 51) and friction between the sole plate to the pier (Figure 50) is $44 + 280 = 324$ kips (service level), which corresponds to approximately 567 kips (ultimate load) using a factor of 1.75 since the majority of the load is live load. Reviewing the moment arms in section 3.3.1 Preliminary Analysis, the moment arm for the weld is 40.875 inches, which combined with ultimate weld load determined above corresponds to an ultimate moment of 1931 ft-kips, which compares well with the ultimate moment of 1978 ft-kips obtained in the aforementioned section. Again, this moment would be less than that calculated by hand for the reasons discussed in the preceding paragraph.

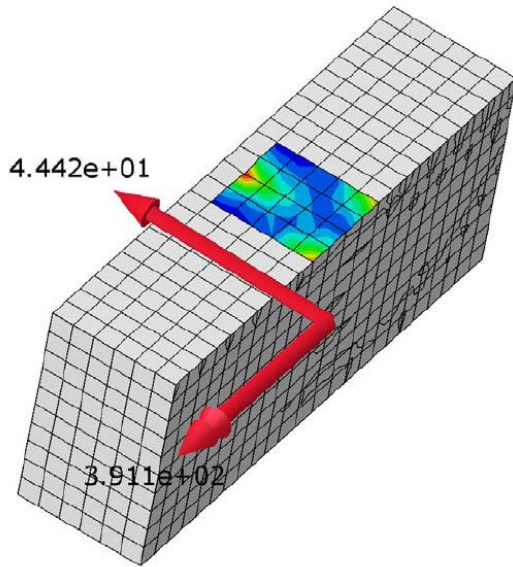


Figure 50 - Axial Force at Pier



Figure 51 - Axial Force at Sole Plate

An alternative FEA was performed on a nearly identical model, the only exception being that the slab was constructed in two parts which abutted at the center and transferred load only through contact and, thus would take only compression at the center. In this run, the moment induced at the center of the support was somewhat less, 1011 ft-kips versus the solid slab case where it was 1130 ft-kips. However, the combined compression and frictional axial loads at the center of the connection were 324 kips, exactly the same; this implies that whether or not the concrete is capable of transferring any tension over the support, the force in the welds will be the same.

4.5.5.2 Material Behavior

Behavior of the material models used was verified by using ABAQUS stress plots at various stages in the analysis.

The stresses in the top of the concrete slab are shown in Figure 52, Figure 53 and Figure 54 at dead load application, 75% of concentrated load application and 100% of concentrated load application, respectively. Based on the ‘Damaged Plasticity’ model, the maximum tensile stress

that the slab may take is 0.50 ksi (Figure 34); once the tensile stress has reached 0.50 ksi and more load is applied, the stress decreases and redistributes elsewhere in the slab or goes to the reinforcing steel; the decrease in tensile stress is apparent in the latter two figures.

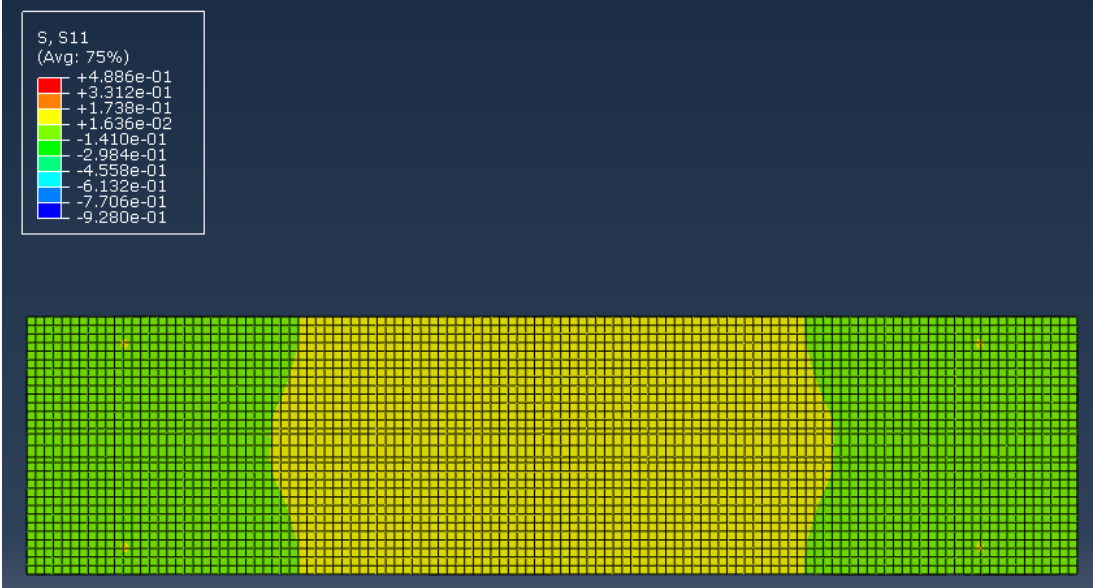


Figure 52 - Concrete Surface Axial Stress after Dead Load Application

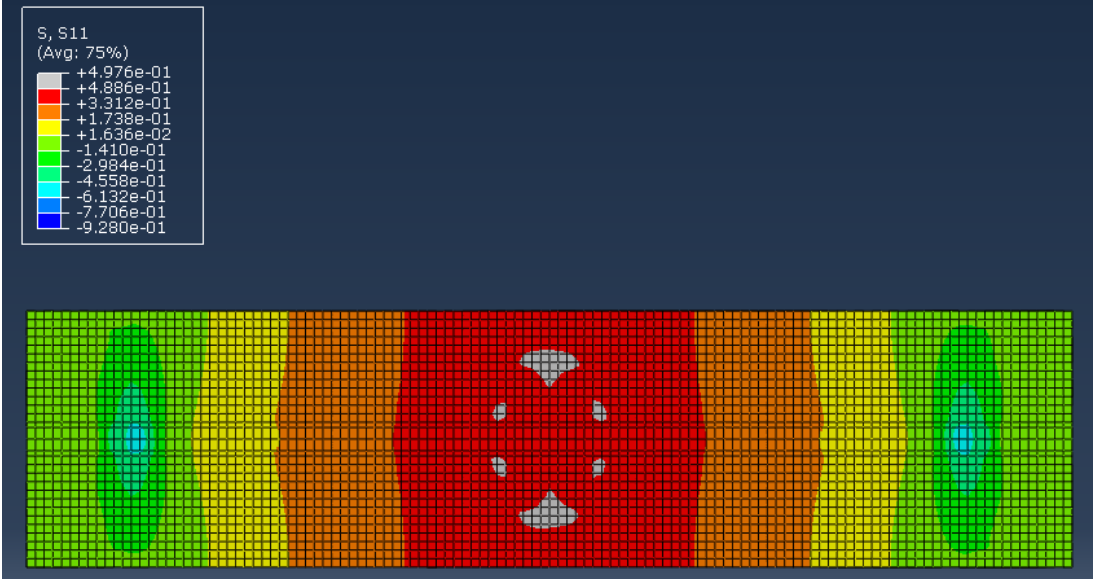


Figure 53 - Concrete Surface Axial Stress after 75% of Concentrated Load Application

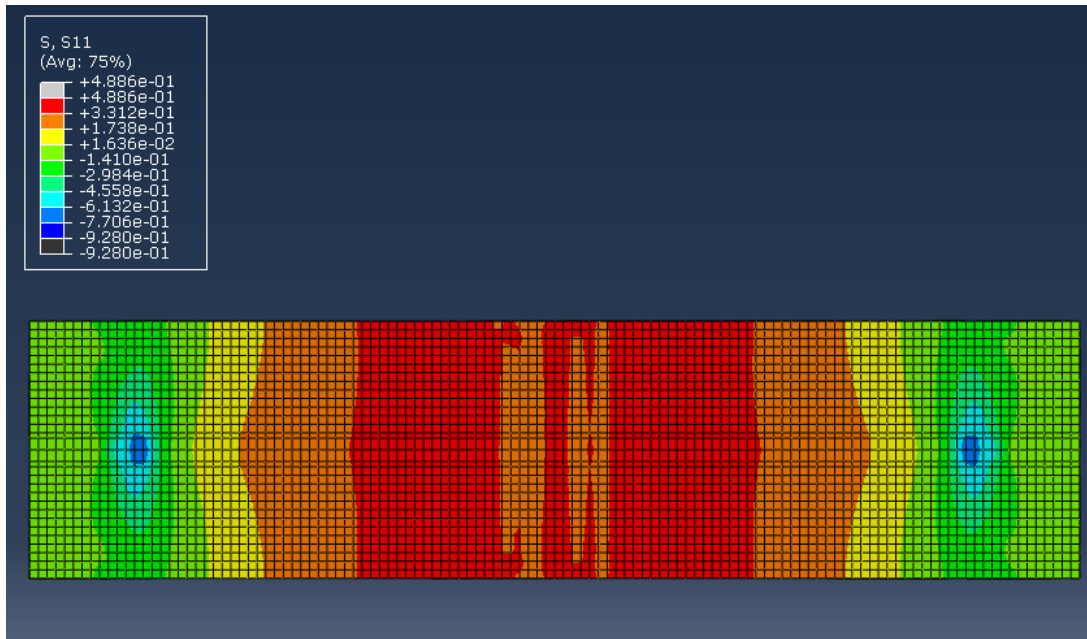


Figure 54 - Concrete Surface Axial Stress after 100% of Concentrated Load Application

The fillet welds to the sole plate, which are the critical element in the SMC behavior, were evaluated for von Mises stress at various stages of the analysis. Specific stages selected were the end of the dead load application (Figure 55), at 75% of the concentrated load application (Figure 56) and 100% of the concentrated load application (Figure 57). None of the von Mises stresses exceeded the ultimate weld stress, $F_u = 70$ ksi, although several exceeded the AWS yield stress, $F_y = 58$ ksi, but by less than 10%.

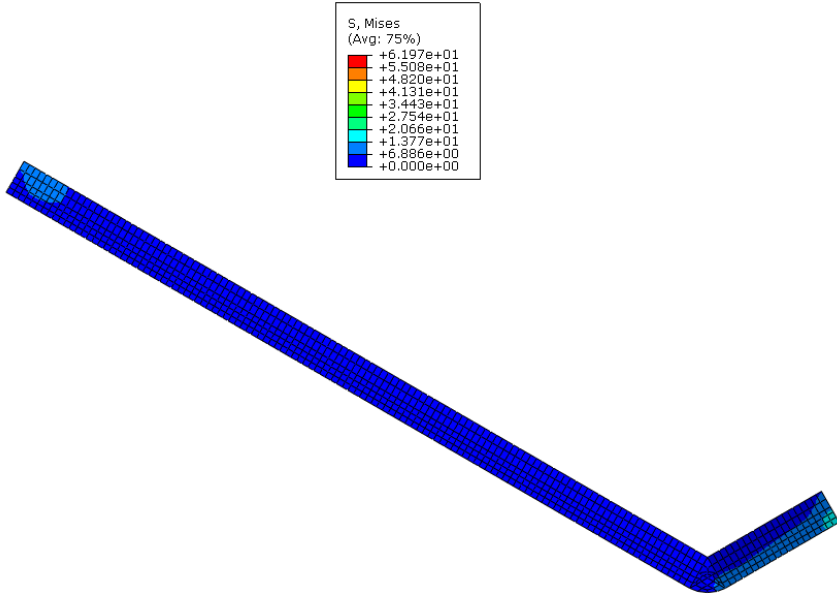


Figure 55 - von Mises Stress in Weld after Dead Load Application

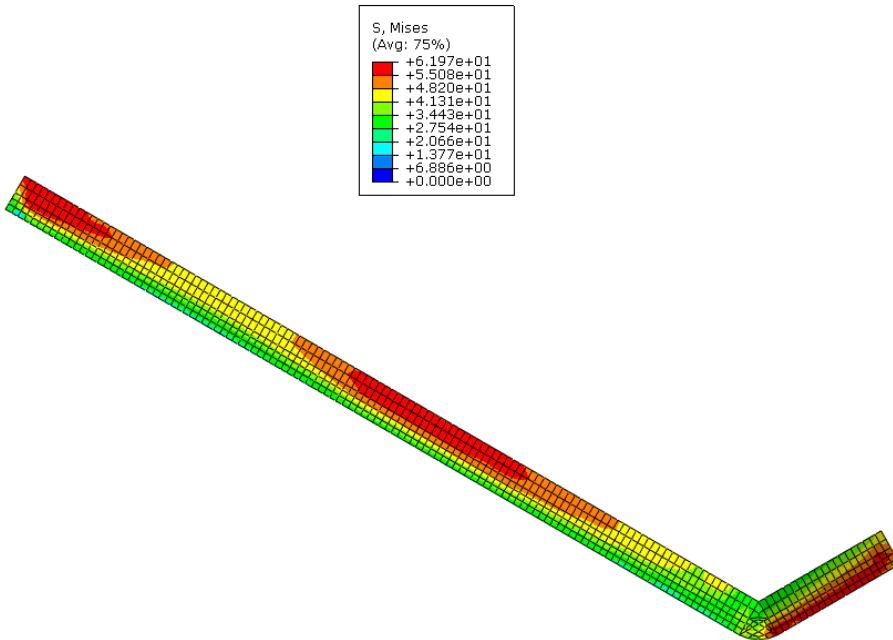


Figure 56 - von Mises Stress in Weld after 75% of Concentrated Load Application

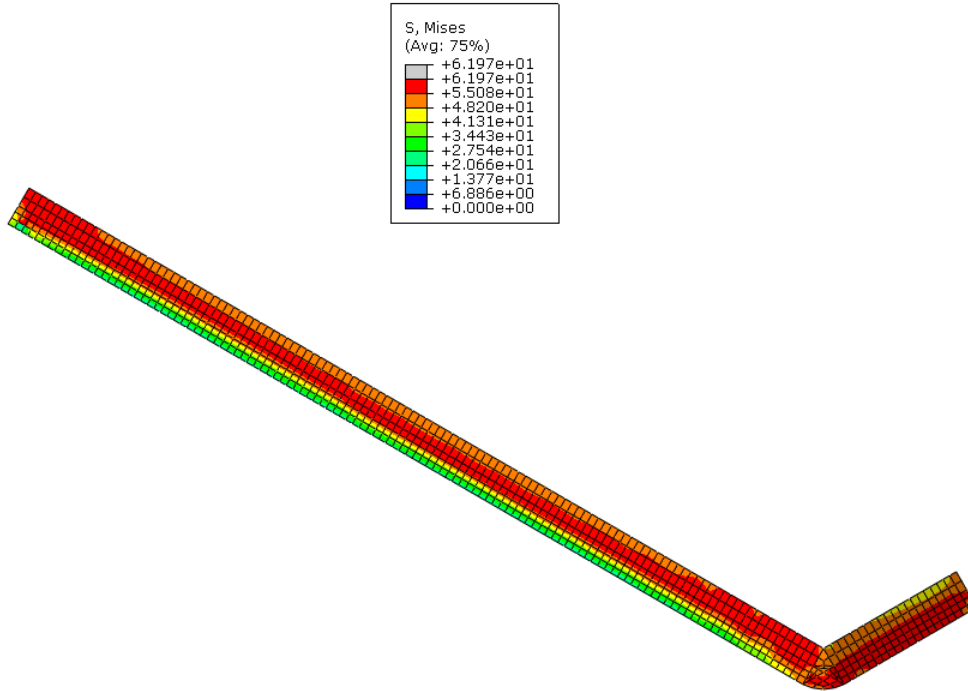


Figure 57 - von Mises Stress in Weld after 100% of Concentrated Load Application

4.5.5.3 Results for Test Reference

Load, displacement and strain data were gathered from the FEA in order to correlate the analysis with the physical test model. However, when compared to the final physical test results, the displacements, stresses and forces determined from the FEA, did not correspond well at all; this is discussed further in 5.7.4 Comparison with Abaqus Results.

CHAPTER 5 PHYSICAL TEST

5.1 LAB DESCRIPTION AND CONSTRAINTS

The physical would be performed in the Structures Lab at the CSU Engineering Research Center. The test was to consist of a double cantilever girder loaded by hydraulic actuators at each end. In order to verify its adequacy for the test, the existing structure required analysis. The floor of the structural lab consists of two areas, one with a 5" unreinforced slab on grade and the other with a heavy load application slab ("strong floor") as the base for all testing. The heavy slab is 24 inches in thickness, reinforced top and bottom with #9 bars at 12 inches each way. An assessment of the heavy load application slab was made and it was determined that a self-reacting load frame would be necessary to perform the testing.

5.2 SELF-REACTING LOAD FRAME

A self-reacting load frame offered several benefits; its location is not restricted to placement on the heavy slab since the only loads it imparted to the slab was its self-weight and the self-weight of the model and test equipment. Also, it was able to be positioned significantly closer to the rolling door for bringing in the structural steel and the concrete truck was able to back directly up to the pour areas. Detailed drawings of self-reacting frame are provided in Appendix 5 – Self-Reacting load frame.

The self-reacting frame was designed to support a total test load of 440 kips in order to match the capacities of the existing actuators used. Thus, the frame was useful for not only the bridge girder test, but will remain useful for other load tests where the heavy floor load carrying capacity is not adequate. The final constructed frame is shown in Figure 58 with the bridge girders installed.



Figure 58 - Self-Reacting Load Frame – Upper Frames for Actuators (March 2014)

5.3 TEST SPECIMEN DESCRIPTION

The test specimen consisted of a reinforced concrete pier supporting an anchored steel sole plate with a neoprene bearing between. The bridge girders were two cantilevered W33x152 steel beams (Figure 60), both of which were welded to the sole plate. Welds to the sole plate were different for each girder; the north girder was welded in accordance with the original bridge design, 14 inches of 5/16 inch fillet weld on each side. The 5/16 inch fillet weld was anticipated to fail at a test load of 90 to 100 kips. The south girder was welded with 14 inches of 5/8 inch fillet weld on each side, which was determined to be adequate for the bridge test and actual design loads. A partial W27x84 diaphragm beam (Figure 61) was installed on the west side the girder for stability; the beam size chosen is the same as in the actual bridge. Additionally, due to the potential for damage to the specimen and injury of personnel when the 5/16" fillet welds failed, a safety device (Figure 59) was installed between the beam ends to limit the movement of the beam at failure. The safety device when engaged would transfer the axial compression

component directly between the girder bottom flanges. During the time that the safety device would be active, no horizontal loads would be transferred to the welds or the sole plate.

The top flanges of the girders had welded headed stud anchors in rows of three at nine inches on center (Figure 60). The concrete slab was reinforced top and bottom in both directions as in the actual bridge slab (Figure 62). The slab width was 7'-4", the same as the effective slab width allowed per AASHTO (2012), one half of the spacing between girders on each side (Figure 63). Load application beams were installed and anchored near the ends of both cantilevers to accept the actuator and load cell arrangements. The load application beams were anchored to the slab with a total of (6) ½ inch diameter wedge anchors each to keep them from displacing horizontally. The load application beams were sized to uniformly distribute the load from the actuator over a width of 72 inches of slab. The loads were applied by a 220 kip actuator at the north end (Figure 64) and two 110 kip actuators at the south end (Figure 65).

The dimensions of the final physical test model of the study girder connection were set to match those of the finite element analysis. The selected connection also matched that built in the field, but with shortened girder lengths and load magnitude and application points calculated to create the same resultant moments and reaction at the pier. A plan of the tested model is shown in Figure 66. The entire set of drawings for the construction of the test specimen is provided in Appendix 3 – Model Construction Drawings.

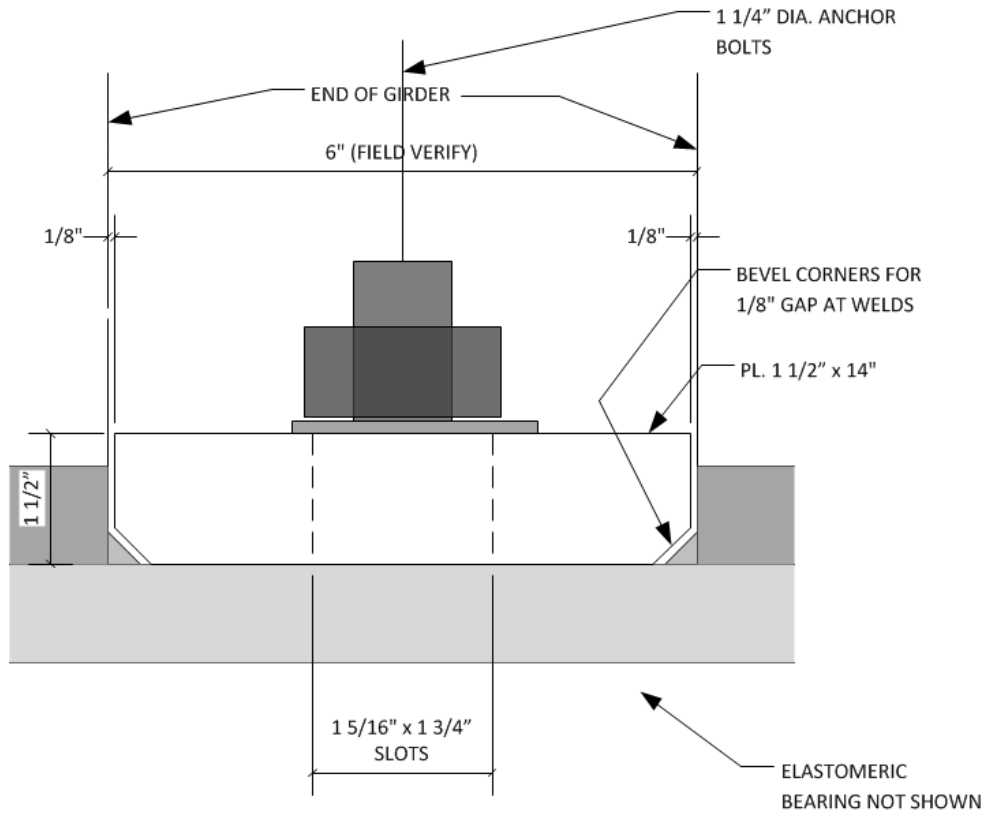


Figure 59 - Safety Device Details



Figure 60 - Bridge Girders with Studs (March 2014)



Figure 61 - Steel Diaphragm Beam (March 2014)



Figure 62 - Slab Reinforcing Placement (March 2014)



Figure 63 - Concrete Deck Slab (April 2014)



Figure 64 - 220 kip Actuator and Load Application Beam (May 2014)

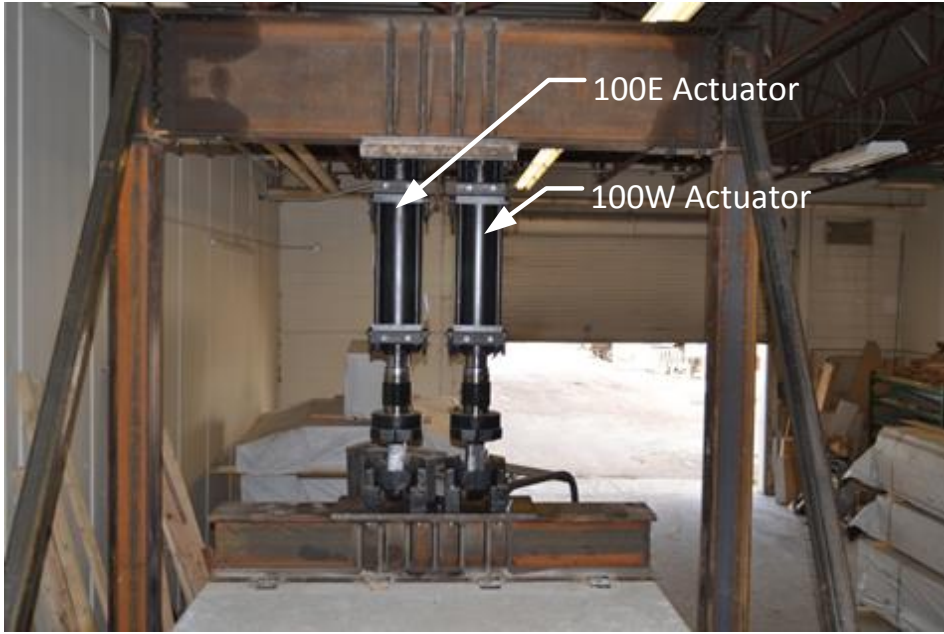


Figure 65 - (2) 110 kip Actuators and Load Application Beam (May 2014)

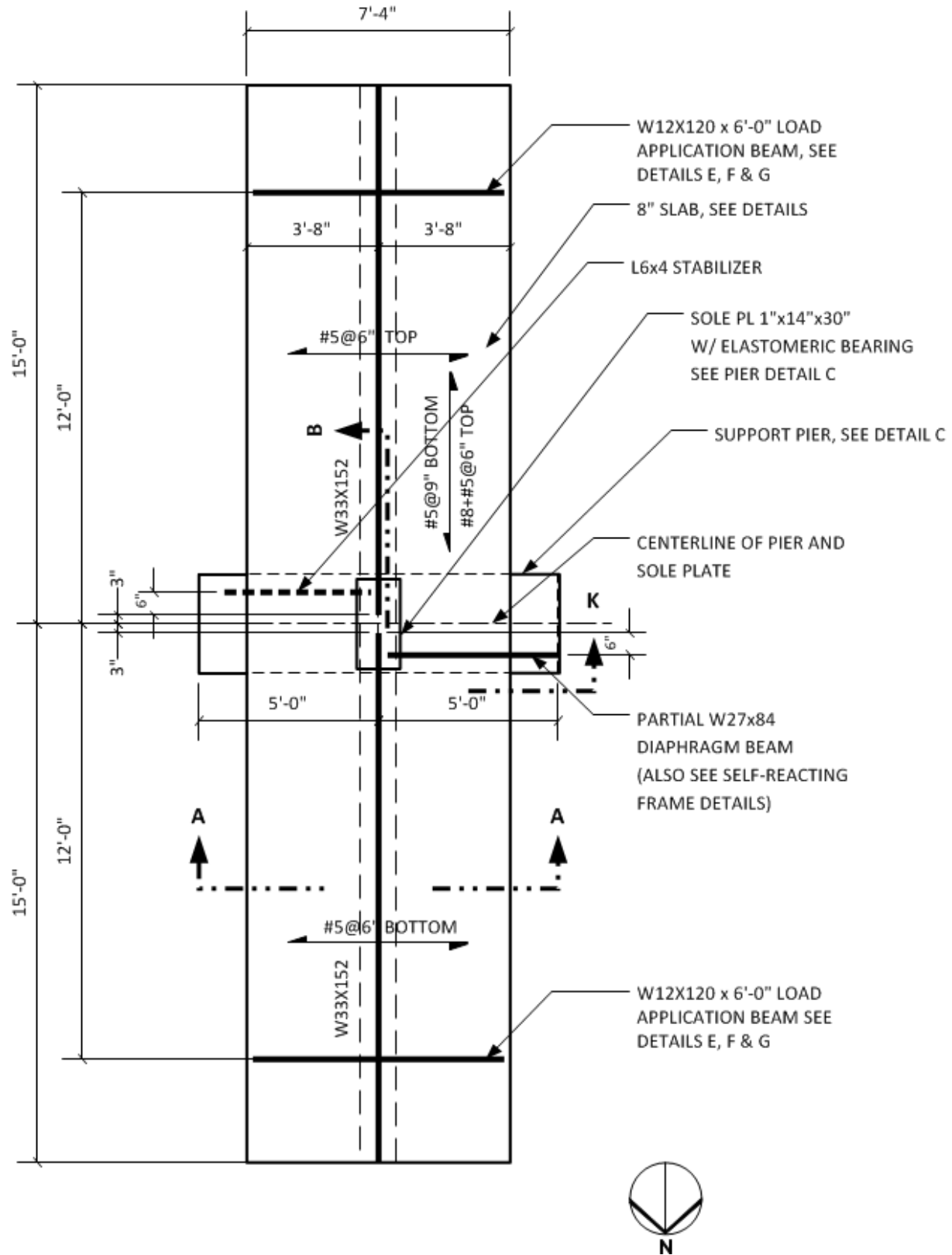


Figure 66 - Plan of Constructed Physical Model

5.4 TEST SPECIMEN INSTRUMENTATION

The physical test specimen was instrumented at key locations based on results of the finite element analysis for later validation of the finite element model. The physical model was instrumented with electrical surface mounted strain gages and string and linear potentiometers. The various devices were positioned as shown in Figure 68 through Figure 75; a legend is given in Figure 67. Rationale for the placement of gages is given below the figures. The numbers shown in ovals are the gage numbers and the numbers shown in rectangles are the corresponding channel numbers for the DAQ.






INSTUMENTATION LEGEND		CONCRETE SURFACE (CS)
		STEEL SURFACE LARGE (SSL)
		STEEL SURFACE SMALL (SSS)
		STEEL SURFACE ROSETTE (SSR)
		POTENTIOMETER (POT)

Figure 67 - Legend for Instrumentation Layouts

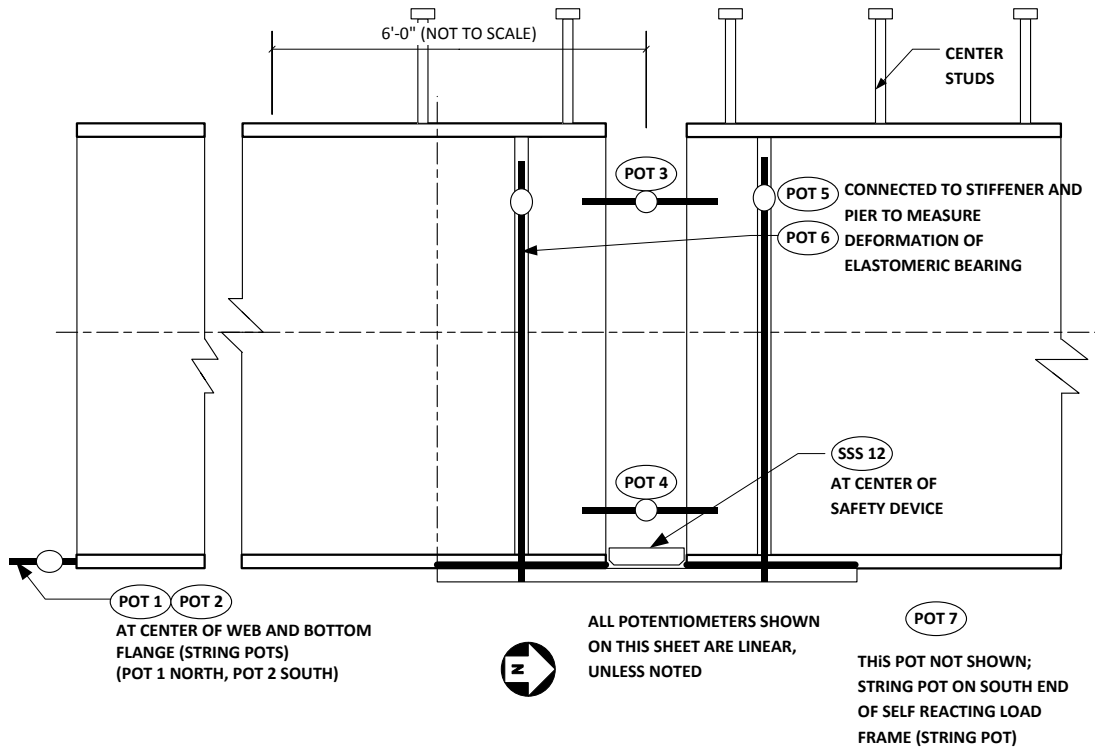


Figure 68 - Instrumentation Layout at the Girder Ends – 1

Pot 1 and Pot 2 were connected to girder ends to measure the total cantilever deflection of the bridge girders. Pot 8 was to measure the upward deflection of one of the self-reacting girders, which was in effect a cantilever beam. Pot 3 and Pot 4 were connected to the girder web near the top and bottom to determine the rotation of the girder ends. Pot 5 and Pot 6 were connected between the stiffeners and the top of the concrete pier to measure the deflection of the elastomeric bearing.



Figure 69 - Pots 3, 4, 5 and 6 in Position during Testing (July 2014)

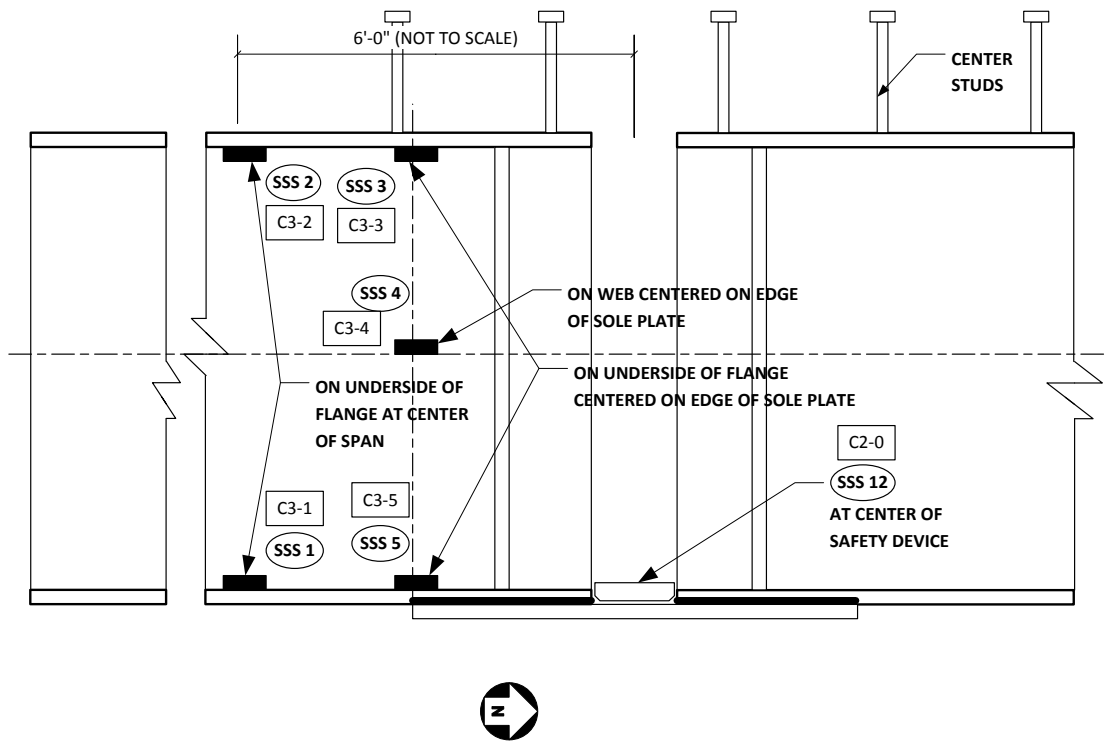


Figure 70 - Instrumentation at the Girder Ends -2

Steel girder: The areas instrumented with strain gages were to provide the strains near the connection to determine the flow of stresses in the girder in the area where the load was anticipated to transfer through the web to the bottom flange and finally to the welds.

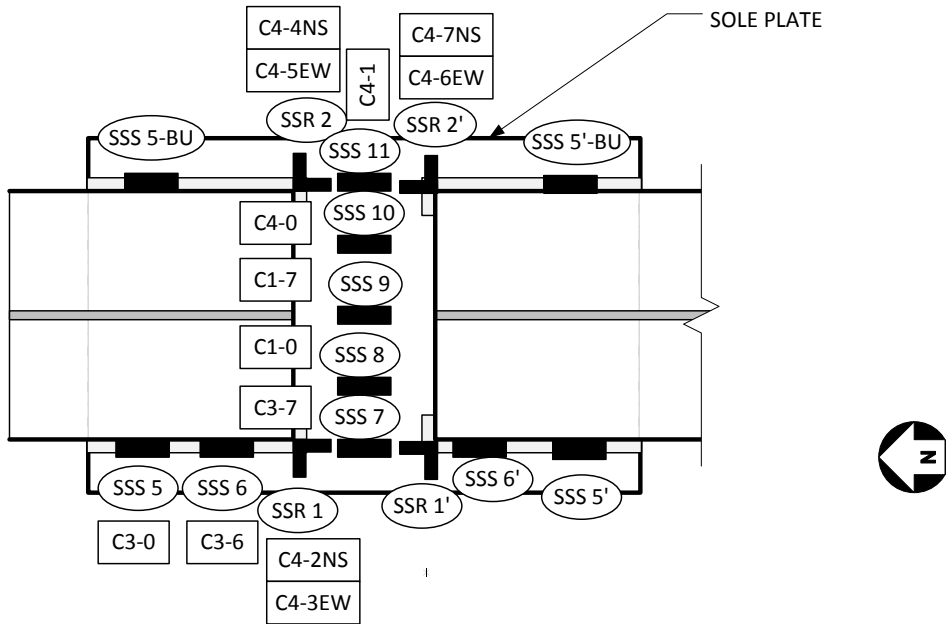


Figure 71 - Instrumentation Layout at the Sole Plate

Sole plate: The sole plate instrumentation was set up to measure the strains going through the sole plate where the compression load transfer is occurring between the girders and particularly, to measure the strains at the welds (Figure 72). As previously mentioned, the welds were believed to be the most critical parts of the SMC connection. An additional strain gage was positioned at the center of the safety device (Figure 70) to determine its loading, once it became active.



Figure 72 - Gage Placement at 5/8" Sole Plate Fillet Weld (July 2014)



Figure 73 - Strain Gage Attached to Top of Slab (July 2014)

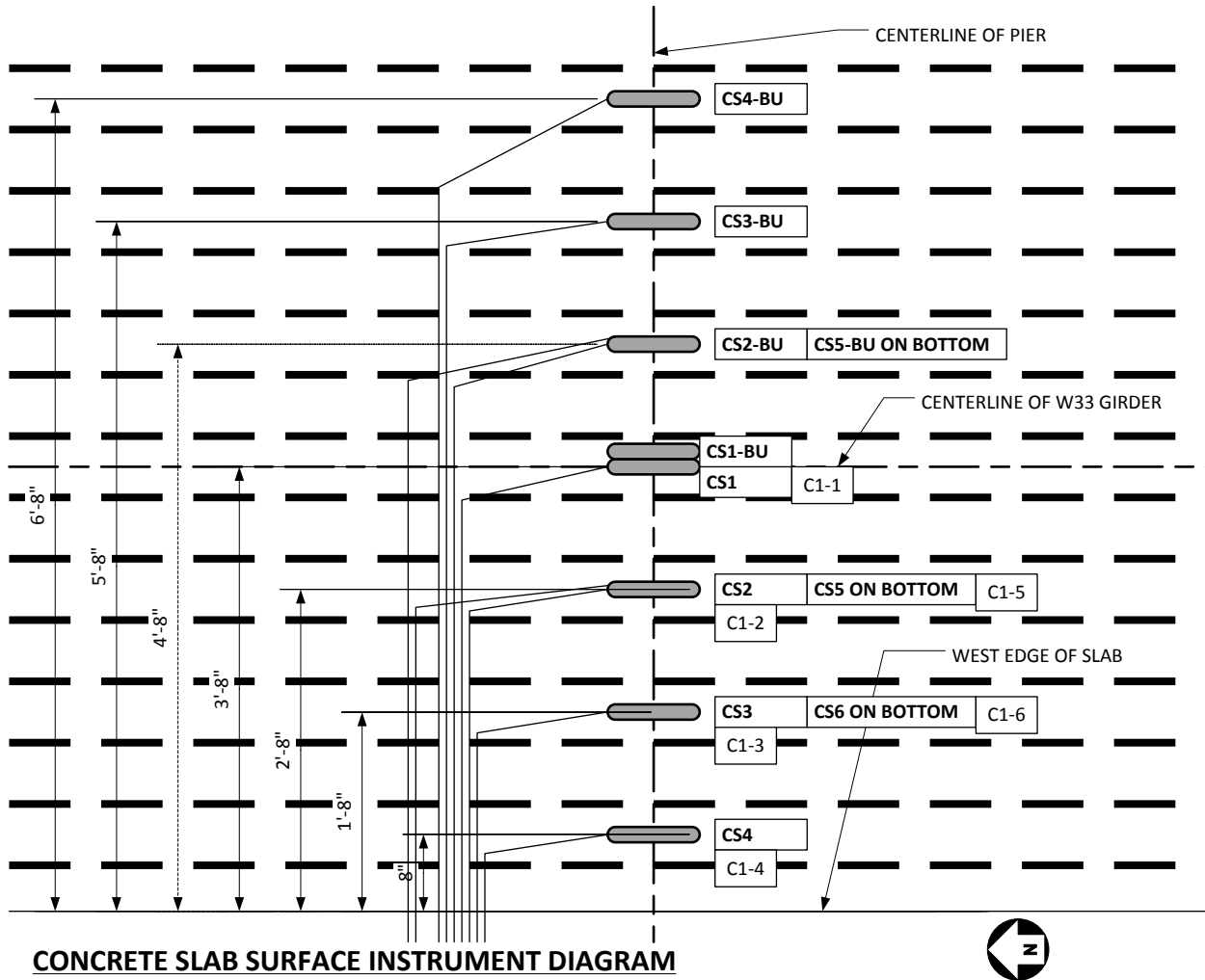


Figure 74 - Instrumentation Layout on the Top and Bottom of Slab

Top of slab: This area is instrumented to determine strains on the top and bottom of the concrete slab in order to see the effects of shear lag in the top of the slab (Figure 74 and Figure 73).

Bottom of slab: This area is instrumented to determine the strain in the bottom of the slab in order to create an accurate force balance in the end connection.

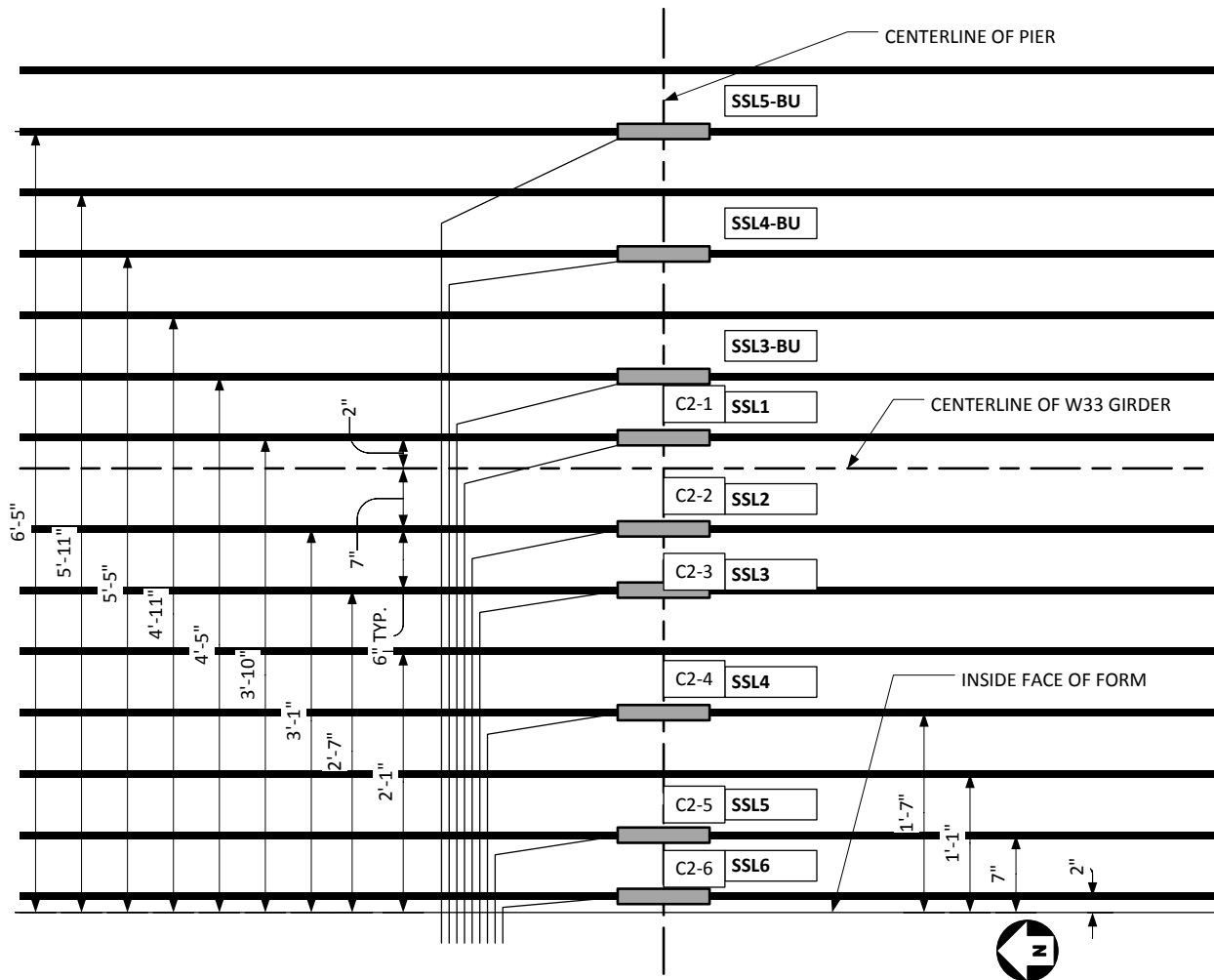


Figure 75 - Instrumentation Layout on the Slab Reinforcing

Top reinforcing bars: These bars are instrumented for strains to determine tension forces in bars and then, based on their relative locations, to observe the shear lag effects in the SMC top reinforcing and the slab (Figure 75 and Figure 76). Due to the location of shear studs on the bridge girder, the reinforcing bars could not be placed symmetrically.

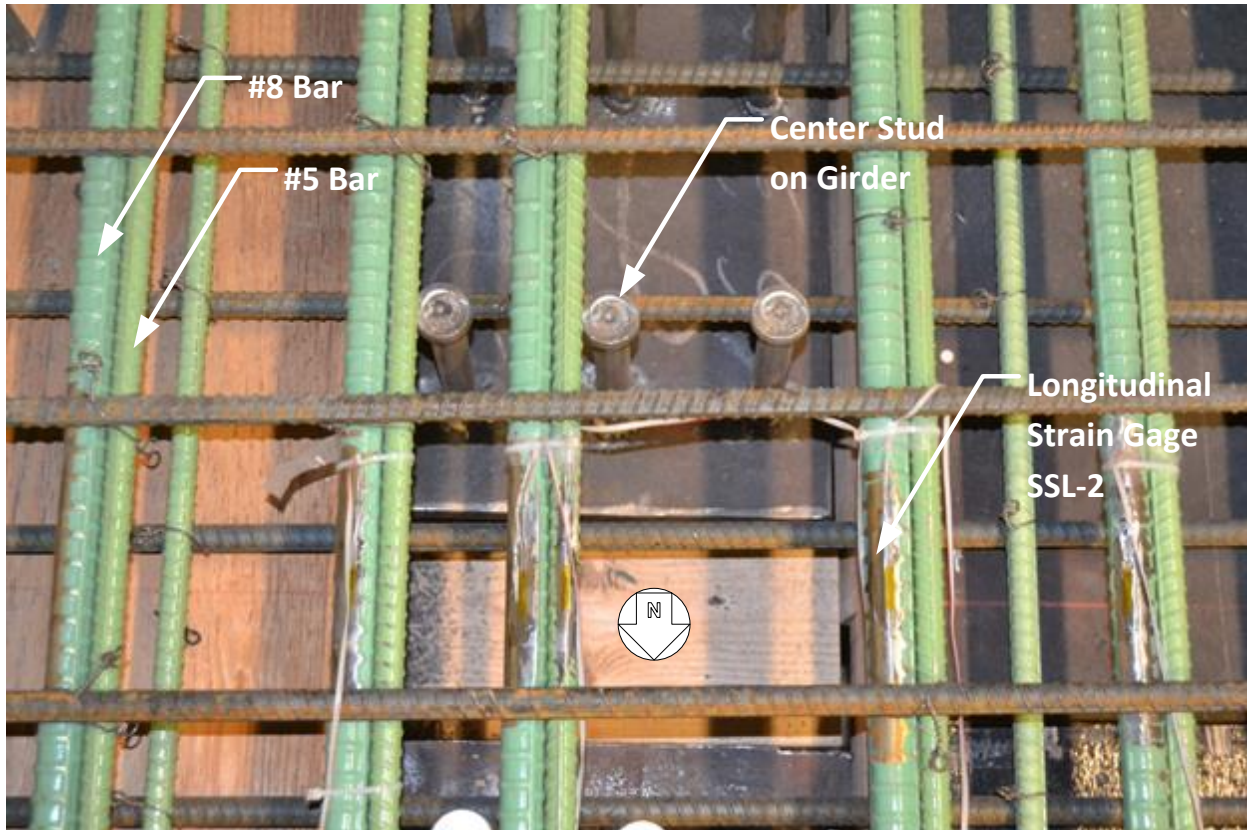


Figure 76 – Strain Gages Attached to Reinforcing Steel (April 2014)

5.5 PHYSICAL TEST

The test specimen was constructed with temporary shoring supports for each girder at center and end points. Once the concrete had attained its design strength, the shores were to be removed and during this process, the instrumentation would be tested to verify functionality and to measure strains from the dead load of the model being active. However, due to concrete shrinkage from drying and reaction with mix water, the slabs actually lifted not only themselves, but also the steel girders slightly off of the temporary supports. Due to the upward shrinkage displacement it was not possible to verify the gage functionality prior to the load test.

Following the removal of the shores, the test equipment which consisted of a MTS Flextest unit for applying load through displacement control, was started. The Flextest unit controlled all

three actuators through the use of a program to apply a displacement of 0.5 mm/minute to the load application beams. The program was written such that user intervention was required after every five minutes, which in effect required the operator to push a button after each 2.5 mm of applied displacement. The operator intervention acted as an additional safety mechanism in the event of a sudden malfunction or failure. The Flextest unit simultaneously recorded the actuator displacement, the applied force and the time. The unit was set up to record at 10 Hz, but for some reason it internally set the time increment value to 0.0996 seconds.

Data was collected with a National Instruments NI PXIe-1082 Data Acquisition Unit (DAQ). The DAQ had a limitation of 32 channels for strain gauges and eight channels for linear potentiometers. The locations of the gages and potentiometers were discussed in Section 5.4 Test Specimen Instrumentation.

The test began on Tuesday, July 22, 2014 and concluded on Wednesday, July 23, 2014. Initially, a shakedown load of 10 kips was applied at each end of the model to verify all equipment was functioning properly. The test equipment was verified to be working properly, however several gages gave questionable data; fortunately, redundant gages were already active for the suspect gages. The structure was then unloaded and the test begun.

The displacement controlled loading of the connection was begun and the bridge was gradually loaded to develop an increasing negative moment at the center of the pier. Originally, the maximum anticipated load to be applied was 90 kips in combination with the dead load moment of the model, which would develop the negative moment due to the design truck (1172 kip-feet). However, due to the lack of dead load deflection and dead load stresses due to concrete shrinkage, it was estimated that a load of 98 kips with a moment arm of 12 feet would be required in order to develop the design moment of 1172 kip-feet. It was also anticipated that

the model could possibly fail at a load of 61 kips, the load at which the failure of the welds to the sole plate were predicted. At an applied load of about 85 kips, a sudden bang was heard and it appeared that the safety device had been engaged. The loading was temporarily stopped. A visual examination of the welds indicated that no cracking failure had occurred and review of the strain gage data confirmed this. The decision was made to continue applying load to the model in an attempt to fail the north (smaller) weld.

The test continued on until a load of approximately 132 kips was applied at each end and no signs of failure or distress were evident. The load was removed from the model and the decision was made to recommence testing the following day. That evening, it occurred to the author that the sole plate may have compressed enough that the safety device became engaged; this would require a total shortening of the sole plate of 1/8 inch for which the corresponding strain would be 0.0208. A strain of 0.0208 indicates that that the sole plate had somehow entered the plastic range. Upon review of the calculations for the sole plate capacity given in Table 7, the plate appeared to have enough capacity. However, from review of Figure 7 and Appendix 2 – Hand Calculations, it was noted that the sole plate is also subjected to a moment as shown in the free body diagram in Figure 77. Due to a combination of normal stresses from the axial compression and moment, the sole plate had a theoretically applied stress of 99.3 ksi, which results in axial and bending deformation of the plate. The applied stress was well in excess of the yield stress of the sole plate, $F_y = 50$ ksi, thus the sudden failure and activation of the safety device.

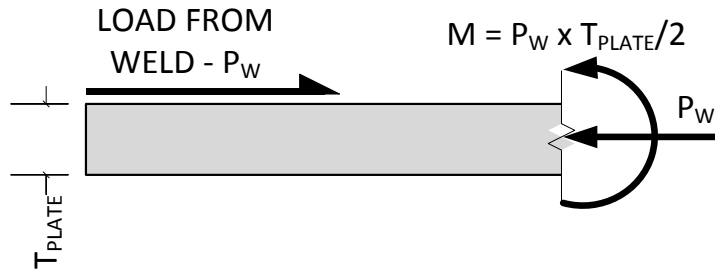


Figure 77 - Free Body Diagram of Sole Plate

The remainder of the test was basically moot as far as the welds to the sole plate were concerned since the safety device was active and thus, the axial load was transferred directly between the girder bottom flanges.

The following morning, knowing the cause of the sole plate activation, the model was jacked up and the safety device was removed. The safety device was modified by machining an additional 1/16 inch from each side. The safety device was subsequently reinstalled between the girder ends and bolted down.

A new load test was begun in which the displacement was applied at a rate of 1 mm/second, again with operator control for each step. This test was to run until either the maximum test load of 200 kips was reached or some anomaly occurred, whichever came first. At an applied load of approximately 120 kips, there was loud bang and the loading was stopped. An examination of the girder ends indicated that again the safety device had been activated and that the welds on the south end of the north girder had failed in several places. The damage was photographically documented and the strain and displacement data stored. The cracked welds are shown in Figure 78 and Figure 79. It is also interesting to note the extreme displacement of the elastomeric bearing in Figure 78.

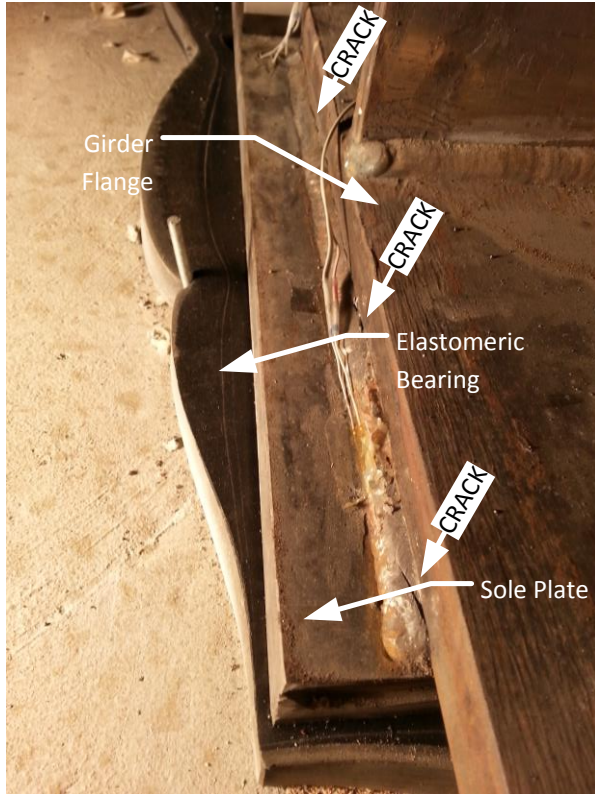


Figure 78 - Failed Weld on East Side of North Girder (July 2014)

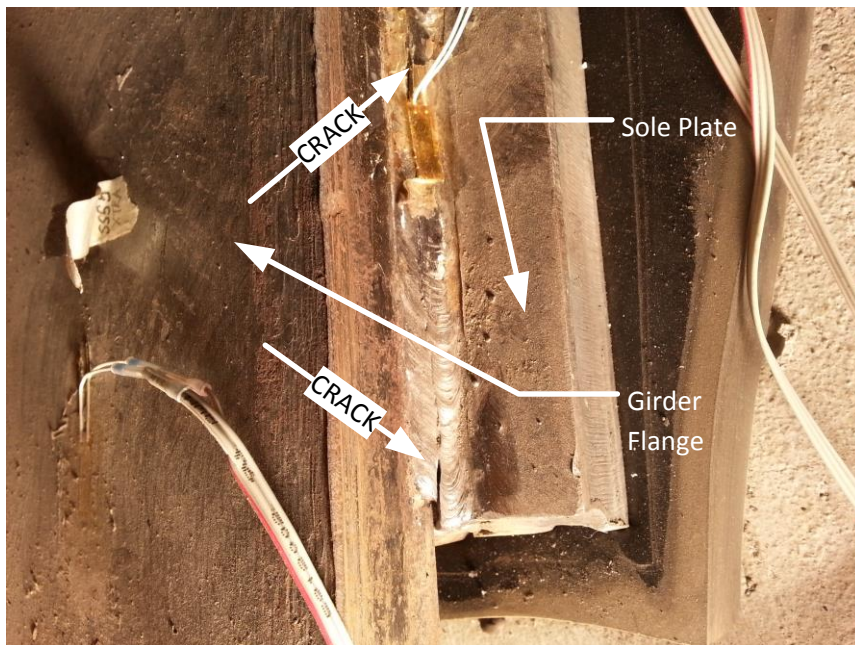


Figure 79 - Failed Weld on West Side of North Girder (July 2014)

The test was recommenced at the same displacement rate and was continued until a load of 198 kips was applied, which was deemed close enough to 200 kips. No signs of additional failure were evident after the load was removed and the model closely examined. As previously mentioned, once the safety device became active, load was transferred directly between the girder bottom flanges and thus, the welds and the sole plate were no longer loaded by any of the forces in the SMC connection.

5.6 TEST RESULTS

The test results consisted of sets of strain gage readings, potentiometer readings, load cell readings and actuator displacement data. Additionally, photographic evidence of model behavior was taken. The strain gage and potentiometer data was recorded as strain or displacement values vs. time intervals of 0.10 second. The load cell and actuator displacement readings were taken vs. time intervals of 0.0996 second as mentioned previously. In order to correlate the strain/model displacement data to the load/displacement data, the load/actuator displacement data was recalibrated to a time set at 0.10 seconds. With a consistent time scale charts of strain/model displacement vs. time and strain/model displacement vs. actuator displacement could easily be created.

Two completely different sets of data were collected, the first for the testing performed on July 22, 2014 and the second for the testing performed on July 23, 2014; these will be referred to as the Day 1 Test and the Day 2 Test, respectively from here on.

5.6.1 Day 1 Test Results

Actuator data for Force vs. Displacement for the Day 1 Test is shown in Figure 80. From review of this chart, it is evident when the safety device became activated at approximately 85 kips of applied load. Aside from the point at which activation of the safety device occurred, the

load vs. displacement curves are relatively linear for both the north and south sets of actuators. The final applied load at the end of testing was 135 kips.

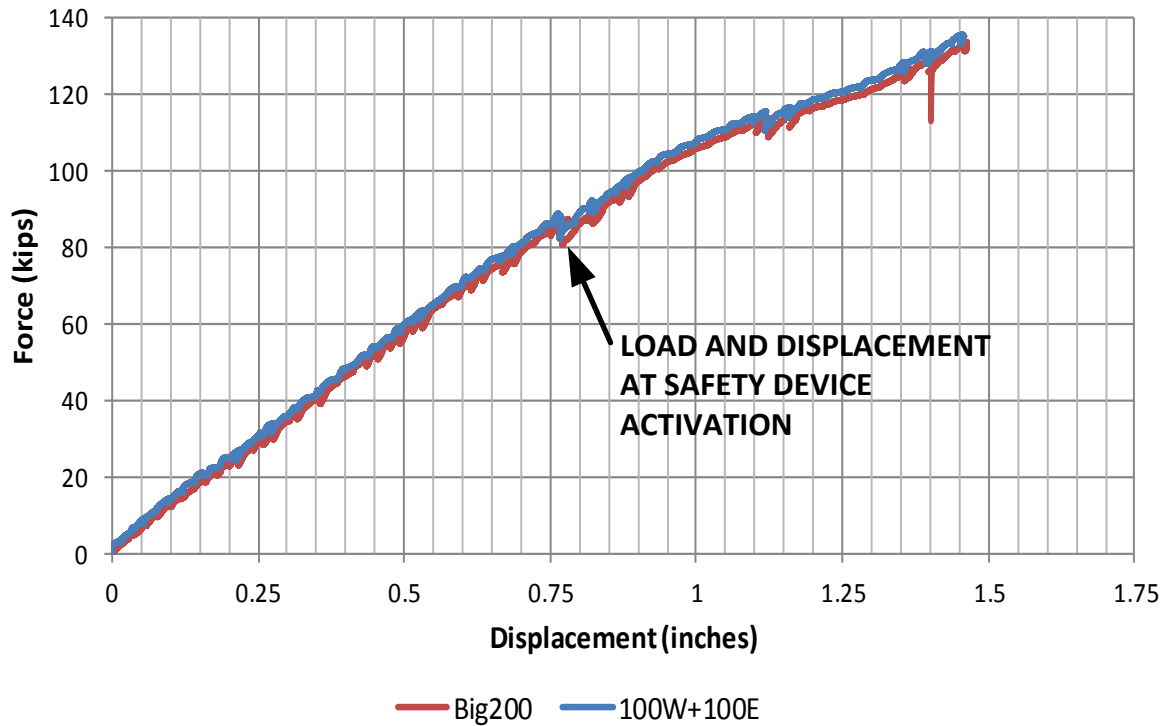


Figure 80 - Actuator Force vs. Displacement – Day 1 Test

The final strains for the day 1 test in the top SMC reinforcing bars were converted to forces and a plot of these force values is presented in Figure 81. While only the #8 bars were instrumented, each #8 bar had a #5 bar adjacent to and centered on it, so force values for the #8's alone and the #8's in combination with the #5's are plotted. From review of the forces in the reinforcing bars, there is a significant drop in the load taken by the bar near the edge of the slab as well as the center bar, SSL-1 (refer to Figure 75 for gage locations). The position of the center bar, directly over the girder, consistently showed lower force in other reports where similar testing was performed (Azizinamini A. , 2005), et al. The Abaqus analysis results also showed this same behavior. The force decrease in the bar near the edge of the slab is most likely

due to shear lag in the slab and its proximity to the edge of the slab, which is two inches away.

The ultimate capacity of a #8 plus a #5 reinforcing bar is 66.0 kips, whereas, the factored ultimate capacity is 59.4 kips. The most highly loaded set of bars is that at gage SSL-2, which has a calculated load of 55.3 kips. The load of 55.3 kips is less than the ultimate capacity of 59.4 kips, thus based on this data no yielding of the SMC reinforcing bars occurred.

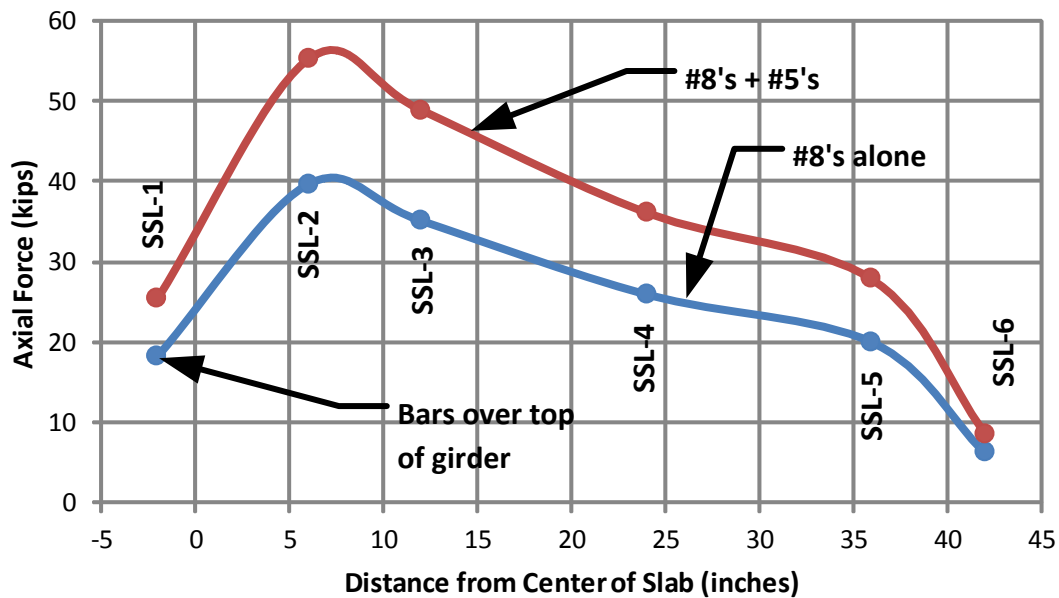


Figure 81 - Shear Lag in Top SMC Bars - Day 1 Test

Concrete top surface strain gage values were plotted vs. load and are shown in Figure 82. At an applied actuator load of 50 kips, all of the gages with the exception of CS1 (refer to Figure 74 for locations of gages), which is at the center are no longer functioning properly. Gage CS1 eventually malfunctions at an actuator force of 57 kips. The gages most likely malfunctioned due to excessive cracking or loss of bond between the gage epoxy and the concrete surface.

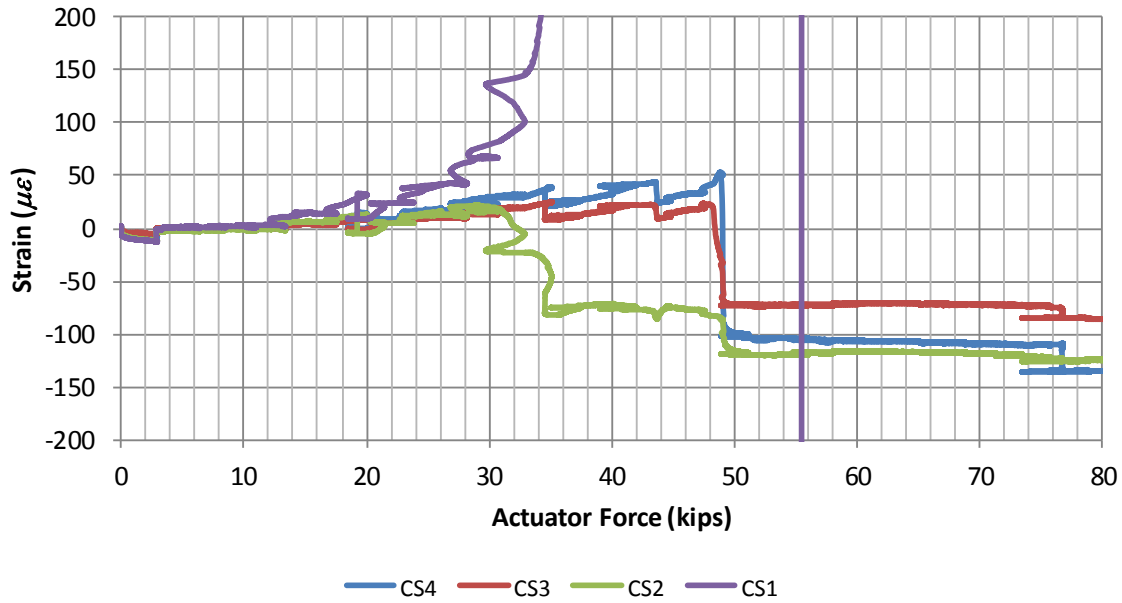


Figure 82 - Concrete Top Surface Strains vs. Actuator Force – Day 1 Test

Concrete bottom surface strain gage values are shown in Figure 83. Gage CS6 was in tension for a short time and then began to follow the trend of CS5 when it went into compression. Both gages showed a drop in strain at a load of nearly 80 kips, close to the load at which the safety device became activated. After the activation the strain at CS5, which is closer to the center of the girder, decreased and approached the values of CS6. Both gages trended toward less negative stress as the girder was loaded, which is reasonable as the neutral axis should have been moving downward.

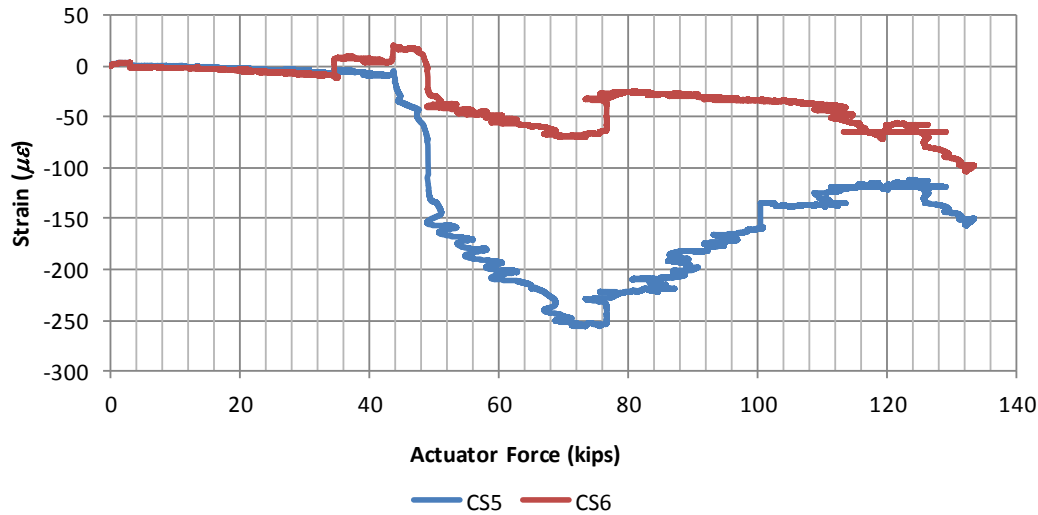


Figure 83 - Concrete Bottom Surface Strains vs. Actuator Force – Day 1 Test

Upon review of the concrete strain gage data at the locations where there were gages on both the top and bottom of the slab at the end of day 1, all four gages had readings of between -100 $\mu\epsilon$ and -150 $\mu\epsilon$, which would indicate that there is compression throughout the full depth of the slab. This cannot be true since the top of the concrete slab must be in tension due to the fact that the top SMC reinforcing steel was in tension. It is likely that the top of the concrete slab gages had some initial strain due to concrete shrinkage or began to malfunction after the concrete cracked and thus, their readings after the point of cracking will be ignored. The presence of compression in the bottom of the slab would mean that there would be a slight compressive component of force from the slab to partially counteract the tensile forces in the top SMC reinforcing bars and tension in the concrete above the neutral axis (see further discussion in Section 5.7).

Final strains in the sole plate were determined from strains at gages SSS7, SSS 9, SSS 10 and SSS 11. Gage SSS 8 malfunctioned, thus the value for the symmetric gage, SSS10, was substituted. A plot of the sole plate strains measured at the end of the Day 1 Test and their

corresponding stresses is shown in Figure 84. The strains are significantly higher at the locations of the welds, one inch from either side vs. the center of the plate.

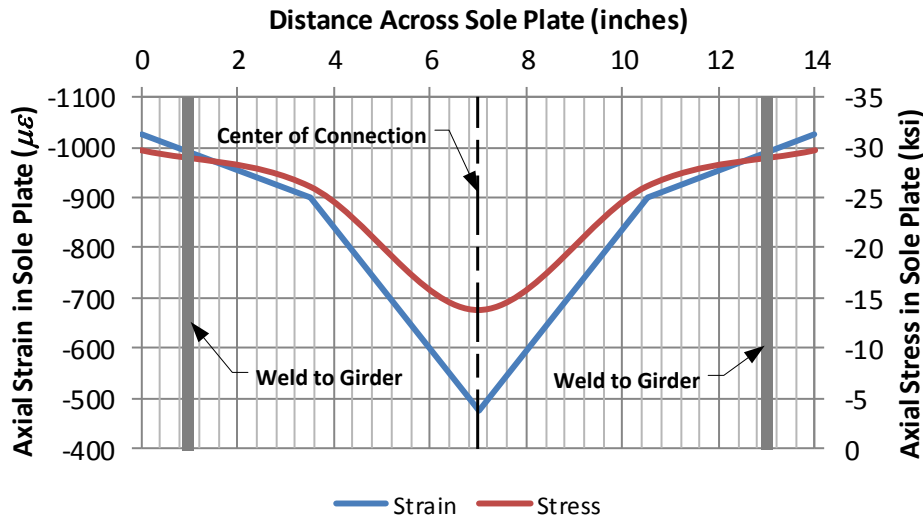


Figure 84 - Sole Plate Strains and Stresses at the end of Day 1 Test

Although the safety device became activated, its gage recorded no appreciable strain and thus no plot is provided herein. The only gage on the device was at the center of the plate and based on the strains in the sole plate, it's likely that the higher strains were near the extremities where no gages were present. The ends of the girders were manually flame cut during fabrication, whereas the safety device edges were precisely machined, thus there was not a perfect fit up when the safety device became engaged. It was noted that the device was not in contact with the girder web and most likely the bottom flange at that location due to roughness in the cut of the girder end. Contact was noted to be occurring at either end of the girder bottom flange, which also the location of the welds to the sole plate.

Displacements of the girder ends are shown in Figure 85 and Figure 86. Reviewing the displacement at the north girder, the jump in displacement at activation of the safety device is quite evident, whereas in the south girder there is only a subtle dip in the displacement. Also

evident is the relatively linear decreasing behavior of the displacement at the south girder, while the north girder is almost a straight line until a load of about 65 kips is applied. The difference in the behavior of the two girder ends is likely due to various internal interactions between all of the dissimilar materials achieving composite action.

Along with differences in behavior under load, there was also a significant difference in displacement at the ends of about 0.30 inches. The reason for this appears to be the variation in displacements of the elastomeric bearing at the center of the connection; the elastomeric bearing displacements are shown in Figure 87 and Figure 88, which show the displacements at the north and south potentiometer locations, respectively (Pot 1 and Pot 2). The north end of the elastomeric bearings displacement at the end of testing was 0.14 inch while at the south end, the displacement was 0.17 inch. The differential between the readings is -0.03 inches towards the south end over 18 inches (1.5 feet) between gages; this corresponds to a total differential of -0.30 inches from end to end over the 30 foot total span of the girders. Accordingly, both end displacements may be adjusted to reflect this slope effect and the corrected displacement at each end is 0.95 inches.

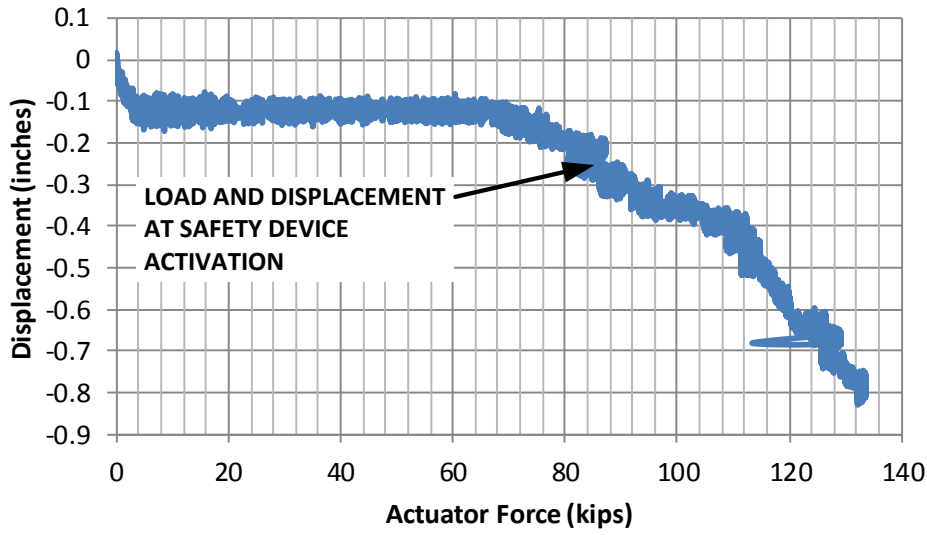


Figure 85 - Displacement at North End of North Girder vs. Actuator Force – Day 1

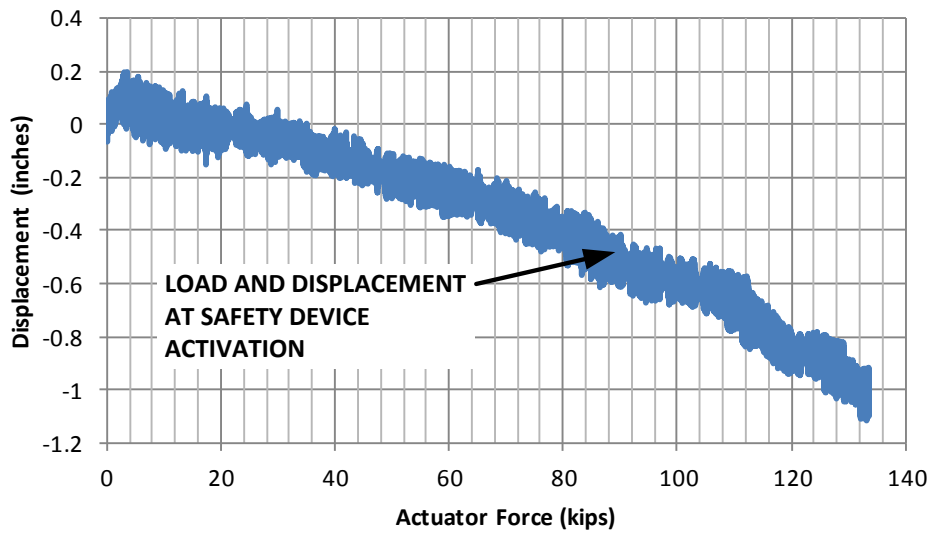


Figure 86 - Displacement at South End of South Girder vs. Actuator Force – Day 1

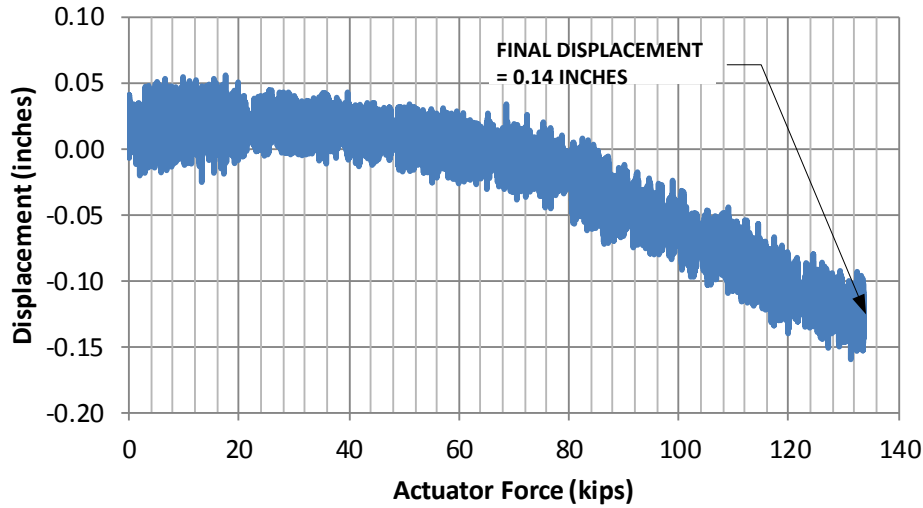


Figure 87 - Displacement of North Elastomeric Bearing vs. Actuator Force – Day 1

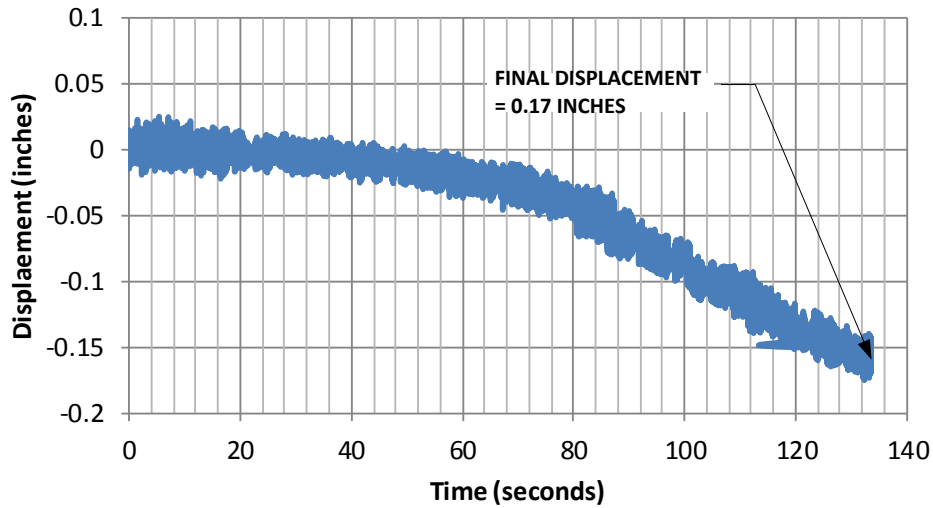


Figure 88 - Displacement of South Elastomeric Bearing vs. Actuator Force – Day 1

5.6.2 Day 2 Test Results

Actuator data for Force vs. Displacement for the Day 2 Test is shown in Figure 89. From review of this chart, it is evident when the safety device became activated at approximately 120 kips of applied load. Aside from the point at which activation of the safety device occurred, the load vs. displacement curves are relatively linear for both the north and south sets of actuators with just slight curvature of both sets after activation of the safety device. Also, due to the

increased loading rate of 1 mm/second for the Day 2 Test from 0.5 mm/second for the Day 1 Test, the curves are considerably less jagged; it's quite possible that the concrete being previously cracked may have also contributed to this more linear behavior.

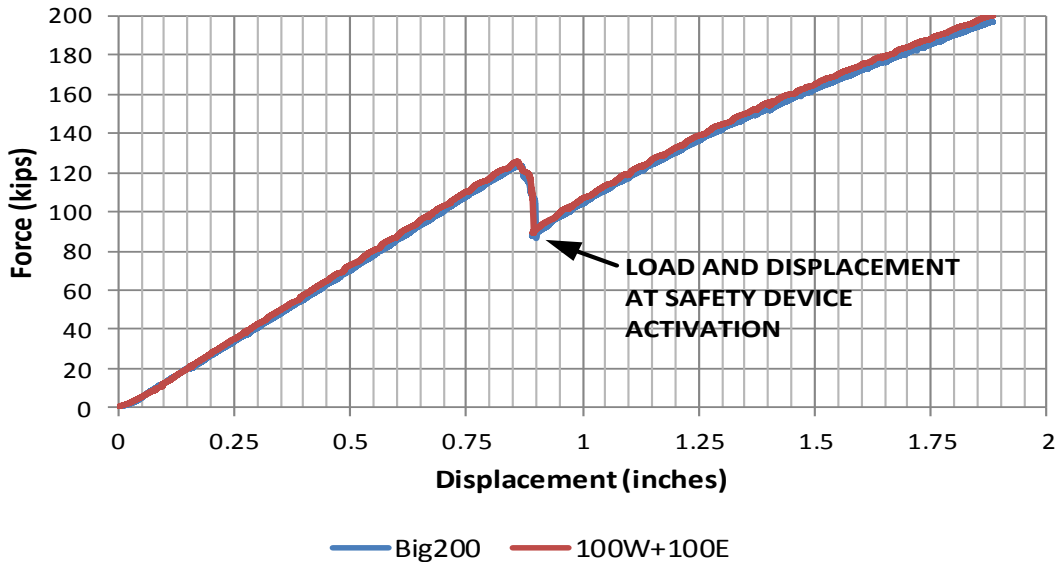


Figure 89 - Actuator Force vs. Displacement - Day 2 Test

The top SMC reinforcing bar strains for the Day 2 Test were examined for consistency with the Day 1 Test values for the same bars and some anomalies were discovered. As may be seen in Figure 107, the strain at the end of the Day 2 Test for the subject bar, instrumented with gage SSL-1, was nearly equal to the strain at the end of the Day 1 Test. The end load for the Day 1 Test was 132 kips, while the end load for the Day 2 Test was 198 kips. Considering the fact that this test specimen is statically determinate, a difference in end loading of 60 kips should not produce the same strains in the subject reinforcing bar. Upon further review, the initial strain in the bar varied between the two tests. There are many likely reasons for the difference in initial strain, effects of concrete cracking causing the aggregate to interlock and not allow the cracked concrete to fully close back up, relief of initial concrete shrinkage stresses, etc.

The original initial unloaded strain for gage SSL-1, was +660 $\mu\epsilon$ for the Day 1 Test, while the unloaded strain was +320 $\mu\epsilon$ for the Day 2 Test. Somehow the difference between these two initial strains must be incorporated into the Day 2 Test strain vs. actuator load charts. There are two possible methods; the first would be to start the Day 2 Test strain at the difference in the two strains, 340 $\mu\epsilon$ as shown in Figure 91. This scheme is not logical and the slopes of the two lines should be relatively parallel, at least until the Day 2 Test weld break. The second possible method would be to proportion the difference in strain to the measured strain in the reinforcing bar linearly along the chart. This method uses the following formulation:

$$\epsilon_{revised} = \epsilon + \frac{\epsilon}{\epsilon_{max}} \Delta\epsilon$$

Where:

$\epsilon_{revised}$ = the modified strain

ϵ = the original strain reading

ϵ_{max} = the maximum unmodified (original) strain

$\Delta\epsilon$ = the difference between the Day 1 Test and Day 2 Test initial strains

Using this formulation yielded the results shown in Figure 91; these results appear to be very reasonable, considering that both lines are nearly parallel and almost overlap up until their respective safety device activations. Also, the reinforcing steel strains remained linear which reflects the fact that the strains and resulting forces in the top SMC reinforcing steel must increase if load is increased. On the basis of this analysis, the scheme 2 methodology will be used to modify the strain curves of the instrumented structural elements from the Day 2 Test. Subsequent internal force analysis should support or refute the validity of this selection. The reinforcing force results vs. the applied actuator load with the aforementioned adjusted strain values are shown in Figure 93 and Figure 94 for the Day 2 Test at the activation of the safety device and at the end of the test respectively. The analysis of the reinforcing forces and

corresponding internal moments are discussed in Section 5.7.1 Internal Forces and Model Equilibrium. Based on that analysis, the results of the modified load the proposed modification to the curve provided consistently reasonable results.

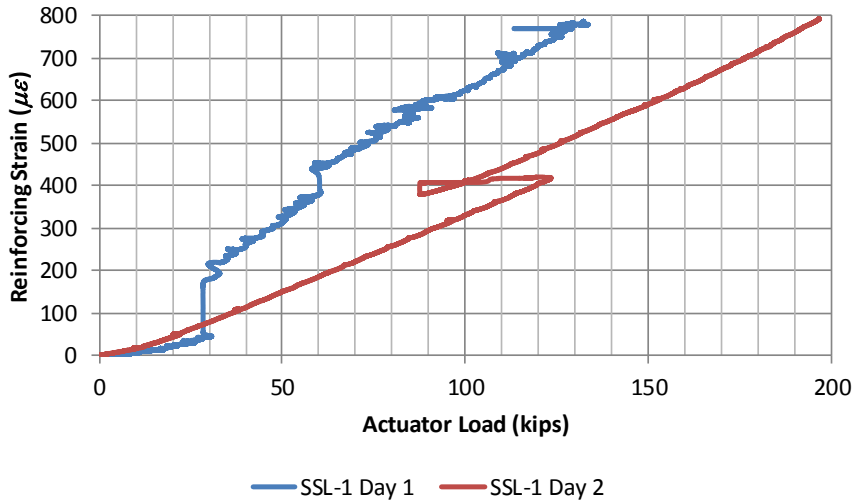


Figure 90 - Comparison of Days 1 and 2 Actuator Load and Reinforcing Strain

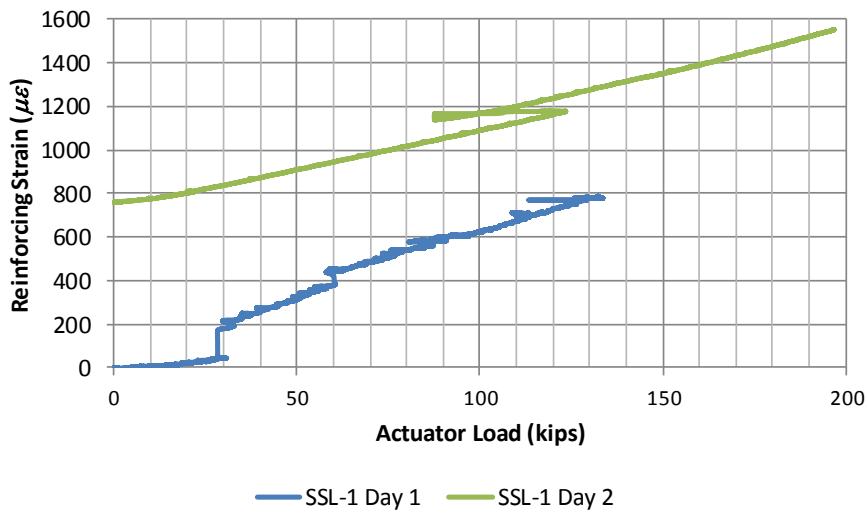


Figure 91 - Comparison of Days 1 and 2 Actuator Load and Reinforcing Strain - Scheme 1

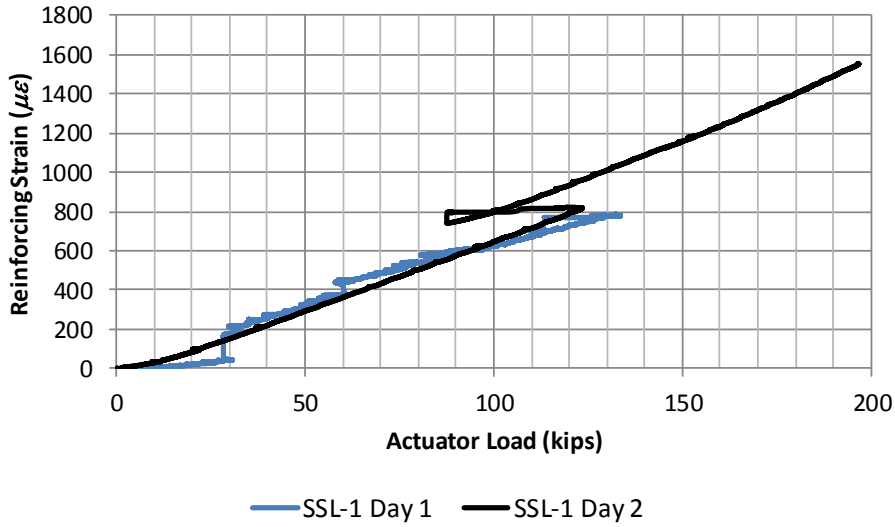


Figure 92 - Comparison of Days 1 and 2 Actuator Load and Reinforcing Strain - Scheme 2

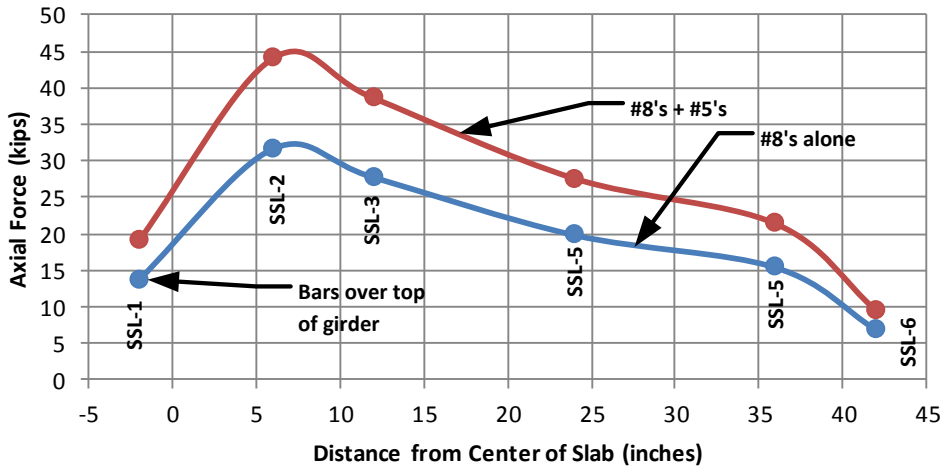


Figure 93 - Shear Lag in Top SMC Bars - Day 2 Test - Safety Device Activation

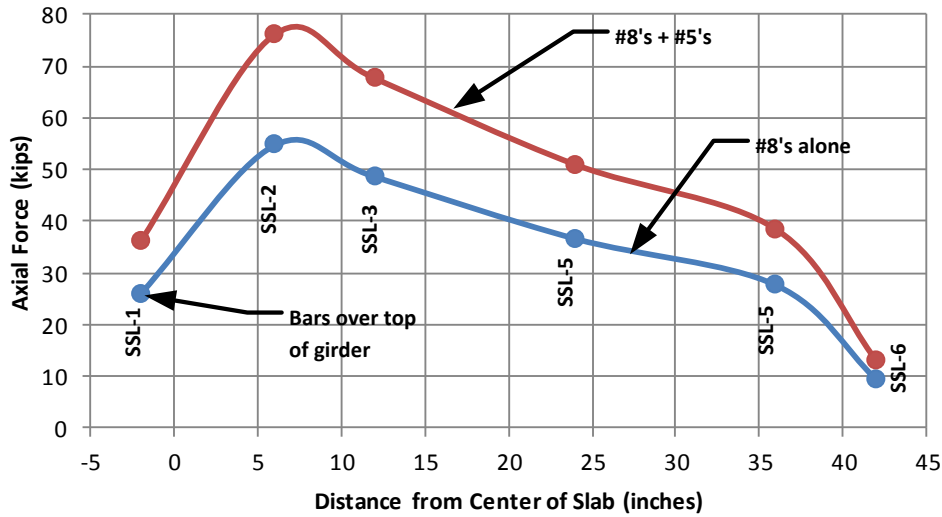


Figure 94 - Shear Lag in Top SMC Bars - Day 2 Test - End of Test

Concrete top strain gage values were unreliable due to cracking damage from the Day 1 Test and additional cracking from the Day 2 Test, thus no data from these gages will be presented.

Concrete bottom strain gage values are presented in Figure 95. It can be seen that up until about 120 kips, the bottom of the slab is in tension. The location of the safety device activation is shown; at this location there is a decrease in strain along with a corresponding decrease in load. This is due to the rapid displacement at the center connections when the south weld cracked/failed and the actuators had to reapply the load lost in the sudden displacement. Once load was reapplied, the strains turned positive again indicating tension in the bottom of the slab, although, just slightly in the case of CS6.

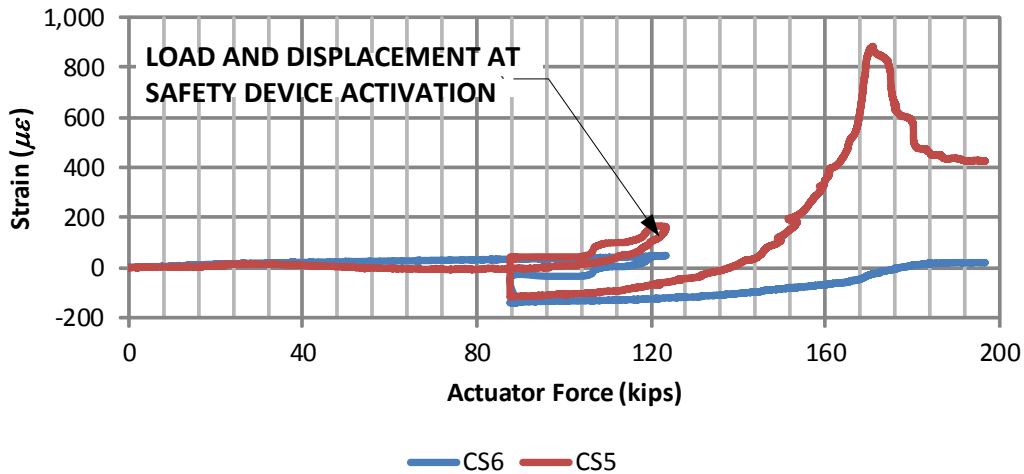


Figure 95 - Bottom Concrete Strains vs. Actuator Force - Day 2

The strains at the center of the sole plate are shown in Figure 96. Based on review of the strain diagram, the sole plate is in compression as expected until the activation of the safety device. At activation, the strain starts increasing and eventually turns into tensile strain; this may be due the behavior of the bottom flanges bowing slightly since they are only partially in contact with the safety device due to bevels shown in Figure 99, which were to accommodate for the welds to the sole plate. Strains in the sole plate were determined from the gages SSS7, SSS 9, SSS 10 and SSS 11. A plot of the measured sole plate strains and corresponding stresses at the point of the activation of the safety device for the Day 2 Test are shown in Figure 97. The strains were significantly higher near the locations of the welds, which is similar to the previous results. Due to machining additional material off of the safety device, it was possible to put more load into the sole plate before safety device activation; in this instance, the load was increased by roughly 40 kips over the Day 1 Test, a 50% increase. Also, the high stresses near the welds have almost reached the factored ultimate capacity of the plate. The unloading path of the sole plate follows the loading path reasonably well, Figure 96 . Once load begins to be

reapplied, there is a straight decrease in the negative strain in the plate. Subsequently, the strain goes from negative to positive strain until the end of the Day 2 test.

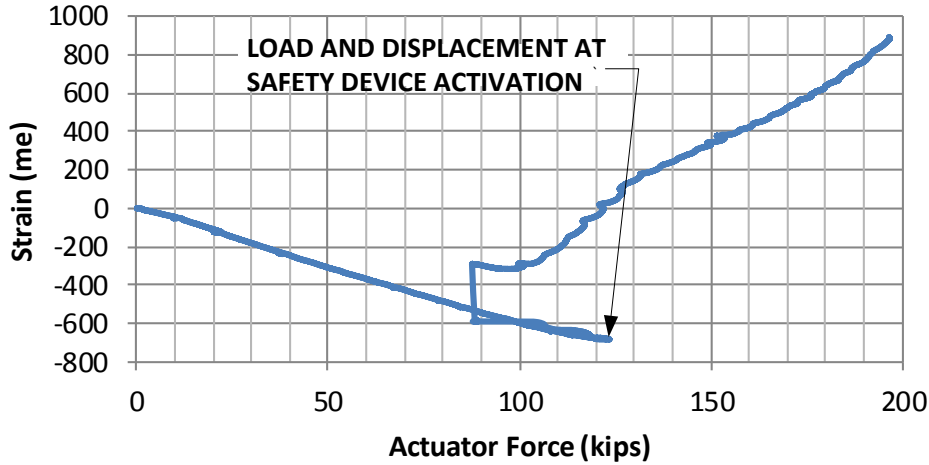


Figure 96 - Strains at Center of Sole Plate – Day 2 Test

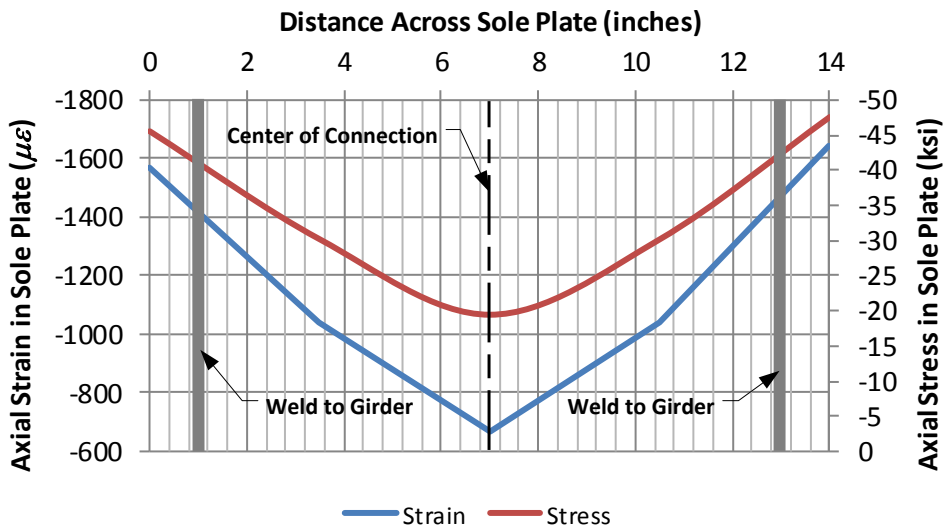


Figure 97 - Sole Plate Strains and Stress at Safety Device Activation - Day 2 Test

The strains in the safety device for the entire Day 2 Test are shown in Figure 98. The location where the safety device became activated is obvious and as in the previous charts, the strain reduces and then begins to increase again. The reason for the tension may be due to the top of the safety device being 1/2 inch higher than the top of the top of the bottom flange and

possibly some negative bending occurring in the top of the device until the load in the device partially equalizes. Following the tensile strains, the plate has a non-linear increase in negative strain to a maximum value of $1490 \mu\epsilon$.

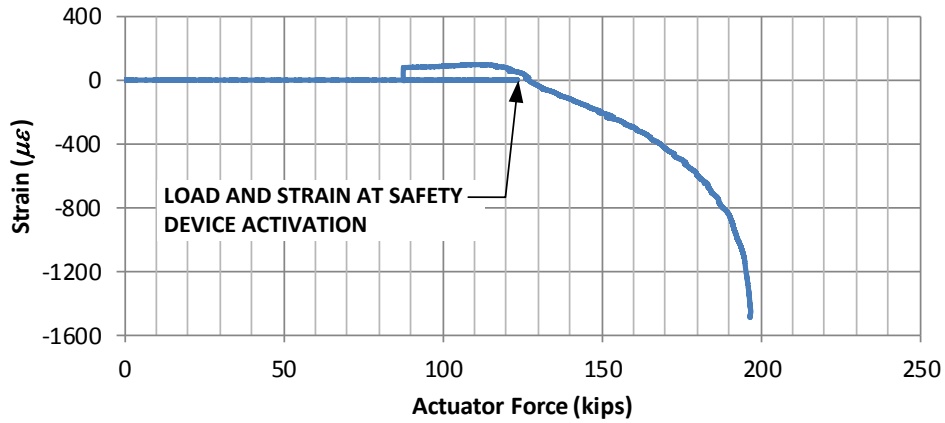


Figure 98 - Strains at Center of Safety Device vs. Actuator Force - Day 2 Test



Figure 99 - Detail of Safety Device Showing Bevel at Weld

Vertical Displacements at the girder ends are shown in Figure 100 and Figure 101. The north end displacement vs. force is not quite linear up an applied load of 123 kips, whereas the curve is very linear for the south end displacement vs. force. The most likely reason for the behavior is the more excessive deformation of the elastomeric bearing at the north end of the sole plate, Figure 102. The location at which the safety device became activated is noted on both charts and it is obvious that a large displacement occurred along with a 25% decrease in applied load. Subsequently, the load was increased and displacement became fairly linear for both ends. The difference in the total readings is again an effect of the non-uniform compression of the elastomeric bearing. However, during this test, the displacements for the girder mounted potentiometers became somewhat unreliable because the deformation of the bearing was so extreme that it actually deformed enough laterally to distort the anchors for the potentiometers (Figure 102).

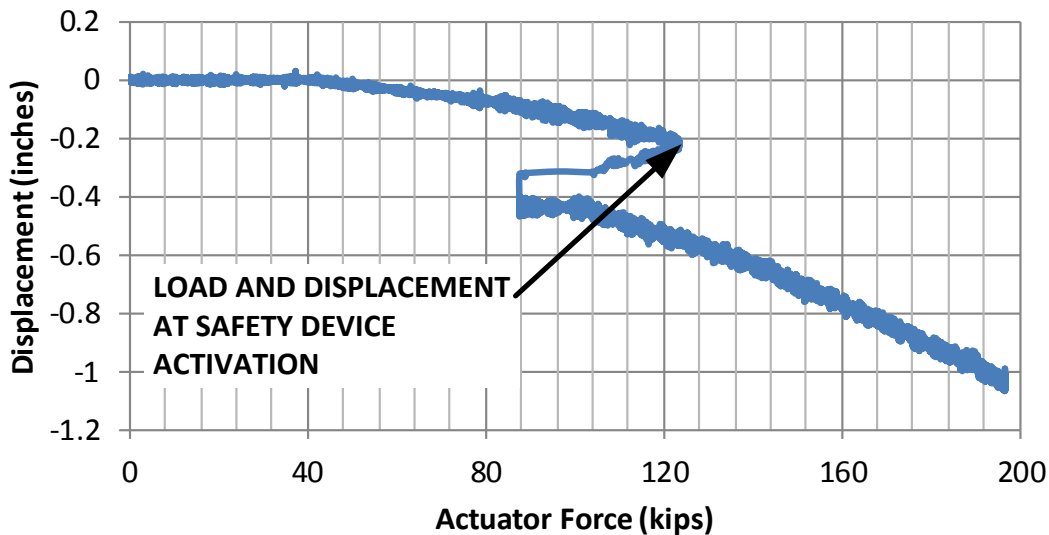


Figure 100 - Displacement of North Girder - Day 2 Test

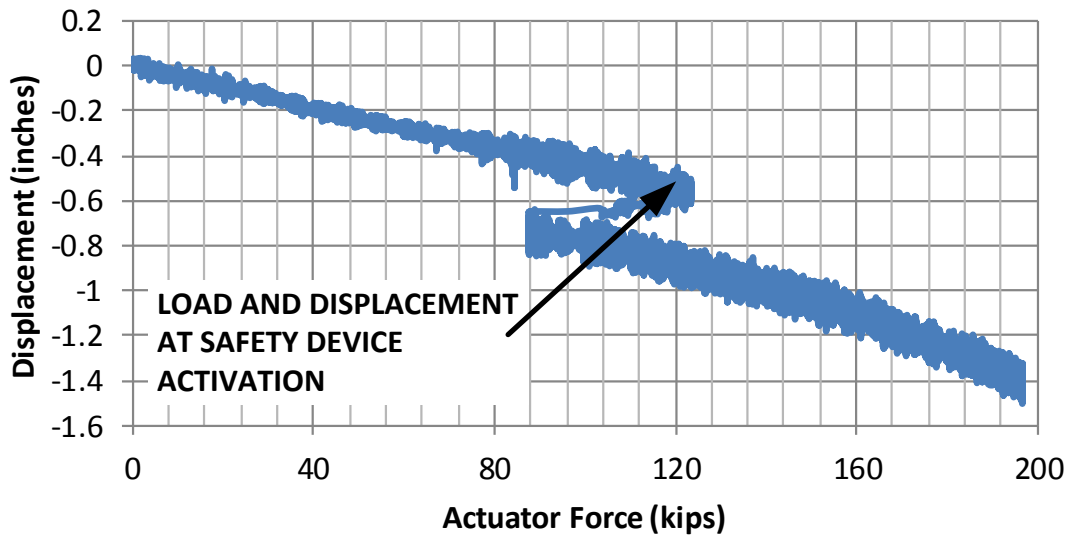


Figure 101 - Displacement of South Girder - Day 2 Test

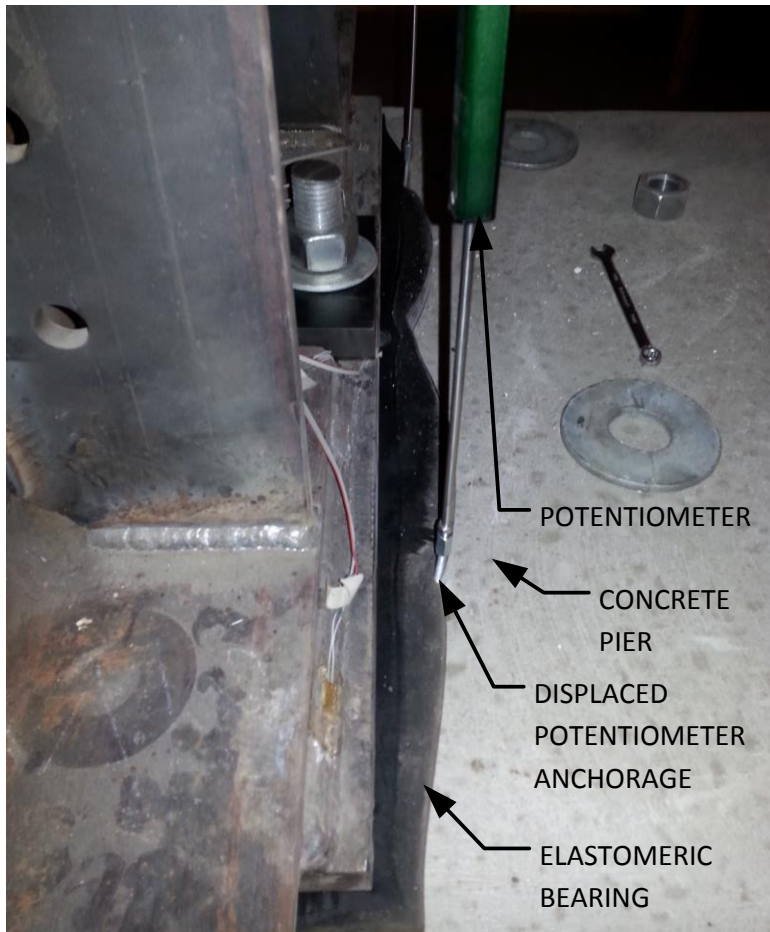


Figure 102 - Distorted Potentiometer Anchorages - Day 2 (July 2014)

The crack pattern in the top of the concrete slab was documented photographically. A representative photo is shown in Figure 103 and a plotted diagram is shown in Figure 104. The crack pattern was only mapped to within three feet of the load application beams; mapping nearer to the load application beams was not considered reliable due to the localized load effects of the beams. The pattern was as anticipated with the majority of the cracking occurring perpendicular to the direction of stress. It is also interesting to note that the cracking somewhat follows the shear lag in the reinforcing bars, reduced in the center and increasing away from the center on either side.

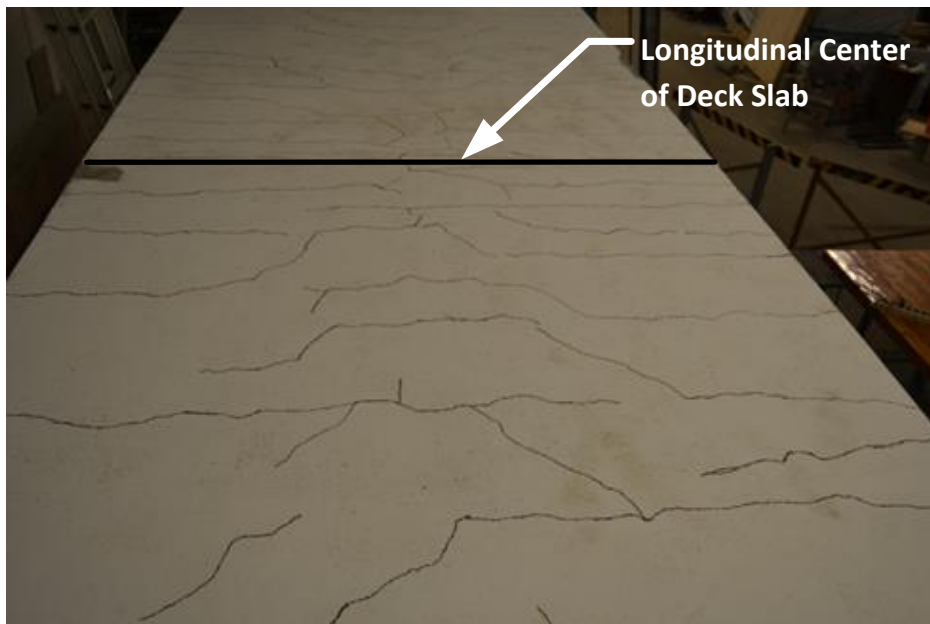


Figure 103 - Final Crack Pattern in Top of Deck Slab Looking South (July 2014)

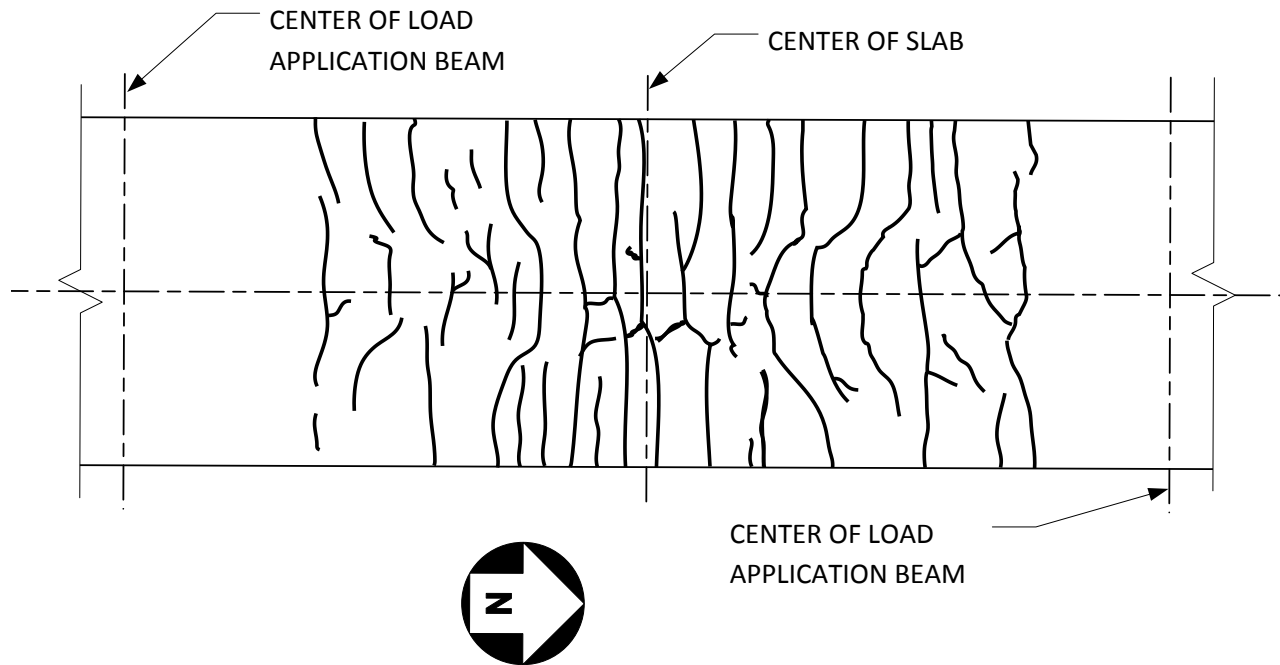


Figure 104 - Crack Pattern in Top of Deck Slab

5.7 ANALYSIS OF TEST RESULTS

The test results were analyzed to verify the internal forces/equilibrium of the physical model for comparison to the hand calculations and to the results of the Abaqus finite element analysis.

5.7.1 Internal Forces and Model Equilibrium

The cross-section of the model at the center was selected for analysis as it was the most heavily instrumented. Casual consideration of the connection would indicate that the largest moments would occur at the center of the connection; however, observing the arrangement of the pier, bearing plates and the locations of the ends of the girders, it became apparent that the maximum moment would be away from the center since the shear is zero at the end of the girder and the girder ends are each 3" from the center of the pier. Based on the Abaqus analysis, the majority of the girder reaction goes into the pier in the first six to twelve inches of bearing; this

arrangement of shear actually reduced the moment at the centerline of the connection and also proved to be true in the physical model.

At the end of the Day 1 Test, the theoretical moment was determined to be 1620 kip-feet at the center of the bridge based on an applied load of 135 kips and a moment arm of 12 feet. The actual moment based on the reinforcing bar forces, shown in Figure 81, creating a couple with the sole plate and safety device was determined to be 1488 kip-feet. On the basis of an applied load of 135 kips and a resultant moment of 1488 kip-feet, the moment arm was determined to be 11.0 feet, or 12 inches from the centerline of the connection. This result is reasonable as the center of bearing is three inches from the edge of the bearing plate nearest to the face of the pier. This behavior is diagrammed in Figure 105.

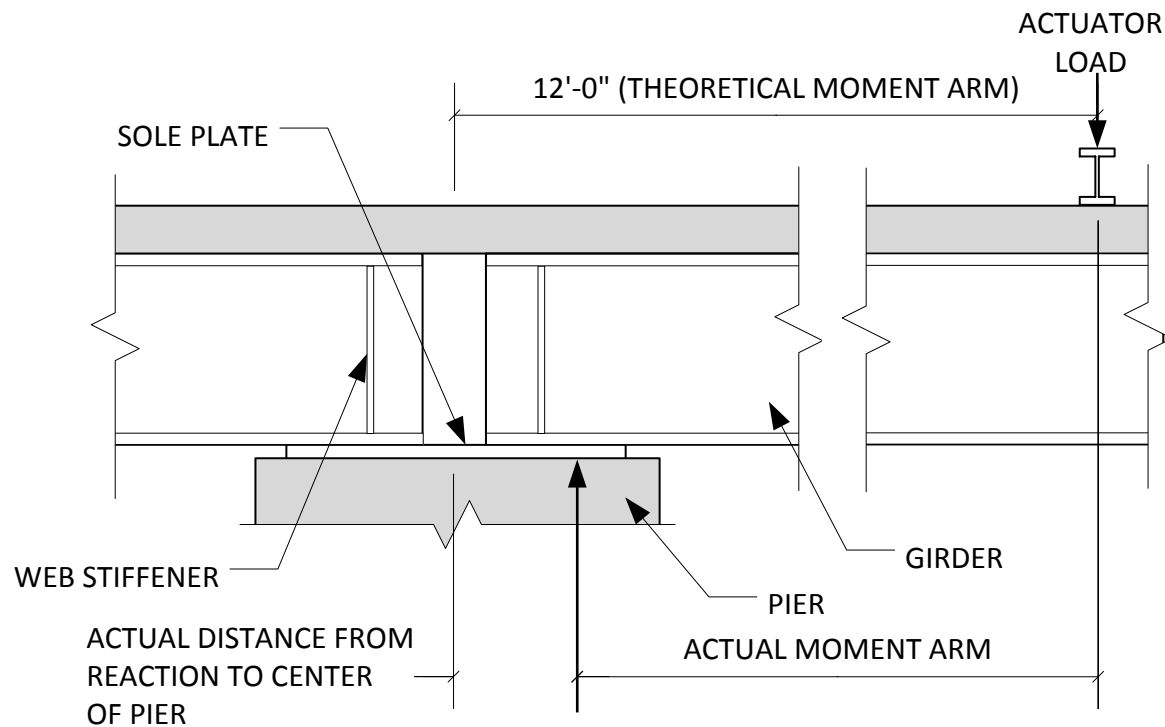


Figure 105 - Girder Support Behavior

Similar resultant moment behavior to the Day 1 Test was noted in the Day 2 Test and is summarized for both days' tests in Table 24. The possible reason for the relative differences in

moment arm at the end of Day 1 Test and at the activation of the safety device in the Day 2 Test was the failure of the elastomeric bearing to regain its shape, which may have caused it more effectively distribute the loads. Also, once the safety device was active, the sole plate was subjected to negative bending, which may have caused the effective reaction location to shift slightly. The locations of the center of bearing also indicate, that although stiffeners are installed to aid in stiffening the web for buckling, it doesn't necessarily mean that the load will go through them; the bearing stiffener in this case is nine inches from the center of the sole plate.

Table 24 - Location of Resultants for Various Loadings

Event	Theoretical Moment	Actual Moment	Center of Actual Bearing from Center of Sole Plate
End of Day 1 Test Load = 135 kips	1620 kip-feet	1488 kip-feet	15'' - 3'' = 12''
Activation of Safety Device Day 2 Test	1476 kip-feet	1367 kip-feet	15'' - 4.5'' = 10.5''
End of Day 2 Test Load = 196.5 kips	2358 kip-feet	2228 kip-feet	15'' - 7'' = 8''

5.7.2 Deflection and deformation compatibility

The deflections at the ends of the north girder are presented in Table 25. The deflections from the test do not correspond well to those calculated by hand nor could they be used for comparison to the actual bridge since it is continuous. Analysis of the deflections indicate that there is a shear component to the displacement, which is reasonable considering that $L/d = 3$ for the physical model. The actual bridge should not have shear deflections of any significance since the actual $L/d > 21$. Thus the deflection values are shown for reference only.

Table 25 - North Girder End Deflections

Test Day and Event	Recorded Deflection	Deflection Correction for Elastomeric Bearing	Corrected Deflection	Applied Actuator Load
Day 1 – Safety Device Activation	-0.24 inches	-0.09 inches	-0.15 inches	85 kips

Test Day and Event	Recorded Deflection	Deflection Correction for Elastomeric Bearing	Corrected Deflection	Applied Actuator Load
Day 1 – End of Test	-0.80 inches	-0.15 inches	-0.65 inches	135 kips
Day 2 – Safety Device Activation	-0.44 inches	-0.12 inches	-0.24 inches	123 kips
Day 2 – End of Test	-1.02 inches	-0.15 inches ⁽¹⁾	-0.87 inches	196 kips

⁽¹⁾ Estimated since values were unreliable due to excessive lateral deformation of the bearings

5.7.3 Discussion/Conclusions from experimental test

Based on a review of the test results, the following key findings were identified:

For simple-made-continuous bridges in general:

1. The mechanism to transfer the compressive force component of the SMC moment is the most load transfer critical element since the top SMC reinforcing steel doesn't ever become fully stressed.
2. The actual maximum negative moment occurs within the length of the beam on the bearing plate and is less than the theoretical maximum negative moment, which would occur in a fully continuous girder that is considered point supported. Thus, it is slightly conservative to design the simple-made-continuous reinforcing and any transfer plates for the force components of the theoretical maximum negative moment.
3. The shear lag in the slab as indicated by the reinforcing steel forces, concrete strains and concrete crack pattern was as expected, based upon comparison to test results by others (Farimani M. , 2006) for this type of connection.

4. The top SMC reinforcing bars on either side of the center bar each take approximately 8% of the total tension load component of the tensile component of the moment and are thus, the critical bars for design. This corresponds reasonably well with the Nebraska studies in which similar bars are taking approximately 9% of the total tension load (Azizinamini A. , 2005). Thus, the more conservative 9% value will be used herein.

For the CDOT simple-made-continuous bridge in particular:

1. The most load critical element of the connection is the sole plate as it is not only required to transfer the entire compressive component of the SMC moment, but it is also subjected to a moment due to load eccentricity.
2. The welds of the girder to the sole plate must be increased in size in order to transfer the full compressive component of the SMC moment.to the sole plate in accordance with AASHTO requirements (3.3.1 Preliminary Analysis and Table 7).
3. The welded connection and the bottom flange of the girder at the weld must also be designed for fatigue considerations; specifically, AASHTO fatigue categories E and E', which have stress ranges of 4.5 ksi and 2.6 ksi respectively.

As an alternative to items 1, 2, and 3, transfer plates flush with the bottom flanges could be installed between the girder flanges as a direct means of compression transfer; these plates could be field adjusted for fit up between the girder ends. This alternative is economical, safe, simple and not subject to the AASHTO fatigue requirements and will be used in the formulation of the final design equations.

5.7.4 Comparison with Abaqus Results

A comparison of the numerical results of the physical model test with the numerical results from initial Abaqus models showed large differences across all response quantities

including girder end displacements as well as strains in the reinforcing steel, concrete and girder steel. The possible reasons for the lack of agreement are many; the major culprits could likely be the concrete damage model, and the constraints used between the concrete and the reinforcing and between the concrete and the girder shear connectors. The axial strains in the reinforcing bars are shown in Figure 107 where the effects of the shear lag across the slab are evident, however, the shapes of the curves of shear lag (Figure 108) are significantly different between the two and the strains from the physical test are three times those of the Abaqus analysis. Another important difference was that the elastomeric bearing was not modeled in Abaqus as its extreme displacements would not allow Abaqus to converge and thus, the runs in which it was modeled would abort prematurely.

While a numerical comparison could not be made, comparison of the overall behavior of the Abaqus model to the physical model did provide some valuable insight into the interpretation of the test results. The behavior at the sole plate in which the actual component of girder reaction is nearer to front of the pier was clearly indicated in the Abaqus results (Figure 106). The location of the bearing stiffener is evident by the flared out, lighter colored sections, which also indicate that the contact forces caused by the stiffeners are significantly lower than those caused by the web. The shear lag in the top of the slab based on the Abaqus analysis is shown in Figure 109; this particular plot was taken from the earlier stages of the analysis prior to the effects of concrete damage became evident.

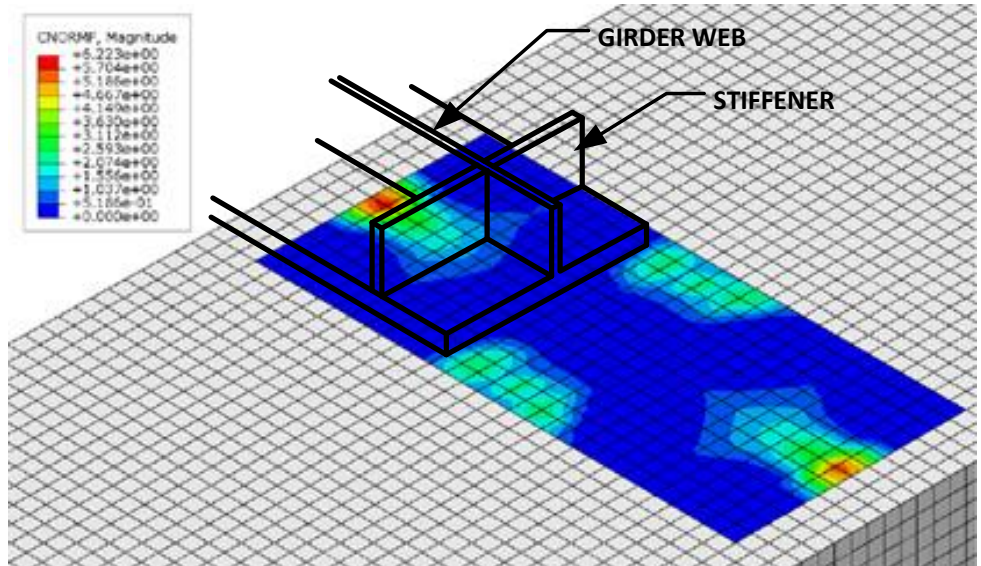


Figure 106 - Normal Forces on Sole Plate – Abaqus

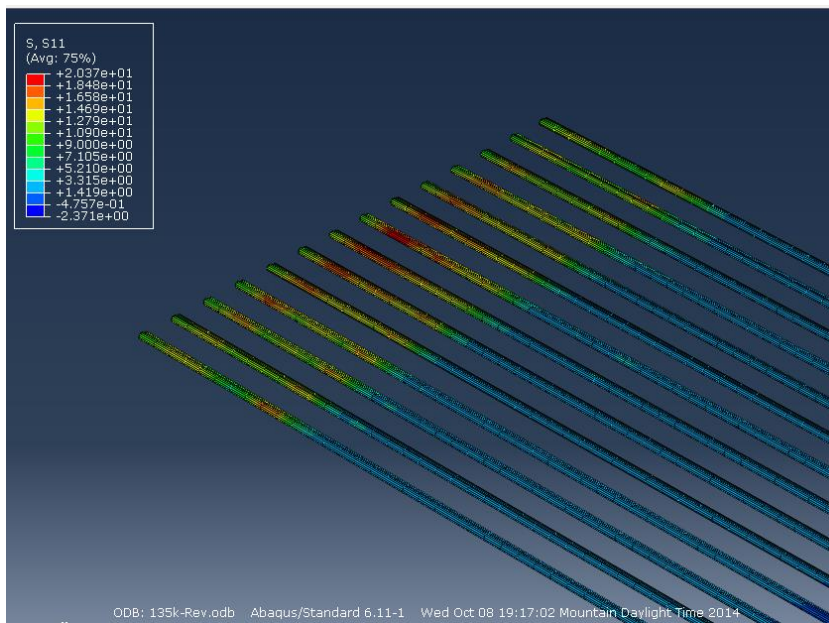


Figure 107 - Axial Stress in SMC Top Reinforcing Steel

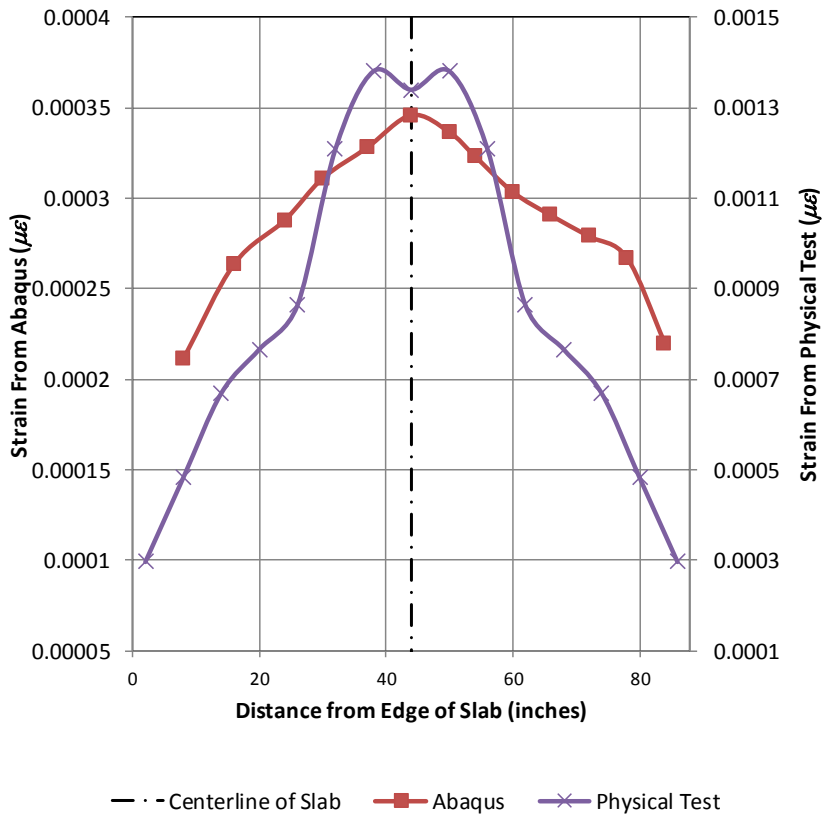


Figure 108 - Comparison of SMC Reinforcing Strains

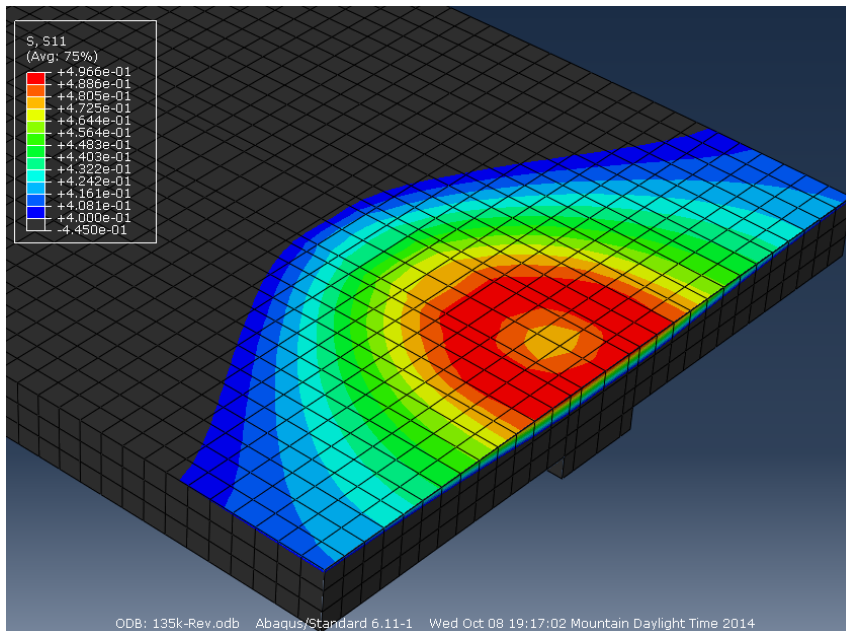


Figure 109 - Early Shear Lag in Top of Concrete Slab

5.7.5 Post-Test Attempts to Correlate Results to Hand and Abaqus Analysis

The significant disparities between the physical test and the original Abaqus analysis might be explained by the concrete in the Abaqus model taking too much tension, particularly in areas which were found to be cracked in the physical test model. These disparities were likely due to the concrete damage model used, which was “concrete damaged plasticity”. Over one hundred different Abaqus models with varying concrete damage parameters were attempted and in every case, both the shear lag in the slab and slab reinforcing did not come close to the actual values noted in the physical test. Also, the deflection of the girder end based on the Abaqus analysis was consistently less than one third of the actual value. Abaqus has an additional concrete damage model, “concrete smeared cracking”, which was not appropriate for the model being considered since the concrete behavior is considered separately from the reinforcing steel and thus, would not give the correct reinforcing strains. Due to significant differences between the results of the Abaqus analysis and the physical test, additional approaches to modeling of the concrete were considered. This included comparison of simple hand calculations to Abaqus and new modeling approaches to avoid using concrete damage models.

Initially hand calculations using the transformed sections of the composite girder and slab as a fixed-end beam were performed for comparison to Abaqus undamaged concrete results. These calculations/Abaqus analyses considered various arrangements of effective structural elements including: beam and slab, and beam, slab and SMC reinforcing. Also, an attempt was made to compare a hand calculation of the beam and SMC reinforcing only to an Abaqus model, but the Abaqus modeling became extremely complicated due to geometry required to tie all of the reinforcing bars to the girder, so instead, this model was created using concrete with a very low modulus of elasticity to create a bond using the embedded constraint between the slab and

the reinforcing steel and using the tie constraint between the concrete slab and the girder. For composite action between the slab and girder a tie constraint was used between the two parts. For all cases, the fixed end reactions compared very well. The free end deflections also compared well for all models, however, all loads applied to the cantilever ends of the girder were well below those that would cause tensile failure of the concrete at the fixed end. When loads were applied that caused tensile failure in the concrete, the results no longer compared well with Abaqus predictions considerably lower than those estimated by hand calculations.

The first new modeling approach was an attempt to simulate the shear lag in the slab by adjusting the stiffness (EI) of the slab across its width. In lieu of modifying the moment of inertia (I) of the slab, the modulus of elasticity (E) was modified by varying its value along the width of the slab. The highest values of E used were near the center of the slab and then reduced in steps to the lowest values at the slab edges. The profile of values used is shown in Figure 110 and was developed by examining the actual shear lag across the slab from the physical test results, with the highest modulus of elasticity at the center of the slab and decreasing to the lowest value at the edges. Varying the modulus of elasticity as described was then modeled in Abaqus and an analysis performed; this approach yielded better results for shear lag in the slab and in the reinforcing bars than using the concrete damage model, but the value of the deflection was still considerably less than that of the actual physical model. The concrete damage model produced SMC reinforcing shear lag values, which while similar in shape to the actual shear lag were strained approximately one third of the actual strains determined from the physical test (Figure 108).

The second new modeling approach involved reducing only the stiffness of the concrete at the center of the connection to simulate the significant amount of cracking of the concrete at

the center of the connection. The results of this approach yielded deflection magnitudes higher than those of the first approach, but about only two thirds of the values from the physical test.

The third new modeling approach was a combination of the first two approaches, i.e., reducing the modulus of elasticity across the slab and at the center of the support. This model used the modulus of elasticity profile shown in Figure 110 along with the arrangement of the slab shown in Figure 111. Using this technique yielded results that compared very well in both shear lag in the reinforcing bars and deflection. Based on a run considering both reduced stiffness longitudinally at the edges of the slab and laterally towards the center of the connection, the shear lag in the reinforcing steel is compared to that of the physical test and is shown in Figure 112. The values of strain in the reinforcing bars compare well as opposed to the strains determined using the concrete damage model, Figure 108. The displacement for this case was 0.88 inches vs. 0.87 inches for the physical test, which is very close considering that the Abaqus analysis using the concrete damage model provided displacement results in the neighborhood of 0.2 inches and less.

It is important to note that the results obtained based on the new modeling approach were performed subsequent to the physical test and thus, creating the models to match the physical test was fairly straightforward. In order to be able to pre-analyze models using this method would require the development of modeling rules based on material properties, model geometry, estimated damage, etc., which is beyond the scope of this work.

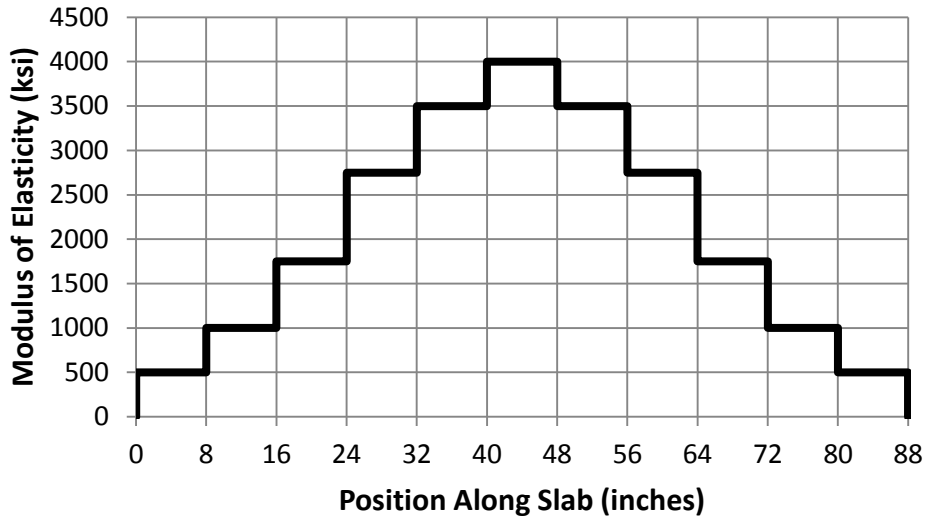


Figure 110 - Profile of Modulus of Elasticity across Slab

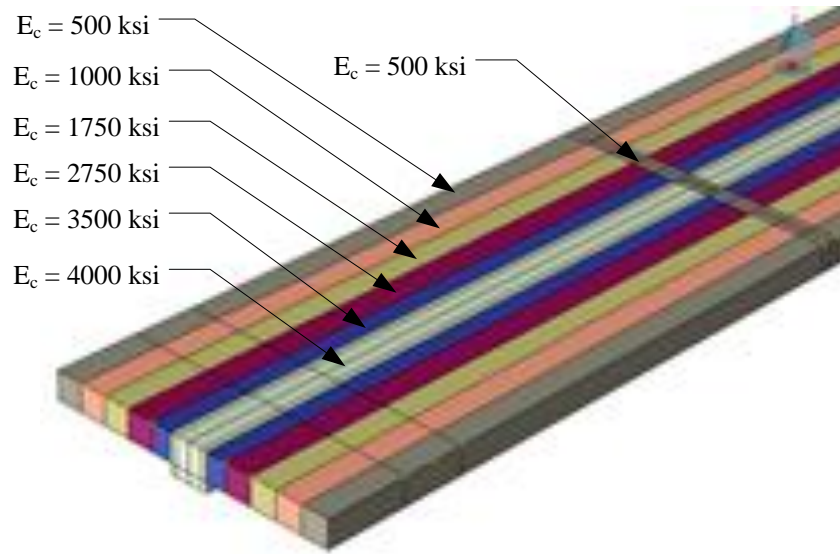


Figure 111 – Third Approach - Moduli of Elasticity

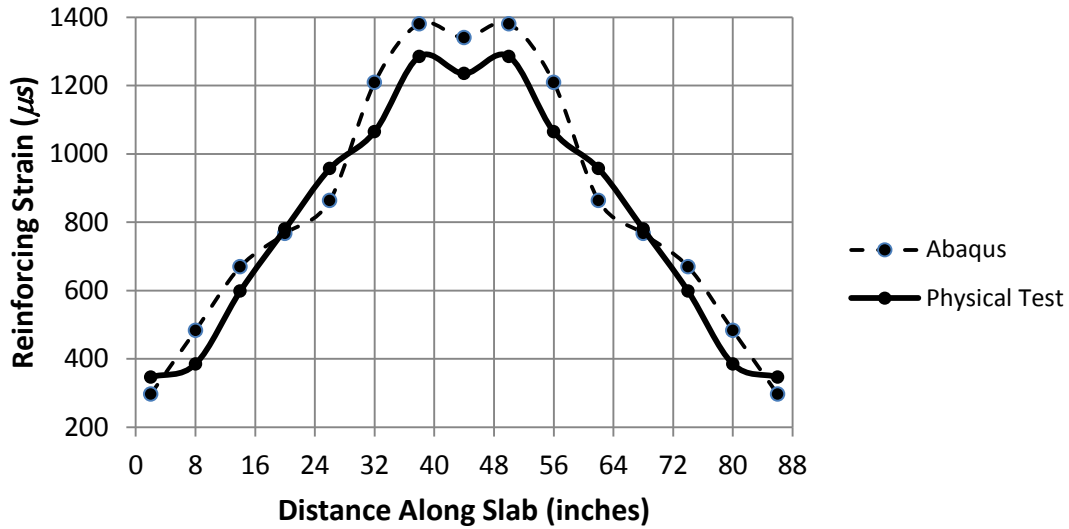


Figure 112 - Comparison of Reduced Stiffness Abaqus Shear Lag to Physical Test

On a final note regarding the third approach, the run times for the Abaqus analyses were less than one hour for all runs compared to over eight hours for a typical concrete damage model run. Thus, this method not only yielded more correct results, it also uses about 15% of the processing time of analyses using damage material models.

CHAPTER 6 PARAMETRIC STUDY

Following the successful completion of the physical model test a parametric study was performed to expand the applicability of the study connection. The parametric study consisted of analyzing ranges of girder spans, numbers of spans, girder spacings (slab spans), slab thicknesses and simple-made-continuous reinforcing arrangements for use in developing design equations for the study connection.

The following sections describe the selection of the various design parameters that helped to define the scope of the parametric study, the study methodology and the results of the study. Design parameters for the study were carefully selected to reflect the practical SMC bridge configurations reviewed and with consideration of the SMC concept under investigation.

6.1 BRIDGED ROADWAY GEOMETRY LIMITATIONS

The range of girder spans was developed assuming that the bridge would be used to span a roadway. Using CDOT standards for road geometry (CDOT, 2012), which are similar or identical to the standards used by other states' departments of transportation, a set of theoretical roadways to be bridged was assumed, forming the basis for spans to be considered. The applied limitations on the roadway based on CDOT were:

1. Lane width = 12 feet
2. Minimum number of lanes = 2
3. Shoulder width = 8 feet
4. Shoulder on each side of the roadway

Additional geometric restrictions made to keep the study within practical limits were::

1. Maximum number of lanes = 6

2. Distance between the roadway and the bottom of the bridge girder = 18 feet (minimum = 16.5 feet)
3. Two horizontal to one vertical slope on the abutments
4. Space between traffic directions = 6 feet

These limitations are shown diagrammatically in Figure 113.

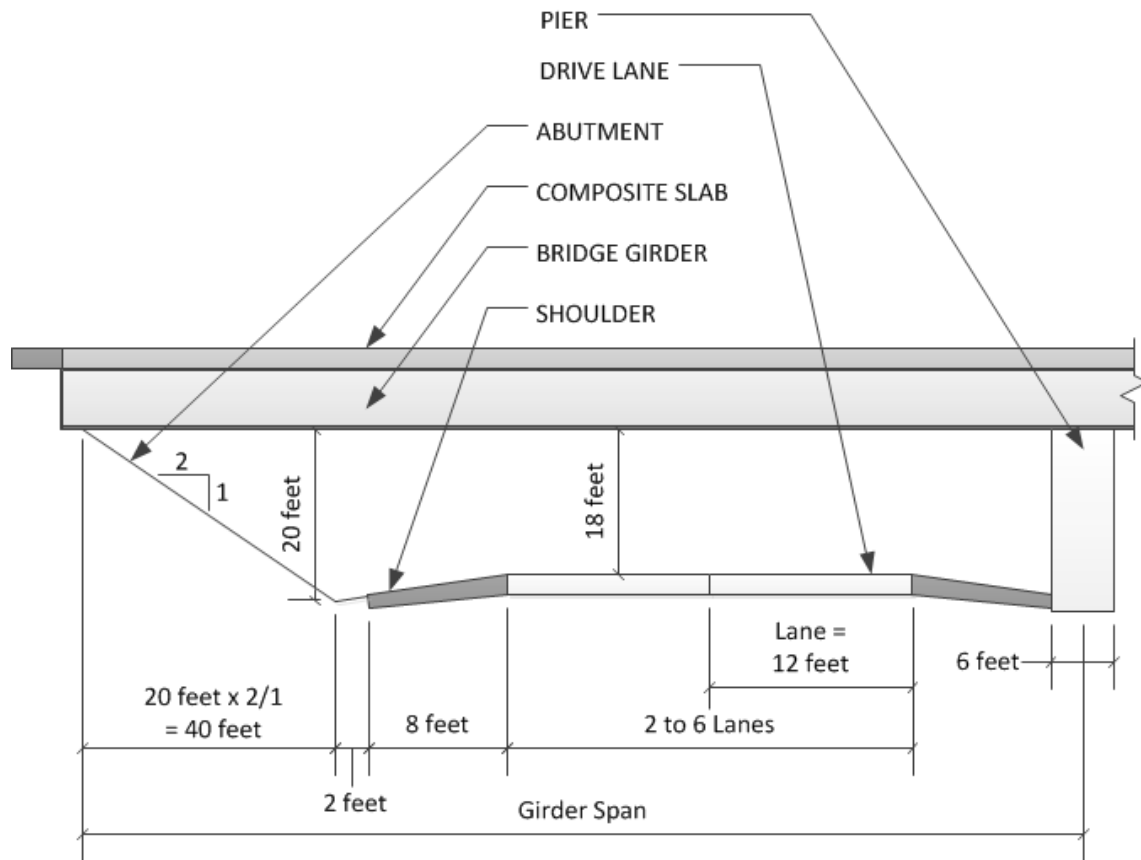


Figure 113 Roadway Limitations

Based on the roadway constraints the range of potential bridge spans was 83 feet to 131 feet. The range selected for the study was set from 80 feet to 140 feet; this range provides for six spans to be considered on twelve foot increments: 80, 92, 104, 116, 128 and 140 feet. The span range of existing SMC bridges varies from 66 feet through 139 feet. The shortest span was for a

rebuilt bridge, the next shortest bridge was 78 feet. Thus, using a minimum length of 80 feet to agree with the original study bridge and a maximum length of 140 feet will extend the applicability of study connection concept to the full range of spans of existing SMC bridges.

6.2 DECK SLAB GEOMETRY AND REINFORCING

6.2.1 General

The slab span/girder spacing plays an important role in the overall behavior of the bridge structure since the slab span affects the load distribution to the girders as well as the effective flange width of the composite section and limits the amount of SMC reinforcing that may be considered to act with the girder to carry the negative moment at the connection. The slab span, which is also the girder spacing, varied from approximately 7'-4" to 10'-4" on the existing bridges reviewed. This range of slab spans was selected for the parametric study, and the spans were incremented in steps of 4 inches. Slab depths of the SMC bridges reviewed varied from 8 to 9 inches. This same range was used for the parametric study with increments of 1/2 inch. The ranges selected for slab spans and slab depths give slab width/depth ratios in the range of 11 to 16, well below the AASHTO limit of 20, after which, prestressing of the slabs is recommended.

6.2.2 AASHTO Limitations

Of the SMC bridges reviewed, the majority of the bridge designs indicated that the slabs were designed using the AASHTO Empirical Design Method, thus the empirical method constraints were used as further limitations of the parametric study.

The Empirical Design Method places specific limitations on minimum slab dimensions and reinforcing steel areas. AASHTO also provides limitations for reinforcing placement relative to the top and the bottom of the slab (clear distances) and spacing requirements between reinforcing bars. The empirical method defined in AASHTO Section 9.7.2 (AASHTO, 2012) specifies

guidelines for maximum slab spans of up to 13'-6" clear between girder flanges and a minimum slab thickness of 7 inches. Minimum reinforcing requirements for these slabs are specified as 0.18 in.²/ft. each way for the top reinforcing steel and 0.27 in.²/ft. each way for the bottom reinforcing steel.

The quantity of the top SMC reinforcing bars which may be placed in the top layer are functions of the effective slab width, the reinforcing bar size and the minimum spacing of the reinforcing bars. In accordance with AASHTO section 5.10.3 – Spacing of Reinforcement, “the clear distance between parallel reinforcing bars shall not be less than 1.5 times the nominal diameter of the bar, 1.5 times the maximum size of the coarse aggregate or 1 1/2 in.. In effect, these requirements may limit the amount of SMC reinforcing and thus the tension force that can be developed at the top of the connection as part of the tension/compression couple resisting the negative moment.

AASHTO section 5.12.3 specifies minimum reinforcing cover dimensions depending upon the location of the reinforcing, specifically, 2.5 inches clear for top reinforcing and 1.0 inch clear for bottom bars up to No. 11 (Figure 114). The clear distances sum to a total of 3.5 inches, which will limit the vertical space available for the SMC reinforcing placement.

Considering that the minimum slab thickness for the empirical method is seven inches and the total of the required clear distances is 3.5 inches, only 3.5 inches (half of the slab thickness) is left available for the placement of four layers of reinforcing. The minimum thickness considered herein, 8 inches, will allow a minimum of 4.5 inches for reinforcing placement. These 4.5 inches of spacing is beneficial in SMC connections because the top reinforcing steel is often larger than the basic top lateral reinforcing in non-SMC bridges.

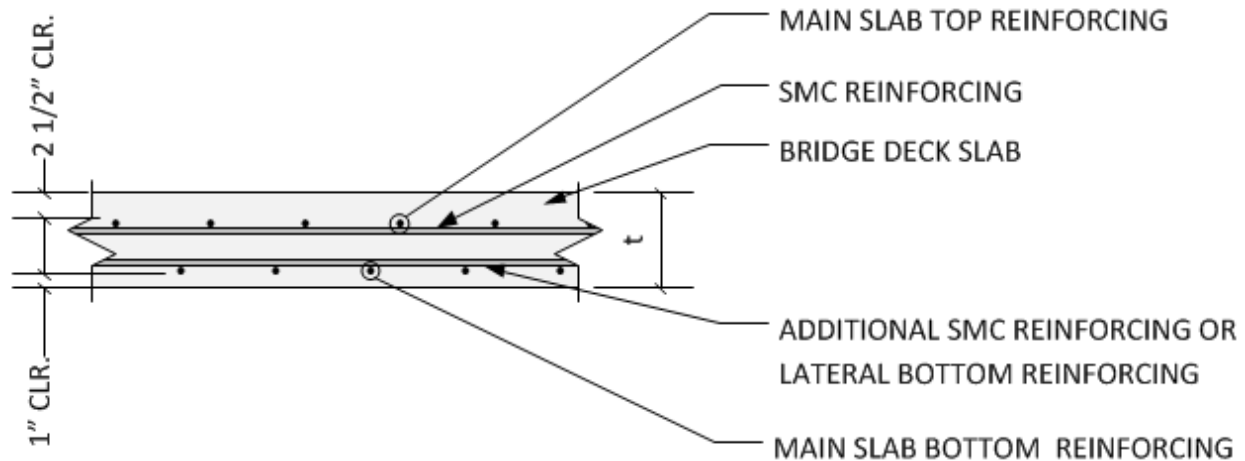


Figure 114 Slab Reinforcing Placement

6.3 GIRDER SELECTION CRITERIA

The depth of the bridge girders is critical in determining the composite properties of the positive moment section, the moment arm for the SMC composite properties and the moment of inertia for deflection calculations. Based on a review of the SMC bridges presently constructed, the ratio of the bridge girder span to nominal girder depth (L/d) varied from 26 to 30; on this basis, an average value of 28 was selected to determine the girder depths for the various bridge spans in this study.

6.3.1 Girder Type Selection

The maximum available standard rolled girder shape is a W44x335 by depth or a W36x800 by weight. Once girders greater than available standard rolled sizes are required, plate girders must be designed. (Also, it is quite possible that plate girders with sections lighter than the standard rolled sizes may be fabricated and have the required section properties. These custom girders may ultimately cost more due to additional fabrication time, and thus this alternative is beyond the scope of this study.)

Plate girders for required bridge girder depths larger than 44 inches were developed to meet the L/d criteria for spans longer than 104 feet, the limit for a 44 inch deep girder. The plate girder depths range from 48 inches to 60 inches depending upon the span requirement; the plate girder designations and dimensions are given in Appendix 5 – Plate Girder Dimensions.

6.3.2 Girder Serviceability Criteria

AASHTO has no required limitations on vertical deflections although it does state that when other criteria are not available, the limitation for deflection under vehicular load should be 1/800 of the span. The AASHTO criterion was used for the selection of girders in the parametric study to eliminate girders from consideration that did not meet this requirement. The service load requirement for deflection is AASHTO load combination ‘Service I’, which has the load factors as shown in Table 3.

The only loads considered in the deflection calculations were the design truck live load and the lane live load; the dead loads of the girders and the slab occur prior to the girders achieving continuity and the girders are typically cambered upward to compensate for these deflections.

6.5 FINAL RANGES OF PARAMETERS

Based on the preceding constraints and criteria, the final ranges of parameters for the study are presented in Table 26. The rolled girder sizes are available standard shapes, whereas the plate girder sizes were developed by the author during the analysis. Full information on the dimensional properties of the plate girders are given in Appendix 5 – Plate Girder Dimensions.

Table 26 - Span and Spacing Ranges for the Parametric Study

Variable	Range	Increment
Girder Span	80 feet to 140 feet	12 feet
Girder Spacing (Slab span)	7'-4" to 10'-4"	4 inches
Slab Depth	8 inches to 9 inches	1/2 inch

Variable	Range	Increment
Rolled Girders	W33, W36, W40, W44	Not applicable
Plate Girders	48 inch to 60 inch depths	6 inches

For each particular girder span considered, there are 30 possible configuration combinations to be considered between the various slab depths and girder spacings. As mentioned previously, the girder depths were defined using the ratio of the span to depth of 1/28; the parametric study girder spans and the corresponding required girder depths are shown in Table 27. The plate girders used for girder depths larger than 44 inches in depth were given reference designations of PG1, PG2, etc., for convenience. The range of rolled and plate girder sizes to be analyzed for the varying ranges of slab depths and girder spacings are given in Table 27. The first value is the nominal depth and weight of lightest girder in the depth series followed by only the weights of the remaining girders in the series. Also presented in Table 27 are the maximum recommended deflections based on L/800. It was likely that the lighter girder sizes may be ruled out by not meeting the deflection criteria, moment capacity, etc.

Table 27- Girder Span to Girder Size Table

Span	Girder Sizes Considered	Maximum Deflection
80 feet	W33x118, 130, 141, 152, 169, 201, 221, 241, 263, 291, 381, 354, 387	1.20 inches
92 feet	W40x149, 167, 183, 211, 235, 264, 327, 331, 392, 199, 214, 249, 277, 297, 324, 362	1.38 inches
104 feet	W44x335, 290, 262, 230	1.56 inches
116 feet	PG1, PG2, PG3, PG4, PG5, PG6, PG7, PG8 (48 inch depth)	1.75 inches
128 feet	PG8, PG9, PG10, PG11, PG12, PG13, PG14, PG22 (52 inch depth)	1.92 inches
140 feet	PG15, PG16, PG17, PG18, PG19, PG20, PG21, PG22 (60 inch depth)	2.10 inches

6.6 ANALYSIS CONSIDERATIONS

The parametric study was intended to determine the appropriate girder size from a range

of sizes for a particular depth range for bridges from two to eight total girder spans, for varying slab thicknesses and varying slab spans. A sensitivity investigation was performed to compare values of maximum positive and negative moments along the bridge for different numbers of girder spans, since the fewer spans that require analysis, the faster the total processing time. This investigation considered a bridge with 80 foot spans and a bridge with 140 foot spans. The 80 foot span bridge was analyzed with W33x118 girders for each span and the 140 foot span bridge was analyzed with PG23 plate girders for each span. The controlling design moments, which are produced by the AASHTO 'Dual Design Truck', are presented in Figure 115 for the minimum and maximum spans to be investigated, 80 feet and 140 feet. As the chart shows, for a given span length, the positive moment is constant for all practical purposes for all span quantities. For two span bridges, there is an increase of approximately 10% in the magnitude of the negative moment; for three spans, the negative moment decreases, but increases slightly at four spans and remains virtually constant for more spans. Based on this investigation, the parametric study performed analysis on two bridges, the first with two girder spans to capture the highest negative maximum moments and the second with four girder spans to capture the approximate envelope of maximum positive and negative moments for bridges of three or more spans. It should be noted that very few of the SMC bridges reviewed had less than three girder spans.

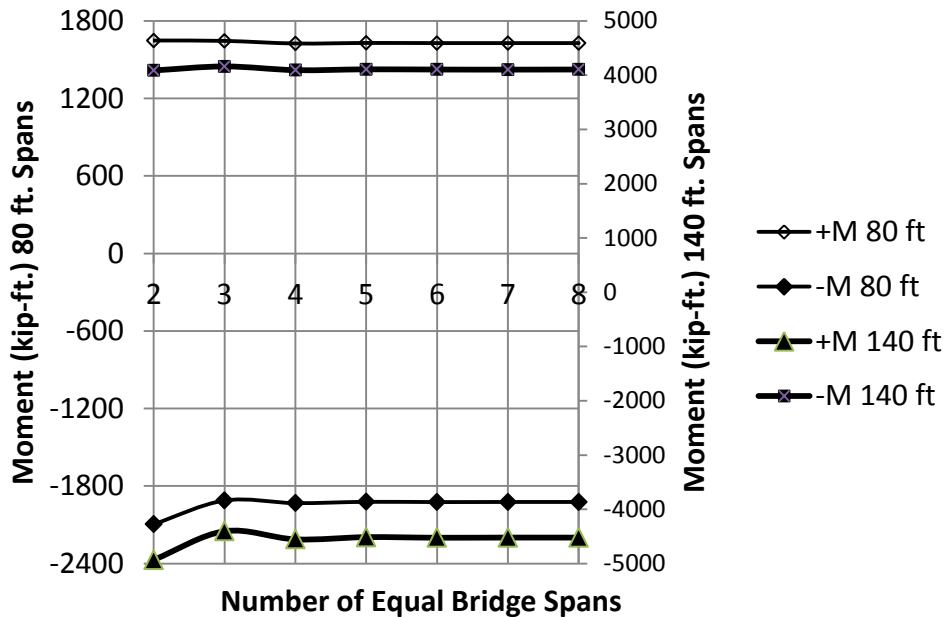


Figure 115 Maximum and Minimum Moments vs. Spans (note: moment scales are different)

6.7 FINAL TRUCK LOAD ANALYSIS

Given the ranges of parameters in Section 6.5 it was necessary to analyze each selected bridge span for ten different girder spacings each with three possible slab thicknesses. Each slab depth, girder spacing and girder size resulted in a different axle load distribution factor to calculate the percentage of the axle loads to the girder. Since the original study girder was constructed with a three inch deep concrete haunch between the slab and girder, a three inch deep haunch was also included in the parametric study analyses. The slab haunch will not only increase the positive moment and negative moment capacity, but it will also increase the composite girder stiffness, thus increasing the axle load distribution factor and correspondingly, the axle load to the girder. If adjacent girders had different depth haunches, the axle load distribution factor for these girders would be based on their specific haunch depth. While it may be conservative to ignore the slab haunch for the composite properties of the girder, it would be unconservative not to consider the haunch in the calculation of the axle load distribution factor.

Along with the axle loads, a uniform lane loading (live load) of 64 psf and a uniform bridge wearing course loading (dead load) of 35 psf were applied.

Each possible girder within the particular span range (as identified in Table 27) was evaluated for the following acceptance criteria:

1. Ultimate positive composite moment capacity greater than or equal to the factored applied positive moment.
2. Service level maximum downward deflection less than or equal to $L/800$, where L is in inches.

The moving load analysis software discussed in Section 3.3.1 Preliminary Analysis, was used to perform the analysis for the various girder and slab combinations. Results of the moving truck load analysis consisted of determining the maximum positive interior moment, the maximum negative SMC moment and the required composite moment of inertia to meet the $Span/800$ vehicular load deflection limit for each case. These results were then analyzed and the lightest girder, which met both the positive moment capacity and had sufficient composite beam stiffness to meet the deflection limit, was selected.

Acceptable girders for a bridge with 80 foot girder spans are presented in Table 28. The tables for bridges with girder spans from 92 feet through 140 feet in 12 foot increments are provided in Appendix 6 – Acceptable Bridge Girders.

Table 28 - Girder Acceptance Table - 80 ft. Span

Girder Spacing	Slab Thickness		
	8 inches	8.5 inches	9 inches
7.33 ft.	W33x152	W33x141	W33x141
7.67 ft.	W33x152	W33x152	W33x152
8.00 ft.	W33x152	W33x152	W33x152
8.33 ft.	W33x169	W33x152	W33x152
8.67 ft.	W33x169	W33x169	W33x169
9.00 ft.	W33x169	W33x169	W33x169

Girder Spacing	Slab Thickness		
	8 inches	8.5 inches	9 inches
9.33 ft.	W33x169	W33x169	W33x169
9.67 ft.	W33x201	W33x201	W33x169
10.00 ft.	W33x201	W33x201	W33x169
10.33 ft.	W33x201	W33x201	W33x201

The maximum SMC negative moments for the acceptable girders were tabulated for use in the development of the top SMC reinforcing design formulation. The final values for a bridge with 80 foot girder spans are presented in Table 29. The tables for bridges with girder spans from 92 feet through 140 feet in 12 foot increments are provided in Appendix 7 – Maximum SMC Negative Moments.

Table 29 - Maximum SMC Negative Moments (kip-feet) - 80 ft. Span

Girder Spacing	Slab Thickness		
	8 inches	8.5 inches	9 inches
7.33 ft.	-2020	-2013	-1988
7.67 ft.	-2080	-2074	-2045
8.00 ft.	-2128	-2123	-2093
8.33 ft.	-2190	-2171	-2140
8.67 ft.	-2239	-2241	-2201
9.00 ft.	-2288	-2289	-2248
9.33 ft.	-2336	-2338	-2295
9.67 ft.	-2408	-2400	-2341
10.00 ft.	-2456	-2448	-2388
10.33 ft.	-2504	-2496	-2459

There are several items of note upon review of Table 29; firstly the SMC negative moments increase with girder spacing. This is logical since an increase in girder spacing will also increase the amount of lane loading and wearing course loading to the girder since both of these are post-composite and thus affect the SMC moment. However, these loads are not the only reason that SMC moments increase, the girder spacing also affects the axle load distribution factor, D_f , (Equation 3), this is due to an increase in the moment of inertia of the composite section as the flange width, which is also one half of the girder spacing is increased. The

increased girder stiffness will cause it to attract more loading from the design truck axles. Secondly, is the decrease in negative moment for thicker slabs; this is actually because the slab dead load is applied prior to the SMC action becoming effective and therefore does not have an effect on the SMC moment. An additional reason for the decrease is again the axle load distribution factor in which the slab thickness affects the slab stiffness, so a thicker slab is better able to distribute loads to the adjacent supporting beams and correspondingly decrease both the positive and negative moments due to truck loadings in the SMC condition.

The determination of acceptable girders was based upon the composite slab and girder sections having adequate strength for the positive bridge girder moment and having sufficient stiffness to meet the selected (L/800) deflection criteria. An approximate method for determining the maximum deflections, which in every case occurred in the first span, was developed; this method involved several simplifications in order to be easily used. On the basis of the maximum deflection, a moment of inertia may be determined based on only the span length and maximum moment; the final formulation is given in Equation 7.

$$I_{\min} \geq \frac{800M_{\max}L}{3452} \approx 0.24M_{\max}L \text{ (Equation 7)}$$

Where:

I_{\min} = Minimum moment of inertia to achieve $l/800$ deflection limitation in inch^4

M_{\max} = Maximum unfactored superimposed load moment in kip-feet

L = Length of the girder span in feet

The moment of inertia formulation was verified using RISA-3D analysis software and found to give acceptable approximations for different span lengths and loading conditions. The calculations for the development of the formula are presented in Appendix 8.

The acceptable girders from the parametric study were then used in the development of the SMC connection design methodology presented in Chapter 7.

CHAPTER 7 PROPOSED DESIGN FORMULATION

7.1 PRELIMINARY CONSIDERATIONS

In the original study connection, the main elements involved in resisting the SMC moment at the support are the girder bottom flange, the weld to the sole plate and the sole plate for the compression component and the top SMC and temperature reinforcing bars for the tension component.

As discussed in Section 5.7.3, several elements of the compression transfer mechanism of the study connection as originally designed and tested were cause for concern, specifically, the sole plate and the weld of the girder bottom flange to the sole plate. The sole plate failed in yielding at an applied moment of 960 kip-ft and the weld from the girder to the sole plate failed in rupture at an applied moment of 1440 kip-ft, both of which were well below the required design ultimate moment of 1782 kip-ft. Both of these elements were crucial to the transfer of the compression component of the maximum internal SMC moment between girders to which the actual study bridge would be subjected. Additionally, the weld between the girder bottom flange and the sole plate was found to be subject to a fatigue stress category E', which has a maximum stress range of 2.6 ksi, well below the actual stress range of approximately 100 ksi. As was also discussed, these concerns may be alleviated through the use of a direct compression transfer plate fitted between the bottom flanges.

A safety device that was used during testing to transfer load in case of weld failure functioned well during the test after both yielding of the sole plate and fracture of the welds of the bottom flange to the sole plate. In order to allow for fit up tolerances in the field, the actual compression transfer plate should consist of two wedge shaped plates as was used in the Tennessee SMC bridges (Appendix 1 – Current SMC Bridges and Chapman, 2008). These types

of plates would allow for both longitudinal and slight angular corrections. The wedge compression plates would subsequently be intermittently field welded to prevent further movement.

This new scheme would not require the welds between the girder bottom flange and the sole plate for axial load transfer since the entire axial load will travel directly through the compression transfer plate. Omitting the extensive welding of the girder to the sole plate would eliminate a significant amount of skilled field labor, but would also require a new method of lateral restraint to be provided for the girder bottom flange. Several options to provide lateral restraint are:

1. Provide anchor bolts through the sole plate and the bottom girder flanges (Figure 116 and Figure 117)
2. Provide field welds for only lateral stability between the sides of the flanges and an anchor bolted sole plate (Figure 118 and Figure 119)
3. Provide welded guide bars on an anchor bolted sole plate with a small space allowance on either side of the girder bottom flange (Figure 120 and Figure 121)

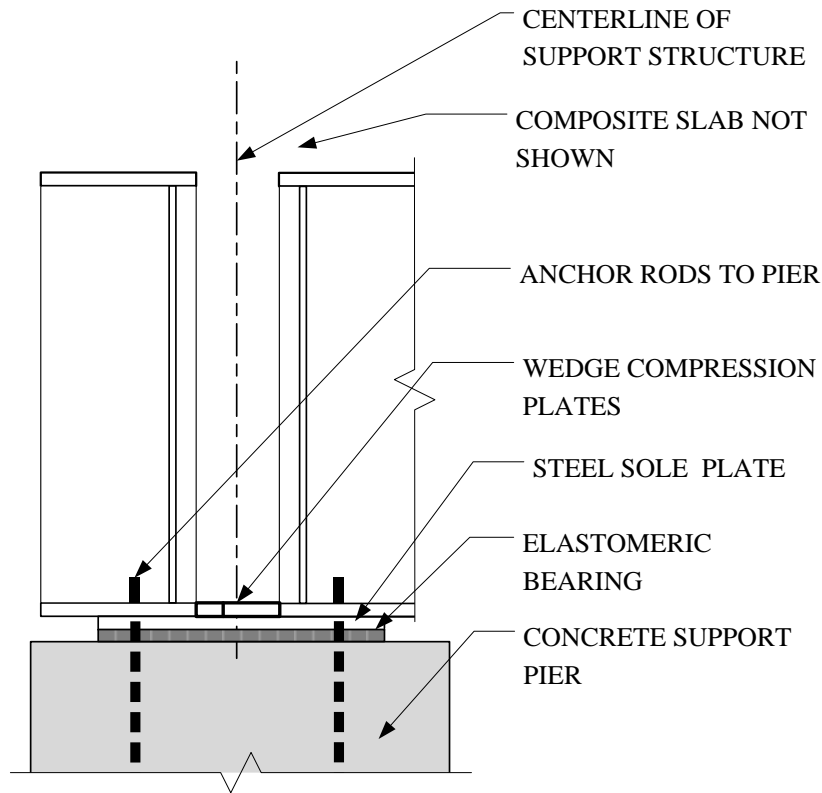


Figure 116 - SMC Girder Support Detail 1 – Side View

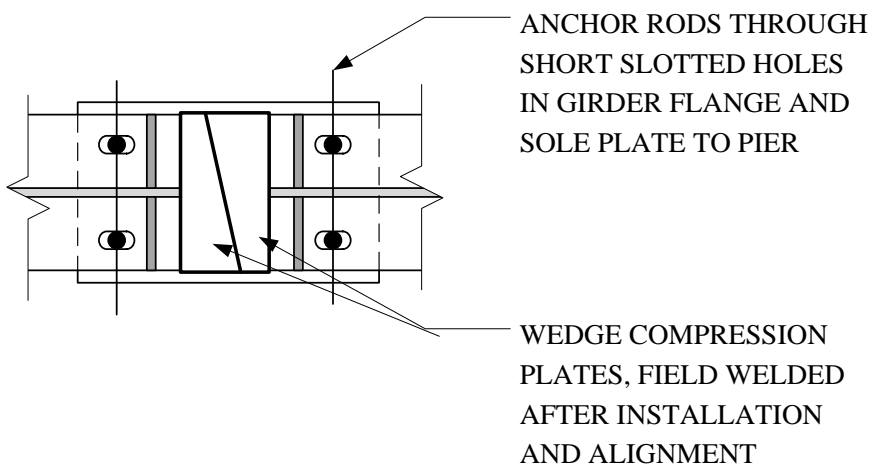


Figure 117 - SMC Girder Support Detail 1 - Plan View

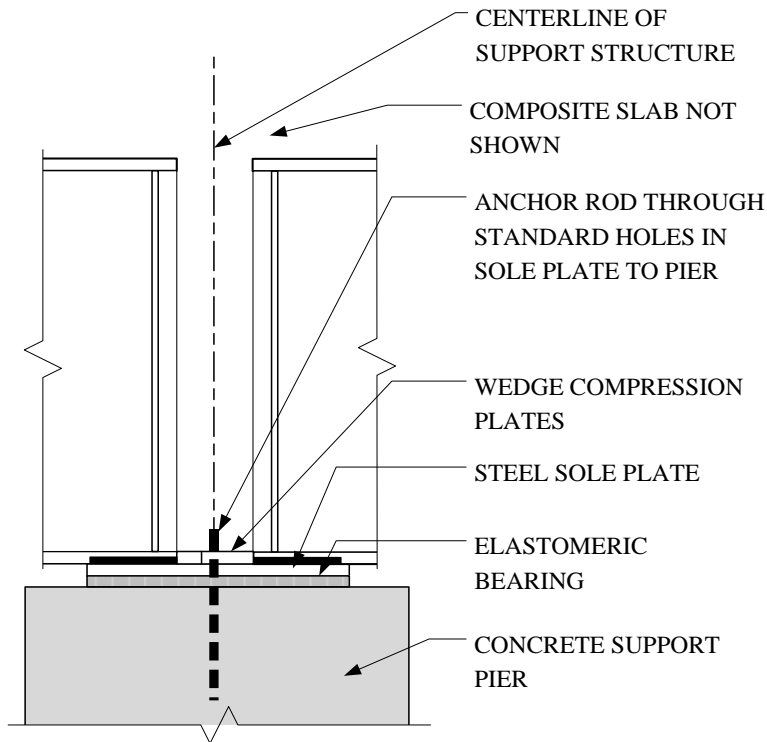


Figure 118 – SMC Girder Support Detail 2 – Side View

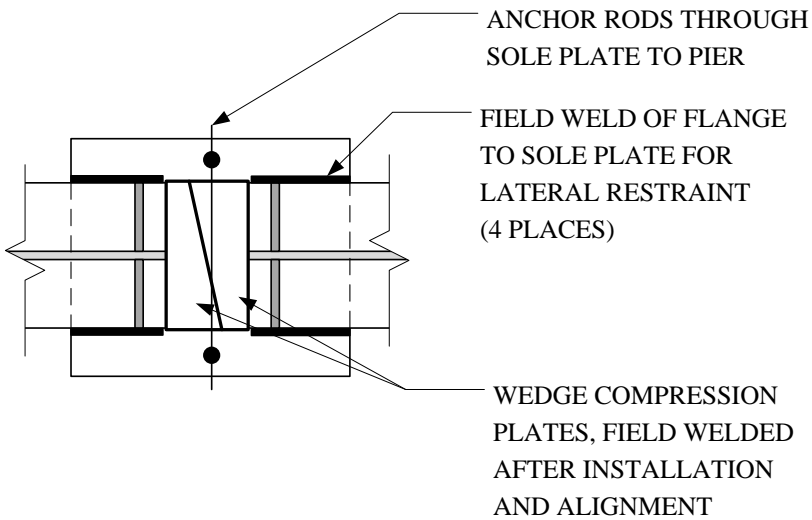


Figure 119 - SMC Girder Support Detail 2 - Plan View

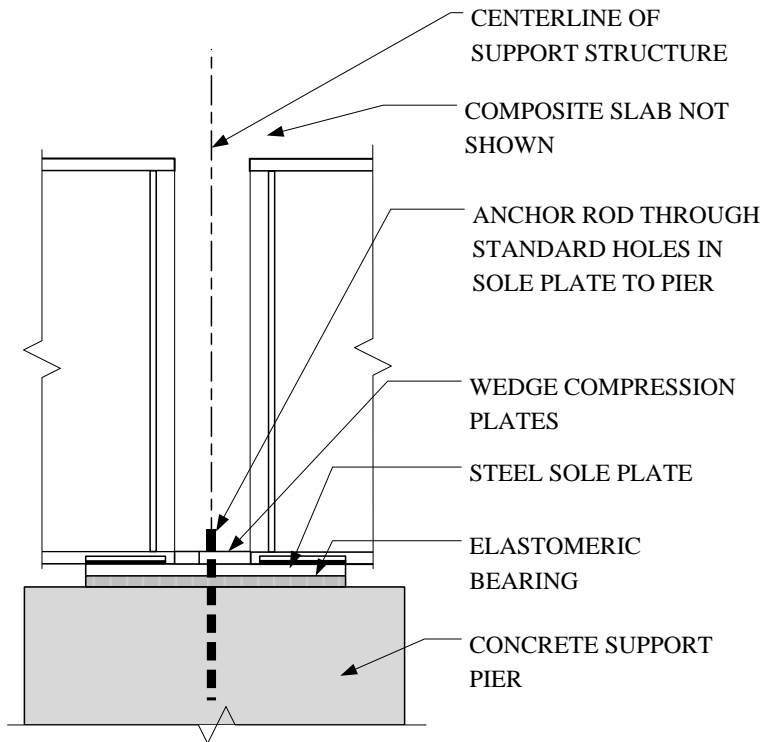


Figure 120 - SMC Girder Support Detail 3 - Side View

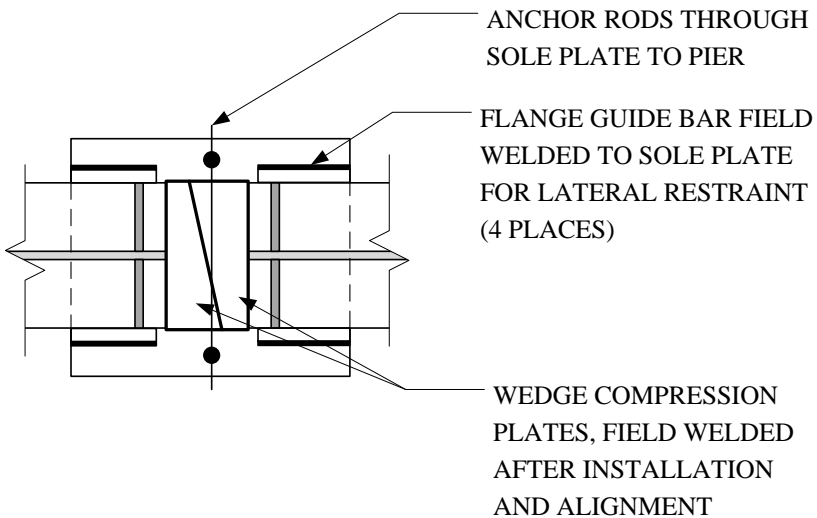


Figure 121 - SMC Girder Support Detail 3 - Plan View

These three possible modifications involve increasing degrees of complexity and consequently, construction cost, also the welds in the second detail could again be subject to

fatigue from compression due to bending in the bottom flange. Therefore, the modifications presented in Figure 116 and Figure 117 will be used in the final connection design strategy.

The wedge transfer plates considered are similar to those used in the Tennessee bridges (Talbot, 2005) and will use the same skew angle of 2.5 degrees between the plates. The design will require the plates to resist the compression load, which will be transferred through direct bearing from the girder bottom flanges. The design will also entail determining the vertical component of the compression force on the skew and designing a partial penetration groove weld for the shear force.

From a review of currently constructed SMC bridges (including the study bridge), all of the bridge slabs were reinforced with SMC top reinforcing and top temperature (longitudinal) bars at the same spacing. It's most likely that this was done for convenience and to avoid the possibility of misplacement of bars in the field. This common, combined placement of the slab SMC and temperature bars will be considered in the formulation and evaluation of the tension component of the proposed design equation. Also, as was seen in the evaluation of the shear lag in the SMC reinforcing steel (Figure 94), the two sets of bars, SMC and temperature, immediately on either side of the girder take a significantly larger share of the tensile load component than the remaining bars.

The final ranges of acceptable girders vs. span and negative moments vs. span were subsequently used in the development of a proposed design equation. These ranges are provided in Table 28 in Section 6.7 and Table 46 through Table 50 in appendix 7, respectively.

7.2 FORMULATION DEVELOPMENT

The basic rationale for the behavior of the connection is the development of an internal couple created by the tension in the simple-made continuous top reinforcing bars being equal to

the compressive component of the bottom flange of the girder. This methodology is not unlike those developed at the University of Nebraska and used in various SMC bridges constructed in Nebraska and elsewhere with the exception that the previous schemes made use of heavy steel blocks to transfer the compressive component of the couple from the flange and a portion of the web and encased the entire connection in a concrete diaphragm.

The starting point for the design would be the selection of a girder, which has sufficient strength and stiffness in the composite condition to meet the strength and serviceability requirements due to the maximum positive moment in the span; girders meeting these acceptance criteria were determined in Chapter 6.

A simple and straightforward approach to design the SMC connection is to directly equate the area of the reinforcing steel to the area of the bottom flange of the girder without regard to the difference in the yield stresses and resistance factors between the two. This method is slightly conservative since $F_y = 50$ ksi for the girder steel and $F_y = 60$ ksi for the reinforcing steel, however, the resistance factors are $\phi = 1.0$ and $\phi = 0.90$ for the girder and reinforcing steel respectively, thus the factored yield stresses are 50 ksi and 54 ksi respectively. Not only is this method conservative, but will also somewhat equalize the strains of the tension and compression components. Equal or approximately equal strains are a desirable behavior because they will enable more accurate calculation of the section stiffness and thus more accurate determination of girder deflections. Once the area is determined, the next step is to multiply the force developed by the area of steel by the moment arm between the two areas and check the value against the required SMC moment capacity. One point of concern is the considerable increase in the stress in the SMC top bars on either side of the girder; this may be remedied by the inclusion of the temperature bars in the capacity of these bars. Thus there must be a requirement that the top

temperature bars be spaced at the same spacing as the SMC top bars. The same reinforcing bar strain behavior in the bars adjacent to the girder was noted in the physical test results of other SMC bridge researchers as well (Farimani R. S., 2014 and Niroumand, 2009). Also, in this other research, the bridge model's loadings were increased during the experimental test such that the reinforcing bars on either side of the girder yielded and as the loading was increased the adjacent bars load increased until they yielded, which continued until the bars at the extents of the slab also yielded. While this is not necessarily a desirable behavior for normal bridge loadings, it does indicate that bridges of this type do have considerable reserve capacity for overload.

The final components are the wedge shaped compression transfer plates, including the weld between the two pieces. Several points to consider are the potential moment induced in the transfer plate if its thickness is greater than the thickness of the bottom flange and the possibility of differences in the yield strengths of the flange and plates. The final modified connection configuration is shown in Figure 122.

On the basis of the preceding, the recommended design methodology would proceed as follows:

1. Equate the area of SMC reinforcing to the area of the bottom flange:

$$A_r \geq A_f = b_f t_f \text{ (Equation 8)}$$

Where:

A_r = required area of SMC reinforcing steel (in.²)

A_f = area of girder bottom flange (in.²)

b_f = width of bottom flange (in.)

t_f = thickness of bottom flange (in.)

The recommended minimum bar size is #8; smaller bars would require a significantly greater number (over 30%) of bars be placed.

2. Determine the moment arm between the couple based on girder and slab geometry:

$$d_m = d_h + t_s - cl - D_t - \frac{D_{SMC}}{2} + d_G - \frac{t_f}{2} \text{ (Equation 9)}$$

Where:

d_h = depth of haunch (inches)

t_s = thickness of slab (inches)

cl = reinforcing clear distance (inches)

D_t = main (lateral) top reinforcing bar diameter (inches)

D_{SMC} = SMC (longitudinal) reinforcing bar diameter, (inches)

d_G = depth of girder (inches)

t_f = thickness of girder flange (inches)

3. Verify the moment capacity of the section using the area and yield stress of the girder

flange:

$$\phi M_n = \phi_f A_f d_m F_{yG} \text{ (Equation 10)}$$

Where:

$\phi_f = 1.0$ Flexure

M_n = Nominal moment capacity (k-in)

A_f = Area of the bottom flange (in.²)

d_m = Moment arm between SMC reinforcing and center of bottom flange (in.)

F_{yG} = Yield stress of girder flange (ksi)

4. Design of the wedge compression plates and weld

- a. Cross-sectional area of the wedge plates, A_{pl} :

$$A_{pl} \geq \frac{A_f \phi_f F_{yw}}{\phi_c F_{ypl}} = t_{pl} b_{pl} \text{ (Equation 11)}$$

Where:

A_f = Area of girder bottom flange (in.²)

$\phi_f = 1.0$ Flexure

F_{yW} = Yield strength of girder (ksi)

$\phi_c = 0.9$ Axial compression

F_{ypl} = Yield strength of plate (ksi)

t_{pl} = Wedge plate thickness (in.)

b_{pl} = Wedge plate width (in.)

- b. Plate thickness shall match the thickness of the girder flange as closely as possible
- c. Check bearing on the plate material from the girder. AASHTO has no specific bearing strength requirements, so these have been taken from the AISC Manual (AISC, 2011).

$$A_p = t_{pl}b_f \geq \frac{\phi_f A_f F_{yW}}{1.8\phi_p F_{ypl}} \text{ (Equation 12)}$$

Where:

A_p = Bearing area of plate against flange

t_{pl} = Thickness of wedge plate (in.)

b_f = Girder bottom flange width (in.)

$\phi_f = 1.0$ Flexure

A_f = Area of girder bottom flange (in.²)

F_{yW} = Yield strength of girder (ksi)

$\phi_p = 0.75$ Bearing

F_{ypl} = Yield strength of plate (ksi)

- d. Design of partial penetration groove weld:

$$w_t = \frac{V_W}{0.6\phi_{e2}F_{exx}} + 0.125 = \text{Minimum weld size (in.) (Equation 13)}$$

Where:

$$V_w = A_f F_{yW} \sin(2.5) = 0.044 A_f F_{yW} = \text{Shear force between the plates (kips)}$$

$$L_w \approx b_{pl} = \text{Wedge plate width (in.)}$$

$$\phi_{e2} = 0.8$$

$$F_{exx} = \text{Ultimate strength of weld metal (ksi)}$$

5. The SMC reinforcing for the girders must meet two criteria:
 - a. The total area of the provide SMC reinforcing steel must equal or exceed the area of the girder bottom flange. This criterion will determine the total number of a specific bar size to be placed at the SMC girder connection within the effective slab width.
 - b. A single SMC top bar considered in conjunction with a single top temperature bar must have the factored tensile capacity to resist a factored tensile load of 9% of the total SMC reinforcing tension component. This criterion is based on the results of the physical test for the study connection and review of test results by other investigators (Farimani R. S., 2014) (Niroumand, 2009) and may affect the size of the reinforcing bars used.

The development of these guidelines is given in section 7.3.

Reviewing the equations, it can be seen that once an acceptable girder and SMC reinforcing bar size is selected, all of the variables required for the equations are known values. Not considered in the design equation formulation was the reaction behavior at the support. As was discussed in Section 5.7.1, the actual negative moment at the end of the girder is less than the maximum theoretical centerline of support moment due to the girder reaction not being at the centerline of the pier, but actually occurring between 8 inches and 12 inches away from the centerline of the support. Neglecting this behavior adds a slight conservatism to the design.

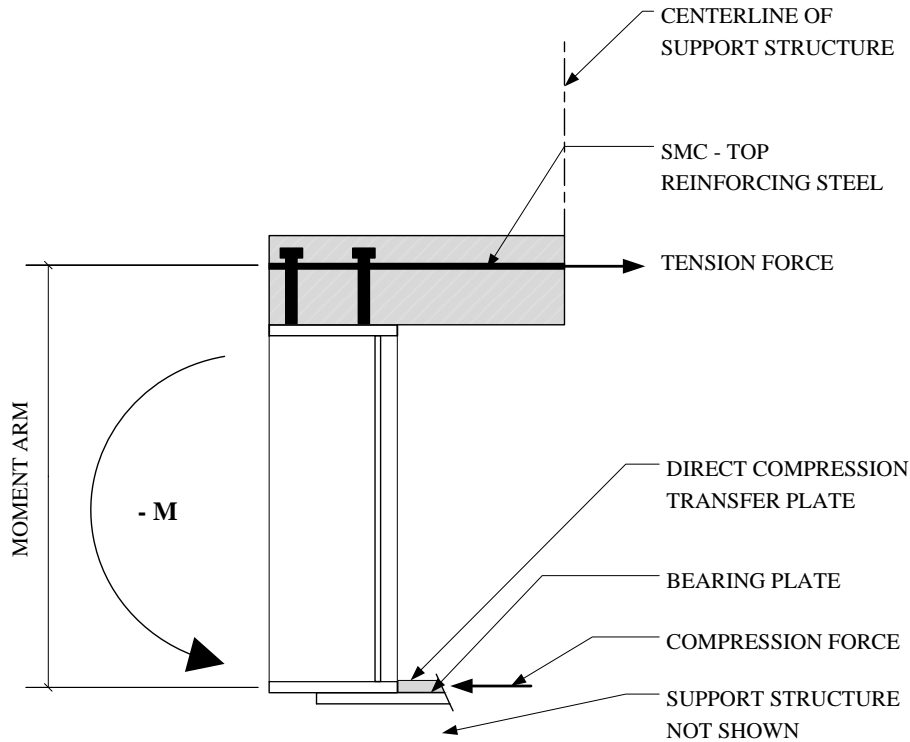


Figure 122 - SMC Behavior

7.3 VERIFICATION/VALIDATION OF DESIGN FORMULATION

To test the proposed design equation, several girders and their corresponding maximum negative moments were compared against the proposed design equation and methodology.

A full example using an 80 foot girder span with a 9 inch thick slab and 9 foot girder spacing and #9 SMC reinforcing bars follows:

From Tables 28 and Table 29 (Section 6.7) the following information is given:

Girder Size: W33x169 $b_f = 11.5$ in., $t_f = 1.22$ in., $d = 33.8$ in.

Negative Moment: $M = -2248$ k-ft

Calculations for the connection design follow:

Determination of required dimensions:

$$A_f = 1.22(11.5) = 14.03 \text{ in.}^2$$

$$d_h = 3 \text{ in.}$$

$$t_s = 9 \text{ in.}$$

$$cl = 2.5 \text{ in.}$$

$$D_t = 0.625 \text{ in. (#5 bar)}$$

$$D_{SMC} = 1.125 \text{ in. (#9 bar)}$$

$$d_g = 33.8 \text{ in.}$$

$$t_f = 1.22 \text{ in.}$$

$$d_m = 3 + 9 - 2.5 - 0.625 - \frac{1.125}{2} + 33.8 - \frac{1.22}{2} = 41.5 \text{ in.}$$

Determine SMC bar quantity and spacing:

$$A_{\#9} = 1.00 \text{ in.}^2$$

$$N = 14.03 \text{ in.}^2 / (1 \text{ in.}^2 / \text{bar}) = 14 - \#9 \text{ bars}$$

$$\text{Slab Width} = 9.0 \text{ ft.} = 108 \text{ in.}$$

$$\text{Spacing} = 108 \text{ in.} / 14 \text{ bars} = 7.7 \text{ in./bar}; \text{ Say } \#9 @ 7 \frac{1}{2} \text{ inches}$$

Verify capacity:

$$\phi M_n = \frac{14.03 \text{ in.}(41.5 \text{ in.})(50 \text{ ksi})}{12 \text{ in./ft.}} = 2425 \text{ kip-ft} > 2248 \text{ kip-ft OK}$$

Design wedge compression transfer plates using $F_y = 50 \text{ ksi}$ plates:

$$A_{pl} \geq \frac{14.03 \text{ in.}^2 (1.0) 50 \text{ ksi}}{0.9(50 \text{ ksi})} = 15.6 \text{ in.}^2$$

$$\text{Try PL } 1 \text{ in.} \times 16 \text{ in.}, A_{pl} = 16.0 \text{ in.}^2 > 15.6 \text{ in.}^2, \text{ OK}$$

$$t_{pl} = 1.0 \text{ in.} \approx 1.06 \text{ in.} = t_f \text{ OK}$$

$$A_p = 1.0 \text{ in.}(11.6 \text{ in.}) = 11.6 \text{ in.}^2 > \frac{1.0(1.06 \text{ in.})(11.6 \text{ in.})(50 \text{ ksi})}{1.8(0.75)(50 \text{ ksi})} = 9.03 \text{ in.}^2$$

Design weld:

$$V_w = 0.044(14.03 \text{ in.}^2)(50 \text{ ksi}) = 30.9 \text{ kips}$$

$$w_t = \frac{30.9}{0.6(0.8)(70 \text{ ksi})(16 \text{ in.})} + 0.125 = 0.183 \text{ in.} - \text{ Use } \frac{1}{4} \text{ in. weld}$$

$$\text{Total weld capacity} = \left(\frac{1}{4} \text{ in.} - \frac{1}{8} \text{ in.} \right) (0.6)(0.8)(70 \text{ ksi})(16 \text{ in.}) = 67.2 \text{ kips} > 30.9 \text{ kips, OK}$$

Verification of area of SMC reinforcing with #5 temperature bars:

$$A_{\#9} = 1.00 \text{ in.}^2, A_{\#5} = 0.31 \text{ in.}^2$$

$$A_{total} = 1.31 \text{ in.}^2$$

$$\phi A_{total} F_y = 0.9(1.31 \text{ in.}^2)(60 \text{ ksi})=70.7 \text{ kips}$$

$$\text{Total flange force} = (14.03 \text{ in.}^2)(50 \text{ ksi})=702 \text{ kips}$$

Check bar force capacity > 9% of flange force

$$70.7 \text{ kips} > 63.2 \text{ kips} = 0.09(702 \text{ kips}), \text{ OK}$$

Table 30 summarizes the reinforcing design results for the preceding example and several other samples. All of the girder and slab arrangements checked were found to be acceptable, although the capacity of case 2 was slightly under, but within 0.5 % of the required value.

Table 30 - Sample SMC Reinforcing and Moment Calculations

Case	0	1	2	3	4	5
Girder Span (ft.)	80	92	92	104	116	116
Girder Size	W33x169	W40x183	W40X183	W44x230	PG1	PG1
Slab t (t _s) (in.)	9	8	9	8	8	9
Girder Spacing (ft.)	8	8	9	8	7.67	10
-M _u (k-ft)	2248	2641	2770	3153	3552	4134
b _f (in.)	11.5	11.8	11.8	15.8	24	24
t _f (in.)	1.22	1.2	1.2	1.22	0.75	0.75
A _f (in. ²)	14.03	14.16	14.16	19.276	18	18
d _h (in.)	3	3	3	3	3	3
cl (in.)	2.5	2.5	2.5	2.5	2.5	2.5
D _t (in.)	0.625	0.625	0.625	0.625	0.625	0.625
D _{SMC} (in.)	1.125	1.125	1.125	1.125	1.125	1.125
d _G (in.)	33.8	39	39	42.9	48	48
Number of Bars	15	15	15	20	19	19
d _m (in.)	41.5	45.7	46.7	49.6	54.9	55.9
φM _n (k-ft)	2426	2697	2756	3984	4120	4195
Status	Adequate	Adequate	Adequate (Within 0.5%)	Adequate	Adequate	Adequate

As was discussed in section 7.2, the SMC reinforcing for the girders must meet an additional criterion besides having a minimum area equal to the girder bottom flange area, which

is that the factored strength of one SMC bar combined with the factored strength of one temperature bar must equal or exceed 9% of the total capacity required. This additional criterion is based on the results of the physical test for the study connection and review of test results by other investigators (Farimani R. S., 2014) (Niroumand, 2009) and may affect the size of the reinforcing bars used.

Thus, the effects of this behavior must also be considered when designing SMC reinforcing. The strain results in the SMC reinforcing bars from the day 2 test are shown in Figure 123 and aside from the jump in curves due to the activation of the safety device, the curves are relatively linear. The physical locations of the individual gages are shown in Figure 75. The two most highly stressed reinforcing bars are those which are located on both sides of the steel girder and are numbers SSL-1 and SSL-2.

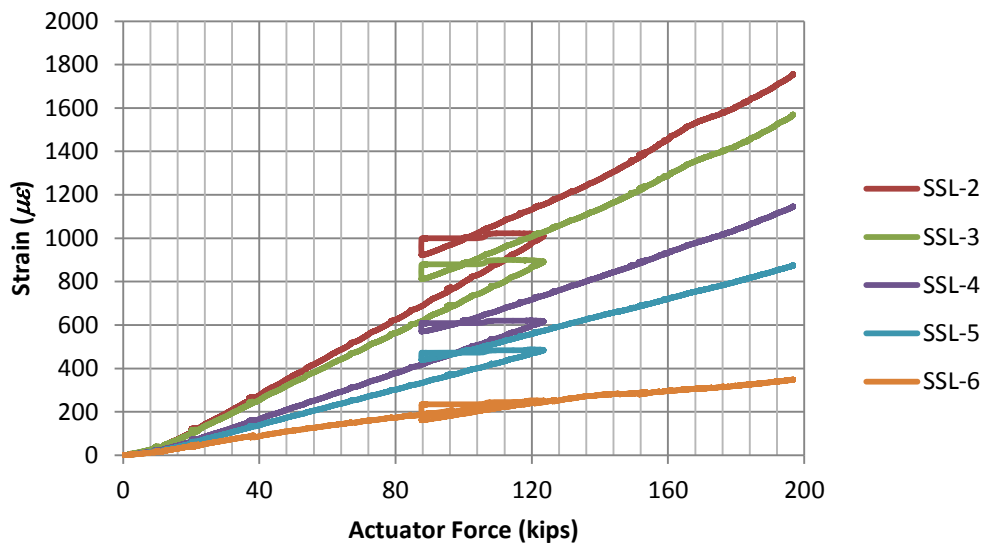


Figure 123 - Day 2 SMC Reinforcing Strains vs. Actuator Force

In order to account for this effect, the total number of reinforcing bars must be known. The area of reinforcing required based on equation $A_r = A_f = b_f t_f$ is 12.3 in² for the W33x152 girder, which has a 11.6 in. wide x 1.06 in. deep flange. Using #8 reinforcing bars, which have

an area of 0.79 in^2 , the total number of bars in the effective flange width must be $12.3/0.79 = 15.6 \approx 16$ bars, which would be spaced at $88/16 = 5.5 \approx 6.0$ inches; coincidentally, this matches the actual test model reinforcing. The tension in each bar adjacent to the girder would be $0.09 \times 2020 \times 12 / 40.35 = 54$ kips (9% of the total tension each). The ultimate capacity of a #8 bar is $\phi F_y A_s = 0.9 \times 60 \times 0.79 = 42.7$ kips, which is less than 54 kips.

A likely reason that the test bridge reinforcing did not yield at the final load, which in effect, applied a moment of 2400 k-ft, was due to #5 temperature bars being adjacent to the #8 SMC bars. There is no reason that these bars may not be considered to act in unison with the SMC reinforcing bars as the SMC reinforcing will aid in reducing shrinkage as well as the temperature bars will aid in resisting the SMC tension. So considering the adjacent temperature bars, the ultimate capacity of the pair is 66 kips, which when factored is 59.4 kips and is greater than 54 kips.

In order to provide assurance that the reliance on #5 temperature bars to help carry the SMC moment near the girder is reasonable for the full range of girders evaluated, all of the acceptable girders were examined. Checking the combined capacity of the bar adjacent to the girder combined with a #5 temperature bar to 9 % of the total SMC tension resulted in a relationship where the size of the main SMC bar required is a function of the ratio of the area of the girder to the area of the bottom flange. The ratio requirements are presented in Table 31 - Minimum SMC Bar Size based on Girder Area/Flange Area. While the table is a reasonable guide, a simple check of the bar capacity is also a very quick and simple calculation.

Table 31 - Minimum SMC Bar Size based on Girder Area/Flange Area

Minimum SMC Bar Size	Range of ratios of Girder Area to Flange Area
#8	$A/A_f > 3.5$
#9	$3.5 > A/A_f > 3.3$
#10	$3.3 > A/A_f > 3.1$

7.4 COST ANALYSIS

As a final investigation of the design practicality of using the steel diaphragm SMC connection, the cost of the steel diaphragm-SMC bridge design is compared to a fully continuous bridge and to a concrete diaphragm SMC bridge. Upon first glance, it appears that SMC bridges will be more economical than standard fully continuous bridges; however other considerations, such as the additional cost of SMC reinforcing, load transfer details, etc., must also be included in the cost analysis. The cost and man hour comparisons presented herein used data from RS Means, *Open Shop Building Construction Cost Data* (Waier, 2003); this particular edition was selected for ease of cost comparisons with other SMC bridge schemes with documented cost information (i.e. concrete diaphragm designs).

A cost comparison of the SMC scheme proposed herein to the most recent SMC scheme proposed by UN/L and used by NDOR (Azizinamini A. , 2014) is presented in Table 32. As may be seen, the steel diaphragm results in a cost savings of 8% for the construction of the diaphragms. The spacing between girders on the two bridges differs, but the estimate is performed based on a unit length of diaphragm basis for comparison. The numbers for the concrete bridge considered the same depth girder as was used in the steel diaphragm bridge, a W33x152.

Table 32 - Cost Comparison - Concrete vs. Steel Diaphragm						
Bridge	Concrete Diaphragm			Steel Diaphragm		
Element	Quantity	Unit Cost	Total Cost	Quantity	Unit Cost	Total Cost
Formwork	57 SFCA	\$6.35	\$362			
Epoxy Coated Reinforcing Steel	0.08 ton	\$2545	\$190			
Cast-in-place Concrete	2.85 CY	\$85	\$242			
Sheet Steel Plate	1.50 cwt	\$41.50	\$62			
W27x84 Girder				7.33 ft.	\$72/ft.	\$528
Wedge Plates				31 lb	\$72/cwt	\$22
Sole Plate Weld				1.33 LF	\$12.75/LF	\$17
Total			\$856			\$567
Diaphragm Length	10.33 ft.			7.33 ft.		
Cost/Foot	\$83			\$77		

A comparison of construction man-hours of the diaphragms is presented in Table 33.

The proposed scheme requires about 14% of the construction man-hours of the concrete diaphragm scheme used in Nebraska; this means considerably less construction time to erect the steel bridge girders with the proposed scheme. Considering a burdened man-hour rate of \$50/hour for the steel diaphragm bridge and \$40/hour for concrete diaphragm bridge, the total cost savings using the proposed SMC concept is nearly 500%/foot. Additionally, NDOR (NDOR, 1996) requires that the concrete diaphragms be cast to only 2/3 of their height and allowed to cure for seven days prior to placing the remainder of the pier and casting the concrete bridge deck; this is a significant detriment to this scheme in that it adds a minimum of seven days to the entire construction schedule. There is no delay required in the proposed steel diaphragm scheme, nor is there such a constraint for conventional fully continuous bridges.

Table 33 - Construction Man-hour Comparison						
Bridge	Concrete Diaphragm			Steel Diaphragm		
Element	Quantity	Man-Hours	Total Hours	Quantity	Man-Hours	Total Hours
Formwork	57 SFCA	0.163/SFCA	9.29			
Reinforcing Steel Placement	0.08 ton	16/ton	1.28			
Cast-in-place Concrete	2.85 CY	1.067/CY	3.044			
Sheet Steel Plate	1	2	2			
W27x84 Girder				7.33 ft.	0.06/ft.	0.5
Install Wedge Plates				2 each	0.25/each	0.5
Weld Wedge Plates				1.33/LF	0.211/LF	0.3
Total			15.6			1.3
Diaphragm Length	10.33 ft.			7.33 ft.		
Hours/Foot	1.5			0.2		

Comparison of cost of the proposed SMC scheme to a fully continuous girder bridge with steel diaphragms of the same geometry is presented in Table 34 . Here the savings for the SMC bridge are substantial at 25% less than a fully continuous girder bridge, and this does not include the effects of the shortened construction time, which has positive economic effects to the motorists who must tolerate construction delays.

Table 34 – Girder Cost Comparison Fully Continuous Bridge to SMC Bridge		
Element	Fully Continuous	Steel Diaphragm Simple-Made-Continuous
Steel Unit Cost	\$2,500/ton	\$2,500/ton
Girder cost	\$19,360 each	\$14,790
Splice cost (2 every other span)	\$4,000 (Azizinamini, 2014)	\$0
Epoxy Coated Reinforcing Steel Unit Cost	\$1,685/ton	\$1,685/ton
SMC Reinforcing cost	N/A	\$2,580
Total Cost	\$23,360	\$17,370
Cost Difference (percent)	25%	

CHAPTER 8 SUMMARY AND RECOMMENDATIONS

8.1 SUMMARY

Steel bridges have been increasingly subject to a smaller market share of bridges in the United States than bridges constructed of both precast/prestressed and reinforced concrete in the short and medium span ranges. The simple-made-continuous concept is a promising option to increase the market share of steel bridges in the United States.

In general, steel SMC bridges are more economical, faster and safer to construct than fully continuous steel bridges. Additionally, SMC bridges do not require closure of the bridged roadway for erection of the hung spans nor for connection of the bolted girder continuity splices, which are required for fully continuous bridges. While not a fair comparison, but for completeness, SMC bridges are not only significantly more economical than simple span multi-span bridges, but they don't have the additional maintenance issue of expansion joints at every support. As a matter of fact, very recently an existing simple span bridge was converted to an SMC bridge by replacing the decks and installing SMC reinforcing and compression transfer mechanisms as retrofits (Griffith, 2014). Many current continuous precast/prestressed bridges were constructed using the SMC concept; the proposed connection and the SMC concept in general is a way for steel to compete against precast/prestressed bridges using their own concept.

The study connection evaluated, developed and modified herein is unique in that the SMC connection is not embedded in a concrete diaphragm as with other SMC bridges. The study connection is also considerably faster to construct and more economical than other SMC schemes since there is no need to wait for concrete diaphragms to cure and attain strength. The following is a summary of benefits of the proposed connection:

1. More economical than fully continuous bridges and other SMC schemes

2. By being exposed, the girder is allowed to properly weather and thereby develop its protective patina
 3. The girder ends and the compression transfer plates are visible for periodic inspection; this is not possible with girders cast into concrete diaphragms
 4. No concerns about cracking of a concrete diaphragm at re-entrant corners around the girders
 5. A significant savings in construction time (seven days minimum) over concrete diaphragms since there is no need to wait for concrete diaphragms to partially cure
- Future designs using the methodology developed by this dissertation can benefit from these advantages.

On the basis of hand analysis, finite element analysis and physical test results, the behavior of the SMC connection was investigated in order to develop design guidelines for the study connection type. A parametric study was performed to expand the applicability of the study to SMC bridges of spans from 80 feet to 140 feet, with various girder spacings and slab depths.

The final design guidelines developed include a methodology for:

1. Determination of the required SMC reinforcing steel
2. Determination of the moment arm between the SMC tension and compression components
3. Calculation of the nominal resisting moment of the SMC connection for comparison to the required ultimate moment
4. SMC reinforcing placement guidelines to address shear lag across the effective slab width

The original connection selected for study was found to have several weaknesses based upon hand analysis of the connection elements, which were subsequently substantiated by physical testing. Based on these findings, recommendations were made to CDOT to perform corrective actions to the bridge; these actions included:

1. Inspection of all of the girder bearings specifically looking for those that appear to have failed welds or other signs of distress
2. Address the connections that appeared distressed immediately by:
 - a. Measuring the distance between the girder flanges and relative locations of existing bolt holes in relation to the flanges
 - b. Fabricating and installing safety plates similar to that presented in Figure 18.
 - c. Carefully grind off failed and partially failed welds which remained.
3. Address the remaining visually non-distressed connections in accordance with item 2 above.

It should be noted that the composite girders installed for the bridge are adequate to support the required bridge loads as simple beams for strength, but not necessarily serviceability under all loading conditions.

8.2 RECOMMENDATIONS FOR FUTURE RESEARCH

The following items are recommendations for future research into SMC schemes, not only for bridges, but for all steel structures in general:

1. It is a well-known fact that continuous girders with increased stiffness at the supports attract more negative moment; the reverse should also be true for bridges with decreased stiffness at the supports. Thus, an investigation into the significance of this behavior in the actual continuous beam analysis would be prudent. It should also be investigated

whether this behavior is significant enough to be included in analysis of SMC type structures.

2. A value of 9% of the total SMC tension was found to be taken by the SMC reinforcing bars adjacent to the composite girder. Additional research and physical testing is recommended to refine the determination of this value based on the possible variables involved: SMC reinforcing location relative to the girder bottom flange, SMC reinforcing spacing and size, etc.
3. Investigation of the possibility of fatigue in parts of the connection, particularly at the weld of the wedge transfer plates. While this weld primarily subjected to compression, there is a slight tension component which will exist.
4. Investigation of the application of the SMC concept to steel buildings using composite beams. This would be a considerably simpler method than welded moment connections to achieve ductile continuity behavior for lateral loads due to stability, wind and earthquakes.
5. AASHTO section 4.6.4 discusses various methods of redistribution of negative moments at the supports in continuous beam bridges. Investigation of the applicability of this section to SMC bridges could possibly lead to even more economical SMC bridges.
6. As an alternative to the use of concrete damage models in Abaqus, adequate and oftentimes better results were obtained by simulating concrete damage using reduced stiffness by modifying the modulus of elasticity of the concrete. Further investigation into this approach may provide a means to save both modeling and analysis time by using this alternative to concrete damage models.

BIBLIOGRAPHY

- AASHTO. (2012). *AASHTO LRFD BRIDGE DESIGN SPECIFICATIONS*. Washington, DC: American Association of State Highway and Transportation Officials.
- AISC. (2011). *Steel Construction Manual*. Chicago: American Institute of Steel Construction.
- Azizimanini, A. &. (2004, November 8). Bridges Made Easy. *Roads & Bridges*.
- Azizimanini, A. (2005). *Development of a Steel Bridge System-Simple for Dead Load and Continuous for Live Load, Volumes 1 and 2*. Lincoln: University of Nebraska.
- Azizimanini, A. (2014). Simple for Dead Load - Continuous for Live Load Steel Bridge Systems. *Engineering Journal - American Institute of Steel Construction*, 59-82.
- Barber, T. L. (2006, December). Simple-Made-Continuous Bridges Cuts Costs. *Modern Steel Construction*.
- Barker, R. M. (2007). *Design of Highway Bridges: An LRFD Approach*. Hoboken: John Wiley & Sons, Inc.
- Barros, M. H. (2002). elastic degradation and damage in concrete following nonlinear equations and loading function. *Proceedings of the Sixth Conference on Computational Structures Technology* (pp. 255-256). Edinburgh, UK: ICCST.
- Carreira, D. J. (1985). STRESS-STRAIN RELATIONSHIP FOR PLAIN CONCRETE IN COMPRESSION. *Journal of the American Concrete Institute*, 797-804.
- CDOT. (2012, July 24). Bridge Design Manual. *CDOT Staff Bridge - Bridge Design Manual*. Denver, CO, USA: CDOT.
- Chapman, D. H. (2008). EVALUATION OF THE DUPONT ACCESS BRIDGE. *Experimental Techniques*, 31-34.

- Farimani, M. (2006). *RESISTANCE MECHANISM OF SIMPLE-MADE-CONTINUOUS CONNECTIONS IN STEEL GIRDER BRIDGES*. Lincoln: University of Nebraska/Lincoln.
- Farimani, R. S. (2014). Numerical Analysis and Design Provision Development for the Simple for Dead Load - Continuous for Live Load Steel Bridge System. *Engineering Journal - American Institute of Steel Construction*, 109-126.
- FHWA. (2005 through 2012). *Annual Materials Report on New BRidge Construction and Bridge Rehabilitation*. Washington, DC: Federal Highway Administration.
- Gopalaratnam, V. S. (1985). Softening Response of Plain Concrete in Direct Tension. *ACI Journal*, 310-323.
- Griffith, D. J. (2014). Existing Simple Steel Spans Made Continuous: A Retrofit Scheme for the I-476 Bridge over the Schuylkill River. *Engineering Journal - American Institute of Steel Construction*, 199-208.
- Grook. (2010, July 30). *Steel Reinforcement*. Retrieved July 8, 2013, from Grook.net: <http://www.grook.net/forum/civil-engineering/construction/steel-reinforcing>
- ICC. (2012). *ICC0ES Evaluation Report ESR-2856*. Whittier, CA: ICC Evaluation Service.
- Javidi, J. A. (2014). Experimental Investigation, Application and Monitoring of a Simple for Dead Load - Continuous for Live Load Connection for Accelerated Modular Steel Bridge Construction. *Engineering Journal - American Institute of Steel Construction*, 177 - 198.
- Karsan, I. D. (1969). Behavior of Concrete Under Compressive Loadings. *Journal of the Structural Division, ASCE*, 2543-2563.

- Lampe, N. J. (2001). *STEEL GIRDER BRIDGES ENHANCING THE ECONOMY - A THESIS*.
Lincoln: University of Nebraska/Lincoln.
- Lampe, N. M. (2014). Development and Experimental Testing of Connections for the Simple for Dead Load - Continuous for Live Load Steel Bridge System. *Engineering Journal - American Institute of Steel Construction*, 83-108.
- Lin, M. (2004). *VERIFICATION OF AASHTO-LRFD SPECIFICATIONS LIVE LOAD DISTRIBUTION FACTOR FORMULAS FOR HPS BRIDGES*. Cincinnati: University of Cincinnati.
- Lu, Z. H. (2010). Empirical Stress-Strain Model for Unconfined High-Strength Concrete under Uniaxial Compression. *Journal of Materials in Civil Engineering, ASCE*, 1181-1186.
- Lubliner, J. J. (1989). A PLASTIC-DAMAGE MODEL FOR CONCRETE. *International Journal of Solids and Structures*, 229-326.
- Malm, R. (2009). *Predicting shear type crack initiation and growth in concrete with non-linear finite element Method*. Stockholm: Royal Institute of Technology (KTH).
- Nakamura, S. Y. (2002). New technologies of steel/concrete composite bridges. *Journal of Constructional Steel Research*, 99-130.
- NDOR. (1996). *Nebraska Bridge Office Policies and Procedures Manual (BOPP)*. Omaha: Nebraska Department of Roads.
- Nelson. (2011). 2011 Nelson Stud Welding Stud and Ferrule Catalog. *2011 Nelson Stud Welding Stud and Ferrule Catalog*. Elyria, Ohio, USA: Nelson Stud Welding, Inc.
- Niroumand, S. J. (2009). *RESISTANCE MECHANISM OF SIMPLE-MADE-CONTINUOUS CONNECTIONS IN SKEW AND NON-SKEW STEEL GIRDER BRIDGES USING*

- CONVENTIONAL AND ACCELERATED TYPES OF CONSTRUCTION*. Lincoln:
University of Nebraska/Lincoln.
- NSBA. (2006, September). Steel Bridge Uses Simple-Span-Made-Continuous Construction.
Modern Steel Construction.
- Ricles, J. M.-W. (2000). *Development and Evaluation of Improved Details for Ductile Welded Unreinforced Connections - Report No. SAC/BD-00/24*. Los Angeles: SAC Joint Venture.
- Salmon, C. (2009). *STEEL STRUCTURES Design and Behavior Emphasizing Load and Resistance Factor Design*. Upper Saddle River, NJ: Pearson Prentice-Hall.
- Simula. (2011). *ABAQUS Analysis User's Manual (6.11)*. Providence, RI: Simula.
- Solis, A. V. (2007). *Field Evaluation of a SDL-CLL Steel Bridge in New Mexico*. Las Cruces: New Mexico State University.
- Talbot, J. (2005, October). Simple Made Continuous. *NSBA Steel Bridge News*, pp. 1-5.
- Waier, P. R. (2003). *Open Shop Building Construction Cost Data*. Kingston, Mass: R S Means.
- Yakel, A. A. (2014). Field Application Case Studies and Long-Term Monitoring of Bridges Utilizing the Simple for Dead - Continuous for Live Bridge System. *Engineering Journal - American Institute of Steel Construction*, 155 -176.

APPENDIX 1 – CURRENT SMC BRIDGES

At the time of this writing, at least ten SMC bridges were found to have been constructed and put into service. Details of these bridges and their SMC connection behavior follow.

State Highway No. 16 over US 85, Fountain, Colorado – February, 2004

Table 35

Bridge Element/Dimension	Value
Drive Lanes	2
Spans	4
Span Lengths	107'-0", 128'-2", 128'-2" and 57'-5"
Girder Spacing	7'-4"
Girder Size/Material	Plate Girder: Top Flange 3/4"x16", Web 1/2"x48", Bottom Flange Ends 3/4"x16", Centers 1 1/8"x16" AASHTO M270 Grade 50
Slab Thickness/Material	9" / $f'_c = 4500$ psi
Slab Haunch Depth (0 means none)	Min. 1 7/8", Max. 5 3/8"
Wearing Course?/Thickness/Density	None
Comments	

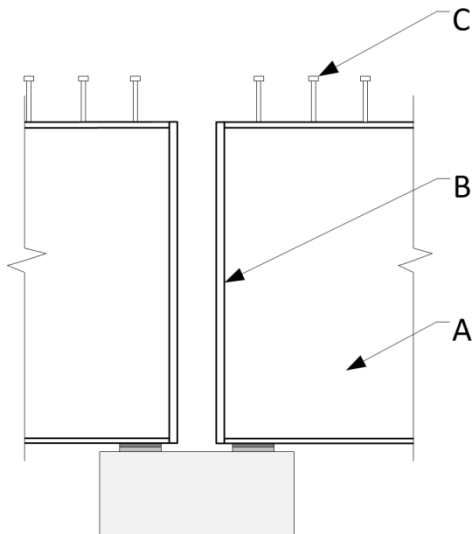


Figure 124 - Girders

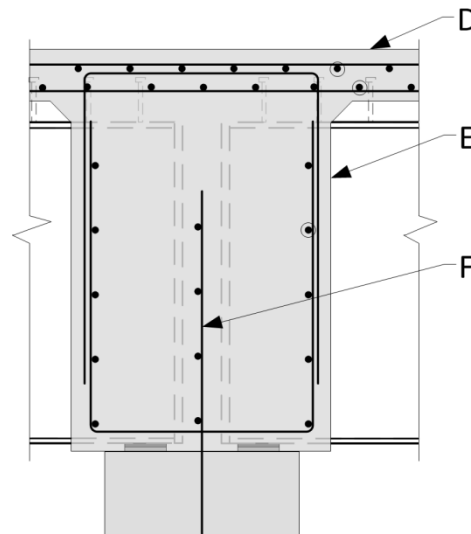


Figure 125 – Diaphragm and Slab

SMC detail Figure 124 and Figure 125:

A = Steel Plate Girder

B = Compression Pl 1 1/4"

C = (3) 7/8" diameter x 7" long headed studs

D = 9" concrete slab reinforced with #6 bars at 8" O.C. top

E = Concrete diaphragm reinforced with #5 longitudinal bars at 10" each side and #5 "U" ties top and bottom at 12" O.C.

F = #9 vertical dowels at 6" O.C. and #5 horizontal bars at 12" O.C.

Notes:

This bridge has more than two spans, thus having the potential of positive moments over one or more of the interior supports.

The beams are placed in pockets in the diaphragms and are not cast into the diaphragms.

The thickness of compression concrete between the end stiffeners of the bridge girders is 6".

State Highway No. 36 over Box Elder Creek, Watkins, Colorado – June, 2005

Table 36

Bridge Element/Dimension	Value
Drive Lanes	2
Spans	6
Span Lengths	77'-10" Typical
Girder Spacing	7'-4"
Girder Size/Material	W33x152 AASHTO M270 Grade 50W
Slab Thickness/Material	8" / $f'_c = 4500$ psi
Slab Haunch Depth (0 means none)	3" Minimum
Wearing Course?/Thickness/Density	Asphaltic – 35 psf
Comments	

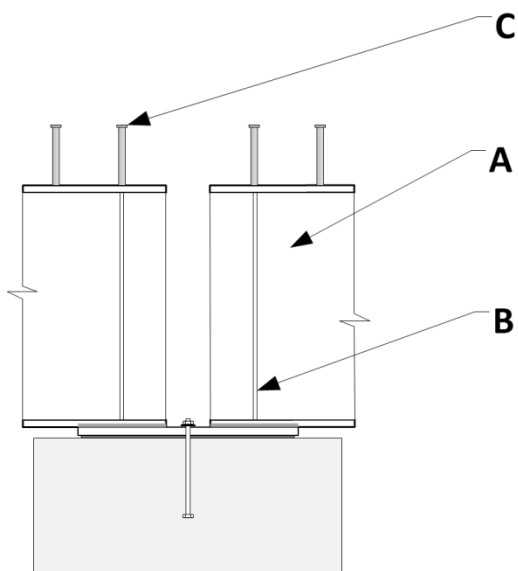


Figure 126 - Girders

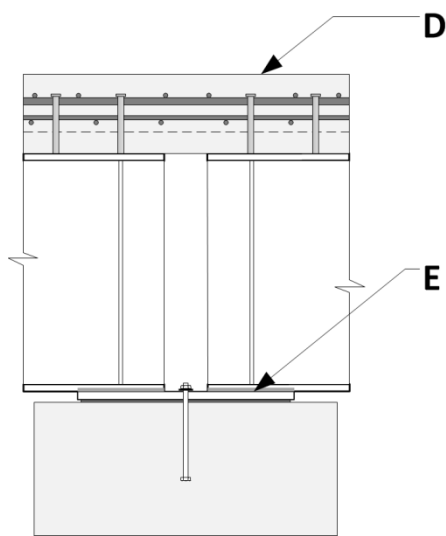


Figure 127 – Girders and Slab

SMC detail Figure 126 and Figure 127:

A = W33x152 girder

B = Plate 1/2" bearing stiffener (diaphragm beam not shown for clarity)

C = (3) 7/8" diameter x 8 3/16" long headed studs

D = 8" concrete slab with #5+#8 bars at 6" O.C. top

E = 5/16" fillet weld x 14" long fillet weld each side of W to 1" minimum sole (bearing) plate

Notes:

This bridge has more than two spans, thus having the potential of positive moments over one or more of the interior supports.

This is the only bridge of those reviewed that does not have a concrete diaphragm but rather a steel wide flange diaphragm (not shown), thus leaving the girder ends exposed.

Sprague St. over Interstate 680, Omaha, Nebraska – May, 2003

Table 37

Bridge Element/Dimension	Value
Drive Lanes	2
Spans	2
Span Lengths	97'-0" Typical
Girder Spacing	10'-4"
Girder Size/Material	W40x249 ASTM A709 Grade 50W
Slab Thickness/Material	8" / $f'_c = 4000$ psi
Slab Haunch Depth (0 means none)	1"
Wearing Course?/Thickness/Density	None
Comments	

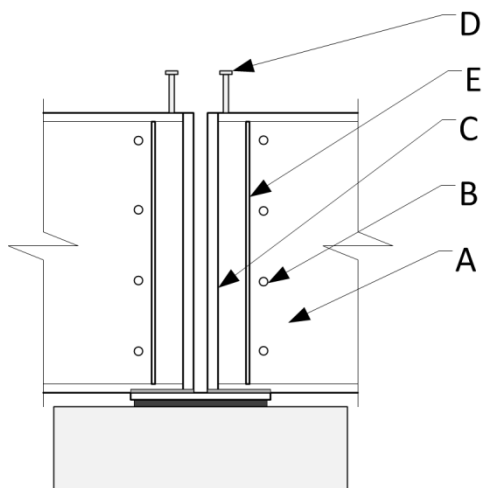


Figure 128 - Girders

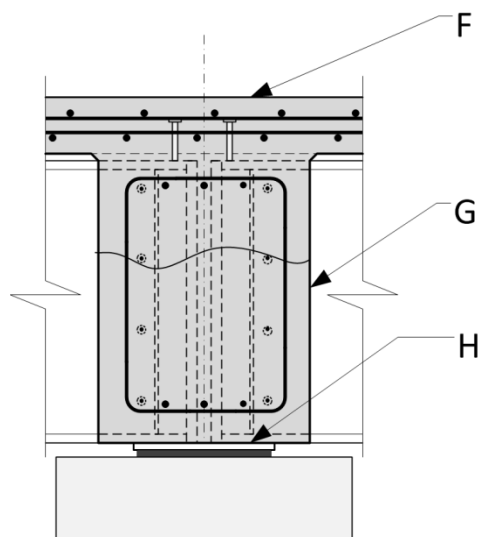


Figure 129 – Diaphragm and Slab

SMC detail Figure 128 and Figure 129:

A = W40x249 girder

B = Holes in beam web for longitudinal diaphragm reinforcing bars

C = 1 1/2" x 16" wide compression plate

D = (3) 7/8" diameter x 5" long headed studs

E = Plate 3/8" bearing stiffener

F = 8" concrete slab with #4+#6 bars at 12" O.C. top

G = Reinforced concrete diaphragm; longitudinal side bars are continuous through girder webs

H = 5/16" fillet weld x 10" long fillet weld each side of W to 1 1/2" sole (bearing) plate

Notes:

This bridge has openings drilled or punched through the girder web at the ends at the abutments in order to make them integral with the abutment concrete. However, there are expansion joints at the abutments which may not perform as anticipated due to the monolithic behavior of the abutment and the girder.

State Highway N-2 over Interstate 80, Hamilton County, Nebraska – November, 2002

SMC detail: Tub (box) girders supported by concrete piers and cast into concrete diaphragms (5000 psi concrete vs. remainder is 4000 psi). The tub girders have a 12'-0" long concrete slab in the bottom for additional compression resistance in the negative moment zone.

Note: While this bridge is unique in that it does not use I-shaped beams, it will not be discussed further since the scope of this work is SMC with I-shaped girders.

US 75 over North Blackbird Creek – Macy, Nebraska – May 2010

Table 38

Bridge Element/Dimension	Value
Drive Lanes	2
Spans	3
Span Lengths	49'-3", 65'-8", 49'-3"
Girder Spacing	11'-8"
Girder Size/Material	W36x135 Ends, W36x150 Center ASTM A709 Grade 50W
Slab Thickness/Material	8 1/2" / $f'_c = 4000$ psi
Slab Haunch Depth (0 means none)	1/2" to 13/16"
Wearing Course?/Thickness/Density	None
Comments	

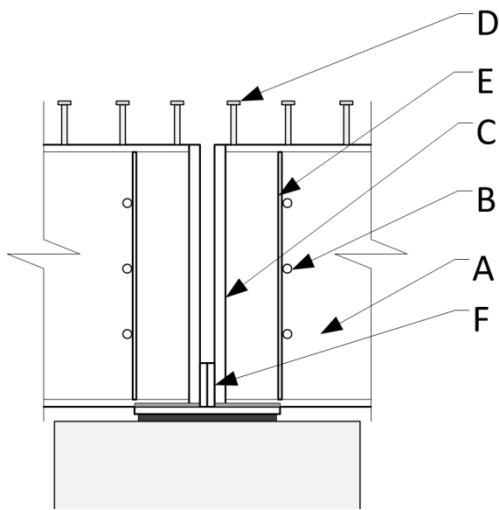


Figure 130 - Girders

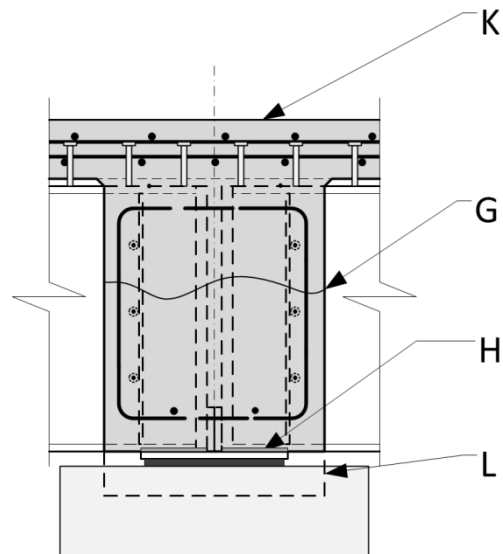


Figure 131 – Diaphragm and Slab

SMC Detail Figure 130 and Figure 131:

A = W36x135 or W36x150 girder

B = Holes in beam web for longitudinal diaphragm reinforcing bars

C = 2" x 12" wide compression plate

D = (3) 7/8" diameter x 5" long headed studs

E = Plate 3/8" bearing stiffener

F = Plate 2"x6"x11.975" beam end plates

G = Reinforced concrete diaphragm; longitudinal side bars are continuous through girder webs

H = 5/16" fillet weld x 6" long fillet weld each side of W to 1 1/2"x12" wide sole (bearing) plate

K = 8" concrete slab with #8 bars at 12" O.C. top

L = Diaphragm extends down on either side of girder concrete bearing stubs

Notes:

The bottom flange width of both a W36x150 and W36x135 is 12.0" which is the same as the width of the sole plate, thus, as detailed on the design drawings, the field weld of the W's to the sole plate would be not be possible to construct.

US 75 over South Blackbird Creek – Macy, Nebraska – May 2010

Table 39

Bridge Element/Dimension	Value
Drive Lanes	2
Spans	3
Span Lengths	55'-0", 73'-6", 55'-0"
Girder Spacing	11'-8"
Girder Size/Material	W36x135 Ends, W36x150 Center ASTM A709 Grade 50W
Slab Thickness/Material	8 1/2" / $f'_c = 4000$ psi
Slab Haunch Depth (0 means none)	1/2" to 13/16"
Wearing Course?/Thickness/Density	None
Comments	

SMC Detail Figure 130 and Figure 131:

This bridge is identical in detailing to the US 75 over North Blackbird Creek bridge with the exception of the girder spans.

Table 40

Bridge Element/Dimension	Value
Drive Lanes	2
Spans	5
Span Lengths	31.75, 32, 32, 32, 31.75 m (104'-2", 105'-0", 105'-0", 105'-0", 104'-2")
Girder Spacing	2.625 m (8'-7")
Girder Size/Material	Plate Girder: Top Flange 22x350 (7/8"x13 3/4"), Web 12x1326(1/2"x52 1/4"), Bottom Flange 22x440(7/8"x17 5/16") AASHTO M270 $F_y = 27.6$ MPa (50 ksi)
Slab Thickness/Material	0.23 m (9") / $f'_c = 27.6$ MPa (4000 psi)
Slab Haunch Depth (0 means none)	0.05 m (2")
Wearing Course?/Thickness/Density	None
Comments	Bridge drawings are metric

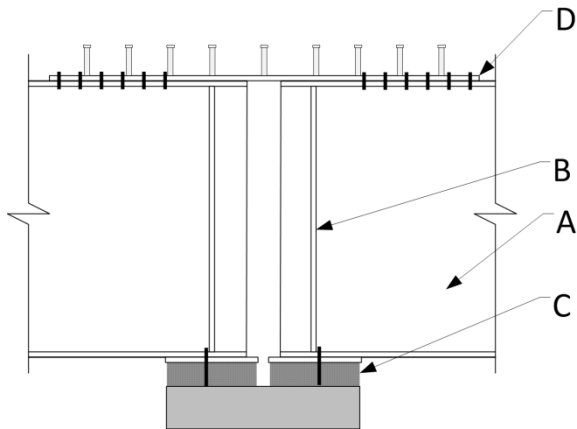


Figure 132 - Girders

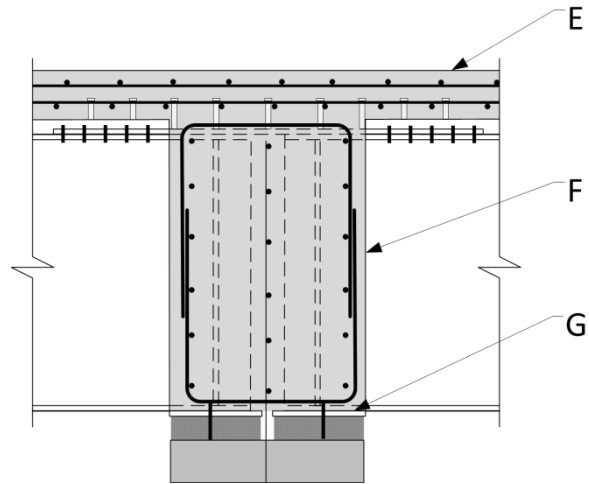


Figure 133 – Diaphragm and Slab

SMC Detail Figure 132 and Figure 133:

A = Plate girder

B = 7/8" Bearing and SMC compression stiffener

C = Elastomeric bearing (no SMC load transfer to pier)

D = Splice plate 7/8" with 9 rows of (3) 7/8" diameter x 5" long headed studs; connected to girder with (8) 7/8" dia. A325-SC bolts each side (see note e)

E = 9" concrete slab with #8 at 6" O.C. top

F = Reinforced concrete diaphragm; center bars are continuous through gap between girders

G = 5/16" fillet weld x 6" long fillet weld each side of plate girder to 1 1/2"x13 3/4" wide sole (bearing) plate

Notes:

This is the only set of bridge drawings reviewed that was in metric.

This bridge was discussed in an article in "Steel Bridge News" (Barber, 2006), where the shear connectors were shown as steel channels; whereas the as-built drawings indicate that the shear connectors are headed studs.

For as environmentally friendly as the bridge and all of the surrounding site work was, there is no bike lane on the bridge.

Spans are greater than two, potential for positive moments over supports.

The bolts to connect the splice plate were installed in short slotted holes in the splice plate and standard holes in the top flange of the beam. The nuts were to be "snug" tightened after the concrete was placed, not set. No other notes were provided as further tightening of these nuts to achieve slip critical action. It would seem more appropriate to have put the slots in the girder flange since there is the potential for the bolts to bind in the concrete and move with the slab as it

shrinks since they are only snug tight. Also, there is the potential for the bolt heads to crack the slab and slip, thus they could not be tightened.

A possibly better solution would be to have the splice plate with high strength welded threaded studs placed into short slotted holes in the slab.

Table 41

Bridge Element/Dimension	Value
Drive Lanes	2 + Pedestrian/Bike
Spans	6
Span Lengths	87.79', 112.58', 112.46', 112.67', 89.87'
Girder Spacing	9'-0"
Girder Size/Material	Girder: Top Flange 7/8"x 18", Web 1/2"x54", Bottom Flange 1 1/2"x18" ASTM A709 Grade 50W
Slab Thickness/Material	8 1/2" / $f'_c = 4500$ psi
Slab Haunch Depth (0 means none)	1/2" to 13/16"
Wearing Course?/Thickness/Density	1" monolithic concrete (145 psf)
Comments	Galvanized steel stay-in-place slab forms HS-25 and Alt. Military Loading

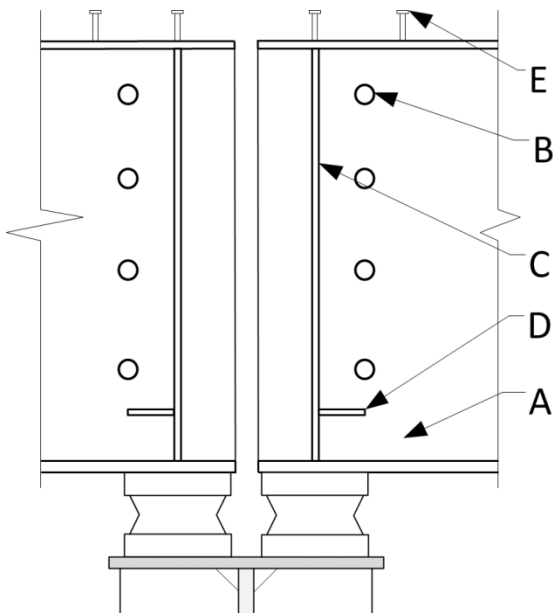


Figure 131 - Girders

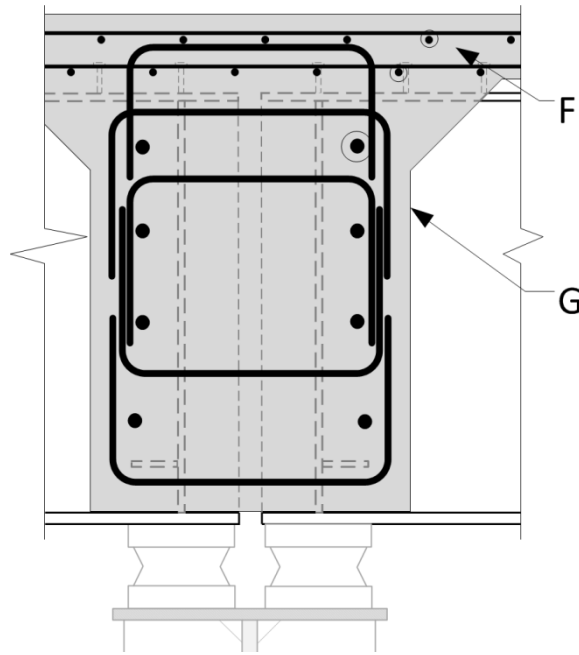


Figure 132 – Diaphragm and Slab

SMC detail Figure 134 and Figure 135:

A = Plate girder

B = Holes in beam web for longitudinal diaphragm reinforcing bars

C = Bearing/SMC compression stiffener plate 7/8"

D = Compression stiffener support stiffener

E = (3) 7/8" diameter x 4" long headed studs

F = 8 1/2" concrete slab reinforced with #8+#4 bars at 9" O.C. top

G = Reinforced concrete diaphragm; longitudinal side bars are continuous through girder webs

Notes:

This bridge is a rebuild and used existing piers and their foundations without modification for loads, although the piers were widened for a wider bridge. Obviously there will be increased loads at the interior supports due to the continuity invoked by the SMC concept

The bridge has more than two spans, thus having the potential of positive moments over one or more of the interior supports.

Church Ave. over Central Ave., etc., Knox County, Tennessee – January, 2005

Table 42

Bridge Element/Dimension	Value
Drive Lanes	2 + 1 Pedestrian/Bike + 1 Parking
6	6
Span Lengths	79'-6", 100'-0", 100'-0", 100'-0", 93'-0", 90'-4"
Girder Spacing	8'-2"
Girder Size/Material	W30x173 ASTM A709 Grade 50W (see notes)
Slab Thickness/Material	8 1/4" / $f'_c = 4500$ psi (see notes)
Slab Haunch Depth (0 means none)	1 3/4"
Wearing Course?/Thickness/Density	None
Comments	Girder continuity plates connected prior to placement of deck slabs.

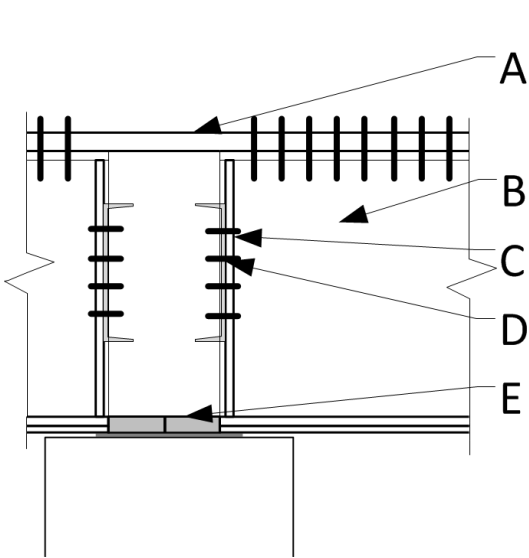


Figure 133 - Girders

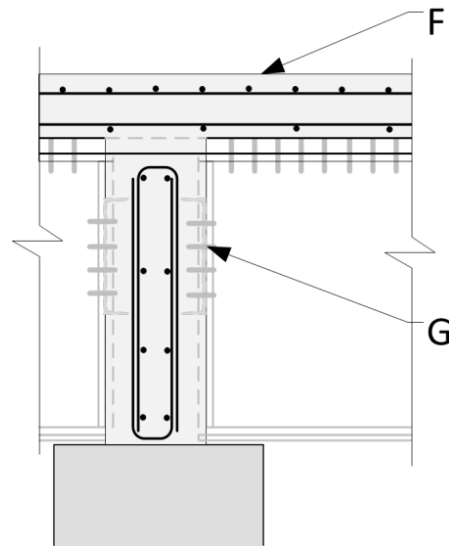


Figure 134 – Diaphragm and Slab

SMC Detail, Figure 136 and Figure 137:

A = Plate girder

B = Bearing stiffener

C = Stabilizer/bracing channel

D = Field welded wedge compression blocks

E = Field bolted splice plate

F = 8 1/4" concrete slab reinforced with #6 bars at 14" O.C. top

G = Reinforced concrete diaphragm

Dupont Access Road over State Route 1, Humphrey's County, Tennessee – 2002

Table 43

Bridge Element/Dimension	Value
Drive Lanes	2
Spans	2
Span Lengths	87'-0", 76'-0"
Girder Spacing	7'-5"
Girder Size/Material	W33x240 ASTM A709 Gr. 50W
Slab Thickness/Material	8 1/2" / (Material not on drawings provided)
Slab Haunch Depth (0 means none)	4 1/2"
Wearing Course?/Thickness/Density	Wearing course shown on drawings without dimensions or material information.
Comments	Girder continuity plates connected prior to placement of deck slabs.

SMC Detail, Figure 136 and Figure 137, except a rolled girder instead of a plate girder.

Massman Drive over Interstate 40, Davidson County, Tennessee – November, 2001

Table 44

Bridge Element/Dimension	Value
Drive Lanes	2
Spans	2
Span Lengths	138'-6", 145'-6"
Girder Spacing	9'-9"
Girder Size/Material	Plate Girder: Top Flange 1 1/2"x18" Web 5/8"x60", Bottom Flange 1 1/2"x18" ASTM A709 Grade 50W
Slab Thickness/Material	8 1/4" / $f'_c = 3000$ psi (see notes)
Slab Haunch Depth (0 means none)	4 1/2"
Wearing Course?/Thickness/Density	None
Comments	Girder continuity plates connected prior to placement of deck slabs.

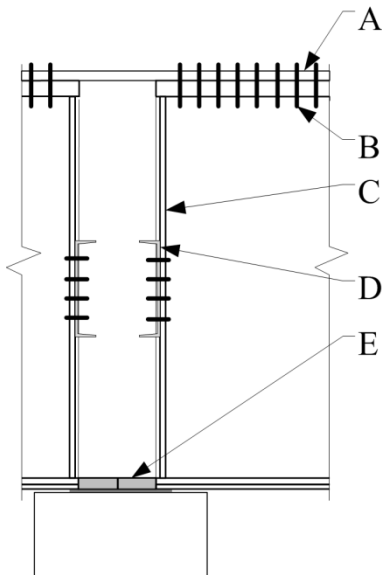


Figure 135 - Girders

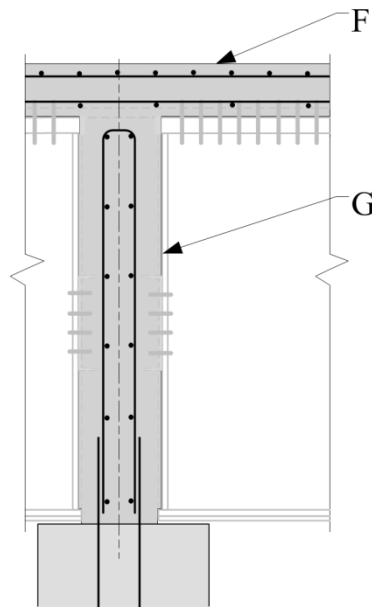


Figure 136 – Diaphragm and Slab

SMC detail:

A = Plate girder

B = Holes in beam web for longitudinal diaphragm reinforcing bars

C = Bearing/SMC compression stiffener plate 7/8"

D = Compression stiffener support stiffener

E = (3) 7/8" diameter x 4" long headed studs

F = 8 1/2" concrete slab reinforced with #8+#4 bars at 9" O.C. top

G = Reinforced concrete diaphragm; longitudinal side bars are continuous through girder webs

Steel girders with top and bottom splice plates cast into concrete diaphragms over piers.

The bottom flanges have welded "wedge" plates between them and the top flanges have bolted top cover plates, additionally, there are full height web stiffeners at the ends of the girders.

Girders are plate girders, web = 5/8"x60", top and bottom flanges = 1 1/2"x18".

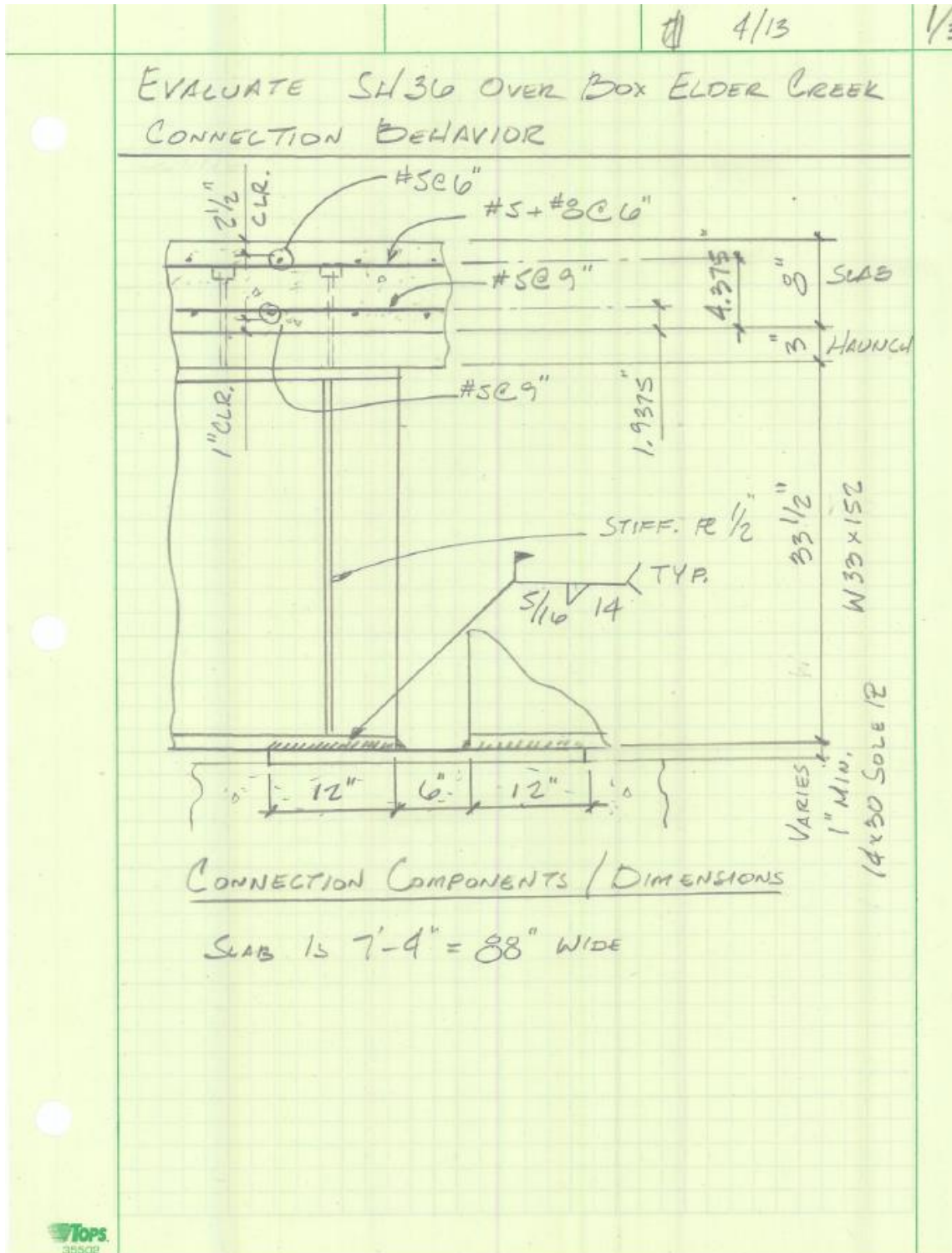
Note: There is an alternative moment splice detail, which shows splice plates on the top and bottom of the top flange; unfortunately, this detail is not constructible since the bottom plate cannot be installed due to the aforementioned web stiffeners. Fortunately, based on review of photos of the bridge it's apparent that the base splice detail was selected. Also, as with the previous Tennessee bridge (Church Ave.), this bridge is simple for only the self-weight of the steel framing.

Notes on bridge information:

Spans are given to centerlines of supports unless noted.

APPENDIX 2 – HAND CALCULATIONS

Calculations of SMC Components of State Highway 36 over Box Elder Creek



CONNECTION BEHAVIOR

• COMPONENTS TO CONSIDER

SOLE PLATE - COMPRESSION

WELDS - SHEAR

W33 - COMPRESSION & POSSIBLE BENDING

#8 + #5 @ 6" - TENSION

#5 @ 9" BOTTOM - POSSIBLE TENSION

- SOLE PLATE $A = 1" \times 14" = 14 \text{ in}^2$ $F_y = 50 \text{ ksi}$ $\phi = 1.0$
 $\phi P_n = 1.0 \times 50 \text{ ksi} \times 14 \text{ in}^2 = \underline{700 \text{ k}}$

- WELDS 5/16 - EFF. THROAT = 0.3125×0.707
 $= 0.221 \text{ in}$
 $F_u = 70 \text{ ksi}$ $r_n = 70 \times 0.221 = 15.5 \text{ k/in}$
 $\phi_{LONG} = 1$ $\phi_{LAT} = 0.8$
 $\phi R_n = 2 \text{ WELDS} \left[12 \times 15.5 \times 1.0 + 2 \times 15.5 \times 0.8 \right]$
 $= \underline{420.8 \text{ k}}$

- W33 TRAY BOTTOM FLG. ONLY:
 $A_g = 1.06 \times 11.6 = 12.30 \text{ in}^2$
 $\phi P_n = 12.30 \times 50 \text{ ksi} = \underline{615 \text{ k}}$

#8 + #5 @ 6" $A_s = 0.79 + 0.31 = 1.10 \text{ in}^2/6"$
 $A_{TOTAL} = \underset{\substack{\uparrow \\ \text{SLAB WIDTH}}}{88} \times 1.10 / 6 = 16.13 \text{ in}^2$
 $\phi P_n = 1.0 \times 16.13 \times 70 \text{ k} = \underline{1129 \text{ k}}$

• BASED ON PRECEEDING LRFD CAPACITIES, WELDS WILL CONTROL DESIGN:

$$\text{MOMENT ARM} = 33.5 + 3 + 4.375 = 40.88 \text{ in}$$

N33 HAUNCH #8+#5

$$\phi M_n = \text{MOMENT ARM} \times \phi P_n = 40.88 \text{ in} \times 420.8 \frac{\text{k}}{12 \frac{\text{in}}{\text{ft}}} \\ = \underline{1433 \text{ ft}\cdot\text{k}}$$

BASED ON ANALYSIS OF WORST CASE LOAD,

$$M_u = 1782 \text{ k}\cdot\text{ft} > 1433 \text{ k}\cdot\text{ft}$$

- WELD MAY NOT BE ADEQUATE -

$$\phi P_n (\text{REQ'D}) = 1782 \times 12 / 40.88 = 523 \text{ k}$$

LESS THAN CAPACITY OF OTHER COMPONENTS \therefore WELD ONLY IS AN ISSUE

SIMPLE-MADE-CONTINUOUS BRIDGE GIRDER TEST MODEL

STRUCTURAL NOTES:

GENERAL

ALL WORK SHALL BE PERFORMED IN ACCORDANCE WITH ALL APPLICABLE CODES AND STANDARDS, INCLUDING BUT NOT LIMITED TO AASHTO AND OSHA.

CONCRETE

ALL CONCRETE SHALL HAVE A MINIMUM ULTIMATE COMPRESSIVE STRENGTH, f'_c , OF 4500 PSI AT 28 DAYS. PROVIDE MIX DESIGN WITH STATISTICAL DATA FOR APPROVAL.

ALL REINFORCING STEEL SHALL BE ASTM A615 GR. 60. PROVIDE MILL CERTIFICATES FOR ALL BARS TO BE PROVIDED.

ALL BARS SHALL BE PROVIDED FULL LENGTH WITHOUT SPLICES.

PROVIDE SHOP DRAWINGS FOR REVIEW AND ACCEPTANCE PRIOR TO FABRICATION OF REINFORCING BARS.

STRUCTURAL STEEL

ALL STRUCTURAL STEEL SHAPES AND PLATES SHALL BE ASTM A992, $F_y = 50$ ksi. PROVIDE MILL CERTIFICATES FOR ALL STEEL PROVIDED.

ALL STRUCTURAL STEEL RODS SHALL BE ASTM F1554, WITH COMPATIBLE NUTS AND WASHERS AS SHOWN AND REQUIRED.

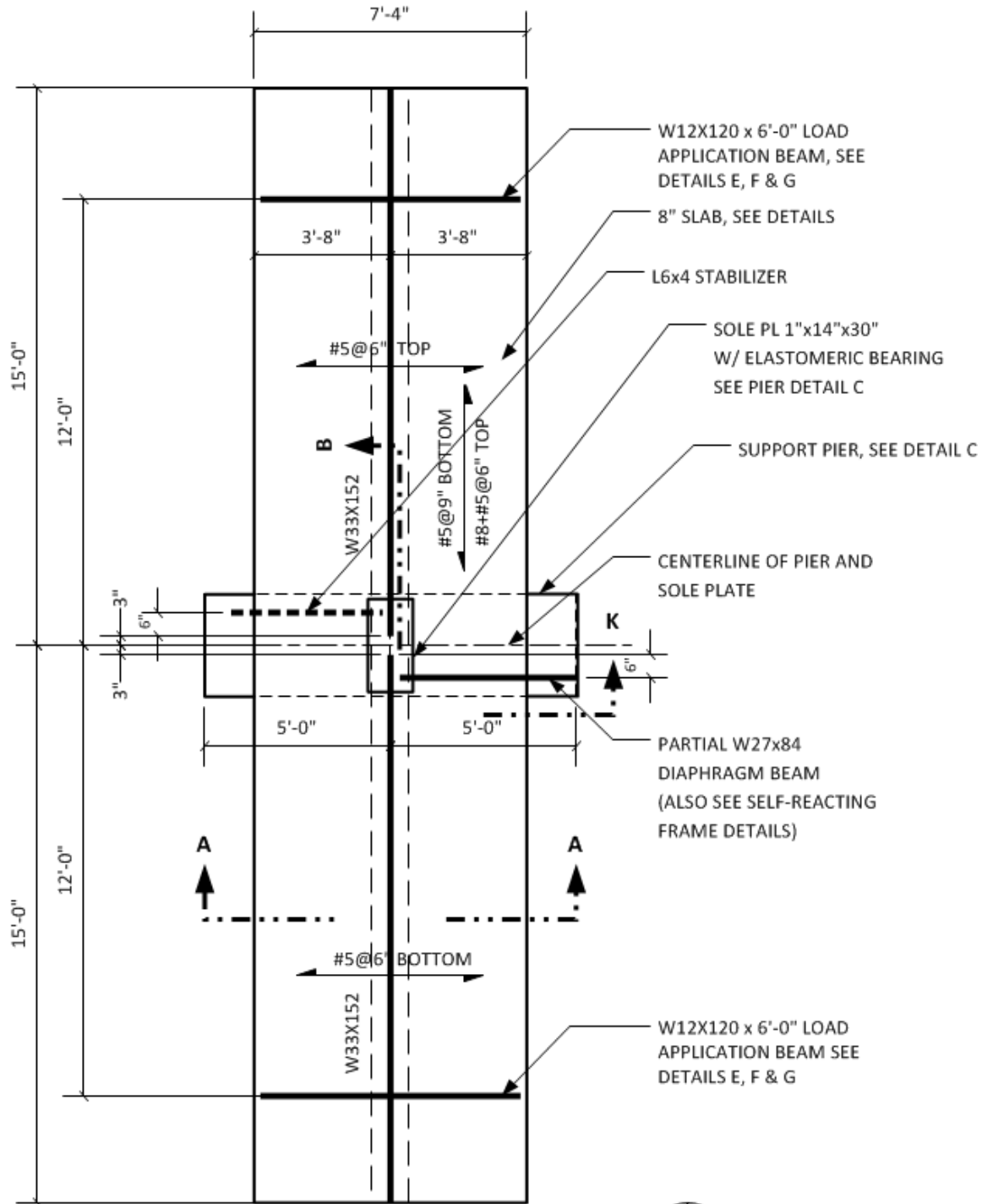
ALL WELDING SHALL BE PERFORMED IN ACCORDANCE WITH AWS D1.1 USING E70XX ELECTRODES.

HEADED STUDS SHALL BE IN ACCORDANCE WITH ASTM A108.

PROVIDE SHOP DRAWINGS FOR REVIEW AND ACCEPTANCE PRIOR TO FABRICATION OF ALL STRUCTURAL STEEL.

SHORING LUMBER

ALL SHORING LUMBER SHALL BE A MINIMUM OF HEM-FIR NO. 2.

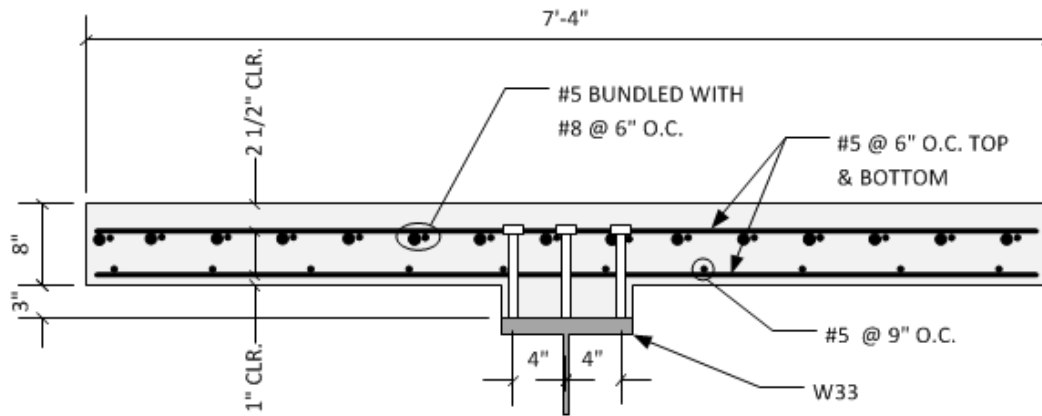


1 FRAMING PLAN

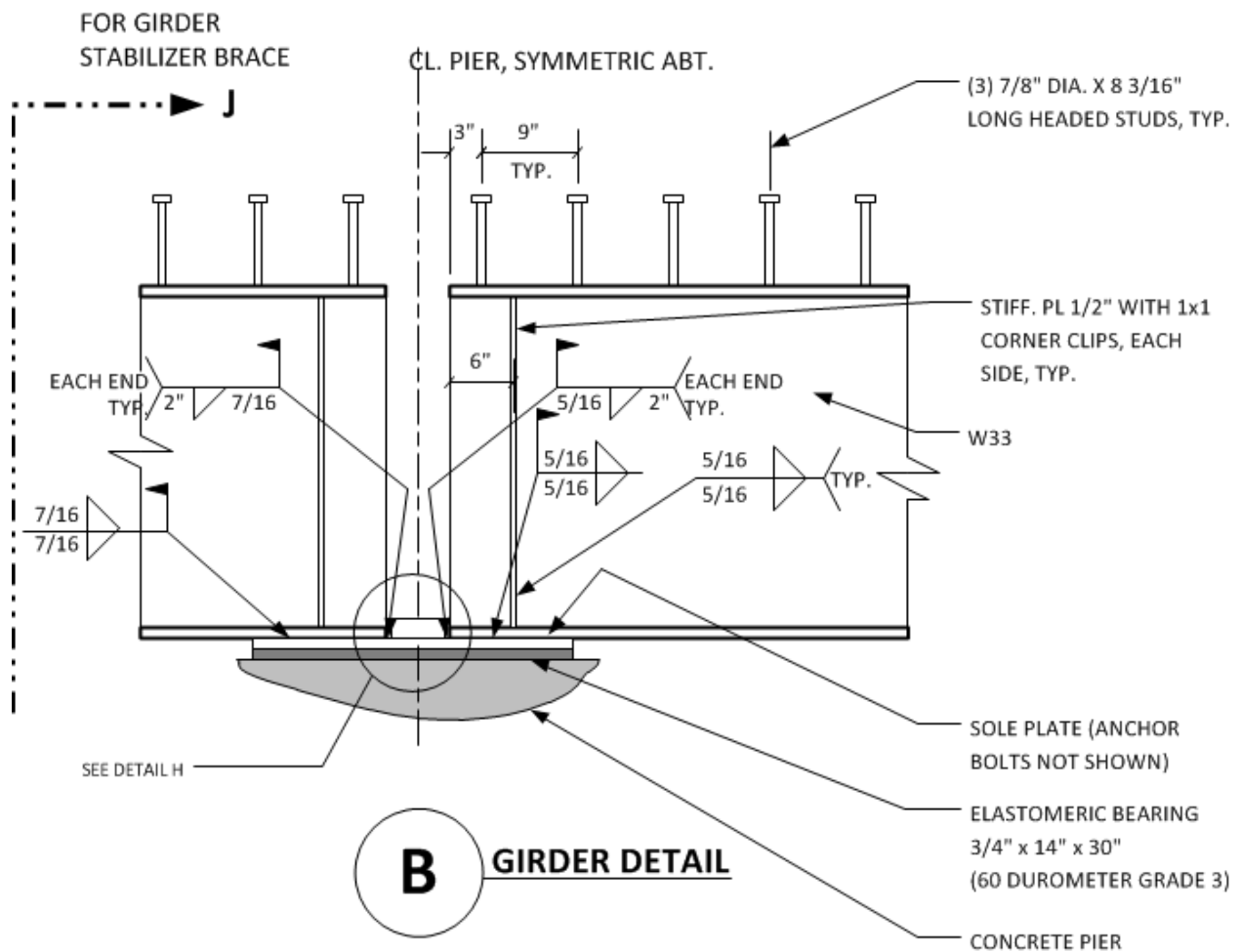


NOTES:

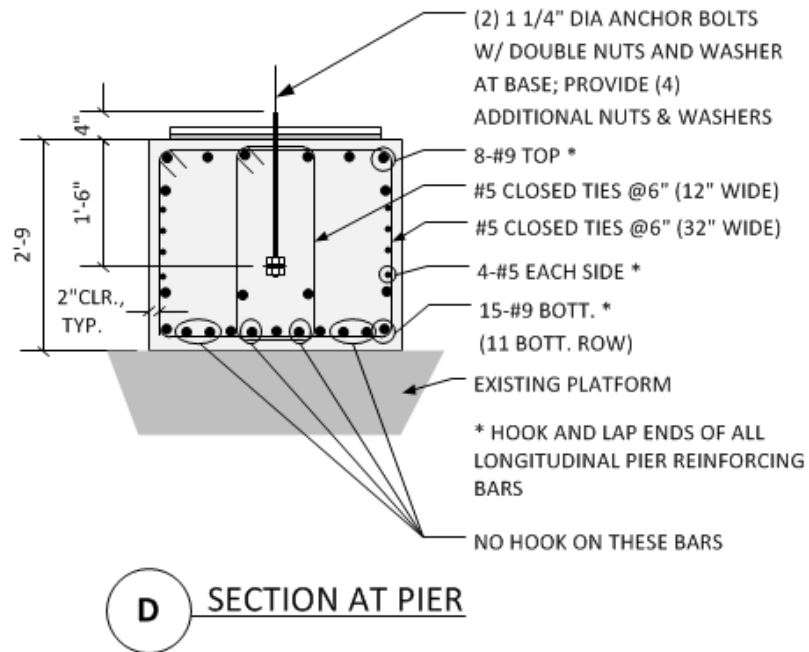
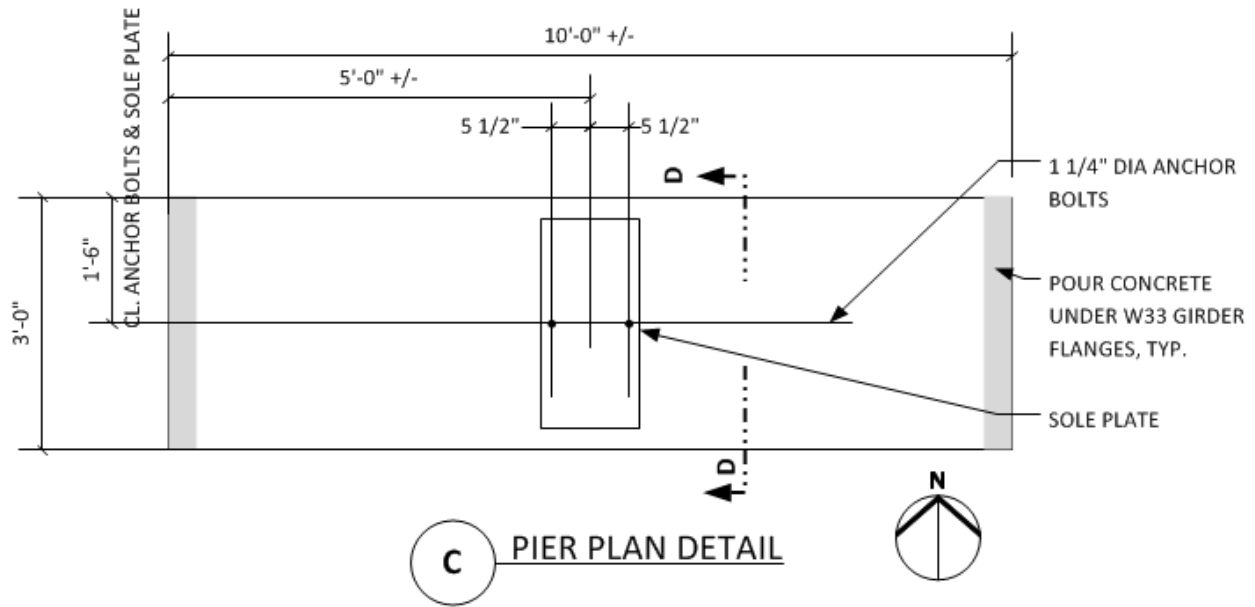
DO NOT INSTALL GIRDER UNTIL CONCRETE PIER HAS ATTAINED DESIGN STRENGTH, 28 DAYS MINIMUM.
SEE SHORING PLAN FOR TEMPORARY SUPPORT DETAILS.

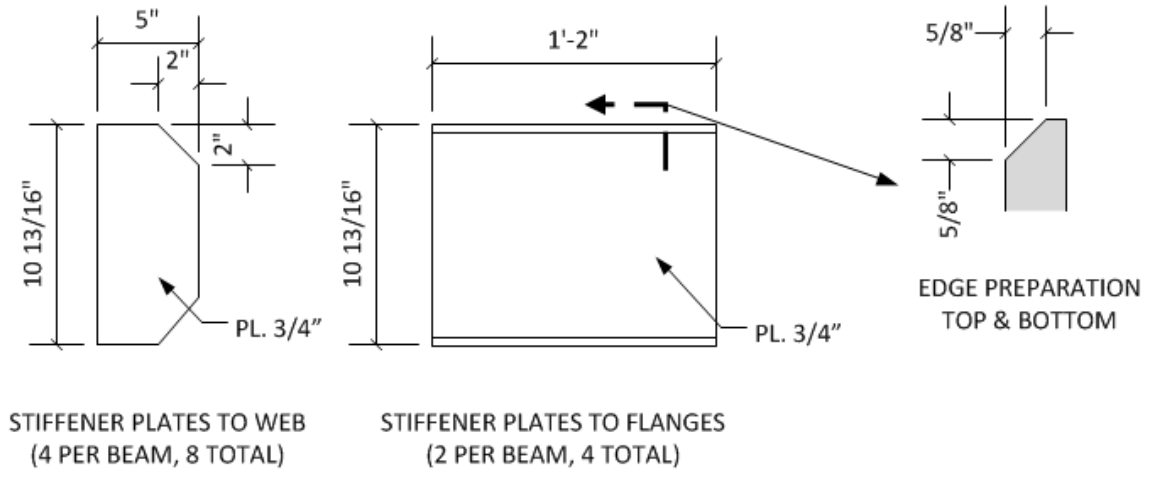
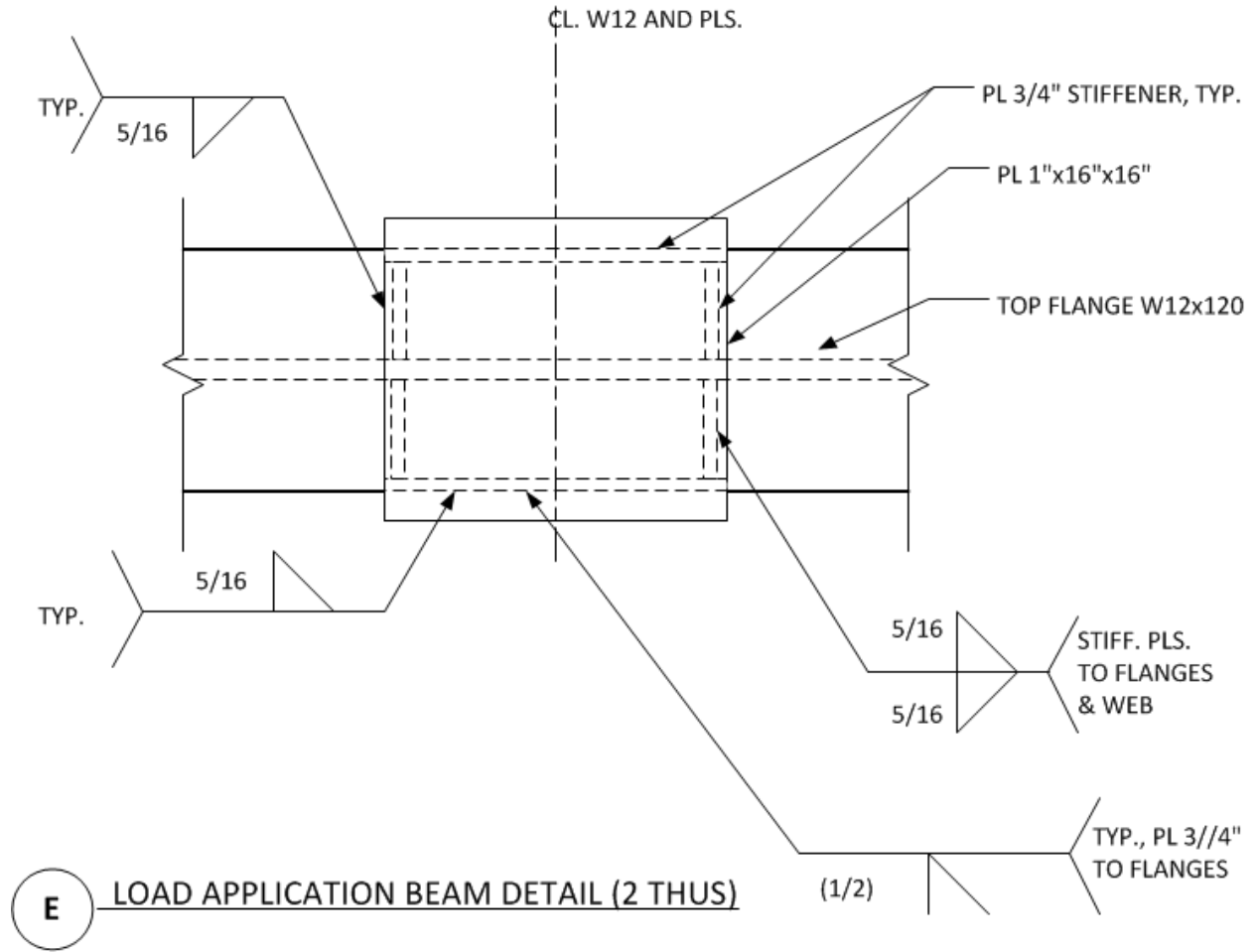


A SLAB SECTION

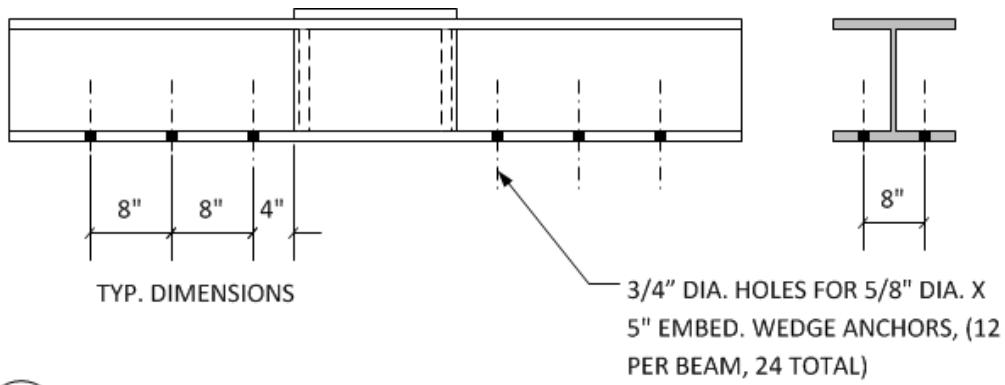


B GIRDER DETAIL

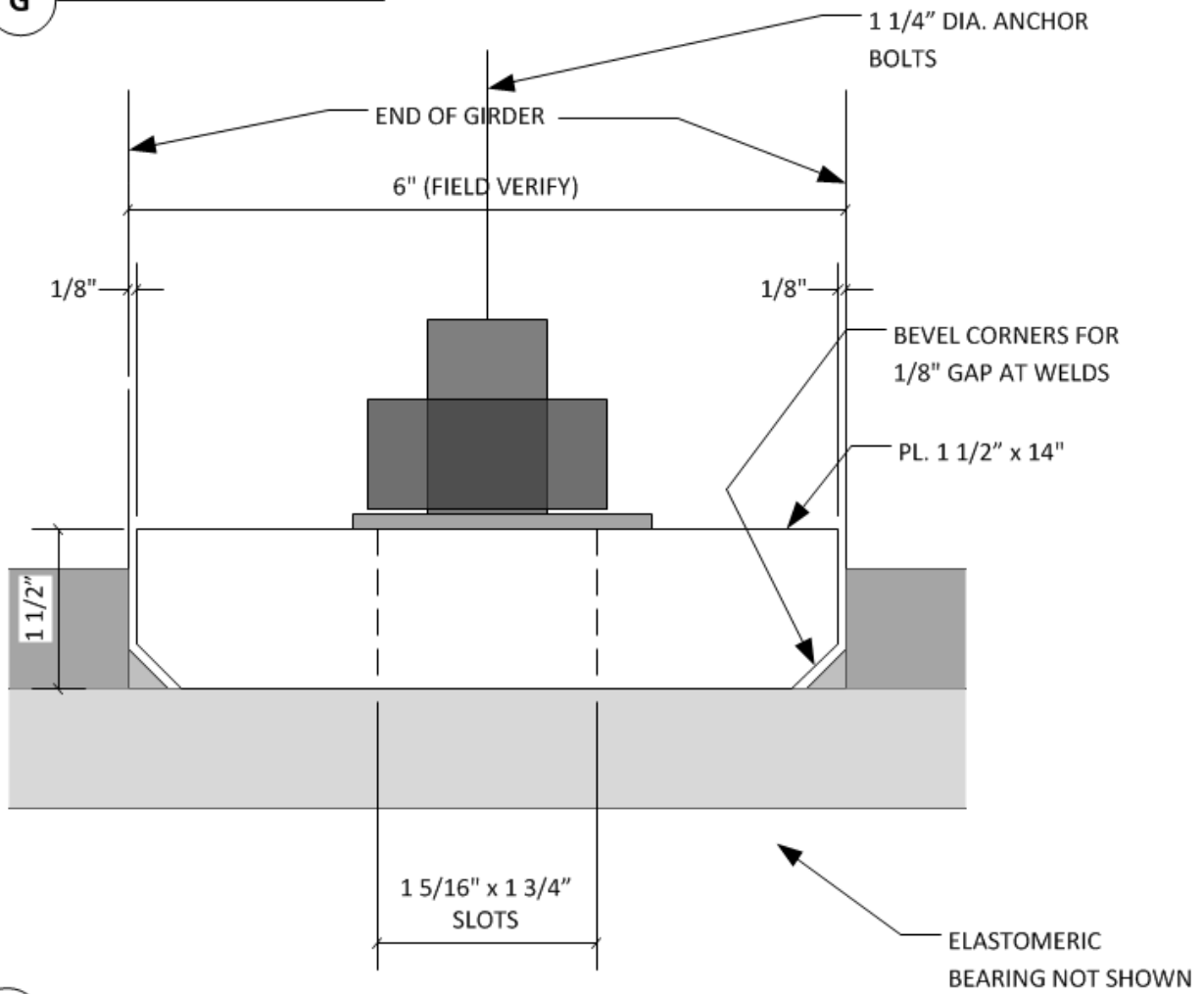




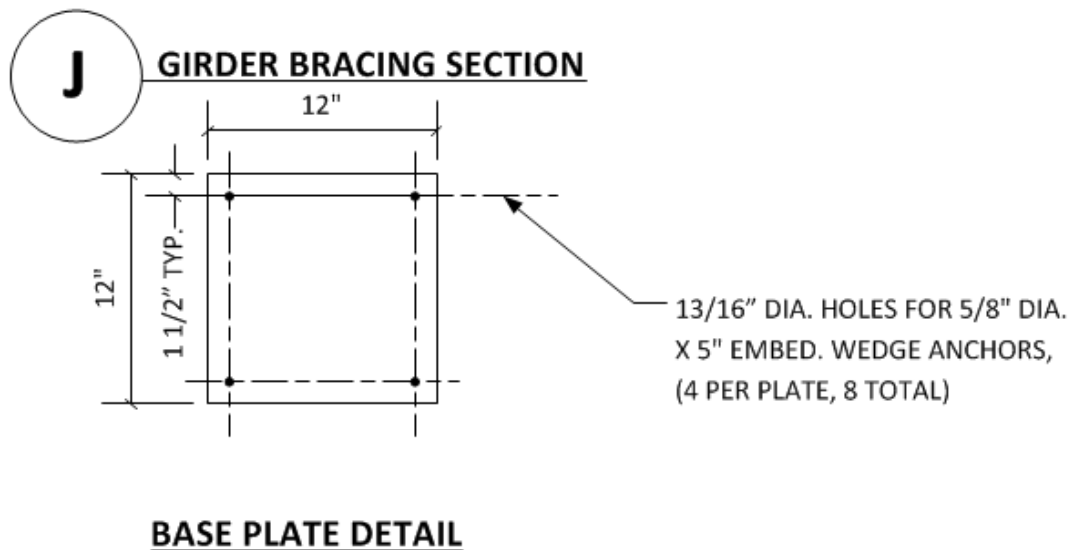
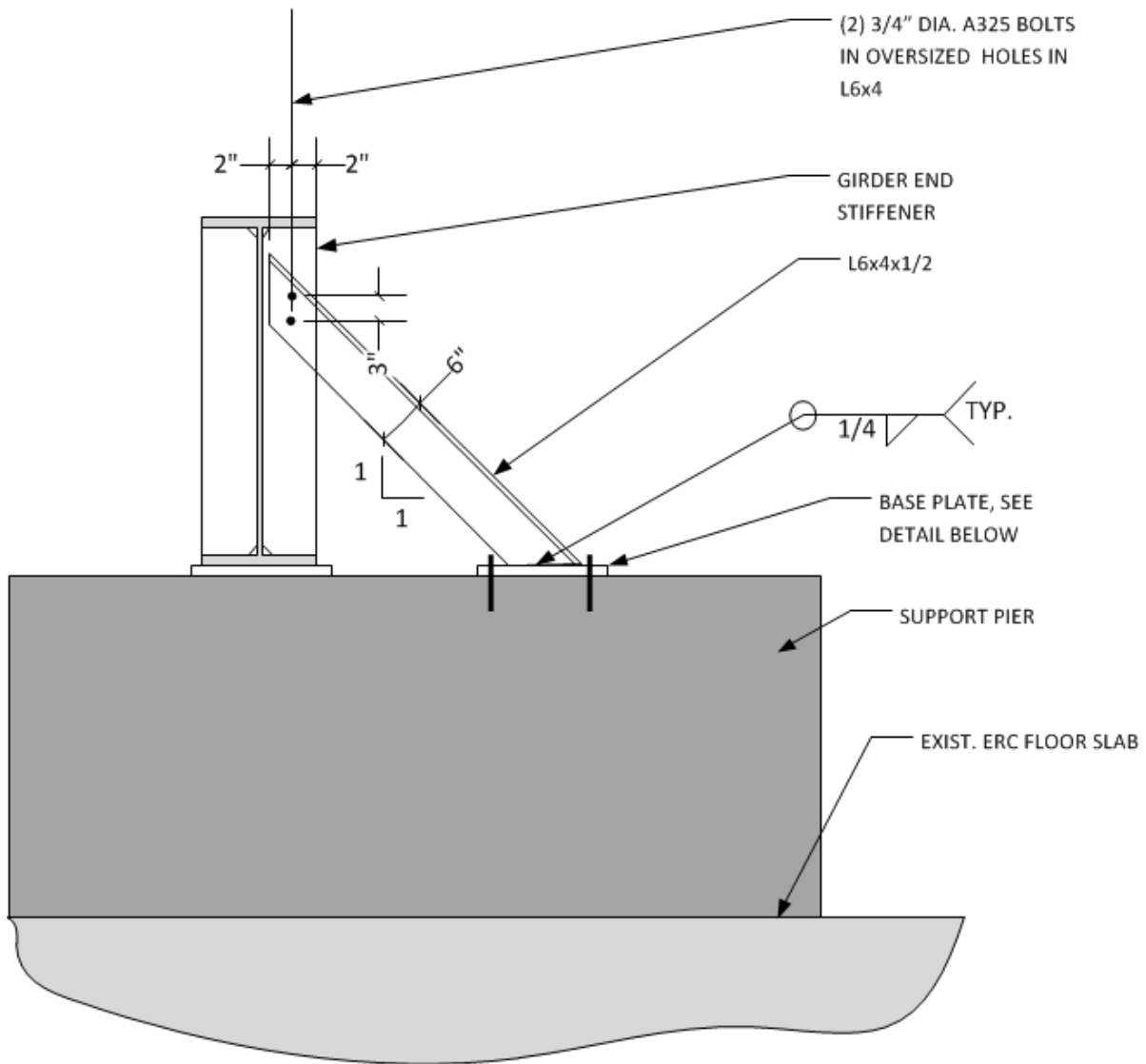
F PLATE DETAILS

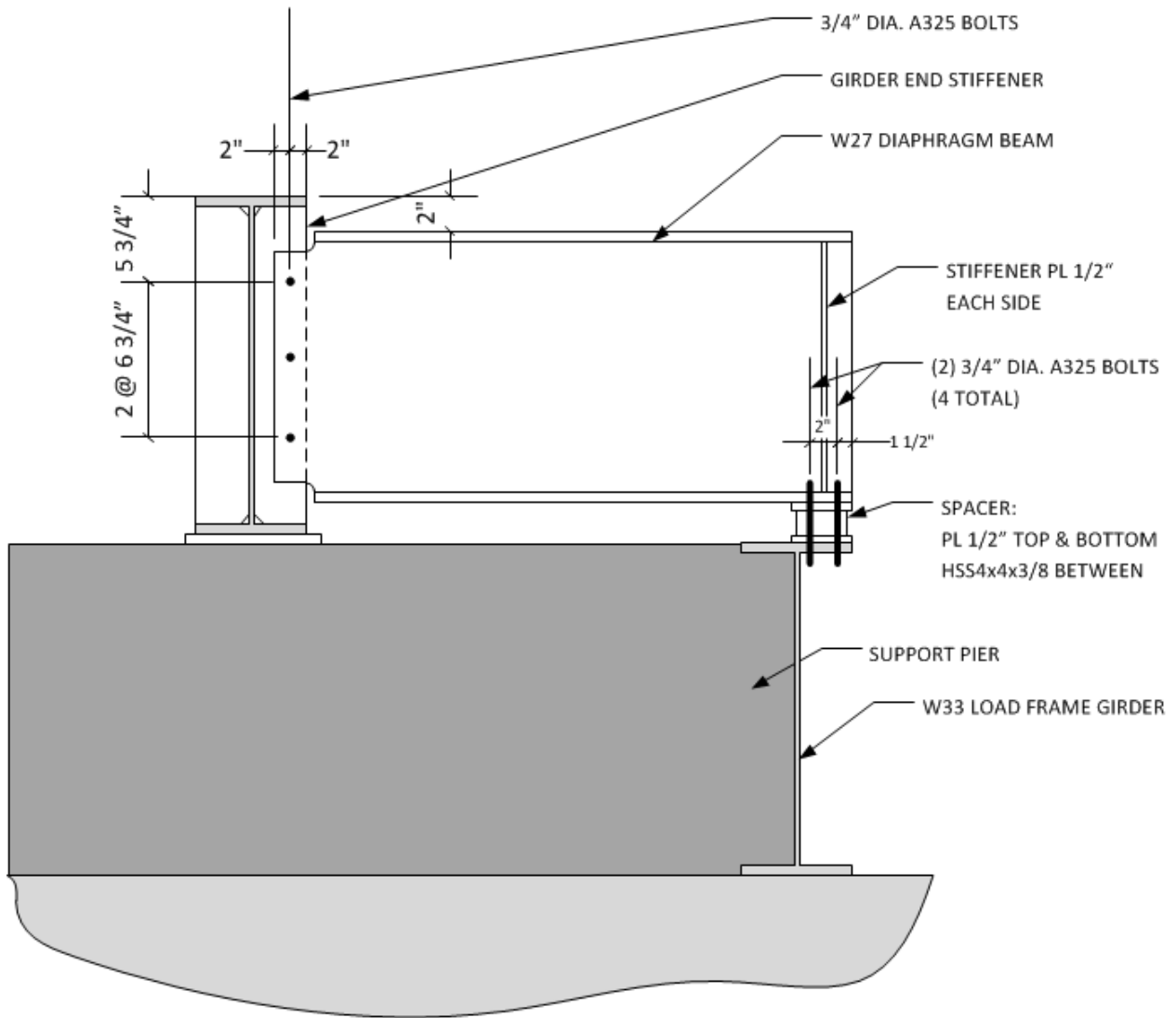


G ANCHORAGE DETAILS

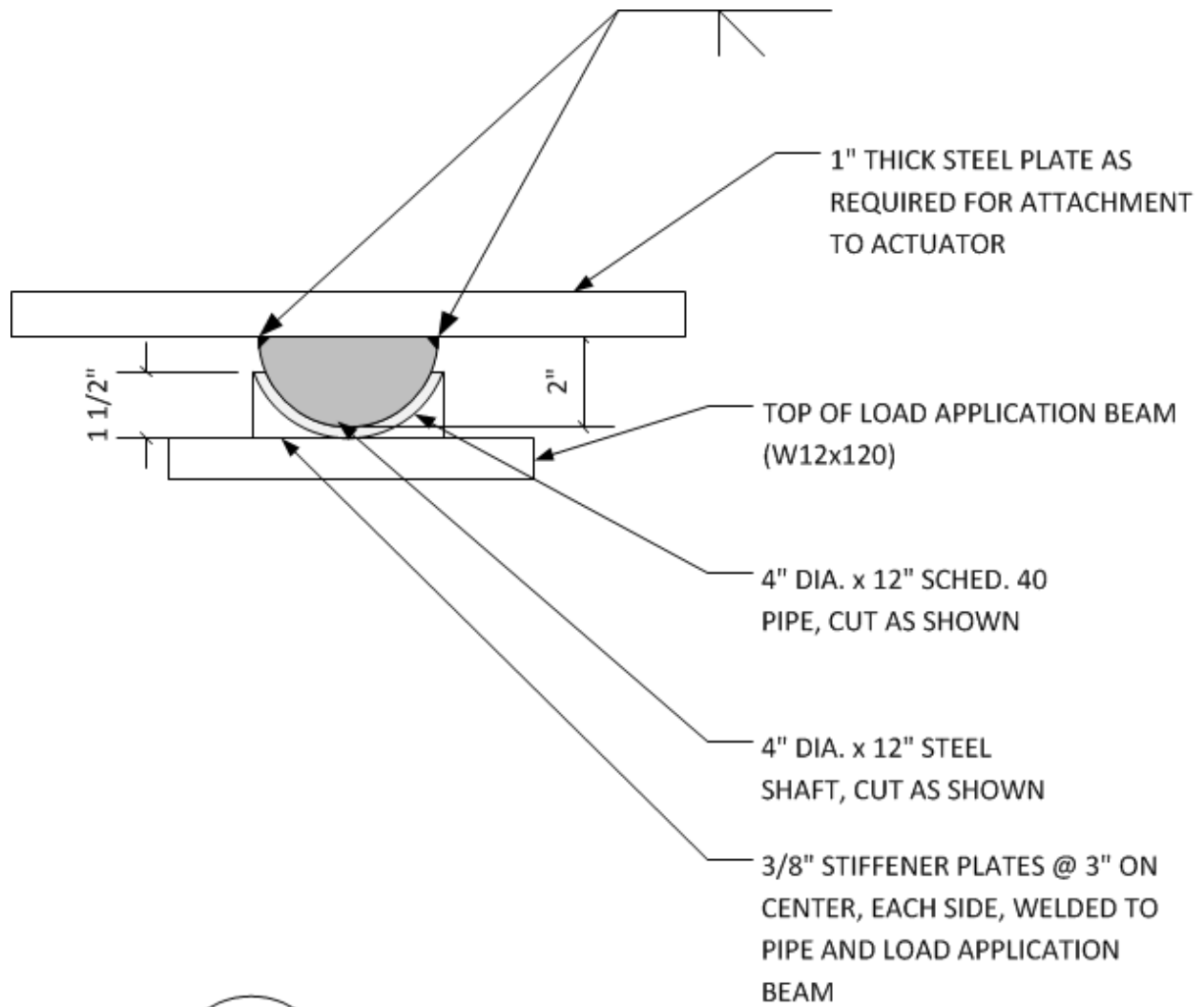


H SPACER PLATE DETAILS





K GIRDER DIAPHRAGM SECTION

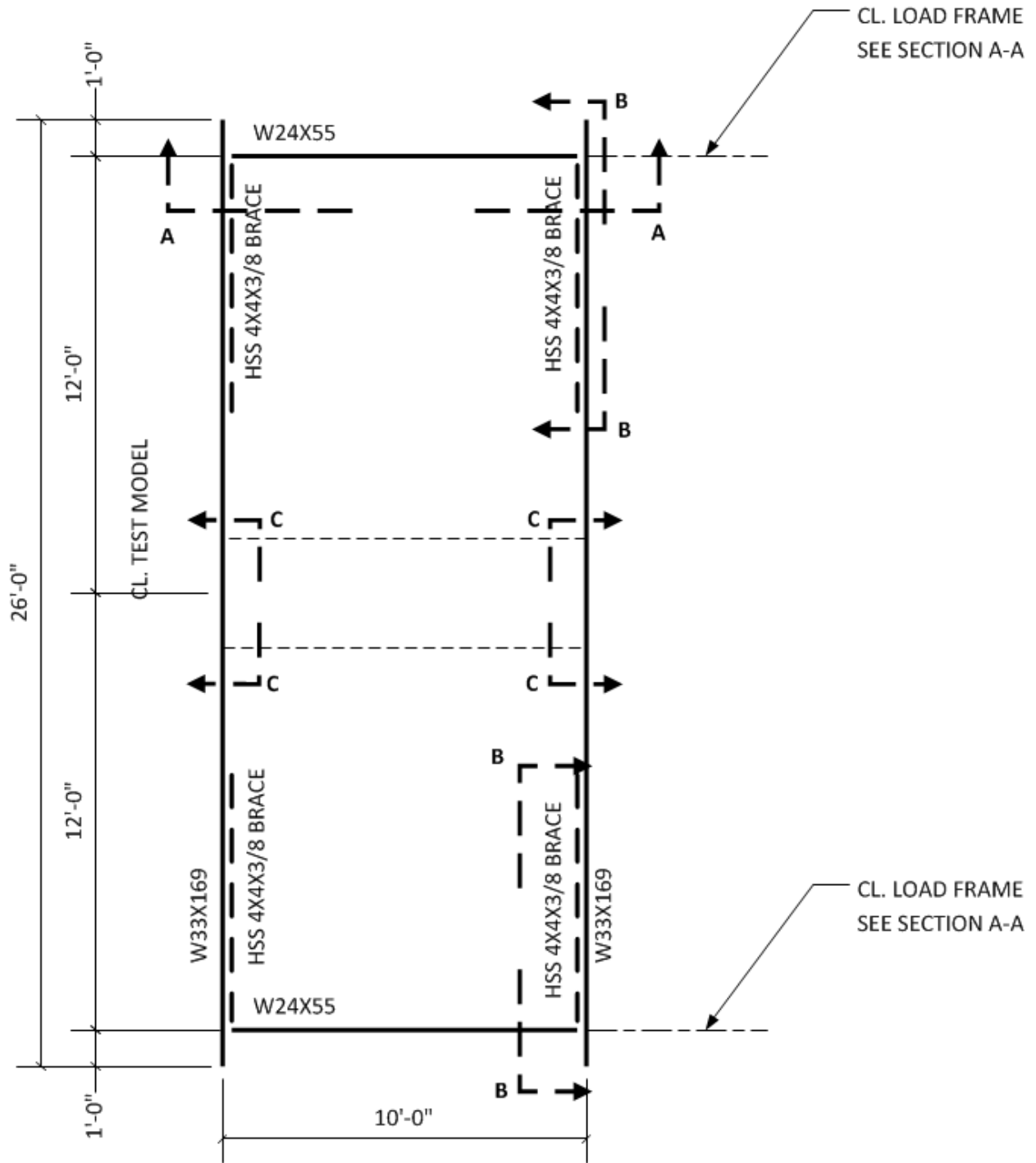


NORTH ACTUATOR 'HINGE' DETAIL

SELF-REACTING LOAD FRAME

GENERAL NOTES:

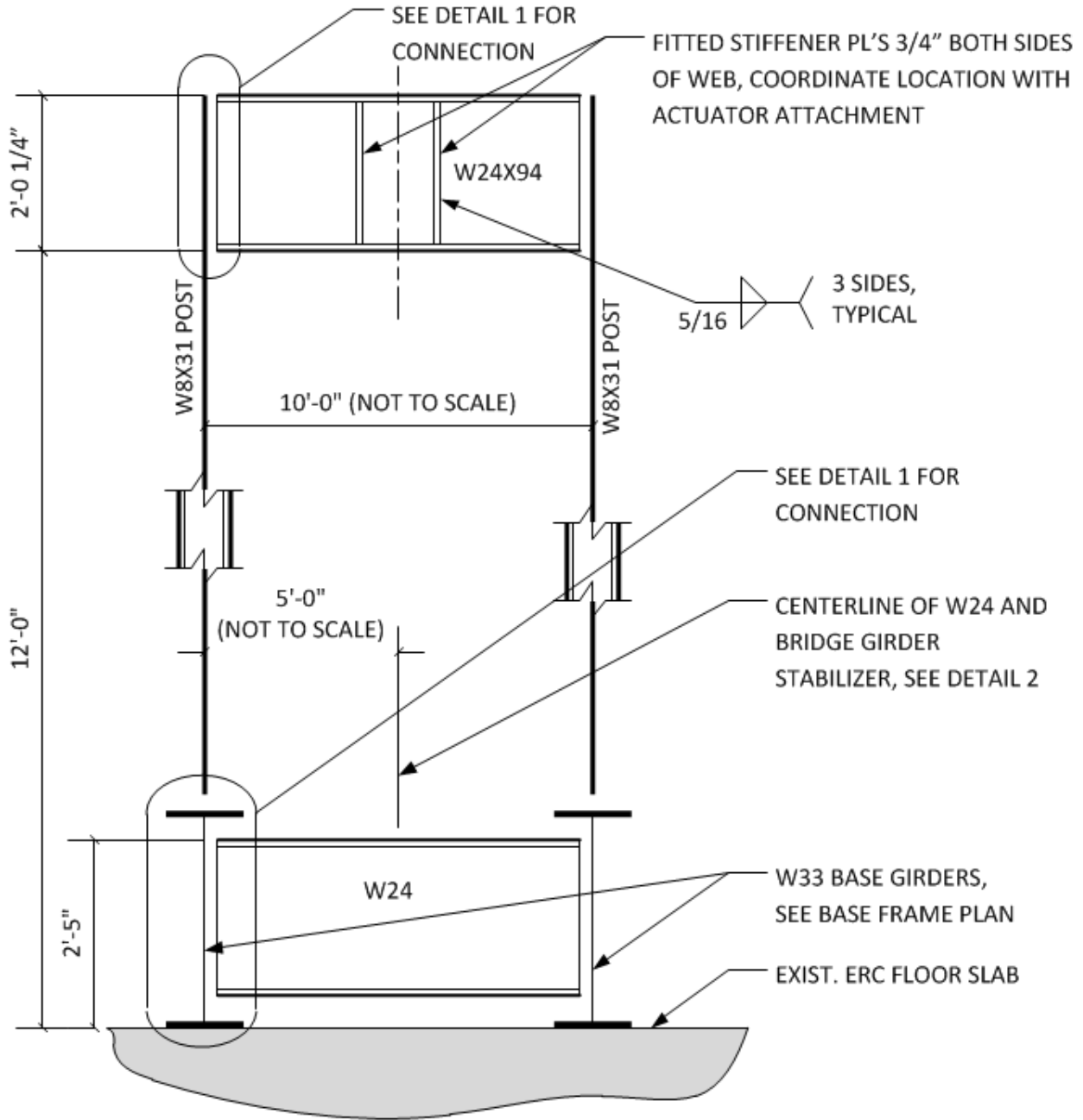
1. FIELD VERIFY ALL EXISTING DIMENSIONS
2. ALL STRUCTURAL STEEL SHAPES SHALL BE ASTM A992, GRADE 50, $F_y = 50$ ksi
3. ALL STRUCTURAL STEEL PLATES SHALL BE ASTM A36, $F_y = 36$ ksi
4. ALL STRUCTURAL STEEL CONNECTIONS SHALL BE MADE WITH 3/4" DIA. A325N BOLTS IN 13/16" DIA. HOLES. DO NOT REAM OR OTHERWISE OVERSIZE HOLES.
5. DRILL OR PUNCH ALL HOLES, DO NOT FLAME CUT.
6. ALL WELD ELECTRODES SHALL BE E70XX.



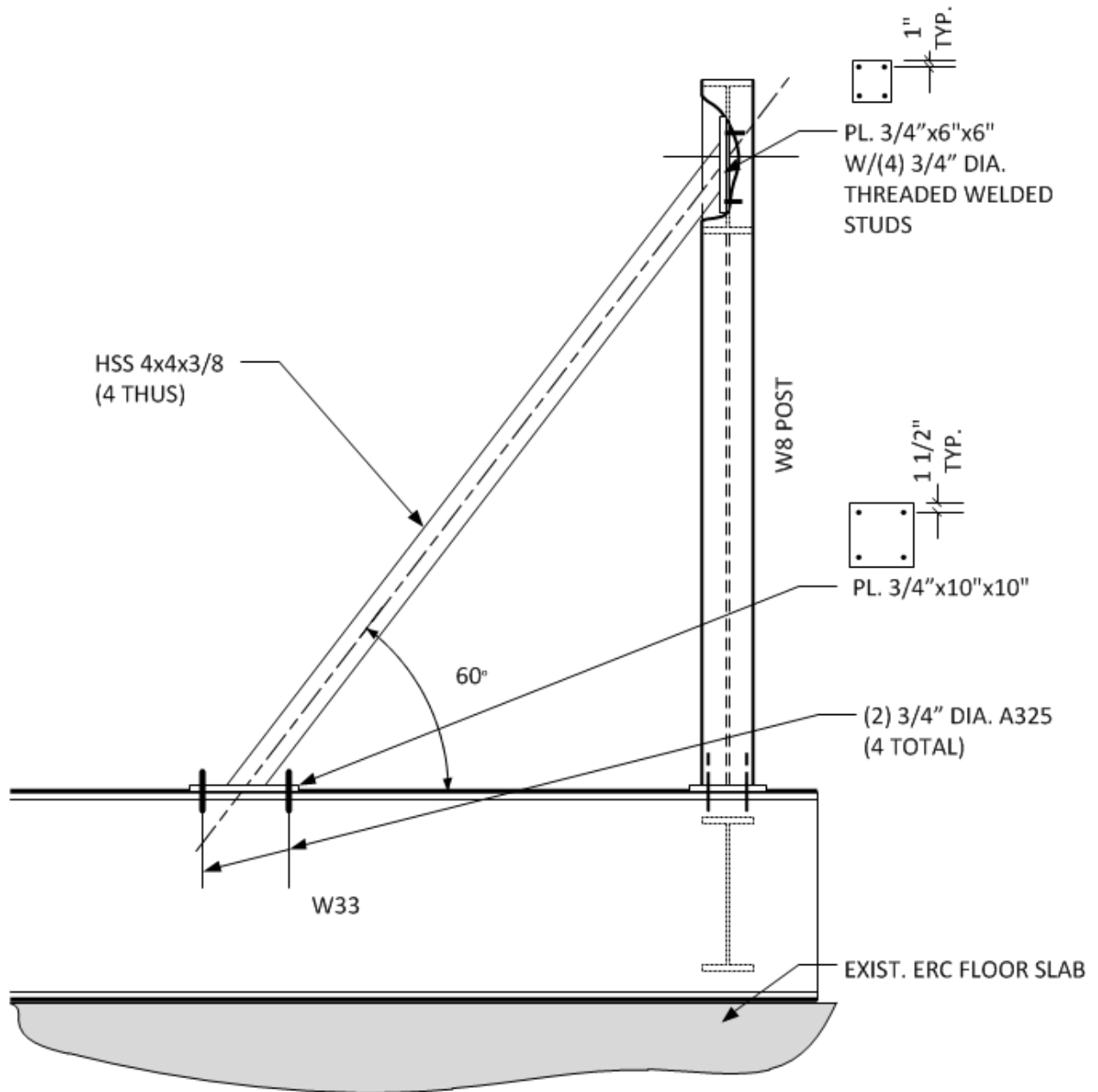
SELF-REACTING LOAD FRAME
BASE FRAMING PLAN

1/4" = 1'-0"





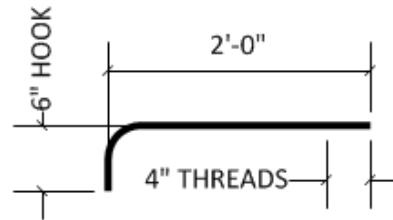
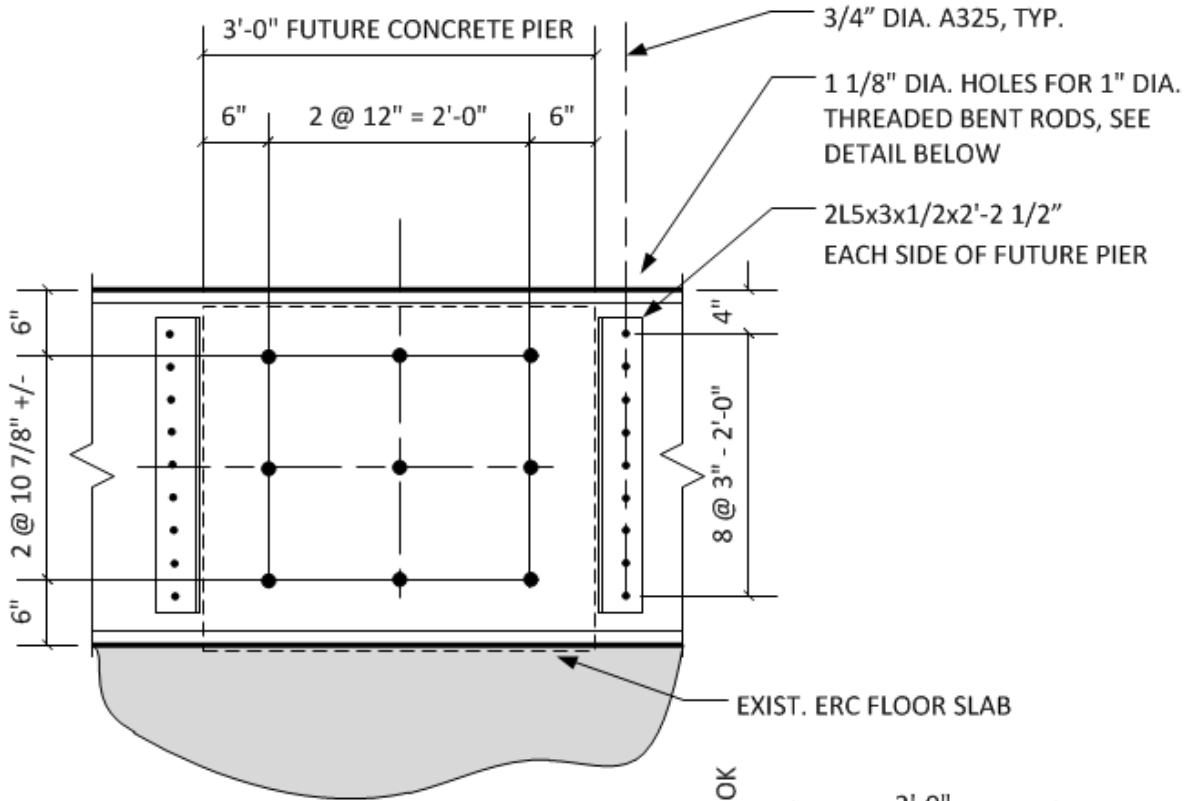
A **LOAD FRAME SECTION**
 1/2" = 1'-0"



B

BRACE ELEVATION

1/2" = 1'-0"



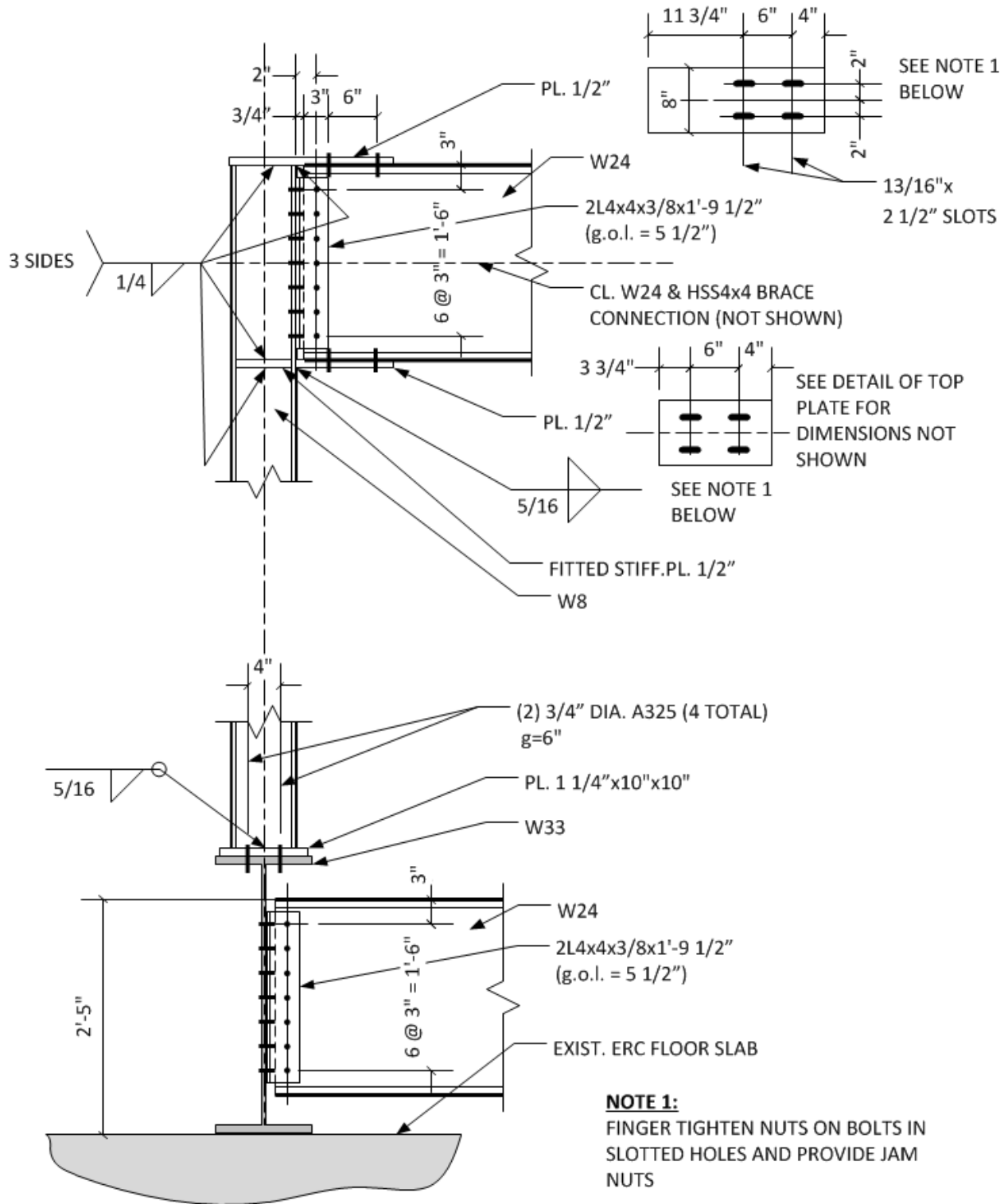
PROVIDE 2 NUTS & 1 WASHER FOR EACH ANCHOR ROD

BENT ROD DETAIL

C

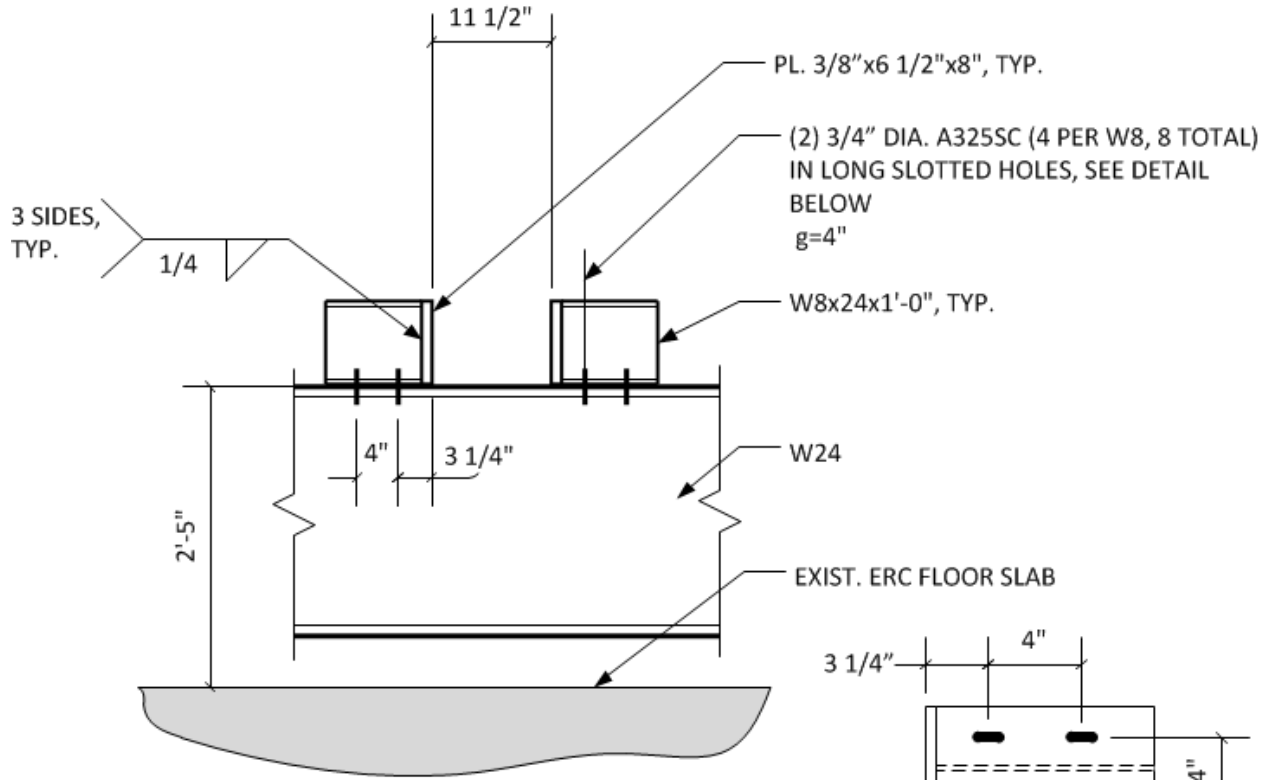
SECTION AT TEST PIER ANCHORAGE

3/4" = 1'-0"



1

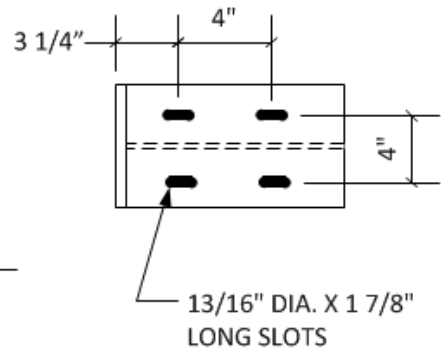
FRAMING CONNECTION DETAILS



2

BRIDGE GIRDER STABILIZER

3/4" = 1'-0"



**W8 FLANGE HOLE
DETAIL**



3/25/13

1

SELF REACTING FRAME

PURPOSE: DESIGN SELF-REACTING LOAD FRAME TO TAKE FULL LOAD OF ACTUATORS (220K). FRAMING WILL BE STEEL GIRDERS WITH MOVEABLE STEEL CROSS BEAMS. DESIGN FOR 10' WIDTH.

MATERIALS: STRUCTURAL STEEL:
SHAPES (W) — ASTM A992 $F_y = 50$ ^{ksi}
P'S & SHAPES — ASTM A36 $F_y = 36$ ^{ksi}
BOLTS — $3/4"$ ϕ ASTM A325SC
WELD ELECTRODES — E70XX
EXIST. CONCRTE $f'_c = 3000$ ^{PSI} (ASSUMED)

CODES, ETC.: STEEL DESIGN — AISC — ASD/LRFD
CONC. DESIGN — ACI — LRFD

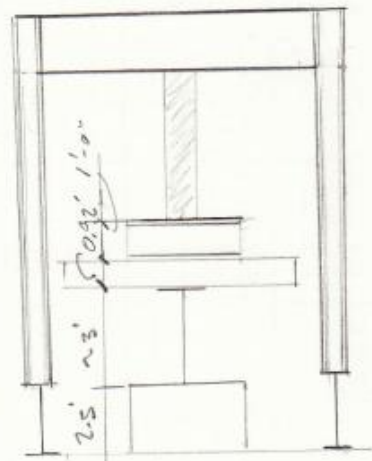
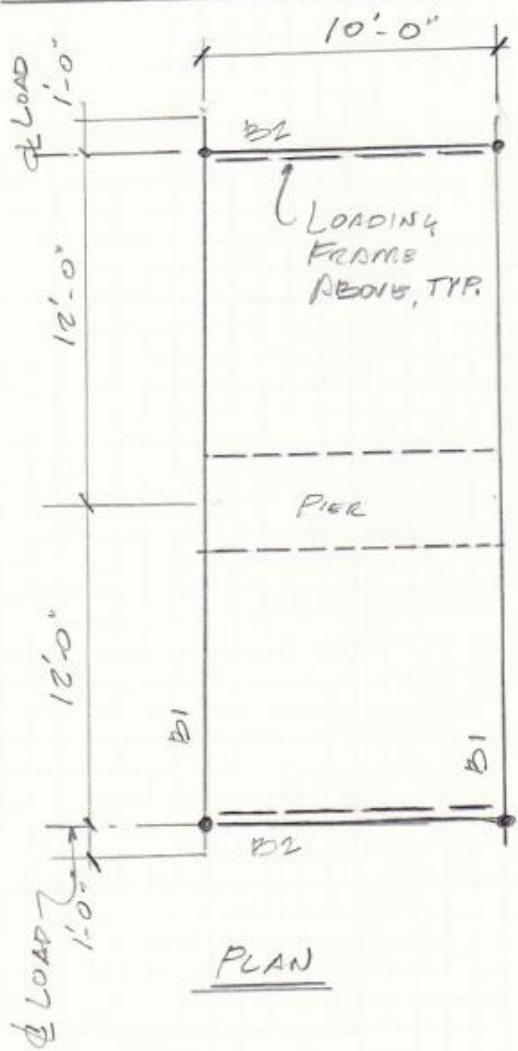
LOADS: DESIGN FOR 220K ACTUATOR LOAD AT EACH END TO BE COUNTERACTED BY DOWNWARD LOADS OF EQUAL & OPPOSITE MAGNITUDE AT CENTER OF GIRDERS. ^(UP)



8/20/13

2

SELF REACTING FRAME



FRAME ELEVATION

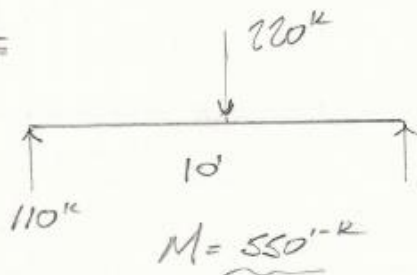
#

8/26/13

3

DESIGN LOAD FRAME

GIRDER



W24x94
 $M_n = 585'·k$
 $\frac{S_x}{E} = 10'$

Check props: $d = 24.3''$ $t_w = 0.515''$ $b_f = 9.07''$ $t_f = 0.875''$
 $K = 1.38''$ ← Assumed

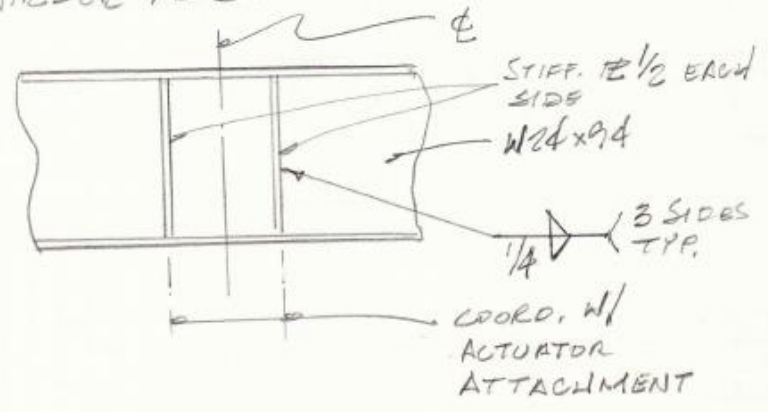
• Web Local Yielding $R_n = (5 \times 1.38 + 10) 50 \times 0.515 = 435'k$
 $R_n / \Omega = 240'k > 110'k \text{ ok}$

• Web Lipping $R_n = 0.80 \cdot 0.515^2 \left[1 + 3 \left(\frac{10}{24.3} \right) \left(\frac{0.515}{0.875} \right)^{1.5} \right] \left[\frac{E F_y 0.875}{0.515} \right]$
 $= 519'k$
 $R_n / \Omega = 259'k > 110'k \text{ ok}$

• Web Sidesway Buckling
 $(h/t_w) / (2/b_f) = [(24.3 - 2 \times 1.38) / 0.515] / (12 \times 10 / 9.07)$
 $= 3.10 > 1.7$ NOT APPLICABLE

STIFFENERS NOT REQ'D, BUT USE ANYWAY.

Use GIRDER AS SHOWN



STEUTS

$T = 110^k$ (slr. 3)

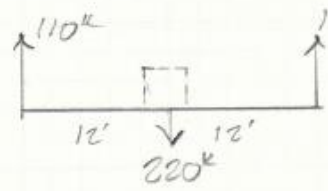
TR4 W8 STEUT



DESIGN CONNS. AFTER
B1 IS DESIGNED

USE
W8x31
 $F_u/S_u = 273^k$
 $A = 9.12 \text{ in}^2$

B1



$M = 110 \times 12$
 $= 1320 \text{ ft-k}$
 $L_b = 12'$

TR4 W33x109 $M_n/S_u = 1470 \text{ ft-k}$

CHECK WEB: $d = 33.8''$ $t_w = 0.670''$ $b_f = 11.5''$ $t_f = 1.22''$
 $k = 1.92''$

- WEB LOCAL YIELDING $R_n = (5 \times 1.92 + 10) 50 \times 0.67 = 657^k$
 $R_n/S_u = 438^k > 110^k$ OK
- FLANGE LOCAL BENDING $R_n = 6.25 \times 1.22^2 \times 50 = 465^k$
 $R_n/S_u = 279^k > 110^k$ OK
- WEB CRIPPLING $M/d = 10/33.8 = 0.30 > 0.2$
 $R_n = 0.40 \times 0.67^2 \left[1 + (4 \times 0.3 - 0.2) \left(\frac{0.67}{1.22} \right)^{1.5} \right] \sqrt{\frac{E F_y \cdot 1.22}{0.67}}$
 $= 411^k$ $R_n/S_u = 205^k > 110^k$ OK
- WEB SIDESWAY - NOT A PROBLEM SINCE CROSS GIRDER FRAMING IN

USE W33x109
NO STIFFS. REQ'D

#

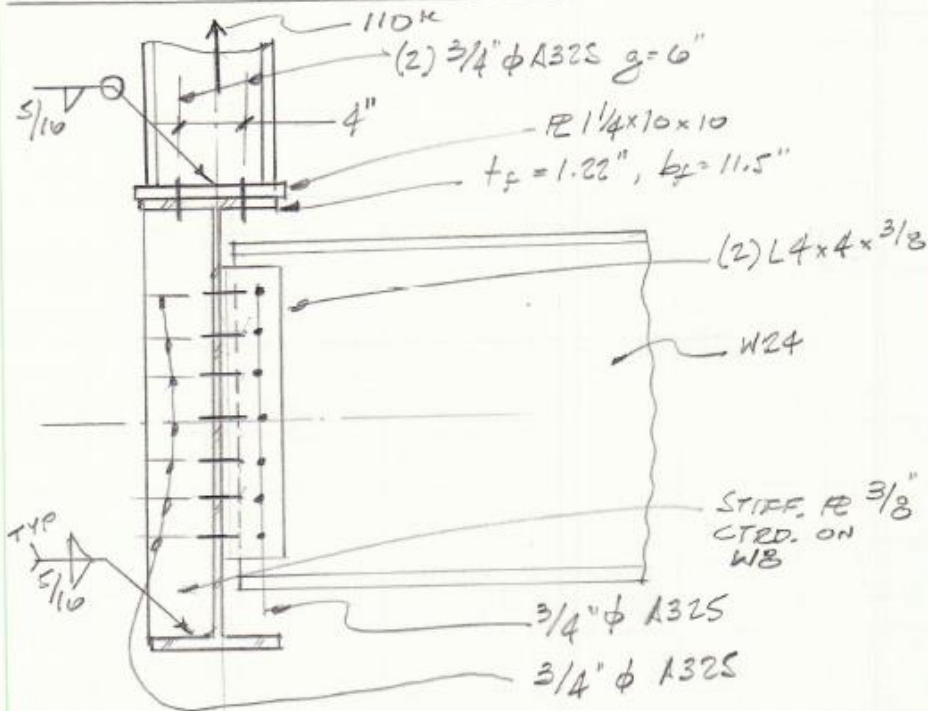
8/26/13

5

PL STABILIZER ONLY
Use SMALLEST W24

Use
W24x55

CONN. W24 & WB STENT TO WBS



STENT CONNECTION Ten (6) $\frac{3}{4}$ " ϕ BOLTS

$$T/\text{BOLT} = 110/6 = 18.3^k$$

$$g = 6" \quad p = 4" \quad b' \sim \frac{6 - 0.285}{2} - \frac{18}{32} = 2.45"$$

$$t_{\min} = \sqrt{\frac{6.06 \times 18.3 \times 2.45}{4 \times 55}} = 1.07" < 1.22"$$

No PAYING @ WB

$$CR \quad t_{\min} = \sqrt{\frac{6.06 \times 18.3 \times 2.45}{4 \times 55}} = 1.13" \Rightarrow PL \frac{1}{4}"$$

• WELD $l_{weld} \sim 2 \times 5.75 + 2(8 - 0.285) = 26.9"$

$$F_r = 110/26.9 = 4.1^k/in \quad \text{Use } 5/16 \quad F_r = 4.64^k/in$$

- CONT. -

#

8/20/13

U

W24 + WB TO W33 - CONT. -

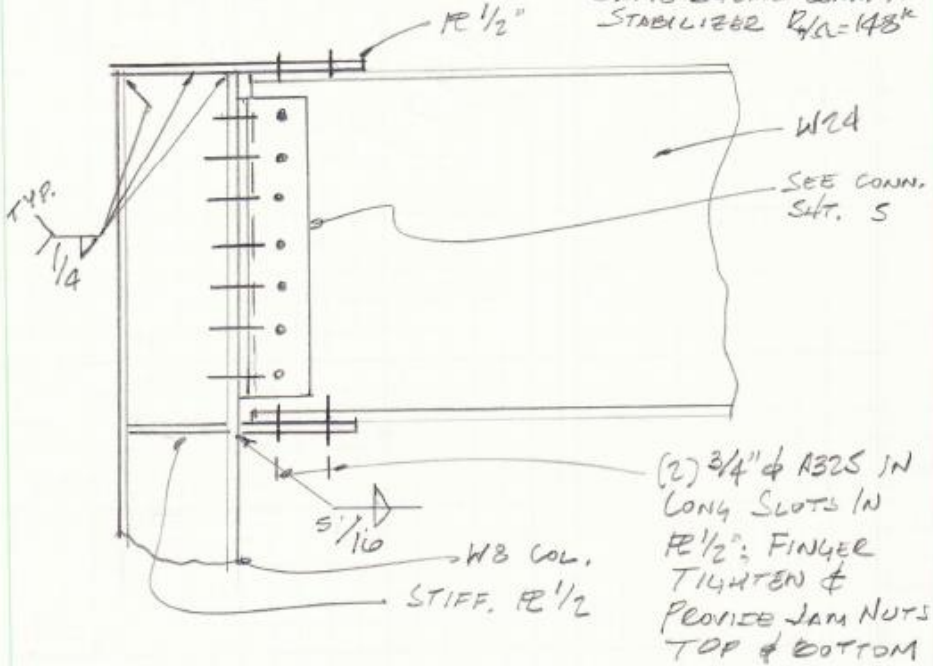
W24 TO W33 JUST FILL UP CONNECTION

SEE SHT. 5 FOR
DETAIL

FRAME Conn. W24 TO WB

R = 110"K

SAME SHEAR Conn. AS
STABILIZER R/A = 148"K



APPENDIX 5 – PLATE GIRDER DIMENSIONS

Table 45 - Plate Girder Dimensions

Name	d _w	t _f	b _f	t _w	d	A	I _x	Wt./ft.
PG1	46.5	0.75	24	0.625	48	65.1	25331	221
PG2	46.5	0.75	26	0.625	48	68.1	27006	232
PG3	46.25	0.875	28	0.625	48	77.9	32360	265
PG4	46.25	0.875	30	0.625	48	81.4	34304	277
PG5	46.25	0.875	32	0.625	48	84.9	36247	289
PG6	46	1	34	0.625	48	96.8	42628	329
PG7	46	1	36	0.625	48	100.8	44838	343
PG8	50.5	0.75	26	0.625	52	70.6	32319	240
PG9	50.25	0.875	28	0.625	52	80.4	38630	274
PG10	50.25	0.875	30	0.625	52	83.9	40918	286
PG11	50.25	0.875	32	0.625	52	87.4	43205	297
PG12	50	1	34	0.625	52	99.3	50733	338
PG13	50	1	36	0.625	52	103.3	53334	351
PG14	49.75	1.125	38	0.625	52	116.6	61746	397
PG15	52.5	0.75	27	0.625	54	73.3	36249	249
PG16	52.25	0.875	28	0.625	54	81.7	42005	278
PG17	52.25	0.875	30	0.625	54	85.2	44475	290
PG18	52.25	0.875	32	0.625	54	88.7	46945	302
PG19	52	1	34	0.625	54	100.5	55082	342
PG20	52	1	36	0.625	54	104.5	57891	356
PG21	51.75	1.125	38	0.625	54	117.8	66987	401
PG22	51.75	1.125	40	0.625	54	122.3	70132	416
PG23	58.25	0.875	30	0.75	60	96.2	58238	327
PG24	58.25	0.875	31	0.75	60	97.9	59768	333
PG25	58.25	0.875	32	0.75	60	99.7	61297	339
PG26	58	1	33	0.75	60	109.5	69637	373
PG27	58	1	34	0.75	60	111.5	71377	379
PG28	58	1	35	0.75	60	113.5	73118	386
PG29	58	1	36	0.75	60	115.5	74859	393

APPENDIX 6 – ACCEPTABLE BRIDGE GIRDERS

Table 46 - Girder Acceptance Table - 92 ft. Span

Girder Spacing	Slab Thickness		
	8 inches	8.5 inches	9 inches
7.33 ft.	W40x167	W40x167	W40x167
7.67 ft.	W40x167	W40x167	W40x167
8.00 ft.	W40x183	W40x183	W40x183
8.33 ft.	W40x183	W40x183	W40x183
8.67 ft.	W40x183	W40x183	W40x183
9.00 ft.	W40x183	W40x183	W40x183
9.33 ft.	W40x199	W40x199	W40x183
9.67 ft.	W40x199	W40x199	W40x183
10.00 ft.	W40x199	W40x199	W40x183
10.33 ft.	W40x199	W40x199	W40x183

Table 47 - Girder Acceptance Table - 104 ft. Span

Girder Spacing	Slab Thickness		
	8 inches	8.5 inches	9 inches
7.33 ft.	W44x230	W44x230	W44x290
7.67 ft.	W44x230	W44x230	W44x290
8.00 ft.	W44x230	W44x230	W44x290
8.33 ft.	W44x230	W44x230	W44x290
8.67 ft.	W44x230	W44x230	W44x290
9.00 ft.	W44x230	W44x230	W44x290
9.33 ft.	W44x230	W44x230	W44x335
9.67 ft.	W44x230	W44x262	W44x335
10.00 ft.	W44x230	W44x262	W44x335
10.33 ft.	W44x230	W44x262	W44x335

Table 48- Girder Acceptance Table - 116 ft. Span

Girder Spacing	Slab Thickness		
	8 inches	8.5 inches	9 inches
7.33 ft.	PG1	PG1	PG1
7.67 ft.	PG1	PG1	PG1
8.00 ft.	PG1	PG1	PG1
8.33 ft.	PG1	PG1	PG1
8.67 ft.	PG1	PG1	PG1
9.00 ft.	PG1	PG1	PG1

Girder Spacing	Slab Thickness		
	8 inches	8.5 inches	9 inches
9.33 ft.	PG2	PG2	PG2
9.67 ft.	PG2	PG2	PG2
10.00 ft.	PG2	PG2	PG3
10.33 ft.	PG2	PG3	PG3

Table 49 - Girder Acceptance Table - 128 ft. Span

Girder Spacing	Slab Thickness		
	8 inches	8.5 inches	9 inches
7.33 ft.	PG8	PG8	PG8
7.67 ft.	PG8	PG8	PG8
8.00 ft.	PG8	PG8	PG8
8.33 ft.	PG8	PG8	PG9
8.67 ft.	PG9	PG9	PG9
9.00 ft.	PG9	PG9	PG9
9.33 ft.	PG9	PG9	PG9
9.67 ft.	PG9	PG9	PG9
10.00 ft.	PG9	PG9	PG9
10.33 ft.	PG9	PG9	PG9

Table 50 - Girder Acceptance Table - 140 ft. Span

Girder Spacing	Slab Thickness		
	8 inches	8.5 inches	9 inches
7.33 ft.	PG16	PG16	PG16
7.67 ft.	PG16	PG16	PG16
8.00 ft.	PG17	PG17	PG17
8.33 ft.	PG17	PG17	PG17
8.67 ft.	PG18	PG18	PG18
9.00 ft.	PG18	PG18	PG18
9.33 ft.	PG19	PG19	PG18
9.67 ft.	PG19	PG19	PG18
10.00 ft.	PG19	PG19	PG18
10.33 ft.	PG19	PG19	PG18

APPENDIX 7 – MAXIMUM SMC NEGATIVE MOMENTS

Table 51 - Maximum SMC Negative Moments (kip-feet) - 92 ft. Span

Girder Spacing	Slab Thickness		
	8 inches	8.5 inches	9 inches
7.33 ft.	-2509	-2489	-2470
7.67 ft.	-2569	-2548	-2528
8.00 ft.	-2641	-2619	-2598
8.33 ft.	-2700	-2677	-2656
8.67 ft.	-2759	-2735	-2713
9.00 ft.	-2818	-2792	-2770
9.33 ft.	-2890	-2864	-2827
9.67 ft.	-2948	-2922	-2884
10.00 ft.	-3006	-2979	-2940
10.33 ft.	-3064	-3036	-2996

Table 52 - Maximum SMC Negative Moments (kip-feet) - 104 ft. Span

Girder Spacing	Slab Thickness		
	8 inches	8.5 inches	9 inches
7.33 ft.	-3013	-2989	-3003
7.67 ft.	-3083	-3058	-3072
8.00 ft.	-3153	-3127	-3143
8.33 ft.	-3222	-3195	-3212
8.67 ft.	-3291	-3263	-3280
9.00 ft.	-3359	-3331	-3348
9.33 ft.	-3427	-3398	-3444
9.67 ft.	-3495	-3491	-3512
10.00 ft.	-3562	-3558	-3579
10.33 ft.	-3629	-3625	-3647

Table 53 – Maximum SMC Negative Moments (kip-feet) – 116 ft. Span

Girder Spacing	Slab Thickness		
	8 inches	8.5 inches	9 inches
7.33 ft.	-3473	-3447	-3423
7.67 ft.	-3552	-3524	-3499
8.00 ft.	-3630	-3601	-3575
8.33 ft.	-3707	-3678	-3651
8.67 ft.	-3784	-3754	-3727
9.00 ft.	-3860	-3830	-3801

Girder Spacing	Slab Thickness		
	8 inches	8.5 inches	9 inches
9.33 ft.	-3946	-3914	-3884
9.67 ft.	-4022	-3989	-3959
10.00 ft.	-4098	-4064	-4060
10.33 ft.	-4173	-4167	-4134

Table 54 - Maximum SMC Negative Moments (kip-feet) - 128 ft. Span

Girder Spacing	Slab Thickness		
	8 inches	8.5 inches	9 inches
7.33 ft.	-3957	-3929	-3902
7.67 ft.	-4044	-4015	-3987
8.00 ft.	-4130	-4100	-4072
8.33 ft.	-4216	-4185	-4180
8.67 ft.	-4327	-4295	-4265
9.00 ft.	-4413	-4380	-4348
9.33 ft.	-4499	-4464	-4432
9.67 ft.	-4584	-4548	-4515
10.00 ft.	-4668	-4631	-4597
10.33 ft.	-4752	-4715	-4680

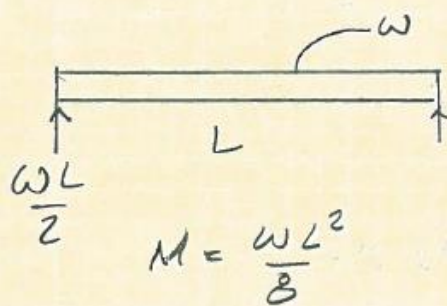
Table 55 - Maximum SMC Negative Moments (kip-feet) - 140 ft. Span

Girder Spacing	Slab Thickness		
	8 inches	8.5 inches	9 inches
7.33 ft.	-4459	-4428	-4401
7.67 ft.	-4554	-4523	-4494
8.00 ft.	-4657	-4625	-4595
8.33 ft.	-4751	-4718	-4687
8.67 ft.	-4854	-4820	-4788
9.00 ft.	-4948	-4912	-4880
9.33 ft.	-5069	-5032	-4970
9.67 ft.	-5163	-5125	-5062
10.00 ft.	-5256	-5217	-5152
10.33 ft.	-5349	-5309	-5243

APPENDIX 8 – DEFLECTION EQUATION DEVELOPMENT

DEVELOP A SIMPLE METHOD TO DETERMINE I_x REQ'D FOR +M DEFLECTION AS A FUNCTION OF MOMENT (M) IN kip-ft LENGTH (L) IN FT. AND SPAN TO DEFLECTION RATIO OF LENGTH (L) IN INCHES AND RATIO LIMIT l/N_D IN INCH/INCH.

EXAMPLE FOR A UNIFORMLY LOADED SIMPLE BEAM



$$M_{\max} = \frac{wL^2}{8} \text{ (k-ft.)}$$

$$\Delta_{\max} = \frac{5wL^4}{384EI_x} \text{ (in.)}$$

$$\Delta_{\max} = C_1 M = C_1 \times \frac{12wL^2}{8} = \frac{5wL^4}{384EI_x}$$

$$C_1 = \frac{8}{wL^2} \times \frac{5wL^4}{384EI_x} = \frac{5}{48} \frac{ML^2}{EI_x}$$

$$\Delta_{\max} = \frac{L}{N_D} \quad N_D = \text{LIMIT NUMBER} \\ 180, 240, 300, 600, 800 \text{ ETC.}$$

$$\frac{L}{N_D} = \frac{5}{48} \frac{ML^2}{EI_x}$$

$$\text{WE WANT } I_x \therefore \left[I_x \text{ MIN} = \frac{5}{48} \frac{ML}{E} N_D \right]$$

IN ORDER TO USE L IN FT. AND M IN k-ft., MULTIPLY BY 12^2 AND DIVIDE BY $E = 29,000 \text{ ksi (STEEL)}$

$$\therefore I_{x \text{ MIN}} = \frac{MLN_D}{1933}$$

M IN K-ft
 L IN ft
 $I_{x \text{ MIN}}$ IN in⁴

FOR SIMPLE-SPAN UNIFORMLY LOADED BEAM, $I_{x \text{ MIN}}$ MAY BE ACCURATELY CALCULATED BASED ON

$$I_{x \text{ MIN}} = \frac{MLN_D}{1933}$$

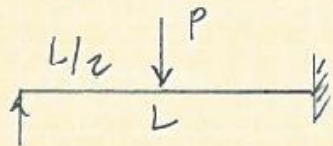
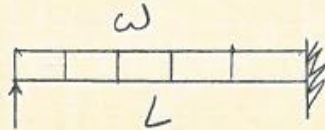
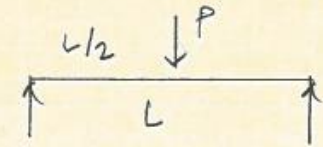
WHERE M IS MAXIMUM MOMENT (K-ft)

L IS SPAN (ft.)

$I_{x \text{ MIN}}$ IS MAJOR AXIS MOMENT OF INERTIA (in⁴)

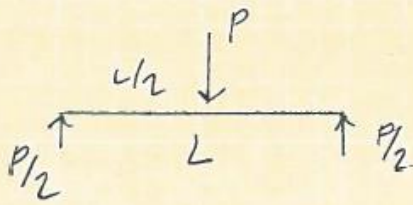
N_D = DEFLECTION LIMITATION AS A FUNCTION OF SPAN, I.E., $\Delta_{\text{MAX}} = L/N_D$

• THIS PROCEDURE MAY BE REPEATED FOR THE FOLLOWING LOAD CONDITIONS FOR COMPARISON



IT'S APPARENT THAT DUE TO INDETERMINACY, THE REQUIRED I_x FOR THESE CONDITIONS WOULD BE LESS THAN THOSE FOR THE CORRESPONDING SIMPLE BEAM CONDITIONS.

POINT LOADED SIMPLE BEAM



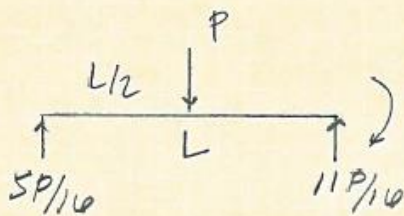
$$M_{\max} = \frac{PL}{4}$$

$$\Delta = \frac{PL^3}{48EI_x} = \frac{ML^2}{12EI_x} = \frac{L}{N_D}$$

$$\frac{ML}{12EI_x} = \frac{1}{N_D} \quad \therefore I_{x\min.} = \frac{MLN_D}{12} \times \frac{144}{29,000}$$

$$I_{x\min.} = \frac{MLN_D}{2417} < \frac{MLN_D}{1935}$$

FIXED-HINGED BEAM LOCK AT +M



$$3PL = -M \quad +M = \frac{5PL}{32}$$

$$\Delta_P = \frac{7PL^3}{768EI}$$

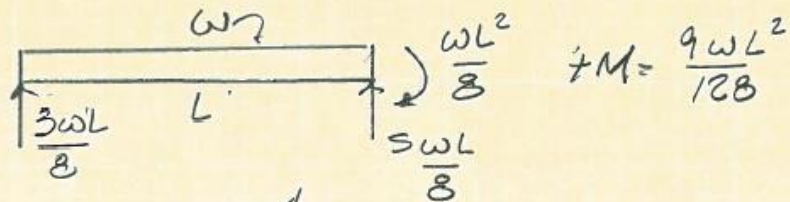
$$\Delta = \frac{32}{5} \frac{7}{768} \frac{ML^2}{EI_x} = \frac{L}{N_D}$$

$$I_x = \frac{224}{3840} \times \frac{MLN_D}{E}$$

$$\text{AT } M_{\max} = 0.009317 \frac{PL^3}{EI}$$

$$= \frac{MLN_D}{3452} = I_{x\min.}$$

$$I_{x\min.} = \frac{MLN_D}{3452} \quad M = M_{\max}$$

FIXED-HINGED BEAM

$$\Delta_{MAX} = \frac{wL^4}{185EI} = \frac{128}{9wL^2} \times \frac{wL^4}{185EI} M$$

$$= \frac{128}{1065} \frac{M}{EI} = \frac{L}{N_D}$$

$$I_{XMIN} = \frac{MLN_D}{2020}$$